Mechanism of Catalysis by *Escherichia coli* Phosphoenolpyruvate Carboxykinase

A Thesis Submitted to the

College of Graduate Studies and Research

In Partial Fulfillment of the Requirements

for the Degree of Master of Science

in the Department of Microbiology and Immunology

University of Saskatchewan

Saskatoon

By

Akosiererem Senibo Sokaribo

PERMISSION TO USE

In presenting this thesis in partial fulfillment of the requirements for a Postgraduate degree from the University of Saskatchewan, I agree that the Libraries of this University may make it freely available for inspection. I further agree that permission for copying of this thesis in any manner, in whole or in part, for scholarly purposes may be granted by the professor or professors who supervised my thesis work or, in their absence, by the Head of the Department or the Dean of the College in which my thesis work was done. It is understood that any copying or publication or use of this thesis or parts thereof for financial gain shall not be allowed without my written permission. It is also understood that due recognition shall be given to me and to the University of Saskatchewan in any scholarly use which may be made of any material in my thesis.

Requests for permission to copy or to make other uses of materials in this thesis in whole or part should be addressed to:

Head of Department of Microbiology and Immunology

2D01, Health Science Building

University of Saskatchewan

107 Wiggins Rd.

Saskatoon, Saskatchewan, Canada

S7N 5E5

ABSTRACT

Escherichia coli phosphoenolpyruvate carboxykinase (ATP:oxaloacetate carboxylase (transphorsphorylating) EC 4.1.1.49) catalyzes the decarboxylation and subsequent phosphorylation of oxaloacetate (OAA) to phosphoenolpyruvate (PEP) in the presence of Mg^{2+}ATP and synergistic catalysis has been observed in the presence of Ca^{2+} or Mn^{2+}. Structural analyses have shown that active site residues Arg333, Ser250 and Tyr207 are coordinated differently in *E. coli* PCK structures complexed with Mg^{2+}ATP-oxalate, Mg^{2+}ATP-Mn^{2+}-pyruvate and Mg^{2+}ATP-Ca^{2+}-pyruvate; hence, we hypothesize that the function of Arg333, Ser250 and Tyr207, depends on the absence or presence of Ca^{2+} or Mn^{2+} during catalysis by *E. coli* phosphoenolpyruvate carboxykinase (PCK).

In order to verify this hypothesis, site directed mutagenesis of the *pckA* gene was used to convert Arg333 to Gln, Ser250 to Ala and Tyr207 to Phe, while $^{14}CO_2$ exchange assay and x-ray crystallography were used to determine the effects of these mutations on catalysis by *E. coli* PCK in the presence of OAA and Mg^{2+}ATP with Ca^{2+} or Mn^{2+} metal ions. Kinetic analysis showed that the Tyr207Phe mutation decrease k_{cat} by 1.7 fold, while Ser250Ala and Arg333Gln reduced k_{cat} by 10.8 and 4,555 fold respectively in the presence of Mg^{2+}ATP and OAA. In the presence of Mg^{2+}ATP, OAA and Ca^{2+}, Arg333Gln, Ser250Ala and Tyr207Phe mutations reduced k_{cat} by 11,688, 44 and 2 fold respectively. In the presence of Mg^{2+}ATP, OAA and Mn^{2+} Arg333Gln, Ser250Ala and Tyr207Phe mutations reduced k_{cat} by 2,880, 4 and 5.5 fold respectively. The crystal structure of Ser250Ala complexed with Mg^{2+}ATP-Mn^{2+}-pyruvate, showed that in the presence of Mn^{2+}, Ser250Ala mutation reduced the angle between the γ-phosphate of ATP and residue 250 by 6.2 Å and increased the distance between the hydroxyl group of Tyr207 and the CH_2 group of pyruvate by 0.5 Å. As a result we conclude that Arg333 is important for

oxaloacetate decarboxylation and phosphorylation. During catalysis in the presence of Mg^{2+}ATP with or without Ca^{2+} or Mn^{2+}, Ser250 functions to maintain one γ-phosphate oxygen of ATP in an eclipsed conformation, while Tyr207 functions to drive oxaloacetate decarboxylation during catalysis in the presence of Mn^{2+} ion.

Kinetic and structural studies of *E. coli* PCK have previously been used to show that Asp269 is involved in metal coordination, while Lys254 and Arg65 are important for Mg^{2+}ATP and OAA binding to *E. coli* PCK respectively. In this study the *E. coli* PCK Asp269Asn-Mg^{2+}ATP-Ca^{2+}-pyruvate crystal structure showed that the Asp269Asn mutation reduced the number of ligands coordinating Ca^{2+} from seven to three, while no electron density was observed for Mg^{2+}ATP and OAA in Lys254Ser and Arg65Gln crystal structures respectively.

ACKNOWLEDGEMENTS

I am very grateful to Elohim for giving me good-health, strength, and everything necessary to complete this program. To my parents, Sokaribo and Ibiada, and brothers, Yahdein, Baruch, Sokaribo, Tonye and Ibim, words cannot even describe how thankful I am for all your support and encouragement. I love you all very much. My sisters, Belema and Ibinabo, I wish you spent more time with us. I will never forget both of you. Hossana Marcus and Victoria Cotterell, thank you guys for all your support and for always being there for me. I love you guys.

I want to thank my supervisor Dr. Hughes Goldie for giving me the opportunity to start graduate school and for all your help, guidance, and understanding. There is no way I would have been able to grow and harvest 12-litre cultures of LB without your help. Thank you, I am truly grateful. I also want to thank Dr. David Sanders for your help with crystallography, for allowing me to work in your laboratory, and for patiently answering all my questions even when I arrived unannounced. Thank you very much. Thank you, Dr. Linda Chelico for been my committee chair and for your helpful recommendations.

I would like to thank Dr. Julien Cotelesage for teaching and helping with data collection and model-building. All the structures in this work would not have been possible without your help. Thank you, Dr. Karen Straaten and Dr. Stanley Moore for patiently teaching, and helping me with crystallography. I would like to thank the faculty and staff of the Department of Microbiology and Immunology for all your help and for providing me with funding for my program, and Rivers State Sustainable Development Agency for all your assistance.

Table of Contents

LIST OF FIGURES

LIST OF TABLES

ABBREVIATIONS

ATP adenosine 5’-triphosphate

cAMP cyclic adenosine 3’,5’-monophosphate

CAM crassulacean acid metabolism

CMCF Canadian macromolecular crystallography facility

COMICS concentration of metal ions and complex species computer program

Cra catabolite repressor activator

CRP cAMP receptor protein

DEAE diethylaminoethyl cellulose

DTT 1,4-dithiothreitol

EDTA ethylenediaminetetraacetic acid

GTP guanosine 5’-triphosphate

LB Luria-Bertani medium

LDH lactate dehydrogenase

MDH malate dehydrogenase

mRNA messenger ribonucleic acid

NADH nicotinamide adenine dinucleotide

NEB New England Biolabs Inc.

OAA oxaloacetic acid, oxaloacetate

PEG polyethylene glycol

PCK phosphoenolpyruvate carboxykinase

PCK-C cytosolic phosphoenolpyruvate carboxykinase

PCK-M mitochondrial phosphoenolpyruvate carboxykinase

PEP phosphenolpyruvate

PPS phosphoenolpyruvate synthase

SDS-PAGE sodium dodecyl sulphate-polyacrylamide gel electrophoresis

TE 10 mM Tris, 1 mM EDTA buffer

Tris Tris[hydroxymethyl]aminomethane

UV ultraviolet

1.0 Introduction

1.1 Gluconeogenesis

1.1.1 Gluconeogenesis in Mammals and its relationship to diabetes

Gluconeogenesis is the central metabolic pathway used for glucose production in the cell. In mammals, it occurs primarily in the liver and kidney. When the blood glucose level is low, glucose can be produced through gluconeogenesis from non-carbohydrate precursor molecules such as lactate, pyruvate, amino acids, and triacylglycerol (Nelson, 2008). When triacylglycerol is used as the starting molecule of gluconeogenesis, it is first converted to glycerol and fatty acids. Fatty acids are oxidized to acetyl-CoA which is used in the Krebs cycle, while glycerol is converted to glyceraldehyde 3-phosphate (a gluconeogenic intermediate) after a series of reactions (Nelson, 2008). Catabolism of gluconeogenic amino acids leads to the production of α-ketoglutarate, fumarate, succinyl-CoA, pyruvate and oxaloacetate which can be converted to glucose, through the gluconeogenic pathway. When lactate is used as the starting molecule of gluconeogenesis, it is first converted to pyruvate, which can be converted to gluconeogenic intermediate, phosphoenolpyruvate (Nelson, 2008).

Insulin resistance and impaired function of pancreatic β-cell are the characteristics of Type 2 diabetics also known as Non-insulin-dependent-diabetes mellitus (NIDDM), (Baudry *et al.*, 2002, Goldstein, 2002). The blood glucose level is tightly regulated, so it is no surprise that increased rate of gluconeogenesis plays a role in the high blood glucose levels of NIDDM patients (Delbaere *et al.*, 2004, Magnusson *et al.*, 1992). Phosphoenolpyruvate carboxykinase (PCK) is the enzyme that catalyzes the first committed step of gluconeogenesis, and RNAi against PCK reduced the blood glucose level of diabetic mice (Gomez-Valades *et al.*, 2006), hence, PCK has been suggested as a potential drug target for the treatment of NIDDM patients (Valera *et al.*, 1994).

1.1.2 Gluconeogenesis in *Escherichia coli*

In *E. coli*, gluconeogenesis is essential for growth on carbon sources such as acetate, and succinate, which are eventually converted to glucose-6-phosphate. Glucose-6-phosphate is an important precursor molecule for glycolysis and the pentose phosphate pathway. During growth on acetate, acetate is eventually converted to acetyl-CoA which is converted to oxaloacetate (OAA) which can be converted to gluconeogenic intermediate phosphoenolpyruvate (PEP). During growth on succinate, succinate is converted to malate which can be converted to OAA or pyruvate depending on the $NAD^+/NADP^+$ ratio in the cell (Figure1.1, Liao *et al.*, 1994). Mutations in gluconeogenic enzymes such as PCK have been associated with the inability of some prokaryotes to grow on succinate or malate. *Rhizobium* with mutations in *pckA*, has been shown to be unable to grow on gluconeogenic substrates such as succinate or malate, but able to grow on glucose or glycerol (Osteras *et al.*, 1991). *E. coli* double mutants with mutations in malic enzyme and *pckA* genes are unable to grow on succinate (Goldie and Sanwal, 1980). In some bacteria the gluconeogenic substrate PEP, is used for the phosphorylation of sugar transported into the cell through the phosphotransferase system; hence gluconeogenic enzyme PCK also plays a role in sugar transport, because it produce PEP required to drive sugar transport into the cell.

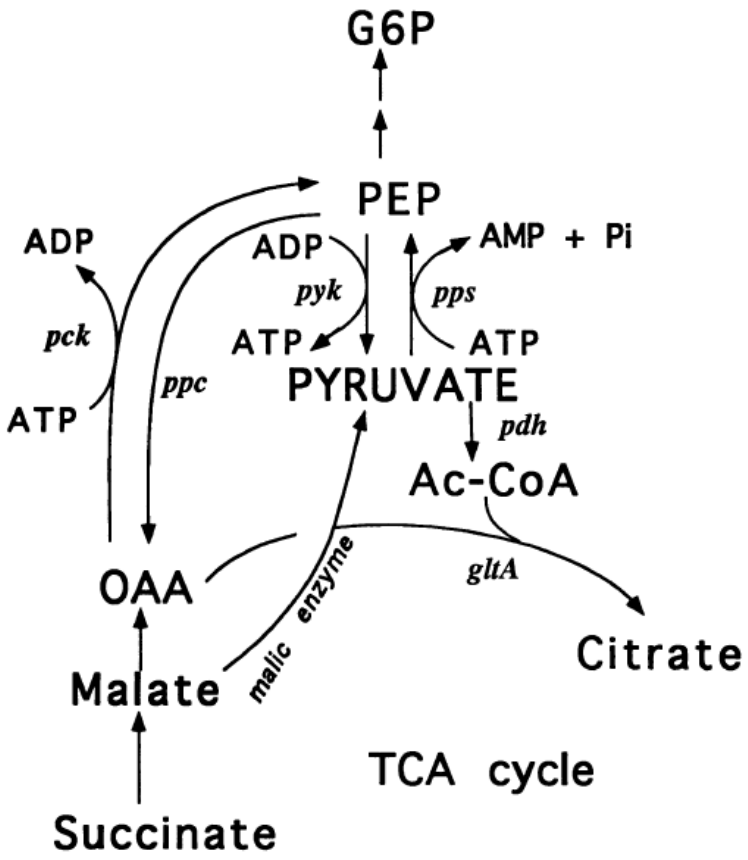

Figure 1.1: Metabolic flux in *E. coli* during growth on succinate. Succinate is converted to malate, which is converted to OAA. OAA is subsequently converted to PEP (phosphoenolpyruvate) by PCK (phosphoenolpyruvate carboxykinase). PEP is eventually converted to glucose-6-phosphate by enzymes involved in gluconeogenesis. Pyk (pyruvate kinase), gltA (citrate synthase) Pdh (pyruvate dehydrogenase) TCA (tricarboxylic acid cycle). (Adapted from Liao *et al.*, 1994).

1.2 Functions of phosphoenolpyruvate carboxykinase

Phosphoenolpyruvate carboxykinase (PCK) catalyzes the reversible conversion of oxaloacetate (OAA) to PEP, and has a strict requirement for a divalent metal cation and a nucleotide triphosphate for catalysis. Based on its specificity for nucleotide triphosphate, the enzyme can be divided into two groups. The ATP-dependent form of the enzyme has the enzyme commission (E.C.) number 4.1.1.49, while the E.C. number for the GTP utilizing enzyme is 4.1.1.32. Enzymes within the same class share 40 – 80% amino acid sequence identity, while no statistically significant sequence homology exist between different groups of PCK; in spite of that, active site residues important for substrate and metal binding are conserved in both PCK

forms and their tertiary structure is easily superimposable (Fig. 1.2), (Aich and Delbaere, 2007, Delbaere *et al.*, 2004).

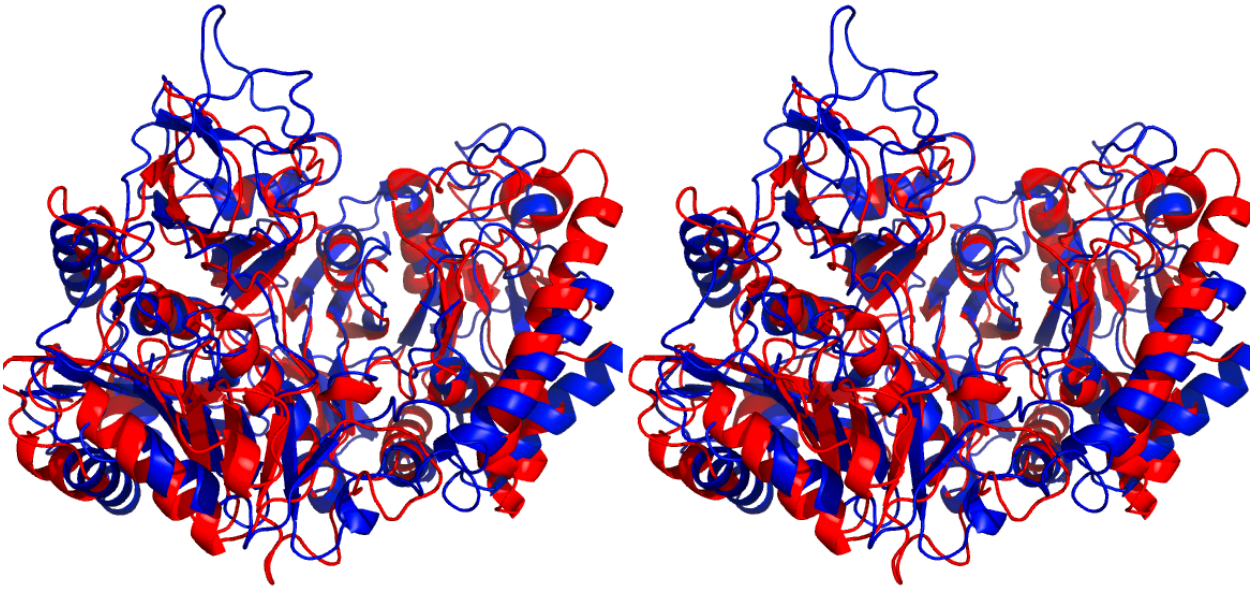

Figure 1.2: Superimposition of ATP dependent *E. coli* PCK (PDB: 1AYL) and GTP dependent Chicken mitochondrial PCK (PDB: 2QZY). Image was made with Pymol using 1AYL and 2QZY PDB. Stereo image was made using Pymol (DeLano 2002).

The reaction catalyzed by PCK is the first committed step of gluconeogenesis, hence the flux of gluconeogenesis can be controlled by regulating PCK expression and activity. *Rhizobium* and *E. coli* with mutations in the *pckA* gene have been shown to be unable to use tricarboxylic acid cycle intermediates as carbon and energy sources, while deletion of the cytosolic PCK gene has been shown to cause hypoglycemia in mice (Chao *et al.*, 1993, Yang *et al.*, 2009). *E. coli* mutants overexpressing PCK have been shown to have increased intracellular concentrations of ATP (Kwon *et al.*, 2008). An altered rate of gluconeogenesis as a result of mutations in *pckA* shows that PCK is an important gluconeogenic enzyme.

In the reverse direction, PCK catalyzes the conversion of PEP, ADP, and CO_2 to OAA and ATP. In *E. coli*, the intracellular concentration of CO_2 is low and the K_m of *E. coli* PCK for CO_2 is high, hence PCK mainly functions to catalyze the forward reaction where PEP is produced.

However, in succinate-producing organisms as such as *Anaerobiosprillum succiniciproducens*, *Actinobacillus succinogens* and *Manheimia succiniciproducens*, PCK functions mainly to catalyze the reverse reaction, which leads to OAA formation (Podkoyrov and Zeikus 1993, Leduc *et al.*, 2005 and Lee *et al.*, 2006).

PCK also plays a role in glyceroneogenesis. In rainbow smelt fish livers, an increase in PCK mRNA levels has been associated with increases in blood glycerol levels during winter periods, while a decrease in PCK mRNA levels has been associated with a reduced rate of glyceroneogenesis in *Drosophila* (Yang *et al.,* 2009). PCK also plays a role in serine biosynthesis and recycling of tricarboxylic acid cycle intermediates back into the tricarboxylic acid cycle for energy production (Yang *et al.*, 2009).

1.3 Distribution of PCK

1.3.1 Species, tissue and cellular distribution

PCK is ubiquitous and has been found in most species. Plants have ATP-dependent PCKs found in the cytosol of most tissues. Plant PCKs are divided into two classes, based on their phosphorylation-dependent kinetic activities. Type one plant PCKs are about 71 to 74 kilodaltons in size. They are phosphorylation-dependent and found in the leaves of some C4 and Crassulacean Acid Metabolism (CAM) plants. Type two plant PCKs are 67 to 70 kilodaltons in size. They are phosphorylation-independent and found in leaves of some C4 plants such as *Urochloa panicodies* (Finnegan *et al.,* 1999). Most microoraganisms such as *Escherichia coli*, *Trypanosoma brucei*, and thermophile *Thermus thermophilius* have ATP-dependent PCKs, however GTP-dependent PCKs are present in *Corynebacterium glutamicum* and hyperthermophlic *Thermococcus kodakaraeusis* (Fukuda *et al.,* 2004, Sugahara *et al.,* 2005 and Medina *et al.*, 1990).

There are two isozymes of GTP-dependent mammalian PCK, cytosolic PCK-C and mitochondrial PCK-M, mainly found in the liver and kidney. Both forms of PCK are used under different metabolic conditions in gluconeogenesis. In mammals, PCK is also present in small intestines, adipose tissues, heart and skeletal muscles (Novakovski 2000). Immunohistochemistry has been used to detect PCK in tissues such as bladder, stomach, vagina, eye, and parotid and submaxillary glands (Zimmer and Magnuson 1990). Using DEAE sephadex column chromatography, chick embryos and very young chicks have been shown to contain four forms of PCK, two in the cytosol and the other two in the mitochondria, (Jo *et al.,* 1974). Chicken and rat PCK have been shown to have 80% amino acid identity, while human, rat and mouse PCK have more than 90% sequence identity (Hanson and Reshef, 1997).

1.3.2 Metabolic significance of PCK distribution

The two isozymes of mammalian PCK function under different metabolic conditions during gluconeogenesis. When pyruvate is the starting molecule for gluconeogenesis, it is first transported to the mitochondria where pyruvate carboxylase converts it to OAA, which is converted to malate by malate dehydrogenase (MDH), with the simultaneous oxidation of $NADH + H^+$ to NAD^+. Malate is transported to the cytosol by the malate/aspartate shuttle, where its conversion to OAA by MDH is accompanied by the reduction of NAD^+ to $NADH + H^+$. Oxaloacetate produced from malate in the cytoplasm is converted to PEP by PCK-C. When lactate is the starting molecule for gluconeogenesis, it is first converted to pyruvate by lactate dehydrogenase (LDH), with the simultaneous reduction of NAD^+ to $NADH + H^+$ in the cytoplasm, and pyruvate is transported to the mitochondria when it is converted to OAA by pyruvate carboxylase. OAA is subsequently converted to PEP by PCK-M, PEP is transported to the cytoplasm where it enters the gluconeogenic pathway (Fig 1.3) (Nelson, 2008).

Mitochondria is the site for oxidative phosphorylation and citric acid cycle, which consume and produce NADH respectively, hence the concentration of NADH in the mitochondria is high, when the flux of oxidative phosphorylation and citric acid cycle are increase. NADH is required for the conversion of malate to OAA in the mitochondria, and since the rate of oxidative phosphorylation and citric acid cycle is reduced under conditions that lead to high lactate concentration, malate cannot be converted to OAA by MDH as a result of low NADH concentration. Hence PCK-M is used to convert OAA to PEP when lactate is the staring molecule for gluconeogenesis (Nelson, 2008).

When the concentration of pyruvate in the cell is high, the rate of oxidative phosphorylation and citric acid are also high, therefore high amount of NADH required for the conversion of OAA to malate is present in the mitochondria. When pyruvate is the starting molecule for gluconeogenesis the concentration of NADH required for the conversion of 1, 3-bisphosphoglycerate to glyceraldehyde-3-phosphate by glyceraldehyde-3-phosphate dehydrogenase in the cytosol is low. Since the mitochondria has higher concentration of NADH under this conversion, malate is transported from the mitochondrial to the cytosol using the malate-aspartate shuttle. Conversion of malate to OAA, is accompanied with the production of NADH, required for gluconeogenesis in the cytosol. OAA present in the cytosol is subsequently converted to PEP by PCK-C (Nelson, 2008). Different isozymes of PCK are used for gluconeogenesis under different metabolic conditions, because the amount of NADH present in cytosol and mitochondria vary under different metabolic conditions.

Under metabolic conditions that lead to increased pyruvate levels in the cell, PCK-C is used for gluconeogenesis, while PCK-M is used when the lactate concentration in the cell is high, hence the PCK-M to PCK-C ratio varies under different metabolic conditions. This ratio

can be used to determine the starting molecule of gluconeogenesis in different species. A significant amount of lactate is produced during flight, hence it is no surprise that avian liver cells have higher amount of PCK-M. On the other hand, rats have higher levels of PCK-C because they mainly use pyruvate as the starting molecule for gluconeogenesis (Hanson and Patel 1994, Wiese *et al.*, 1991).

In unicellular organisms such as *E. coli*, PCK mainly functions to permit growth on other carbon sources, like pyruvate and succinate. In plants, PCK is present in the bundle sheath and mesophyll cells of C4 and CAM photosynthetic plants, where it functions to produce CO_2 for the Calvin cycle through OAA decarboxylation (Dittrich et al., 1973, Leegood and Walker 2003).

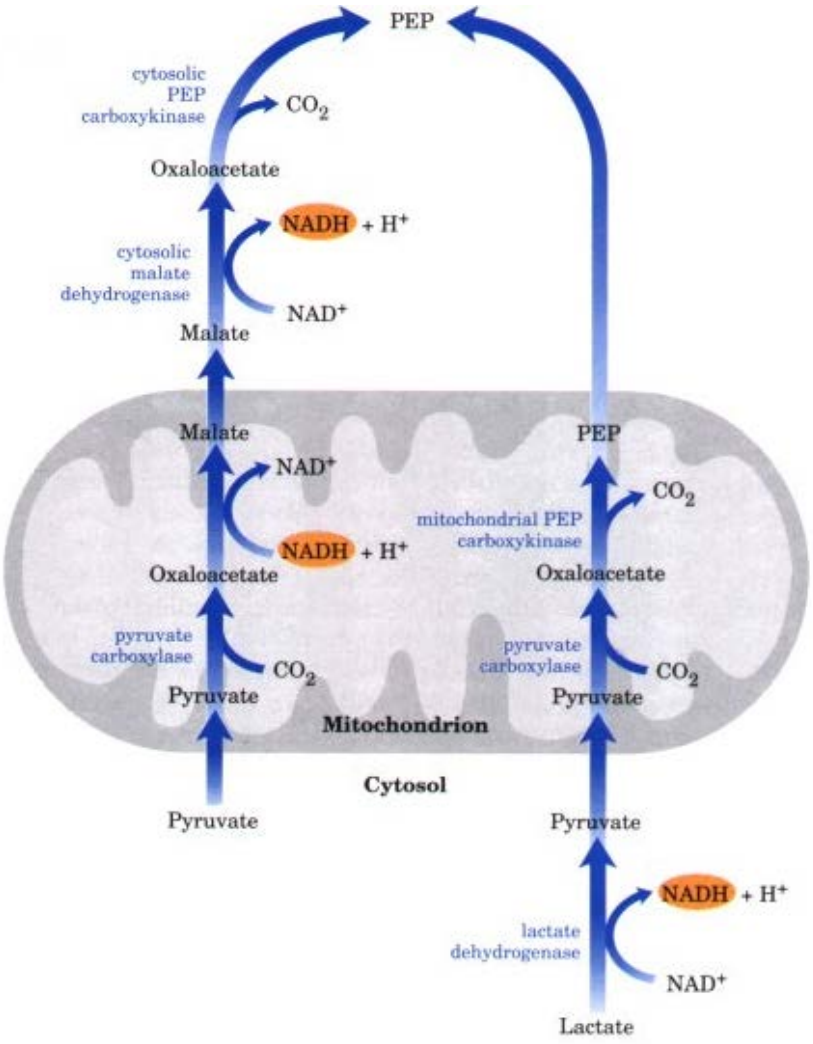

Figure 1.3: Function of cytosolic and mitochondrial PCKS. Mitochondrial PCK is used for OAA production when lactate is the starting molecule for gluconeogenesis, while cytosolic PCK is used when pyruvate is the starting molecule for gluconeogenesis. PCK-C is used when lactate is present because NADH is regenerated when lactate is converted to pyruvate in the cytosol (Adapted from Nelson, 2008).

1.4 Regulation of PCK

1.4.1 Regulation of PCK activity in Eukaryotes

Mammalian PCK expression is regulated by a wide variety of physiological stimuli such as hormones, cellular intermediates, and dietary carbohydrates. Regulation of PCK in mammals occurs primarily at the level of transcription in response to dietary hormonal signals, such as glucagon and insulin (Hanson and Reshef, 1997). During fasting, which leads to high glucagon levels, glucagon acts through cyclic adenosine monophosphate (cAMP) to increase the rate of

PCK translation by stabilizing PCK mRNA. On the other hand, high blood glucose levels lead to increased insulin levels which act to reduce PCK transcription, by blocking transcription from the PCK promoter and decrease PCK translation by reducing the half-life of PCK mRNA (Chakravarty *et al.*, 2005, Christ and Nath 1996). However, regulation of the mammal PCK promoter is more complex than just described, because, as shown in figure 1.4, the promoter region of PCK has more than 15 response elements that can be recognized by many transcription factors, including glucocorticoid and thyroid hormones (Chakravarty and Hanson, 2007; Nelson, 2008).

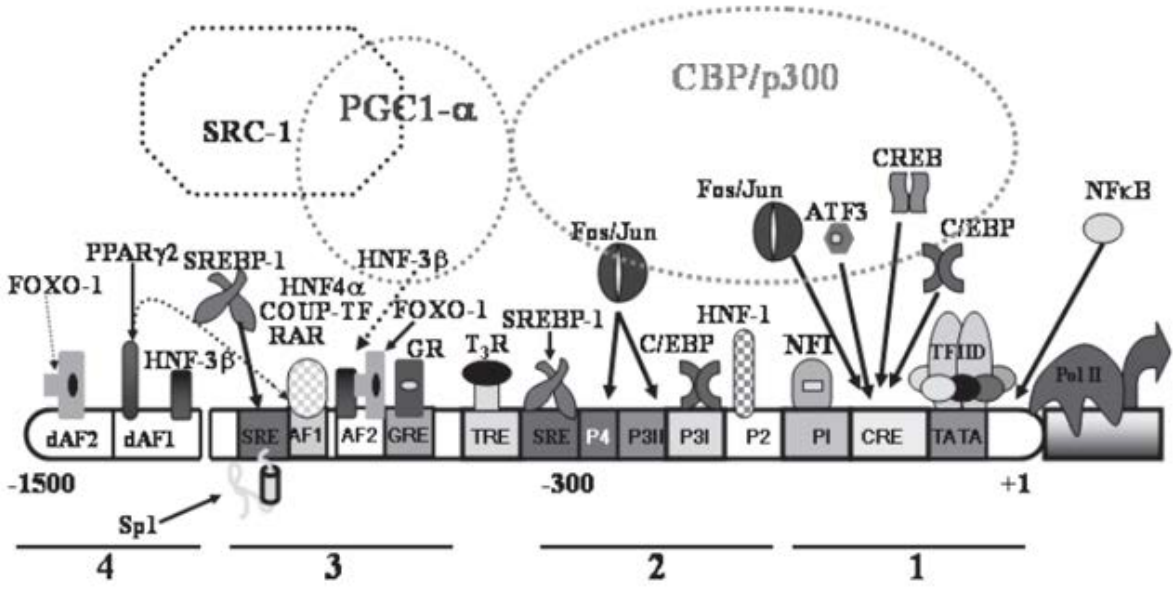

Figure 1.4: Phosphoenolpyruvate carboxykinase C (PCK-C) gene promoter region: Transcription factors such CRE, cAMP bind to specific binding site on the PCK-C promoter. Adapted from Chakravarty and Hanson 2007.

The activity of plant PCK is primarily regulated by phosphorylation and dephosphorylation. Plant PCKs have N-terminal extensions with one or two potential phosphorylation sites. One is a cAMP dependent protein kinase site, while the other has consensus to sites phosphorylated by the SNF-1-related family of protein kinases. The loss of ^{32}P in plant PCK has been attributed to loss of the N-terminal extension (Leegood and Walker 2003).

Phosphorylation of the N-terminal extension leads to PCK inactivation and occurs at night in all C3, CAM, and some C4 plants, while dephosphorylation, which activates the enzyme, occurs during the day (Walker *et al.*, 1997 and Leegood and Walker, 2003).

1.4.2 Regulation of *E. coli* PCK

Phosphoenolpyruvate carboxykinase is involved in gluconeogenesis, hence it is no surprise that its expression is regulated by catabolite repression, where the presence of glucose represses *pckA* expression in *E. coli*. When *lacZ* was fused to *pckA* promoter and expressed in *E. coli*, it was observed that β-galactosidase synthesis was induced during stationary growth phase, and addition of glucose to the growth medium caused a reduction in β-galactosidase levels, hence *pckA* is induced during stationary growth phase and regulated by catabolite repression (Goldie, 1984). Like most gluconeogenic enzymes, *pckA* is activated by cAMP and cAMP receptor protein (CRP), also known as catabolite activator protein in the absence of glucose (Saier, 1996). Analysis of *pckA*, showed that it has two CRP binding sites, one upstream and the other downstream of the transcription start site. Binding of cAMP-CRP to the upstream site has been associated with transcription activation (Nakano *et al.*, 2014).

1.5 *Escherichia coli* phosphoenolpyruvate carboxykinase

1.5.1 Reaction type of *E. coli* PCK

E. coli PCK catalyzes the reversible conversion of OAA and ATP to PEP, ADP, and CO_2. The high K_m of bicarbonate (13 mM) required by the enzyme indicates that *E. coli* PCK mainly functions to produce PEP in *vivo*. Kinetic studies of *E. coli* PCK performed by Krebs in 1980 showed that the reaction catalyzed by the enzyme occurs by a sequential random mechanism, where OAA or ATP can be the first substrate that binds to the enzyme. No phosphoenzyme intermediate was detected when the enzyme was incubated with radioactively labelled ATP and ADP, and the requirement of ATP for OAA – $^{14}CO_2$ exchange to occur, were used to rule out the

possibility of a ping pong mechanism. The almost identical rate of exchange between OAA and $^{14}CO_2$, and between ATP and ADP was used to conclude that the reaction occurs by a random sequential mechanism (Krebs and Bridger, 1980). A sequential random mechanism has also been shown for PCK from *S. cerevisiae* and rat liver PCK-C (Jabalquinto and Cardemil, 1993). The inability of analogues of ATP such as α, β-CH_2-ATP and β, γ-CH_2-ATP to catalyze the reaction shows that the enzyme is specific for ATP, while the inability of OAA analogues such as L-lactate and DL, β-chlorolactate to act as substrates for avian liver PCK shows that the enzyme is very specific for OAA (Ash *et al.*, 1990).

1.5.2 Structural changes cause by substrate binding to *E. coli* PCK

The tertiary structure of *E. coli* PCK is made up of α-helices and β-sheets with a barrel-like fold. It is made up of two domains, an N-terminal domain which includes residues 1 – 216 & 283 – 341, and a C-terminal domain which includes residues 217 – 282 & 342 – 540. The active site of *E. coli* PCK is in a deep cleft between both domains and substrate binding causes them to move towards each other by approximately 20° in a hinge-like fashion. A similar degree of domain movement have been observed in *A. succiniciproducens* ATP-dependent PCK (Cotelesage *et al.*, 2005). Like most kinases, *E. coli* PCK possesses a kinase la (GX_4GKTT) and kinase 2a (X_4D) loop essential for triphosphate and divalent metal ion binding, respectively. The structure of *E. coli* PCK with and without substrates have been solved using x-ray crystallography, and comparison of the native structure with the substrate bound structures has shown that six regions of the enzyme interact with Mg^{2+}-ATP through electrostatic, van der Waals interactions and hydrogen bond formation, and some of these interactions causes domain movements which lead to active site closure (Tari *et al.*, 1997).

The first region includes His232, which interacts directly with the γ-phosphate of ATP in the Mg^{2+}-ATP oxalate structure, but interacts indirectly with the γ- phosphate of ATP by interacting with Ca^{2+} or Mn^{2+} in structures containing Ca^{2+} or Mn^{2+} (Tari *et al.*, 1996, Sudom *et al*, 2003). The kinase la loop made up of $G_{248}LSGTGKT_{255}$ (Fig 1.5) forms part of the second region that interacts with the phosphate groups of ATP and Mg^{2+}. Comparison of the native structure and Mg^{2+}-ATP oxalate structure shows that Gly248 and Gly253 undergo conformational changes upon Mg^{2+}-ATP binding that allow them to adopt conformations that would be considered Ramachandran unfavorable for other amino acids. This change in conformation enables the kinase 1a loop to contract slightly and wrap tightly around Mg^{2+}ATP.

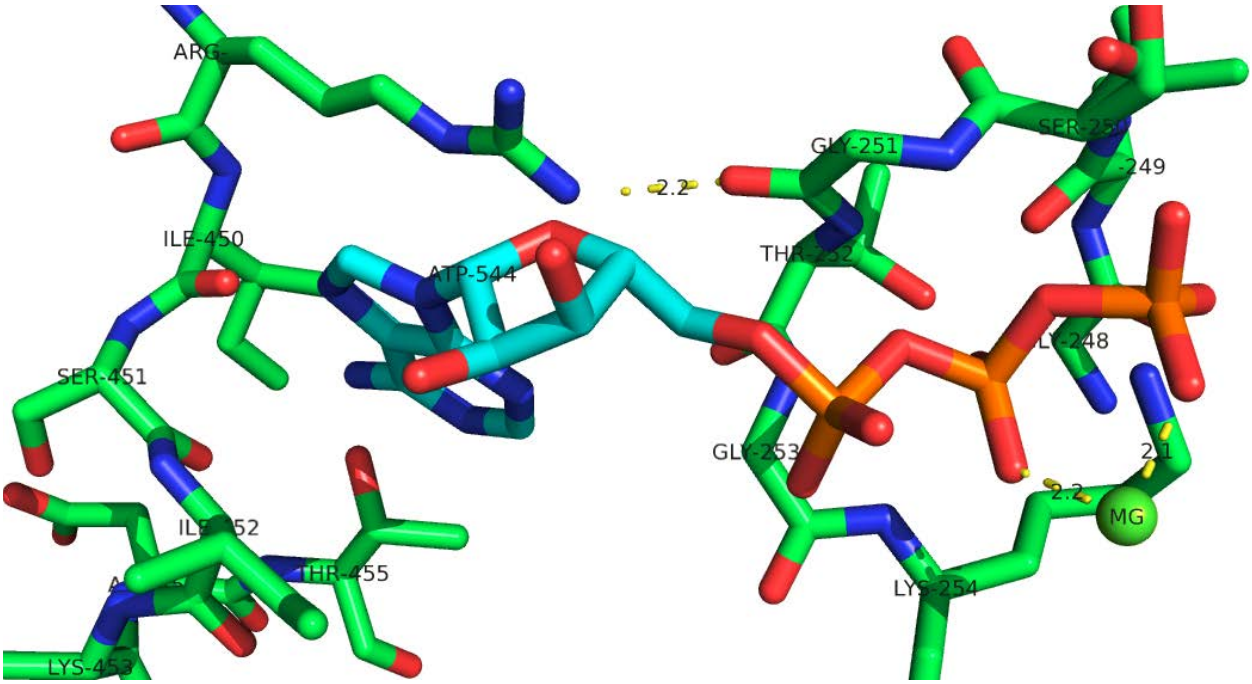

Figure 1.5: Kinase 1a loop and adenine binding region of *E. coli* PCK: Kinase 1a loop is made up of Gly248, Leu249, Ser250, Gly251, Thr252, Gly253, Lys254 and Thr255, interacts with the triphosphate groups of ATP, while Arg449, Ile450, Ser451, Ile452, Lys453, Asp454 and Thr455 make up the adenine binding region, that interacts with the adenine base and ribose sugar of ATP. The adenine binding region is connected to the kinase 1a-loop through Arg449 which is H-bonded to Gly251. Image was made with Pymol (DeLano, 2002) using 1AYL PDB.

The third region of the enzyme, which interacts with Mg^{2+}-ATP, is the Kinase 2 motif, made up of residues $L_{265}IGDD_{269}$ (Fig 1.6) which are involved in metal ion coordination and substrate positioning. Asp268 and Asp269 interact with Mg^{2+} indirectly through two water molecules. In structures containing Mn^{2+} or Ca^{2+}, Asp269 interacts directly with Mn^{2+} or Ca^{2+}. The importance of this motif in substrate positioning was observed when point mutation that changed Asp268 to Asn eliminated the ability of *E. coli* PCK to phosphorylate the reaction intermediate, *enol*-pyruvate (Hou *et al.,* 1995). Residues between Lys288 and Gln297 make up part of the fourth region, that is involved in direct and water mediated interactions with the ribose sugar of ATP, while the fifth region is made up of Arg333 and Ca^{2+} or Mn^{2+}, which connects Mg^{2+}-ATP and OAA (Tari *et al.,* 1996).

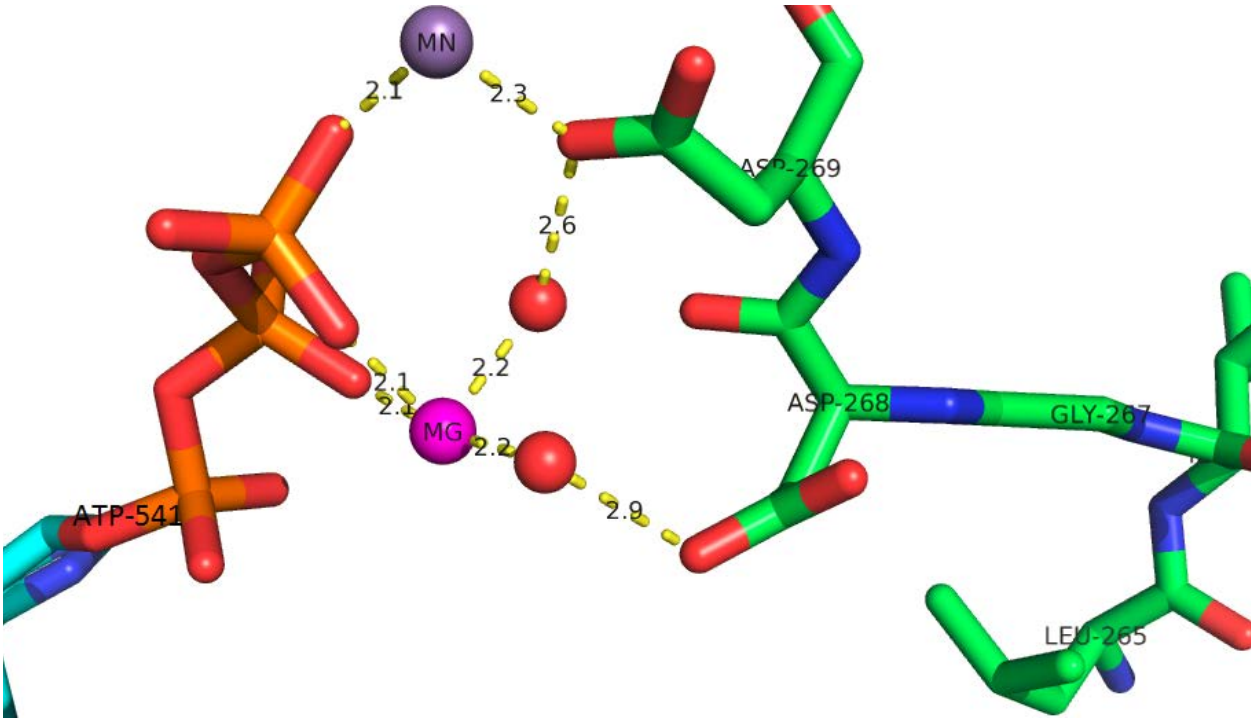

Figure 1.6: Kinase 2a loop: Leu 265 Ile 266 Gly 267 Asp268, and Asp269, make up the kinase 2a loop that coordinate Mg^{2+} in Mg^{2+}-ATP complex bound to *E. coli* PCK. Asp269 is also coordinating Mn^{2+}. Distances are shown in Angstroms. Image was made with Pymol (DeLano, 2002), using PDB: 1AQ2.

The sixth region is made up of residues R_{449}ISIKDT_{455} (Fig 1.5), which interact with the adenine base and the ribose sugar of ATP. Hence, this region is called the adenine/ribose binding region. In *E. coli* PCK, ATP adopts a conformation that puts the adenine base over the ribose sugar, and this sterically strained conformation of ATP is probably similar to the transition state conformation of ATP (Tari *et al.*, 1996). Hence, the enzyme probably reduces the free energy of the transition state by making ATP adopt an energetically unfavourable conformation.

Upon ATP binding, the loop region made up of residues between G_{442} – G_{447} undergoes conformation changes that cause residues between R_{449} – T_{455} to move towards the interior of the active site where they interact with the adenine base (Fig 1.7). This interaction is further stabilized through hydrogen bond interaction between the NH_2 group of Arg449 and the carbonyl oxygen of Gly251, which is part of the kinase 1a loop (Fig 1.5). Changes in the backbone torsion angles of Glycine 442, 445, and 447, are essential for the interaction of residues R_{449} – T_{455} with the adenine base of ATP, upon ATP binding (Fig 1.7), and these Gly residues are conserved in both forms of PCK.

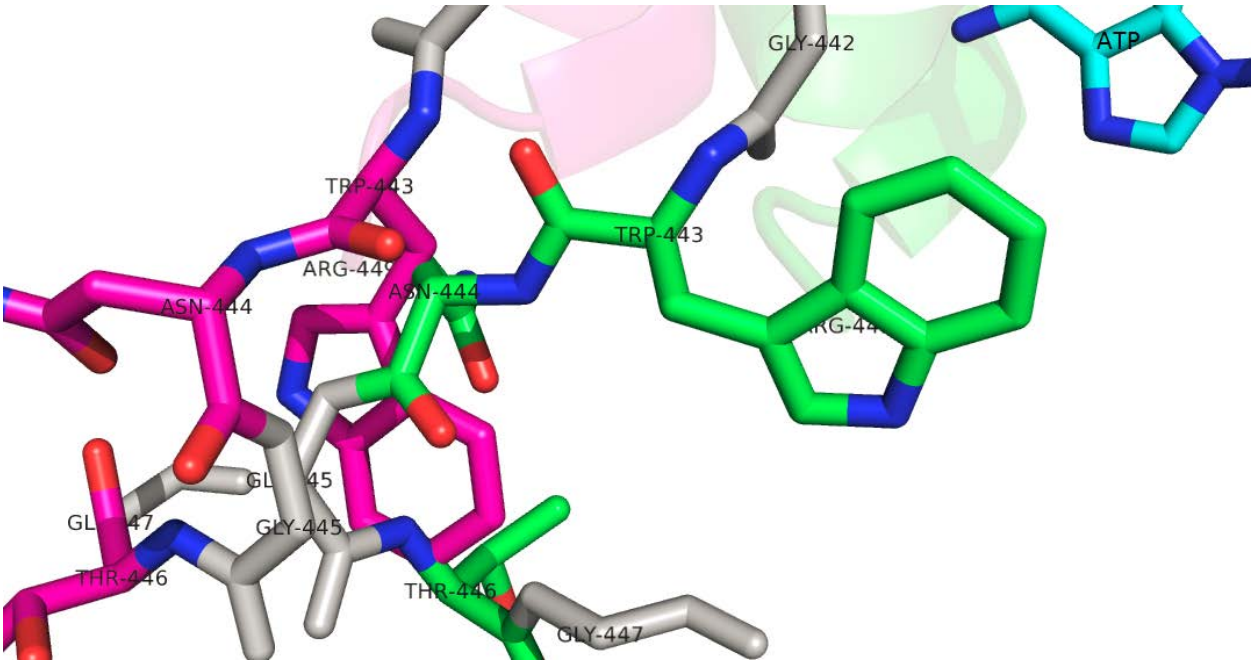

Figure 1.7: Alignment of native *E. coli* structure (1OEN PDB) with *E. coli* PCK-Mg^{2+}-ATP-Mn^{2+}-pyruvate structure (1AQ2 PDB). Changes in the torsion angles of Gly 442, Gly 445 and Gly 447 upon ATP binding cause conformation changes in residues G_{442} – G_{447} which cause the adenine/ribose base binding region (R_{449} – T_{455}) to move close to ATP and interact with adenine base ribose sugar of ATP bound to *E.coli* PCK. Image was made with Pymol (DeLano 2002).

Active site closure is said to be caused by small changes in the polypeptide backbone torsion angles of residues 260 – 272, 208 – 234, and 340 – 356, regions that connect the N and C-terminal domains (Tair *et al.*, 1996). Structural analysis of *E. coli* PCK shows that these residues are arranged in the following order: residues G_{442} – G_{447} are followed by the adenine/ribose binding region (R_{449} – T_{455}), which is followed by the kinase 1a loop; residues 260 – 272, 208 – 234, and 340 – 356 follow the kinase la loop, respectively. This indicates that conformational changes that occur in the region between G_{442} – G_{447} upon ATP binding are probably transferred to the kinase 1a loop through hydrogen bond formation between Arg449 and Gly251, and changes in kinase 1a loop which enabled it to interact with the phosphate group of ATP is subsequently transferred to the other regions which lead to active site closure.

Analysis of the OAA bound *E. coli* PCK structure shows that OAA is bound at a site about 5Å away from the active site, and it has been hypothesized that ATP binding probably moves OAA towards the active site (Cotelesage, 2007). Comparison of *E. coli* PCK structures where oxalate or pyruvate are used as OAA analogues to the native structure have shown that residues involved in OAA binding are in similar positions in both structures. This therefore indicates that OAA binding does not induce structural changes in *E. coli* PCK, and supports a sequential ordered mechanism of catalysis by *E. coli* PCK instead of a sequential random mechanism obtained through kinetic analysis. Hence structural analysis indicates that OAA binds before Mg^{2+}-ATP, which induces active site closure in *E. coli* PCK. Closure of the active site is important for catalysis, because it traps substrates, prevents the escape of reaction intermediates, excludes solvent from the active site, and positions catalytically important active site residues in the right orientations to facilitate catalysis by *E. coli* PCK (Sudom *et al.*, 2003, Tari *et al.*, 1996).

1.5.3 Binding of divalent metal cations to *E. coli* PCK

In vitro E. coli PCK requires millimolar concentrations of Mg^{2+} in the form of Mg^{2+}ATP for catalysis. However, for optimal catalysis, it also requires micromolar concentrations of Mn^{2+} or Ca^{2+}, hence synergistic catalysis by *E. coli* PCK occurs in the presence of Mg^{2+}-ATP and Ca^{2+} or Mn^{2+} (Goldie and Sanwal, 1980). Structural analyses have shown that Mg^{2+}, $Mn^{2+}$and Ca^{2+} preferentially bind to two sites in *E. coli* PCK. Mg^{2+} forms a metal nucleotide complex with ATP (Mg^{2+}-ATP), while Ca^{2+} and Mn^{2+} bind at a site between Mg^{2+}ATP and OAA, hence this site is called the bridging site. Mg^{2+} is bound at a site, 5.2 Å and 5.4 Å away from Mn^{2+} and Ca^{2+} binding site, respectively. One γ-phosphate oxygen of ATP and the side chain of Asp269 act as bridging ligands between Mg^{2+} and Ca^{2+} or Mn^{2+} ions in *E. coli* PCK.

In *E. coli* PCK, Mg^{2+} is coordinated by one β and γ-phosphoryl oxygens of ATP, Oγ of Thr255 and three ordered water molecules (Fig 1.8). The carboxylate groups of Asp268 and 269 form hydrogen bonds with two of the water molecules involved in Mg^{2+} coordination, and this is important to hold the phosphate groups of ATP in the right position that facilitates catalysis (Tari *et al.*, 1997). *E. coli* PCK Asp268Asn mutant PCK catalyzes the conversion of OAA to pyruvate instead of PEP, because it is unable to phosphate the reaction intermediate (Hou *et al.*, 1995, Novakovski 2000).

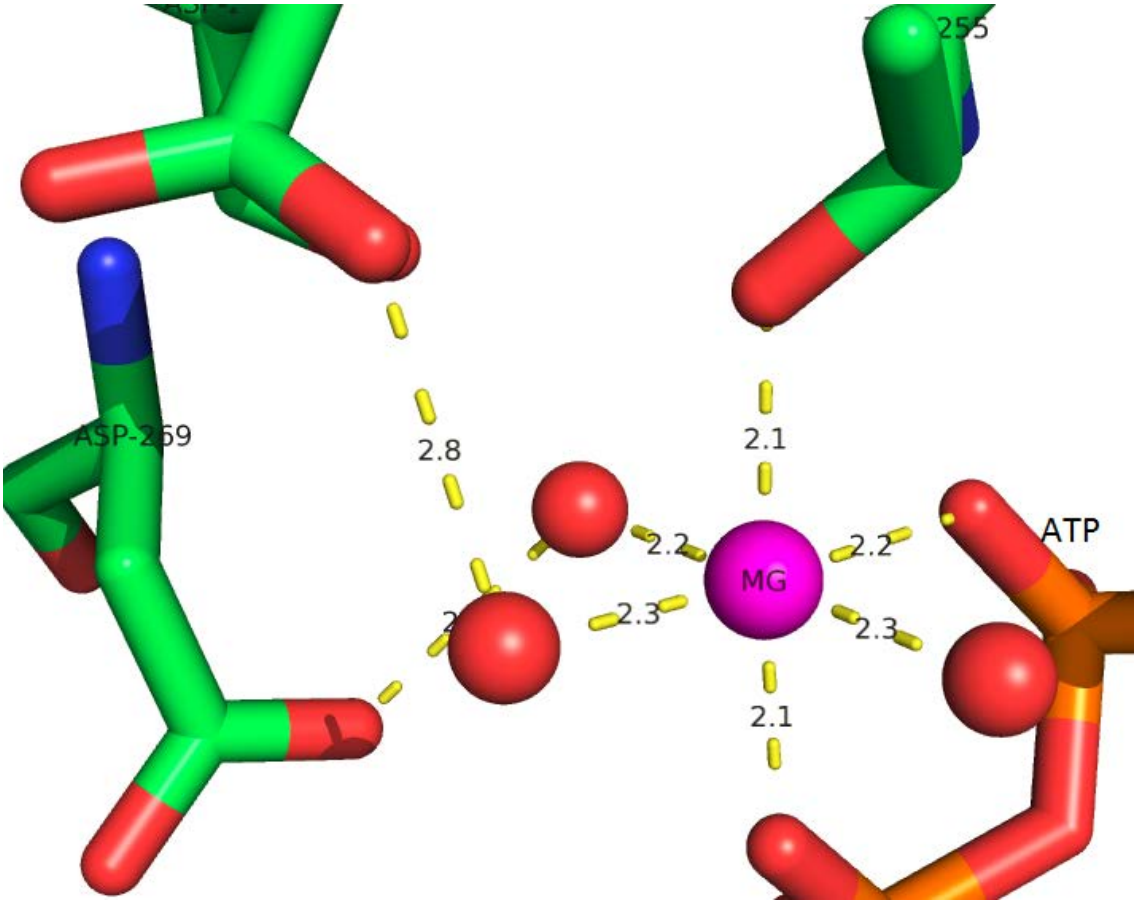

Figure 1.8: Mg^{2+}coordination. Mg^{2+} is coordinated by three water molecules, Thr255, β and γ-phosphate of ATP. Asp268 and Asp269 are indirectly coordinating Mg^{2+} through two molecules. Distances are in Angstroms. Image was made with Pymol (DeLano, 2002) using PDB: 1AYL.

Mn^{2+} is coordinated by six ligands that form a slightly distorted octahedron around it. It is coordinated by two water molecules, one γ-phosphate oxygen of ATP, one oxygen from the side chain of Asp269, Nζ of Lys213, and the Nε2 of His232 (Fig 1.9). Ca^{2+} is coordinated by seven ligands: one of the oxygen atoms of pyruvate, two side chain oxygen atoms of Asp269, one γ-phosphate oxygen of ATP, Nζ of Lys213, Nε2 of His232 and one water molecule (Fig 1.10). Comparison of Ca^{2+} and Mn^{2+} bound *E. coli* PCK structures shows that, Ca^{2+} and Mn^{2+} bind at the bridging site in *E. coli* PCK; however, their coordination slightly differs. Ca^{2+} is coordinated by seven ligands, while Mn^{2+} is coordinated by six ligands. One water molecule, two side chain oxygen's of Asp269, and one carboxyl oxygen of pyruvate directly coordinate Ca^{2+}, while Mn^{2+} is coordinated by one Asp269 oxygen, and two water molecules which directly coordinate pyruvate. The orientation of pyruvate and the distance between the carbonyl oxygen of pyruvate and γ-phosphate of ATP also differs in both structures (Tari *et al.*, 1997; Sudom *et al.*, 2003).

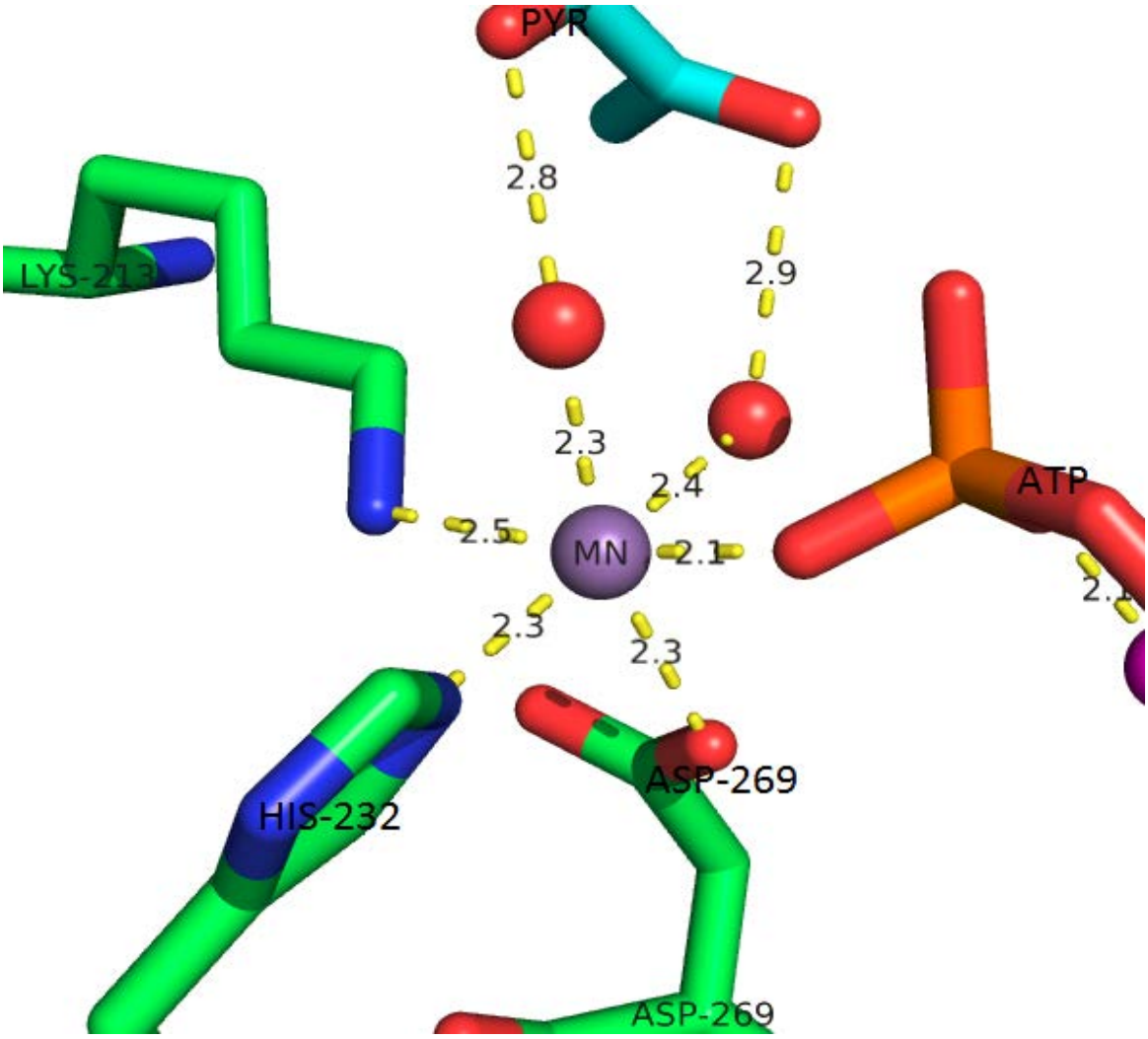

Figure 1.9: Mn^{2+}coordination. Mn^{2+} is coordinated by two water molecules, Nζ of Lys213, the $N^{\varepsilon 2}$ of His232, one oxygen from the side chain of Asp269 and one γ-phosphate oxygen. Distances are in Angstroms. Image was made with Pymol (DeLano, 2002) using PDB: 1AQ2.

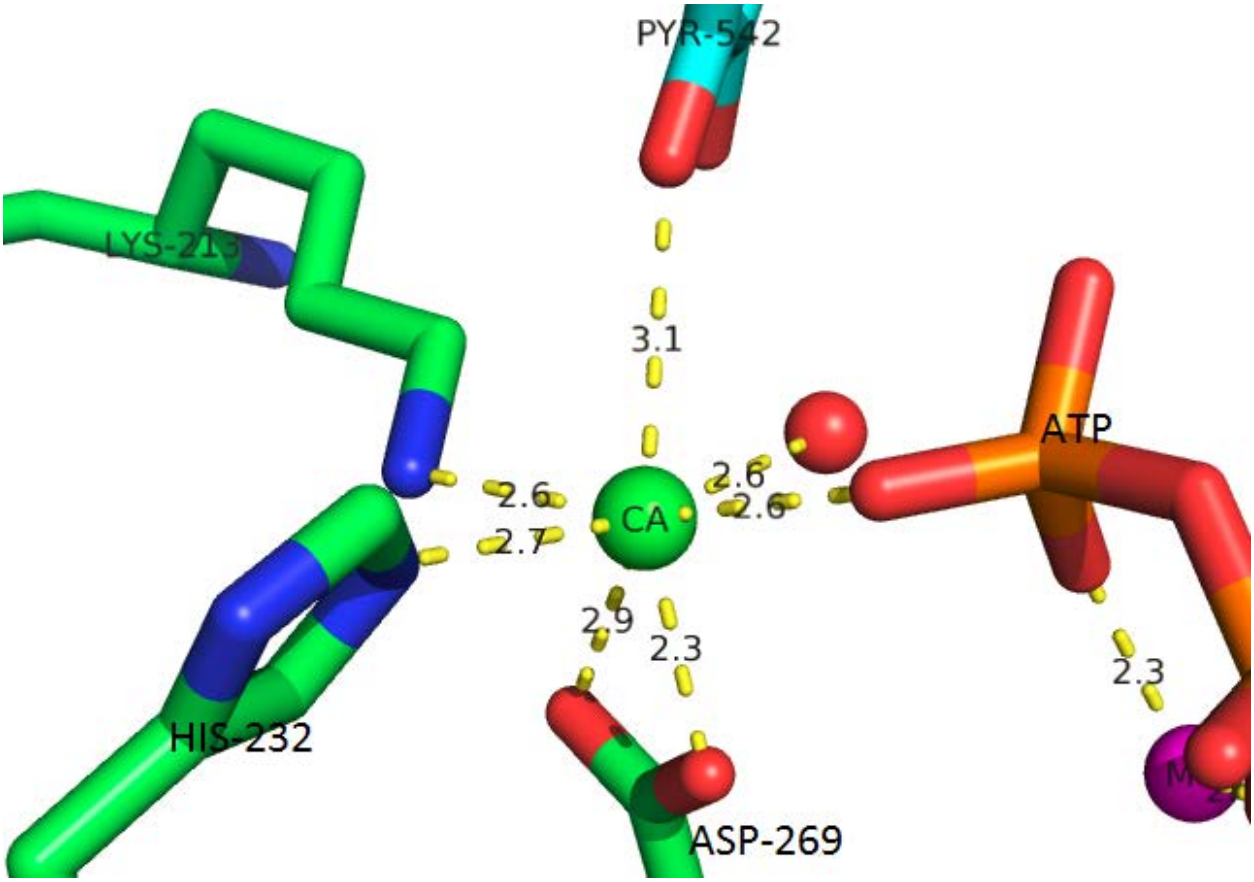

Figure 1.10: Ca^{2+}coordination. Ca^{2+} is coordinated by two water molecules, Nζ of Lys213, the $N^{\varepsilon 2}$ of His232, two oxygen from the side chain of Asp269 and one γ-phosphate oxygen. Distances Angstroms. Image was made with Pymol (DeLano 2002) using PDB: 1OS1.

The specificity of Mg^{2+} and Mn^{2+} or Ca^{2+} for distinct regions of the active site is probably due to their different ionic radius and their preference of oxygen or nitrogen as coordinating ligands. Mg^{2+} is a hard Lewis acid with an ionic radius of 0.65 Å. It strongly favors coordination by hard Lewis bases such as oxygen and has low affinity for sites where nitrogen acts as a coordinating ligand, hence it has reduced affinity for the bridging site where nitrogen atoms are used for metal coordination (Tari *et al.,* 1997). Ca^{2+} favors coordination by oxygen over nitrogen; however, it has an ionic radius of 0.99 Å and is too large to fit into the 1.4 Å sphere created by the all oxygen coordinating ligands at the Mg^{2+} binding site. Therefore, it binds only at the bridging site where it is coordinated by oxygen and nitrogen atoms. Ca^{2+} is usually not coordinated by two nitrogen atoms, however coordination of Ca^{2+} by nitrogen has also been

observed in nitrolotriacetic acid and aminocarboxylate EDTA (Barnett and Uchtman, 1979, Sudom *et al.,* 2003). Mn^{2+}, with an ionic radius of 0.8Å, has higher affinity for nitrogen coordinating environment, hence it is no surprise that Mn^{2+} binds to the bridging site in *E. coli* PCK (Tari *et al.,* 1997).

1.5.3.1 Effects of metal cations on catalysis by *E. coli* PCK

Magnesium binds to nucleotide triphosphate molecules with higher affinity and puts them in the proper orientation for catalysis, and it has a reduced tendency to form reactive hydroxo complexes at physiological pH, hence Mg^{2+} is a better metal for complex formation with ATP, compared to Mn^{2+} or Ca^{2+} (Tari *et al.*, 1996). However, Ca^{2+} and Mn^{2+} are more efficient at water exchange compared to Mg^{2+}, hence are better suited to bind at the bridging site in *E. coli* PCK (Sudom *et al.*, 2003, Tari *et al.*, 1997). In *E. coli* PCK, the interaction between Mg^{2+}, Lys254, and the β & γ-phosphate oxygen's of ATP leads to P-O bond polarization, and increases the susceptibility of the γ-phosphate of ATP to nucleophilic attack. This interaction also causes the β & γ-phosphate oxygen's of ATP to adopt an eclipse conformation, which is essential for an S_N2 mechanism of phosphoryl transfer (Tari *et al.*, 1997). *E. coli* PCK uses residues between Arg449 – Thr455 to promote a sterically strained conformation of the adenine base and ribose sugar of ATP. However, it requires Mg^{2+} to promote a sterically strained conformation of the triphosphate group of ATP, hence the strict Mg^{2+} requirement of the enzyme. One of the way enzymes reduce the transition state energy of a reaction is through bond strain, where the enzymes cause structural rearrangement that strains the substrate bonds to adopt a conformation that is closer to the substrate conformation during the transition state. The energetically unfavourable conformation of ATP in *E. coli* PCK is probably similar to the conformation of ATP during the transition state of the reaction; therefore, Mg^{2+} is required by *E. coli* PCK to reduce the free energy of the reaction through bond strain.

The presence of a second metal binding site in *E. coli* PCK is important for increasing, the reactivity of the reaction intermediate *enol*-pyruvate and the susceptibility of the γ-phosphate of ATP for nucleophilic attack (Sudom *et al.,* 2003, Tari *et al.,* 1997). The interaction between Ca^{2+} or Mn^{2+} and one of the γ-phosphate oxygen's of ATP further increases the susceptibility of the γ-phosphate for nucleophilic attack, and also function to properly orient and bring Mg^{2+}-ATP and OAA in close proximity to each other for catalysis (Tari *et al.,* 1997 and Delbaere *et al.,* 2004). Therefore the rate of catalysis is expected to be increased (high k_{cat}) in the presence of Mg^{2+}-ATP and Ca^{2+} or Mn^{2+}. However, since Ca^{2+} is directly interacting with both substrates, the rate of catalysis with Ca^{2+} is expected to be higher than the rate of catalysis with Mn^{2+}.

1.5.4 How mutations of active site residues affect metal and substrate coordination in *E. coli* PCK

E. coli PCK has been intensely studied kinetically and structurally by Goldie, and the importance of a number of active site residues like Arg65, Asp268, Asp269, His213 Lys212, Lys213 and Lys254 have been investigated. Structural analysis has shown that Lys213, His232, and Asp269 are involved in coordinating Ca^{2+} or Mn^{2+} in *E. coli* PCK. Similar residues (Lys263, His283, Asp220, and Cys307) have also been implicated in Mn^{2+} coordination in GTP-dependent PCK found in humans (Holyoak *et al.,* 2006). Metal coordination by aspartate and histidine residues are not unusual because aspartate is negatively charged while histidine has a pK_a close to neutral. Metal coordination by positively charged lysine is unusual; however, in the active site of *E. coli* PCK Lys213 is close to Lys212 and Phe413, which function to lower the pK_a of Lys213 (Sudom *et al.,* 2003). The importance of phenylalanine in reducing the pK_a of lysine has been demonstrated in *S. cerevisiae* PCK, where Phe216Tyr mutation increased the pK_a of Lys213 from 6.5 to 9.3 and reduced the affinity of the enzyme for Mn^{2+} (Yevenes *et al.,* 2007). Lys212Ser mutation increased the K_m of *E. coli* PCK for Mn^{2+} by 33-fold, and reduced k_{cat} of the

reaction by 40-fold. Hence, Lys212 and Phe413 are required for metal coordination by Lys213. Lys213Ser mutation reduced k_{cat} 5-fold, decreased the K_m for Mg^{2+}-ATP 4-fold and had no significant effect on the K_m for OAA. However, catalysis by this mutant is inhibited in the presence of Mn^{2+}. Crystal structures of the Lys213Ser *E. coli* PCK mutant have shown that Mn^{2+} is coordinated by four instead of six ligands in this mutant. Altered OAA binding and reduced OAA reactivity as a result of the tetrahedral coordination of Mn^{2+} in the Lys213Ser mutant has been attributed to the inhibition of catalysis in the presence of Mn^{2+} displayed by this mutant (Cotelesage, 2007), hence Lys213 is important for metal coordination in *E. coli* PCK. Calcium or manganese bound to the bridging site of *E. coli* PCK can also function to reduce the pK_a of Lys213.

Structural analysis has shown that Asp269 directly coordinates Mn^{2+} and Ca^{2+}, but indirectly coordinates Mg^{2+} in *E. coli* PCK. Mutation of Asp269 to Asn increased the K_m of *E. coli* PCK for Mn^{2+} about 1,000-fold, but had little effect on the K_m for Mg^{2+}-ATP. His232Gln mutation increased the K_m of the enzyme for Mn^{2+} about 7,000-fold and decreased k_{cat} about 14-fold. The huge effects of mutations to Lys213, Asp269, and His232 have on the K_m of *E.coli* PCK for Mn^{2+} shows that these residues are important for the coordination of metals that bind to the bridging site of *E. coli* PCK. Although Cys307 is important for metal coordination and catalysis by GTP-dependent chicken liver PCK (Holyoak *et al.,* 2006), the equivalent residue Cy233 in *E. coli* PCK is not required for metal coordination and catalysis, since no significant change in K_m or k_{cat} was displayed by Cys233Ser *E. coli* PCK mutant. Hence modification of active site cysteine residues inactivates GTP dependent PCK, but has no effect on *E. coli* ATP dependent PCK (Holyoak *et al.,* 2006, Bazaes *et al.,* 1993).

Analysis of the *E. coli* PCK structures have shown that Arg65 is important for OAA binding, and Arg65Gln mutation increased the K_m of the enzyme for OAA about 200-fold (Novakovski, 2000). Lys254 is one of the conserved residues of Kinase 1a motif, and functions together with Mg^{2+} to maintain the energetically unfavourable conformation of the β and γ-phosphate group of ATP. Mutation of Lys254 to Ser reduced k_{cat} 17-fold and increased K_m of the enzyme for Mg^{2+}-ATP about 70-fold (Novakovski, 2000), indicating that Lys254 is required for Mg^{2+}-ATP binding to *E. coli* PCK. Crystal structures of Arg65Gln, Asp269Asn, and Lys254Ser were solved during the course of this project and are described in the results and discussion segment of this report.

Table 1.1: Kinetic results of mutational studies on *E. coli* PCK. Obtained from Novakovski 2000.

Mutant	K_m				k_{cat} min $^{-1}$
	OAA (mM)		Mg^{2+} ATP	Mn^{2+}	
	with Mn^{2+}	without Mn^{2+}	mM	μM	
R65Q	159* ± 34	156*	<0.01	<0.01	14.8 ±2.0
K212S	1.24 ± 0.44	1.05 ±0.23	0.010±0.003	1.0 ±0.03	0.67 ±0.02
K213S	0.26 ±0.09	0.55 ±0.04	0.06 ±0.02	Inhibition	5.20 ±0.17
H232Q	23.7 ±5.9 [a]	66.2 ±0.9 [b]	0.08 ±0.01 [a]	222 ±16	1.84 ±0.06 [a]
C233S	1.31 ±0.33	0.32 ±0.04	0.20 ±0.05	0.09 ±0.02	18.9 ±1.8
K254S	1.78 ±0.39 [b]	6.72 ±1.65 [b]	18.0 ±2.0	0.09 ± 0.02 [b]	1.54 ±0.06 [b]
D269N	n.e.	122 ±15 [a]	0.42 ±0.02 [a]	32.1 ±3.7	1.69 ±0.08 [a]
Wild Type	0.77 ±0.17	0.51 ±0.10	0.26 ±0.07	0.03 ±0.01	26.5 ±1.2

*Value was extrapolated
n.e. – could not be evaluated (OAA was inhibitory at high concentrations)
[a] - values determined at less than saturating concentrations of Mn^{2+}
[b] - Values determined at less than saturating concentrations of Mg^{2+} ATP
Errors are standard errors of the mean

1.6 Mechanism of *E. coli* PCK catalysis derived from crystal structures

Decarboxylation of OAA and phosphoryl transfer from ATP or GTP to the reaction intermediate, are the two steps necessary for the conversion of OAA to PEP (Matte *et al.*, 1997). The crystal structures of *E. coli* PCK with Mg^{2+}-ATP and oxalate, Mg^{2+}-ATP-pyruvate-Mn^{2+} or Ca^{2+} have been solved and analysis of these structures has led to the proposed mechanism of *E. coli* PCK catalysis in the presence of Mg^{2+}ATP and OAA, Mg^{2+}-ATP, OAA and Mn^{2+} and Mg^{2+}-ATP, OAA and Ca^{2+}. Crystals where made with ATP, Mg^{2+}, Mn^{2+} or Ca^{2+} and pyruvate or oxalate instead of OAA to prevent ADP and PEP formation, since *enol*-pyruvate is the reaction intermediate, in some cases interaction between the enzyme and the reaction intermediate is analyzed.

1.6.1 Mechanism of PCK catalysis derived from crystal structures with *E. coli* PCK-oxalate-ATP and Mg^{2+}

The mechanism of catalysis by *E. coli* PCK in the presence of Mg^{2+}-ATP and OAA was derived from analysis of *E.coli* PCK Mg^{2+}-ATP-oxalate structure (PDB: 1AYL). Analysis of this structure shows that Arg333 is directly interacting with Mg^{2+}-ATP and oxalate. One of the carboxyl oxygen's of oxalate is 4.7 Å away from the γ-phosphate of ATP, at an almost linear angle of 159° (Fig. 1.11), indicating an S_N2 associative mechanism of phosphoryl transfer where bond breaking and formation occur simultaneously.

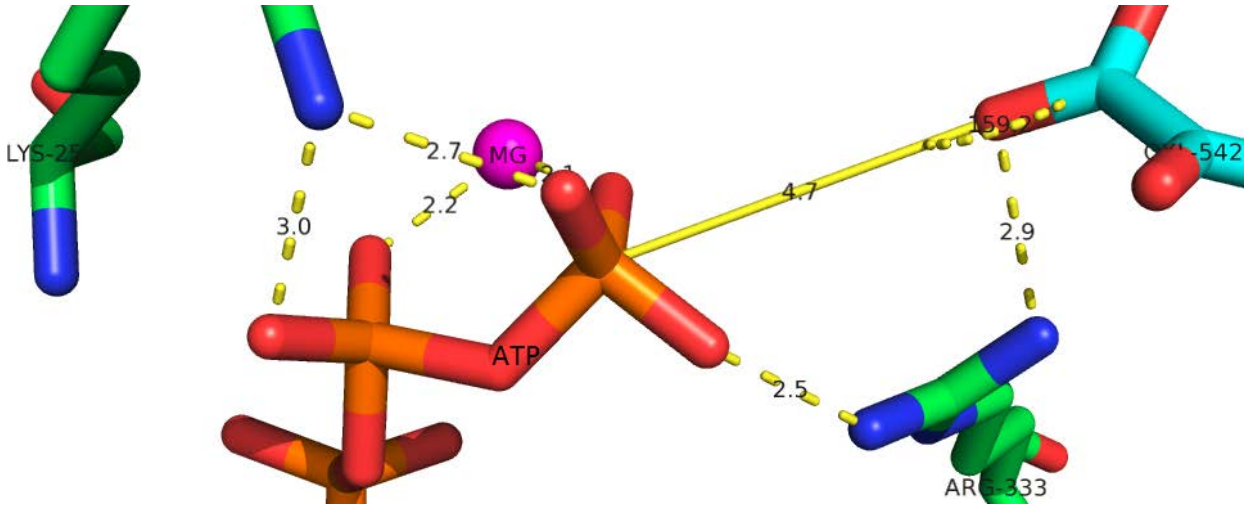

Figure 1.11: Coordination of oxalate and ATP. Oxalate and ATP are coordinated by Arg333. The β and γ-phosphate groups of ATP are interacting with Mg^{2+} and Lys254. One of the carboxyl group of pyruvate is 4.7Å away from the γ-phosphate of ATP, at an angle of 159.2°. Distance in Angstroms. Image was made with Pymol (DeLano, 2002) using PDB: 1AYL.

If the interaction between Mg^{2+}-ATP, OAA and Arg333 is similar to the interaction between Mg^{2+}-ATP, oxalate and Arg333 observed in the crystal structure, then the proposed mechanism of catalysis in the presence of Mg^{2+}ATP and OAA as shown in Fig 1.12 is as follows. Interaction between Arg333 and OAA, drives OAA decarboxylation and the formation of *enol*-pyruvate, which also interacts with Arg333. The proximity of Arg333 allows it to bridge *enol*-pyruvate and Mg^{2+}-ATP, neutralize the electrostatic repulsion between them, and bring them in close proximity to each other. Arg333 also functions with Mg^{2+} and Lys254 to increase the electrophilicity of the γ-phosphate of ATP, by withdrawing electrons from the β and γ-phosphate oxygen's of ATP. Attack of the electrophilic γ-phosphate of ATP by the nucleophilic carbonyl oxygen of pyruvate enolate leads to ADP and PEP formation (Tari *et al.*, 1996).

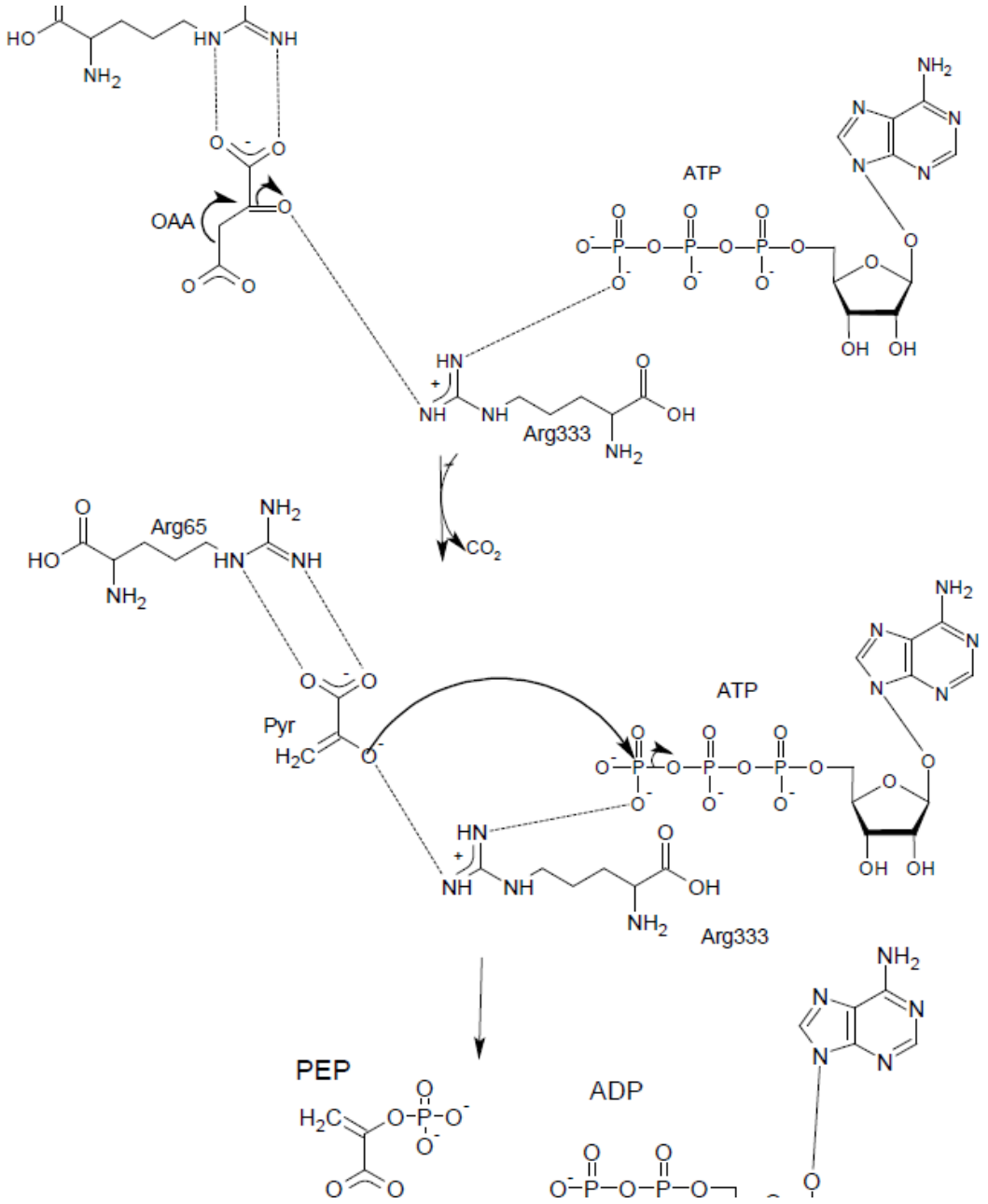

Figure 1.12: Proposed mechanism of PCK catalysis in the presence of Mg^{2+}ATP and OAA. Interaction of Arg333 with both substrates drives the decarboxylation of OAA and the formation of pyruvate enolate. Negatively charged carbonyl oxygen of enoly pyruvate attacks the electrophilic γ-phosphate of ATP leading to PEP and ADP formation (Diagram was made with ACD/ChemSketch).

1.6.2 Mechanism of PCK catalysis derived from crystal structures with *E. coli* PCK-pyruvate-ATP, Mg^{2+} and Mn^{2+}

The mechanism of catalysis by *E. coli* PCK in the presence of Mg^{2+}ATP, OAA and Mn^{2+} was derived from analysis of *E. coli* PCK-Mg^{2+}-ATP-Mn^{2+}-pyruvate structure (PDB: 1AQ2). In the *E. coli* PCK –MgATP-pyr-Mn^{2+} structure Arg333 and Mn^{2+} are in positions that allow them interact with both substrates through electrostatic interactions. Arg333 interacts directly with one γ-phosphate oxygen of ATP and the carbonyl oxygen of pyruvate, while Mn^{2+} interacts directly with one γ-phosphate oxygen of ATP, but indirectly with one carboxyl oxygen and the carbonyl oxygen of pyruvate through two water molecules that are directly coordinating pyruvate (Fig 1.13). This structure also supports an S_N2 mechanism of phosphoryl transfer, because the carbonyl oxygen of pyruvate is 4.3Å away from the γ-phosphate of ATP at an angle of 134°, which is almost linear.

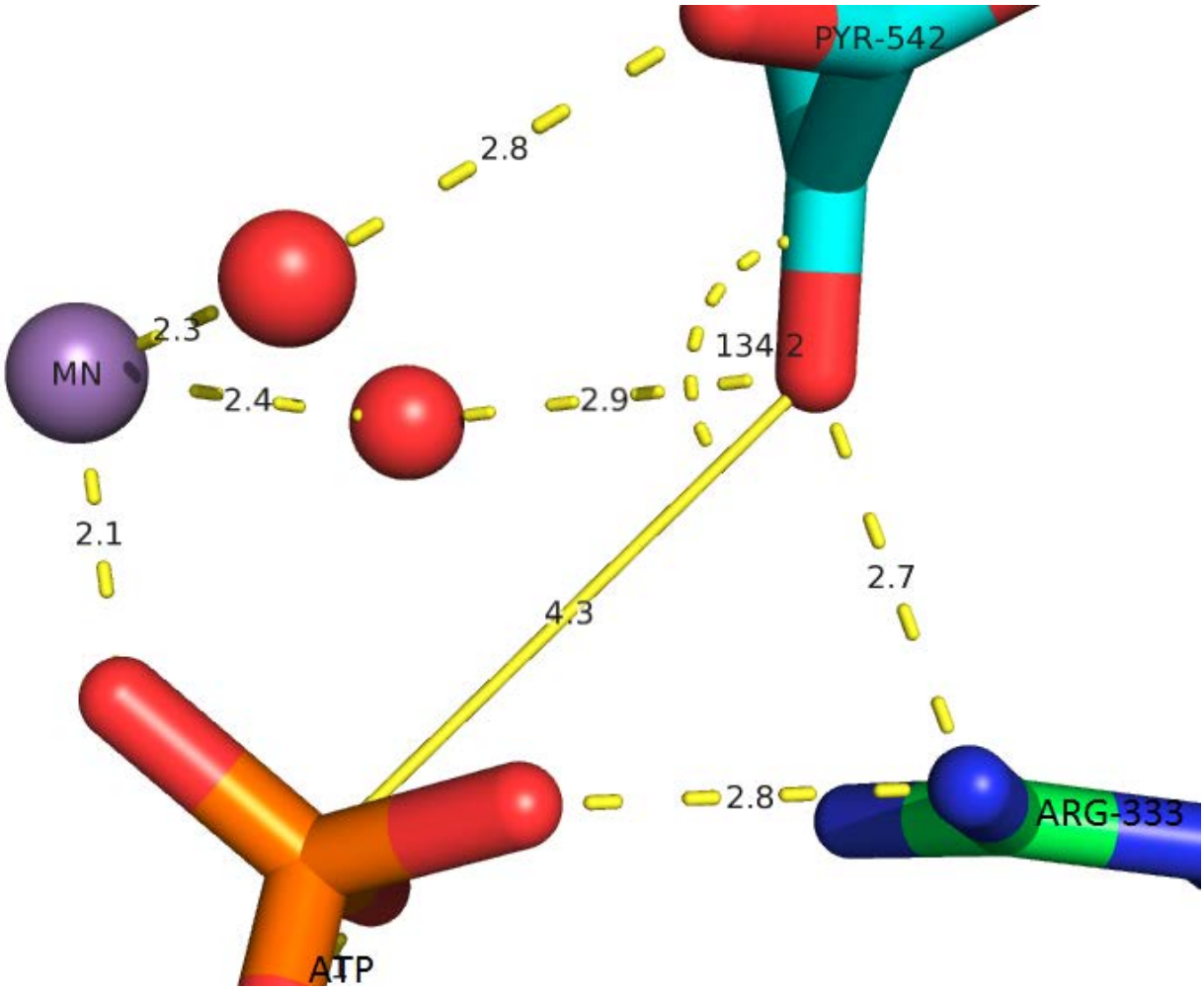

Figure 1.13: Coordination of pyruvate and ATP in *E.coli* structure with Mn^{2+}. Pyruvate is coordinated by two water molecules and Arg333 which is also coordinating ATP. The carbonyl oxygen of pyruvate is 4.3Å away from the γ-phosphate of ATP. Distance are in Angstroms. Image was made with Pymol (DeLano, 2002) using PDB: 1AQ2.

If OAA and pyruvate interactions with Mg^{2+}ATP, Mn^{2+} and Arg333 are similar, then the interaction between Arg333 and OAA drives OAA decarboxylation, the formation of *enol*-pyruvate and displacement of water molecules from the coordination sphere of Mn^{2+}. Interaction of Mn^{2+} and Arg333 with *enol*-pyruvate and ATP, neutralizes electrostatic repulsion between *enol*-pyruvate and ATP, and brings the carbonyl oxygen of *enol*-pyruvate in close proximity to the γ-phosphate of ATP. The electrophilicity of the γ-phosphate of ATP is increased by the action of Mn^{2+}, Mg^{2+}, Arg333 and Lys254, that draw electrons form the β and γ phosphates of

ATP. Nucleophilic attack of the γ-phosphate of ATP by the carbonyl oxygen of *enol*-pyruvate leads to PEP and ADP formation (Fig 1.14, Tari *et al.*, 1997).

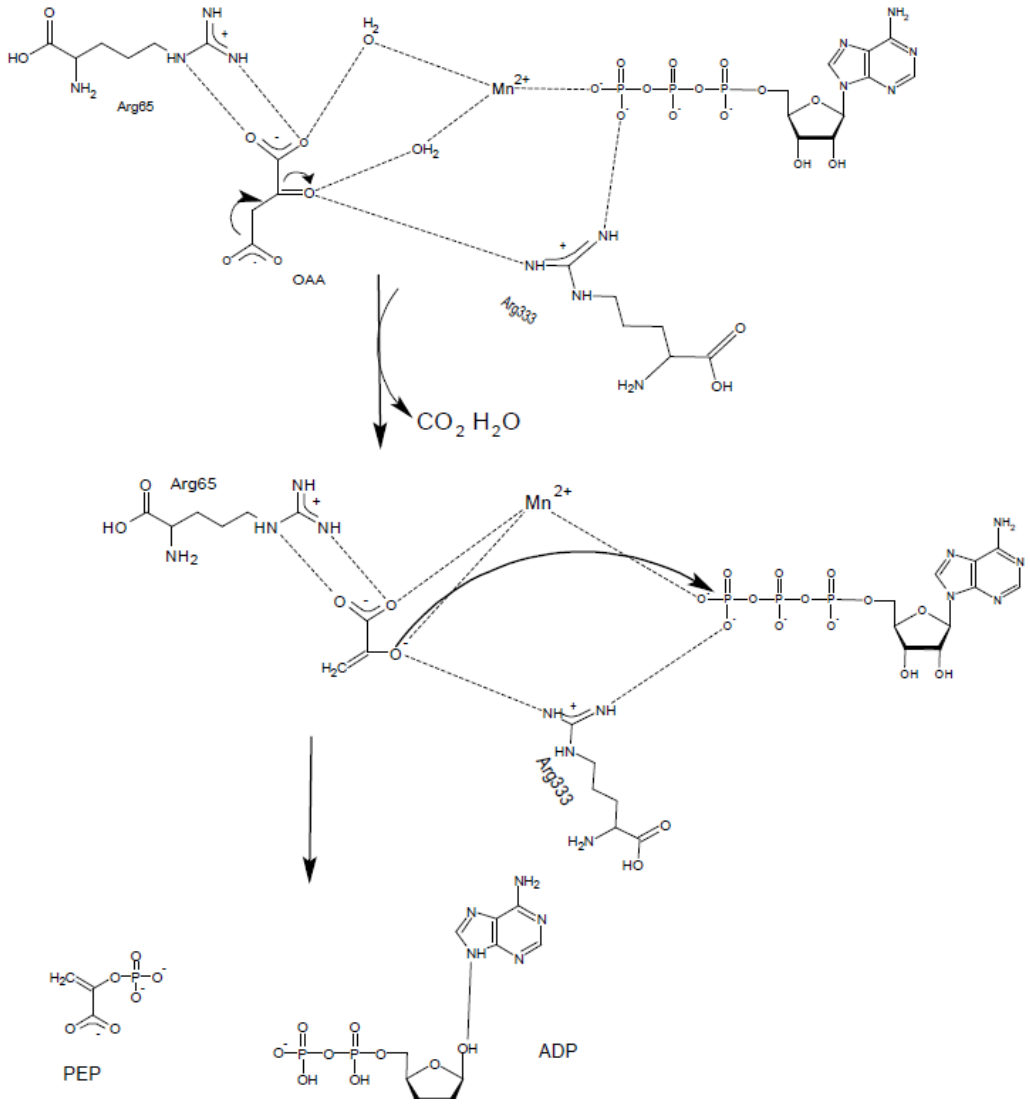

Figure 1.14: Proposed mechanism of PCK catalysis in the presence of Mg^{2+}ATP OAA and Mn^{2+}. Interaction of Arg333 and Mn^{2+} with both substrates drives the decarboxylation of OAA and the formation of pyruvate enolate. Negatively charged carbonyl oxygen of enol-pyruvate attacks the electrophilic γ-phosphate of ATP leading to PEP and ADP formation. Made with ACD/ChemSketch software.

1.6.3 Mechanism of PCK catalysis derived from crystal structures with *E. coli* PCK-pyruvate-ATP, Mg^{2+} and Ca^{2+}

The mechanism of *E. coli* PCK catalysis in the presence of Mg^{2+}ATP, OAA and Ca^{2+}, was derived from analysis of *E. coli* PCK Mg^{2+}ATP- pyruvate-Ca^{2+} structure (PDB: 1OS1). Analysis of the structure with Ca^{2+} shows that Ser250, Arg333, Tyr207 and Ca^{2+} (Fig 1.15) are in positions that allow them interact with Mg^{2+}ATP or pyruvate. Ca^{2+} directly interacts with one γ-phosphate oxygen of ATP and one carboxyl oxygen of pyruvate. Tyr207 directly interacts with the CH_2 group of pyruvate, Arg333 is directly interacting with Ser250 and one γ-phosphate oxygen of ATP. Ser250 is directly interacting with one γ-phosphate oxygen of ATP, one carboxyl oxygen of pyruvate and Arg333. One of the carboxyl oxygen of pyruvate is 4.3Å away from the γ-phosphate of ATP, while the carbonyl oxygen of pyruvate is 6.0Å away from the γ-phosphate of ATP.

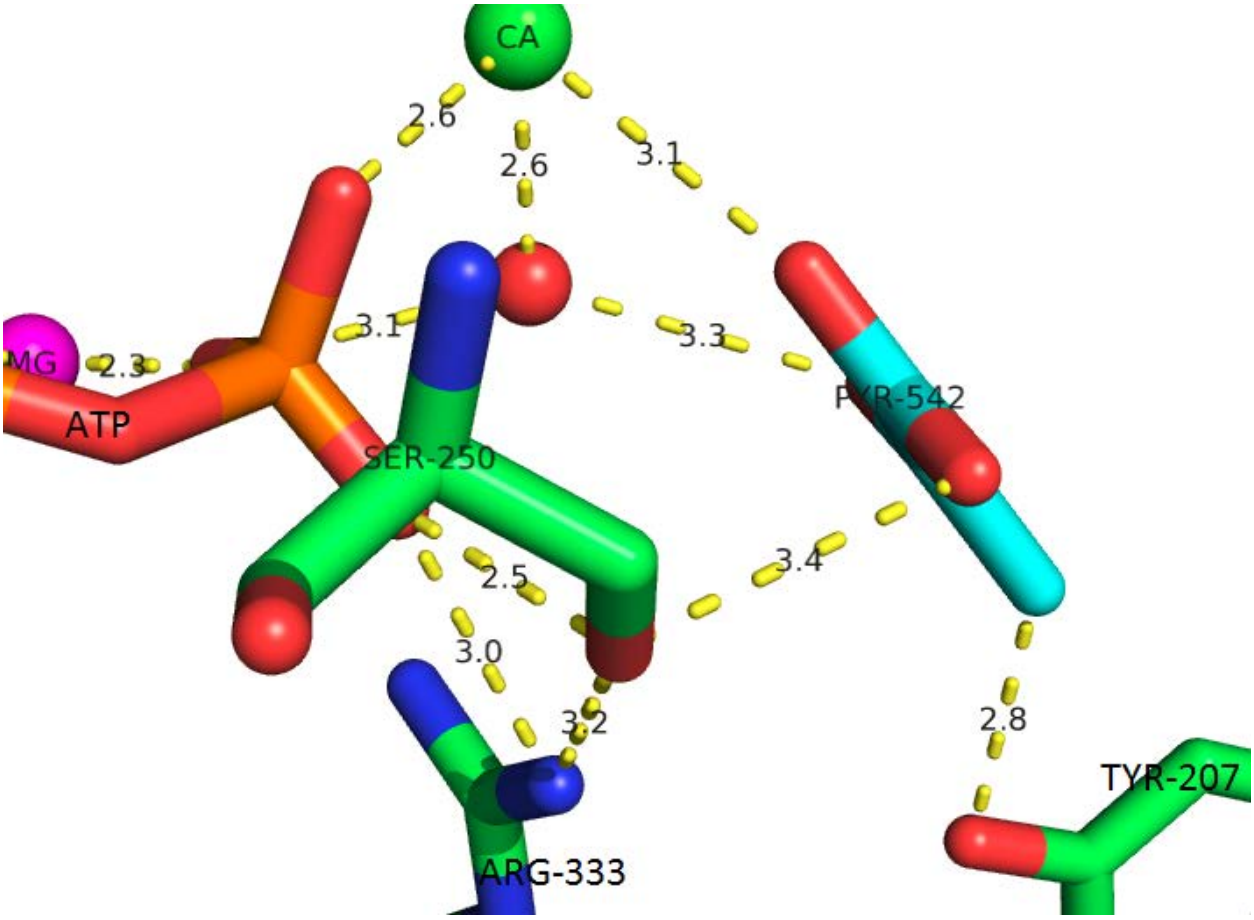

Figure 1.15: Coordination of pyruvate and ATP in the *E.coli* structure with Ca^{2+}. Pyruvate is coordinated by one water molecule, Ca^{2+}, Ser250 and Tyr207, while ATP is coordinated by Mg^{2+}, Ca^{2+} and Arg333. Distance are shown in Angstroms. Image was made with Pymol (DeLano, 2002), using PDB: 1OS1.

The proposed mechanism of *E. coli* PCK catalysis in the presence of Mg^{2+}-ATP, OAA and Ca^{2+} as shown in Fig1.16 is as follows. Binding of OAA to Ca^{2+} drives the decarboxylation of OAA and the formation of *enol*-pyruvate. Ca^{2+} also functions to neutralize the electrostatic repulsion between *enol*-pyruvate and the γ-phosphate of ATP, bringing them in close proximity to each other and orienting the carbonyl oxygen of pyruvate to nucleophilically attack and displace the γ-phosphate of ATP. Electrostatic repulsion between Tyr207 and the CH_2 group of pyruvate functions to move the carbonyl oxygen of pyruvate closer to the γ-phosphate of ATP. According to Sudom *et al.*, 2003, superposition of OAA over pyruvate binding site, has shown that Arg333 can interact with the second carboxyl group of OAA; hence it was proposed that salt

bridge formation between OAA and ATP by Arg333 functions with Ca^{2+} to drive OAA decarboxylation and to maintain the stability of the reaction intermediate (Sudom *et al.,* 2003, Delbaere *et al.,* 2004). The electrophilicity of the γ-phosphate of ATP is increased by Ca^{2+}, Mg^{2+}, Arg333 and Lys 254, which are interacting with the β and γ-phosphate oxygen's of ATP. Formation of PEP and ADP occurs when the nucleophilic carbonyl oxygen of *enol*-pyruvate attacks the electrophilic γ-phosphate of ATP. Since Ser250 is interacting with ATP, Arg333 and pyruvate, we hypothesize that it is required holding both substrate in the right orientation for catalysis, in the presence of Ca^{2+}.

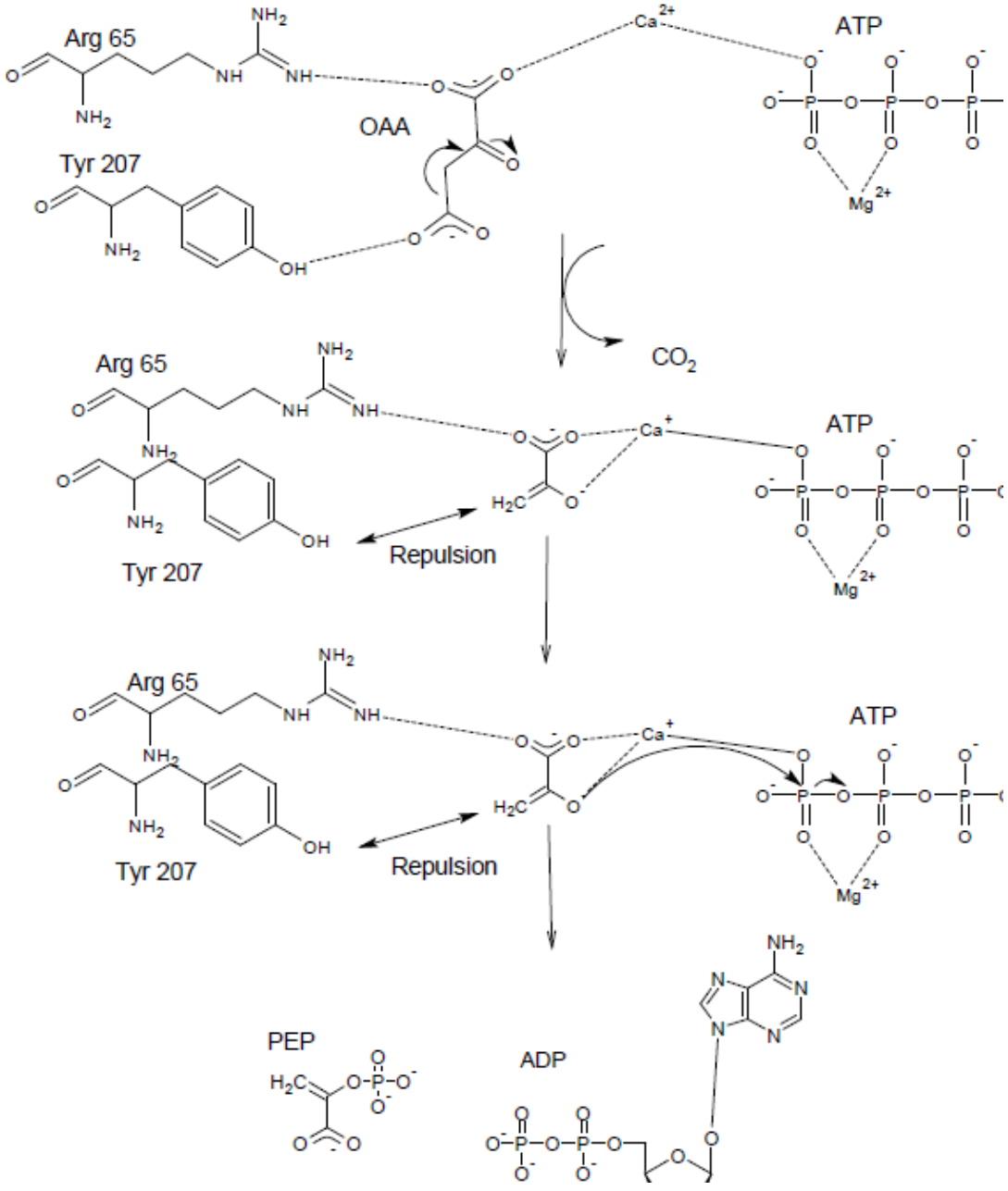

Figure 1.16: Proposed mechanism of PCK catalysis in the presence of Mg^{2+}ATP, OAA and Ca^{2+}. Interaction of OAA with Ca^{2+} leads to OAA decarboxylation. Electrostatic repulsion between Tyr207 and the CH_2 group of enol pyruvate, moves enol pyruvate towards ATP. Interaction between the carbonyl oxygen of enol pyruvate and Ca^{2+}, puts the carbonyl oxygen of enol pyruvate in the right orientation to attack and displace the electrophilic γ-phosphate of ATP leading to PEP and ADP formation (made with ACD/ChemSketch software).

1.7 Hypothesis and objectives

The objective of this study is to confirm the proposed mechanisms of *E. coli* PCK catalysis using site directed mutagenesis, enzyme assays and x-ray crystallography. Arg333 interacts electrostatically with Mg^{2+}-ATP and OAA, with and without Mn^{2+} or Ca^{2+}. It functions to drive OAA decarboxylation, and to bring *enol*-pyruvate and ATP in close proximity to each other for catalysis. As a result Arg333Gln mutation is expected to cause a decrease in the rate of the reaction (reduced k_{cat}). Since glutamine is able to form hydrogen bond with both substrates, this mutation will enable us determine if electrostatic interaction between Arg333, OAA and *enol*-pyruvate is important for catalysis in the presence of Mg^{2+}-ATP and OAA with and without, Mn^{2+} or Ca^{2+}.

In the presence of Ca^{2+} electrostatic repulsion between the hydroxyl group of Tyr207 and the CH_2 group of pyruvate enolate moves the negative charged carbonyl oxygen of *enol*-pyruvate in close proximity to the γ-phosphate of ATP. Mutation of Tyr207 to Phe will eliminate the hydroxyl group, and therefore allow us confirm if the interaction between Tyr207 and the CH_2 group of *enol*-pyruvate is required for catalysis in the presence of Mg^{2+}-ATP, OAA and Ca^{2+}. This mutant is expected to have a reduced rate of catalysis (low k_{cat}) in the presence of Ca^{2+}, but have k_{cat} similar to the wildtype enzyme in the presence of Mg^{2+}-ATP and OAA with and without Mn^{2+}.

Ser250 is part of the kinase 1a loop important for ATP binding; in the presence of Ca^{2+} it directly interacts with ATP, pyruvate and Arg333. Hence when Ca^{2+} is used for catalysis, Ser250 functions to bring both substrates in close proximity to each other. A Ser250Ala mutation will eliminate the hydroxyl group necessary for residue 250 to coordinate ATP, *enol*-pyruvate and Arg333, in the presence of Mg^{2+}-ATP, OAA and Ca^{2+}, as a result this mutation is expected to

cause reduced k_{cat} in the presence of Ca^{2+}, but have little effect on catalysis in the presence Mg^{2+}-ATP and OAA with and without Mn^{2+}. Although Ser250 is part of the kinase 1a loop, Ser250Ala mutation is expected to have a higher effect on catalysis in the presence of Ca^{2+} and a lesser effect on ATP binding since other residues involved in ATP binding are intact.

E. coli PCK Arg333Gln mutant will display a reduced k_{cat} in the presence of Mg^{2+}-ATP and OAA with and without Ca^{2+} or Mn^{2+}, while Ser250Ala and Tyr207Phe mutations will display reduced k_{cat} when Mg^{2+}-ATP, OAA and Ca^{2+} are present for catalysis. Arg333Gln, Ser250Ala and Tyr207Phe mutations are not expected to have a significant effect on the K_m of the enzyme for Mg^{2+}-ATP and OAA, because Arg65Gln and Lys254Ser have been shown by Novakovski 2000, to increase the K_ms of the enzyme for OAA and Mg^{2+}-ATP respectively. Since mutation of Arg333, Ser250 and Tyr207 is expected to have different effect on k_{cat} in the presence or absence of Mn^{2+} or Ca^{2+}, we hypothesize that the function of Arg333, Ser250 and Tyr207 during catalysis by *E. coli* PCK depends on the presence or absence of Mn^{2+} or Ca^{2+}.

Binding of Ca^{2+} or Mn^{2+} to the bridging site of *E. coli* PCK allows them to interact with Mg^{2+}-ATP and OAA and properly orient and bring the reaction intermediate in close proximity to the γ-phosphate of ATP. They also function to increase the susceptibility of the γ-phosphate of ATP for nucleophilic attack; hence, it is expected that the rate of catalysis in the presence of Mn^{2+} or Ca^{2+} will be increased. However since Ca^{2+} is directly interacting with both substrates, the rate of catalysis in the presence of Ca^{2+} is expected to be greater than the rate of catalysis in the presence of Mn^{2+}.

2.0 Materials and Methods

2.1 Site-directed Mutagenesis

2.1.1 Site-directed mutagenesis to form Arg333Gln Ser250Ala and Tyr207Phe mutations

Site-directed mutagenesis using mutagenic primers was used to generate mutations of interest on the *pckA* gene present on plasmid pDBss generated for pBR322 plasmid (Fig 2.1). To allow for preliminary screens of putative mutants, silent mutations that generated unique restriction sites were also introduced into the mutagenic primers. Mutant codons were selected for relatively high codon usage, in order to ensure optimal expression of mutant proteins, using the *E. coli* codon usage table (Genbank).

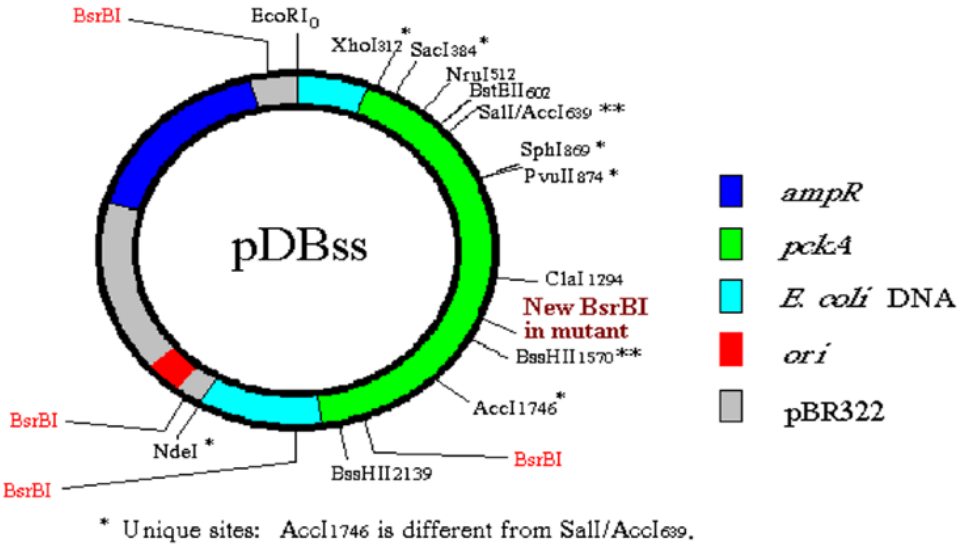

Figure 2.1: 4750bp pDBss plasmid

Tyrosine 207 Phenylalanine mutation was introduced into the *pckA* gene using the forward primer oHG68 and reverse primer oHG67 with silent a mutation that introduced a unique *KpnI* restriction site into the plasmid, as shown in Fig 2.2 below.

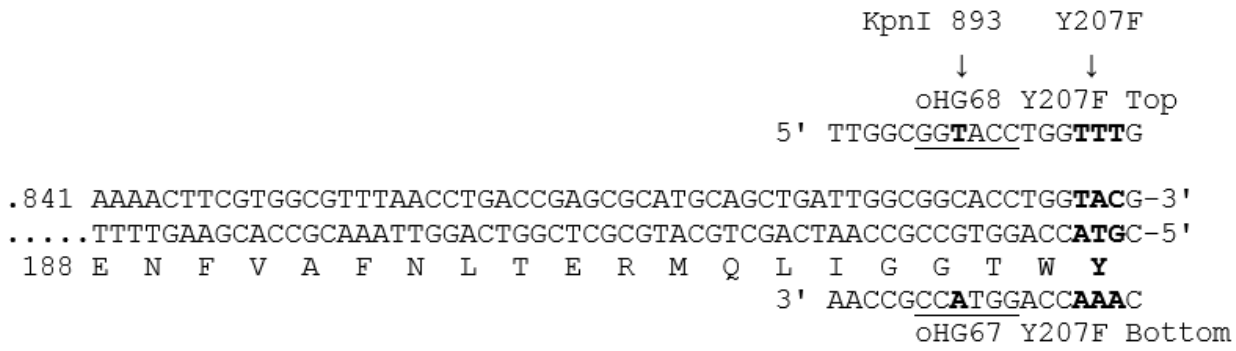

Figure 2.2: Site-directed mutagenesis introducing Tyr207Phe mutation into pDBss plasmid.

Arginine 333 glutamine mutation was introduced into the *pckA* gene using the forward primer oHG209 and the reverse primer oHG210 with a silent mutation that introduced a third *BsaI* restriction site on plasmid pDBss, as shown below (Fig 2.3).

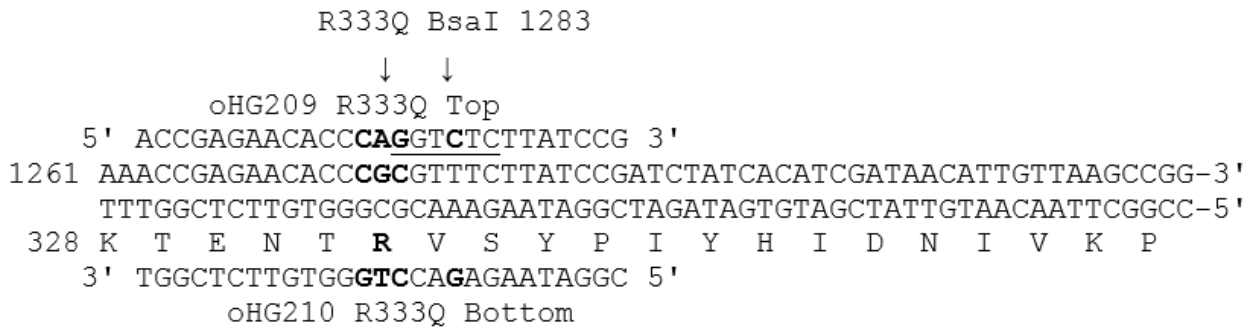

Figure 2.3: Site-directed mutagenesis introducing Arg333Gln mutation into pDBss plasmid.

Serine 250 alanine mutation was made previously in the lab by Patricia Thibeault as shown below, using the forward primer oHG72 and the reverse primer oHG71, with a silent mutation that introduced a unique *Kpn1* restriction site on the plasmid (Fig 2.4).

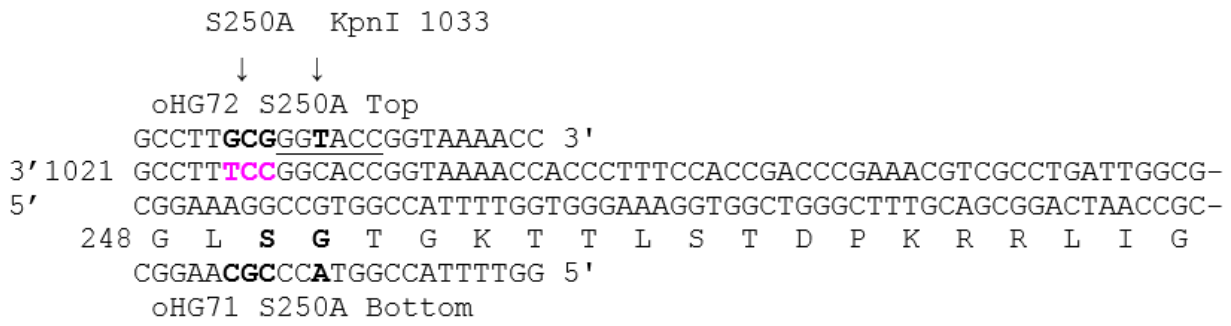

Figure 2.4: Site-directed mutagenesis introducing Ser250Ala mutation into pDBss plasmid.

Concentrations of primers and plasmid templates used for making mutated plasmids were determined by measuring their absorbance at 260 nm. The reaction mixture included the following: 25 ng of plasmid DNA (pDBss), 25 ρmol of each primer, 10X pfu Ultra II fusion buffer, 1 µl pfu UII HS polymerase, and 0.2 mM dNTP mix in a total volume of 50 µl. PCR mutagenesis was carried out in a S1000 thermal cycler under the following conditions: denaturation at 94°C for 30 seconds, annealing at 55°C for 60 seconds and extension at 72°C for 5 min. Reactions were cycled 17 times and completed at 72°C for 5 min. To cleave methylated DNA and therefore reduce the amount of non-mutated plasmid. PCR products were incubated with 1 U of *DpnI* for 1 hour, and used to transform NEB5-alpha competent *E. coli* cells. Cells with mutant plasmid were isolated using growth on 100 µg/ml ampicillin plates, since the plasmid contains the ampicillin resistance gene, which is absent in NEB5-alpha cells (Novakovski, 2000).

Table 2.1: Primer and mutation list

Primer	Size	Sequence	Function
oHG68	29	5'TTGGCGG**T**ACCTGG**TTT**GGCGG CGAAATG 3'	Forward primer used for Y207F mutation Y→Q: TAC → TTT New *KpnI* (GTAC/C) site: GCA → GTA
oHG67	29	5'CATTTCGCCGCC**AAA**CCAGGT**A** CCGCCAA 3'	Reverse primer used for Y207F mutation Y→Q: ATG → AAA New *KpnI* (GTAC/C) site: TGC → TAC
oHG209	40	5'CAAAAACCGAGAACACC**CAG**G T**C**TCTTATCCGATCTATCA 3'	Forward primer used for R333Q mutation R→Q: CGC → CAG New *BsaI* (GGTCTC) site: TTT → TCT
oHG210	40	5'TGATAGATCGGATAAGAGACCT GG**GTG**TT**C**TCGGTTTTTG 3'	Reverse primer used for R333Q mutation R→Q: GCG → GTG New *BsaI* (GGTCTC) site: TTT → TCT
oHG72	31	5'GTTCTTCGGCCTT**GCG**GG**T**ACC GGTAAAACC 3'	Forward primer used for S250A mutation S→A: TCC → GCG New *KpnI* (GTAC/C) site: GCA → GTA
oHG71	31	5'GGTTTTACCGG**T**ACCCGCA**AGG** CCGAAGAAC 3'	Reverse primer used for S250A mutation S→A: AGG → CGC New *KpnI* (GTAC/C) site: CGT → CAT

2.1.2 Preparation of plasmids

2.1.2.1 Alkaline lysis method

Mutated plasmids were isolated from NEB-5α competent cells as follows. To prepare cells for plasmid extraction, ampicillin-resistant colonies of transformed NEB-5α competent cells were grown overnight in 5 ml cultures of LB medium containing 100 µg/ml ticarcillin. Cells were pelleted by centrifugation at 5,000 x g for 5 minutes and plasmids were extracted using the Qiagen miniprep kit according to the protocol described in the Qiagen Plasmid Purification Manual. This kit contains an alkali which is used for cell lyses.

2.1.3 Restriction digest screening

Restriction sites were introduced into mutated plasmid pDBss together with the desired mutation. As a result, preliminary screens were performed on the isolated plasmid. Restriction digests of plasmids were prepared by adding 1 µg of mutate plasmid prep, 1 µl of restriction enzyme, 5 µl of NEB cutsmart buffer, and water to make up the volume to 15 µl. A digest containing *BssHII* was incubated in a 50°C water bath for 15 min, while the *BsaI* and *KpnI* digest was incubated in a 37°C water bath for 1 hour. New restriction sites were introduced together with Y207F and S250A mutations on plasmid pDBss. As a result, a double digest with *KpnI* and *BssHII* was used for the preliminary screening of these mutated plasmids. To perform a double digest with *KpnI* and *BssHII*, the mutant plasmids were first incubated for 15 min at 50°C with *BssHII*, before the addition of *KpnI*, after which plasmids were incubated at 37°C for 1 hour. Table 2.2 shows the expected band sizes for the digest performed on each mutant plasmid.

Table 2. 2: Enzymes and expected fragments of mutant plasmid digests.

Mutants	Restriction enzymes	Cuts *pckA* at (bp)	Expected size (bp) of fragment
R333Q	*BsaI*	833, 1283 and 3832	450, 1751 and 2549
S250A	*BssHII*	2139	1107 and 3643
	KpnI	1033	
Y207F	*BssHII*	2139	1247 and 3503
	KpnI	893	

2.1.4 Sequencing

The entire mutated *pckA* gene was sequenced to confirm the presence of the desired mutation and the absence of undesired mutations using the oligonucleotides which bind to specific region of pDBss plasmid, shown in Table 2.3. Plasmid DNA samples were sent to the DNA sequencing laboratory at the National Research Council in Saskatoon, for sequencing.

Table 2.3: List of oligonucleotides used for sequencing

Oligos	Size	Sequence	Sequence direction
oHG199	25	5’CACTAGCGCCAGCCATCCCCAAAGG 3’	PCK 5’
oHG200	23	5’GCCAATATGTATTGCCTGAATAG 3’	PCK 3’
oHG201	22	5’CCAGATACGTAAATCTATGAGC 3’	PCK 5’
oHG202	23	5’GGTTTGAAACCTGCCAGTTCTTC 3’	PCK 3’
oHG203	23	5’CATCACCGAAGTGGCCTGGCAGG 3’	PCK 5’
oHG204	25	5’GGGTGTTCTCGGTTTTTGAACCATC 3’	PCK 3’
oHG205	23	5’CTATCAAGCTGTCGAAAGAAGCG 3’	PCK 5’
oHG206	21	5’GTGAAGGTTTCTGCATTATCC 3’	PCK 3’
oHG207	22	5’GGCAAACGTATCTCGATTAAAG 3’	PCK 5’
oHG208	24	5’CGCGGGCGCAGGGCACGACAAAAG 3’	PCK 3’

5’ oligos binds to the top strand and sequence from this oligo goes in the 5’ direction. 3’ oligos bind to the bottom strand and sequencing goes in the 3’ direction.

2.2 Purification of Mutant PCKs

2.2.1 Growth of cultures

Mutant plasmids shown to contain desired mutations using restriction digests and sequencing were used to transform competent HG89 *E. coli*. As shown in Table 2.4, *E. coli* strain HG89 has mutations in the *pps, pckA,* and *recA* genes. Since it is lacking PCK necessary for the conversion of OAA to PEP, and phosphoenolpyruvate synthase (PPS) required for the conversion of pyruvate to PEP, HG89 cannot use succinate or pyruvate as its primary carbon and energy source, unless it is transformed with plasmids carrying the *pckA* or *pps* genes. HG89 also requires the presence of amino acids such as histidine, threonine, tyrosine, and arginine for growth, hence the ability of HG89 *E. coli* strains transformed with wild type or mutant pDBss

plasmid to grow on minimum succinate and glucose plates lacking one of the amino acids required for HG89 growth was confirmed.

Table 2.4: Genotype and phenotype of *Escherichia coli* K-12 HG89 strain

Strain	Genotype	Phenotype
HG89 F^-	*argG::Tn5*	Requires arginine for growth, contains a Tn5 insertion
	edd-1	6-phosphogluconate dehydratase (Entner Douderoff dehydratase)
	his-61	Requires histidine for growth
	lac	Lactose fermentation negative
	pckA4	Pck^-, unable to grow with succinate as the sole carbon source when *pps*$^-$ mutation is also present
	pps-3	Pps^- unable to grow with pyruvate as the sole carbon source
	pyrD34	Pyr^-, requires pyrimidine (uridine) for growth
	recA	Defective in general recombination, cannot repair radiation damage, *exoV*, induction of *recB*, *recC*
	rpsL125	Resistant to streptomycin
	thr-1	Requires vitamin B1 for growth
	tyrA2	Requires tyrosine for growth
	srl::Tn10	Sorbitol, PTS system and fermentation. Tn10 insertion closely linked to recA

Colonies that display the expected phenotype on minimum plates were picked from ampicillin plates and inoculated in sterile test tubes containing 5 ml of LB and 100 µg/ml ticarcillin and grown overnight at 37°C while shaking. The overnight-grown 5 ml cultures were used to inoculate 300 ml of LB containing 100 µg/ml ticarcillin. This culture was also grown overnight at 37°C while shaking. Overnight-grown 300 ml cultures were used to inoculate 12 L LB medium contained in sterile 14 L fermenters. Cells were grown in 14 L fermenters until they reached stationary phase, during which *pckA* expression from the plasmid is induced. Cells were harvested by centrifugation at 5,000 x g for 5 min, supernatant was discarded, and pellet resuspended in 0.85% cold NaCl and centrifuged at 5,000 x g for 10 min. Cells were finally

resuspended in a 50 mM Tris 10 mM EDTA buffer and disrupted using a cell disrupter at 15 k.p.s.i.

2.2.2 Protein purification

2.2.2.1 Protein purification on DEAE cellulose and calcium phosphate columns

Diethylaminoethyl (DEAE) cellulose is a weakly basic anionic exchange resin used for column chromatography, and Whatman microgrannular DE32 DEAE cellulose used in this study, and were prepared as follows. DEAE was dissolved in water, stirred for 30 min, and filtered with a Whatman 24 cm circle filter paper in a large Buchner funnel. The DEAE cake was resupended in 0.5 N HCl, stirred slowly for 30 min, filtered, and washed with water until the pH of the filtrate was approximately 4. DEAE at pH 4 was resuspended in 0.5 N NaOH stirred slowly for 30 min, filtered, and washed with water until the pH of the filtrate was equal to 7. DEAE at pH 7 was further washed with 0.2 M Tris pH 7.5, resuspended in 10 mM Tris pH 7.5, and applied to a C-type Pharmacia column. The column filled with DEAE was flushed with several column volumes of 10 mM Tris 1 mM EDTA (TE) buffer, before the addition of 250 µl of crude extract, obtained from the cell disruptor. The column containing crude extract was washed with two column volumes of TE buffer, and column flow-through (fractions) were collected in glass tubes. To elute PCK from the column, a KCl gradient was applied to the column and more fractions were collected at 4°C.

Fractions collected from the DEAE column were applied to a standard sodium dodecyl sulphate-polyacrylamide gel electrophoresis (SDS-PAGE) gel (Ausubel *et al.,* 1996), to enable the identification of PCK containing fractions, through comparison to previously purified PCK. PCK-containing fractions were concentrated and applied to ultra-gel column for further purification. This column was washed with a 20 mM Tris 1mM EDTA buffer, PCK was eluted by gravity, and the purity of eluted PCK fractions was visualized with a SDS-PAGE gel.

2.3 Enzyme assays

2.3.1 $^{14}CO_2$ Exchange assay

The $^{14}CO_2$ exchange assay was used to determine the kinetic parameters of mutant and wild type PCKs (Goldie, 1979). Decarboxylation of OAA by PCK in the presence of ATP leads to PEP, ADP, and CO_2 formation. However, since PCK can also catalyze the reverse reaction, excess $NaH^{14}CO_3$ (20mM) drives the reaction backwards, causing the formation of radioactively labeled OAA (^{14}C-OAA), which can be counted using a scintillation counter. Therefore, in PCK exchange assay, radioactivity is exchanged between labelled and unlabeled CO_2 to produce radioactively labelled OAA.

Assays were performed in duplicate or triplicate and repeated 3 to 4 times in one-dram glass vials containing 4 x 10^5 dpm $NaH^{14}C0_3$, 5 mM ATP, 10 mM OAA, 1 mM Mg, 1 mM Mn^{2+}, 1 mM Ca^{2+}, 40 µM EDTA, 40 mM Na, and 100 mM Tris, at a pH of 7.5 in a total volume of 500 µl. The amount of substrates and metals used in the assay were varied based on the concentration range of the changing substrate. Since a mixture of these reagents can lead to complex formation between the substrates and metal ions present in the solution, thereby reducing the desired concentration of free substrate and metal ion available for the reaction, a modified version of Fortran program “COMICS” (Concentrations of Metal Ions and Complex Species) was used to determine the concentration of each reagent required for the assay (Goldie, 1979).

2.3.2 COMICS program

COMICS calculates the required concentrations of the each reactant that will result in the desired concentrations of bound and free ligands necessary for a given assay (Goldie 1979, Perrin and Sayce, 1967). Since a mixture of the reagents results in the formation of complexes between the various reagents, COMICS uses the cumulative stability constants (log Beta) of the complexes to calculate the concentrations of bound and free ligands in the assay mixture. Table

2.5 shows the stability constants of the complexes that are likely to be formed between the reagents in our assay. Stability constants were obtained from Gelles and Salama (1958), Critically selected Stability Constants of Metal Complexes, Database Version two (1995) and Goldie's Doctor of Philosophy thesis 1979, while Table 2.6 shows a sample assay spread sheet, used for PCK exchange assay.

Table 2.5: Cumulative stability constants of complexes present in assays

Complex		log Beta	Complex		Log Beta	Complex		log Beta
1	$H(OAA)^{2-}$	13.1	13	$Mn(ATP)^{2-}$	4.76	25	$H(EDTA)^{3-}$	10.2
2	$H_2(OAA)^{-}$	17.0	14	MnH(ATP)	8.9	26	$H_2(EDTA)^{2-}$	16.3
3	$H_3(OAA)$	19.2	15	$Mg(ATP)^{2-}$	4.06	27	$H_3(EDTA)^{-}$	19.0
4	CaH(OAA)	15.1	16	MgH(ATP)	8.61	28	$H_4(EDTA)$	21.0
5	$Mn(OAA)^{-}$	15.9	17	$Na(ATP)^{2-}$	1.1	29	$Ca(EDTA)^{2-}$	10.6
6	$Mg(OAA)^{-}$	6.27	18	HCO_3^{-}	9.57	30	$CaH(EDTA)^{-}$	13.8
7	$Mg(OAA)_2^{4-}$	11.1	19	H_2CO_3	15.6	31	$Mn(EDTA)^{2-}$	13.8
8	MgH(OAA)	15.1	20	$CaCO_3^{+}$	3.0	32	$MnH(EDTA)^{-}$	16.9
9	$H(ATP)^{3-}$	6.51	21	$CaHCO_3^{2+}$	10.4	33	$Mg(EDTA)^{2-}$	8.83
10	$H_2(ATP)^{2-}$	10.6	22	$MnHCO_3^{2+}$	10.0	34	$MgH(EDTA)^{-}$	12.7
11	$Ca(ATP)^{2-}$	3.77	23	$MgCO_3^{+}$	2.37	35	$Na(EDTA)^{2-}$	1.64
12	$CaH(ATP)^{-}$	8.46	24	$MgHCO_3^{2+}$	10.3			

EDTA is present in the buffer used for elution of PCK during purification. Complexes present in a particular assay depend on the metal ions used for that assay.

Table 2.6: Sample spreadsheets of calculation using the COMICS program (Mg^{2+}ATP is the varied substrate shown here)

Tube No	Total ATP (mM)	H_2O (µl)	1mM ATP(µl)	10mM ATP (µl)	50.9mM ATP (µl)	100mM Mg^{2+} (µl)	100mM Mn^{2+} (µl)	200mM OAA (µl)	200mM $NaH^{14}CO_3$ (µl)
1	Rx								
2	‘’								
3	‘’								
4	OAA Blk	269.6			31.7	31.2	47.5		50
5	“	269.6			31.7	31.2	47.5		50
6	“	269.6			31.7	31.2	47.5		50
7	0.032	253.5	16			26.3	37.1	47.1	50
8	“	253.5	16			26.3	37.1	47.1	50
9	“	253.5	16			26.3	37.1	47.1	50
10	0.064	237.3	32			26.4	37.2	47.1	50
11	“	237.3	32			26.4	37.2	47.1	50
12	“	237.3	32			26.4	37.2	47.1	50

13	0.161	188.4	80.5			26.5	37.5	47.1	50
14	“	188.4	80.5			26.5	37.5	47.1	50
15	“	188.4	80.5			26.5	37.5	47.1	50
16	0.322	252		16		26.8	38.1	47.1	50
17	“	252		16		26.8	38.1	47.1	50
18	0.644	234.5		32		27.3	39.1	47.1	50
19	“	234.5		32		27.3	39.1	47.1	50
20	1.611	181.3		80.6		28.8	42.2	47.1	50
21	“	181.3		80.6		28.8	42.2	47.1	50
22	3.222	222.5			31.7	31.2	47.5	47.1	50
23	“	222.5			31.7	31.2	47.5	47.1	50
24	6.443	175.4			63.3	36.3	57.9	47.1	50
25	“	175.4			63.3	36.3	57.9	47.1	50
26	16.1	36.2			158.2	51.3	89.2	47.1	50
27	“	36.2			158.2	51.3	89.2	47.1	50

Assay tubes containing the required amount of substrates and metals were incubated for 10 mins at 37°C, and the reaction was stopped with 500 µl of 0.2 N H_2SO_4. To prevent foam formation during aeration, one drop of octanol was added to each assay tube and tubes were aerated by bubbling with compressed air vigorously for 10 min in a fume hood to remove excess radioactive CO_2.

2.3.3 How kinetic values where obtained using GraphPad Prism

Determination of kinetic parameters such as K_m and V_{max} was performed using GraphPad Prism version 3.0 for Windows. This program determines K_m and V_{max} values using Michaelis-Menten (M-M), Lineweaver-Burk, and Eadie-Hofstee plots. Plotting of initial velocities versus substrate concentrations gives a hyperbolic curve (M-M plot) that can be used to determine V_{max} and K_m values. Lineweaver-Burk plots are obtained by plotting the reciprocal of initial velocities against the reciprocal of changing substrate concentration. This produces a straight line with a positive slope, and the reciprocal of the X-intercept (usually negative) gives the K_m, while the reciprocal of the Y-intercept gives the V_{max}. A plot of initial velocities versus initial velocities divided by substrate concentrations gives the Eadie-Hofstee plot, where the negative slope is equal to K_m and the Y-intercept is equal to V_{max}.

2.3.3.1 Definition of kinetic parameters in this study

2.3.3.1.1 Single substrate reactions

The reaction catalyzed by an enzyme can be divided into three stages: the pre-steady state, the steady state, and the final stage. The pre-steady state is used to describe the initial stage of a reaction, when an enzyme is mixed with excess substrate, and the concentration of the intermediate (enzyme-substrate complex) is rapidly increasing. During the steady state, the rate of intermediate formation and degradation is equal (Fersht, 1999). In the final stage, the intermediate is rapidly depleted with product formation, and the enzyme is regenerated. A single substrate reaction is one in which an enzyme catalyzes the conversion of one substrate to one product, and the steady state of this type of reaction has been used to derive Michaelis constant (K_m) and the Michaelis-Menten equation, as described below.

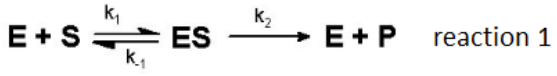

reaction 1

In the single substrate reaction shown above (reaction 1), E, S, ES, and P represent the enzyme, substrate, enzyme-substrate complex, and product, respectively, k_1 is the rate constant for ES formation, k_{-1} is the rate constant for ES dissociation, and k_2 is the rate constant for product formation. Formation of ES is dependent on the concentrations of E and S, while ES can be degraded to E + S or E + P, hence the rate of ES formation and degradation is described by Eq. 3.1 and 3.2 respectively.

$$[ES] = k_1[E][S] \quad 3.1$$

$$[ES] = k_{-1}[ES] + k_2[ES] \quad 3.2$$

During the steady state of a reaction, the rate of ES formation is equal to the rate of ES degradation (Eq. 3.1= Eq. 3.2). However, it is difficult to calculate the concentration of E, S, and ES complex during steady state, hence two steady state assumptions are made as follows. The substrate concentration during the steady state [S] is equal to the total substrate concentration [S_t]

added to the reaction because the amount of substrate in the ES complex is negligible compared to the total substrate concentration. On the other hand, the total concentration of enzyme [E_t] in the reaction is equal to the sum of the substrate bound enzyme (ES) and the free enzyme, hence the concentration of free enzyme during steady state can be described using Eq. 3.3.

$[S] = [S_t]$ Steady state assumption 1

$[E_t] = [E_f] + [ES]$ Steady state assumption 2

$[E_f] = [E_t] - [ES]$ 3.3

Substituting [E] into equation 3.1 gives Eq. 3.4.

$[ES] = k_1([E_t] - [ES])[S]$ 3.4

Since the rate of ES formation is equal to the rate of ES degradation during steady state, Eq. 3.2 is equal to Eq. 3.4, and together gives equation 3.5.

$k_1([E_t] - [ES])[S] = k_{-1}[ES] + k_2[ES]$ 3.5

Rearranging Eq. 3.5 gives Eq. 3.6, where Michealis constant (K_m) is equal to $(k_{-1} + k_2)k_1$

$[ES] = [E_t][S]/[S] + ((k_{-1} + k_2)/k_1)$ 3.6

The breakdown of ES complex to product is the slowest step of a single substrate reaction, hence it is the rate-limiting step of the reaction, and the rate-limiting step of a reaction is used to describe the initial velocity of the reaction, as shown in Eq. 3.7.

$V_0 = k_2[ES]$ 3.7

Substituting Eq. 6 for [ES] in Eq. 3.7 gives Eq. 3.8

$V_0 = (k_2[E_t][S])/S + k_m$ 3.8

The maximum velocity of a reaction occurs when the enzyme is saturated, hence all the enzymes are bound to substrate (ES). As a result, equation 3.9 is used to describe the maximum velocity (V_{max}) of a reaction.

$V_{max} = k_2[E_t]$ 3.9

Rearrangement of Eq. 3.9 and Eq. 3.8 together gives the Michaelis-Menten equation (3.10).

$V_0 = (V_{max}[S])/ K_m + [S]$ 3.10

The initial velocity and the substrate concentration of a reaction can be easily measured using kinetic assays, and M-M plot of initial velocity against the substrate concentration gives a hyperbolic curve from which V_{max} and K_m values can be determined. From the curve, K_m is the substrate concentration at which the rate of the reaction is half its maximum velocity, while V_{max} is the maximum velocity of the reaction for a given enzyme concentration. Since V_{max} changes with enzyme concentration, $k_{cat,}$ which is equal to V_{max} divided by the enzyme concentration, is used to describe the rate of the reaction in this study (Cornish-Bowden, 1995, Nelson, 2008).

2.3.3.1.2 Multi substrate reactions

Single substrate reactions are essential for deriving rate equations but rarely occur *in vivo*. In multi-substrate reactions, two or more substrates are converted to two or more products. Although the rate equations are more complex for these kinds of reactions, the Michaelis constant and Michaelis –Menten equation can be described for these reactions, if one substrate is held constant while the other is varied. As a result, the experimental K_m and V_{max} for these reactions are apparent values, because these values change with changing conditions (Cornish-Bowden 1995). Since PCK catalyzes a multi-substrate reaction, all the kinetic parameters described in this report are apparent values.

2.3.3.1.3 Turn over number

The k_{cat} is a first-order rate constant used to describe the reaction and properties of the enzyme-product, enzyme – intermediate and enzyme – substrate complex (Fersht, 1999). It is also called the catalytic constant because it describes the limiting rate of an enzyme catalyzed reaction. In a single substrate reaction, k_{cat} is equal to k_2, since the conversion of ES to product is the rate-limiting step of the reaction. k_{cat} is also called the turnover number because it also defines the number of catalytic cycles, or turnover, the enzyme can undergo per unit time (Nelson, 2008). Since k_{cat} gives a more accurate representation of the rate at which an enzyme

catalyzes a reaction, changes in k_{cat} are used to describe the how Arg333Gln, Ser250Ala, and Tyr207Phe mutations affect the reaction catalyzed by PCK.

2.3.3.1.4 Kinetic efficiency

Kinetic efficiency is a measure of the ability of an enzyme to accelerate a reaction beyond the rate of the uncatalyzed reaction. It refers to the property and the reaction of the free enzyme and substrate. It is also called specificity constant and is calculated by dividing k_{cat} with K_m (Fersht, 1999, Nelson, 2008).

2.4 X-ray crystallography

2.4.1 *E.coli* PCK Ser250Ala-ATP-Mn^{2+}-Pyruvate Structure

2.4.1.1 Crystallization conditions

Microbatch crystallization under oil was used to grow PCK Ser250Ala crystals complexed with ATP, Mn^{2+} and pyruvate at room temperature. A 2 µl drop containing 3 mg/ml S250A PCK, 5 mM manganese chloride ($MnCl_2$), 5 mM magnesium chloride ($MgCl_2$), 2 mM ATP, 2 mM pyruvate, 1 mM ethylenediaminetetraacetic acid (EDTA), 200 mM ammonium acetate, 100 mM sodium acetate pH 4.8, 0.01 mM 1,4-dithiothreitol (DTT), and 12% (w/v) polyethylene glycol (PEG) 4000 was added to a 2 µl drop containing 0.01 mM nickel chloride, 100 mM Tris(hydroxymethyl)aminomethane (TRIS) pH 8.5, and 20% (w/v) PEG 2000. Rod-like crystals (Fig 2.5) measuring 0.4 mm by 0.2 mm by 0.1 mm formed after 7 days. Crystals were harvested, soaked in cryoprotectant solution containing 30% (v/v) glycerol, 1 mM EDTA, 100 mM sodium acetate, 2 mM ammonium acetate, and 12% PEG 4000 for 10 seconds, and flash-cooled in liquid nitrogen.

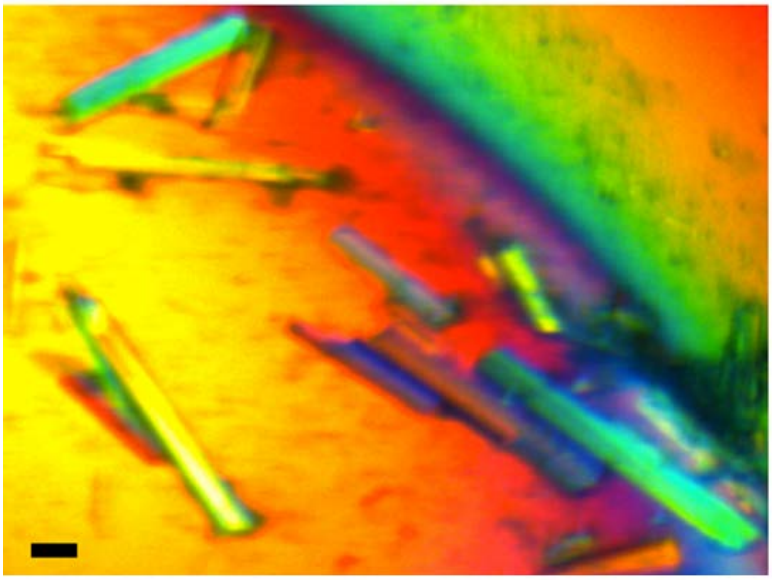

Figure 2.5: Rod-like crystal used for data collection. Scale bar at the bottom left of the figure is 0.1mm

2.4.1.2 Diffraction, Data collection and processing

Diffraction data for Ser250Ala PCK complexed with ATP-Mn^{2+} and pyruvate was collected from a single crystal at a wavelength of 0.88 Å, with a crystal-to-detector distance of 200 mm. Images were recorded on a MX300HE detector using the 08B1-1 beamline at the Canadian Macromolecular Crystallography Facility (CMCF) in Saskatoon. The crystal diffracted to a resolution of 1.5 Å and 250 diffraction images were collected with an oscillation range of 0.5° and an exposure time of 1 second per image. The crystal was kept at 105°K under a cold stream of nitrogen gas during data collection. Diffraction images were processed with d*TREK (Pflugrath, 1999) processing software.

2.4.1.3 Phase Determination, Model Building, Refinement and Structure validation

One molecular replacement solution was found using the coordinates from *E. coli* PCK model PDB accession number 1AYL using Phaser-MR (Mccoy, 2007) in PHENIX (Adams *et al.*, 2010). Since 1AYL is missing residues 390 – 400, and inspection of the electron density for S250A showed that these residues can be built, residues 390 – 400 were built into the S250A model using Coot (Emsley *et al.*, 2010), and structure refinement was performed using

Phenix.Refine (Afonine *et al.*, 2012) in PHENIX . Since the electron density for ATP was very evident in the model, ATP was added to the model. After refinement, the electron densities for pyruvate and Mn^{2+} became evident, and these ligands were also included in the model. After several rounds of model building and structure refinement, no improvement in R-values was observed. As a result, water was added to the model, and the model was built and refined until no improvement in R-values was observed. The model was validated using comprehensive validation (Chen *et al.*, 2010) in PHENIX.

2.4.2 *E.coli* PCK Asp269Asn-ATP-Mg^{2+}-Ca^{2+}-Pyruvate Structure

2.4.2.1 Crystallization conditions

The Asp269Asn *E. coli* PCK mutant previously purified by Novakovski was successfully crystallized by microbatch under oil. A 2 µl drop containing 2 mg/ml D269N PCK, 5 mM $CaCl_2$, 5 mM $MgCl_2$, 2 mM ATP, 2 mM pyruvate, 1 mM EDTA, 200 mM ammonium acetate, 100 mM sodium acetate pH 4.8, 0.01 mM DTT, and 12% (w/v) PEG 4000, was added to a 2 µl drop containing 2 M sodium acetate, 0.1 M Tris pH 8.2, and 30% (w/v) PEG 4000. Rod-like crystals formed after 7days, crystals were harvested, soaked in a cryoprotectant solution containing 30% (v/v) glycerol, 1 mM EDTA, 100 mM sodium acetate, 200 mM ammonium acetate, and 12% PEG 4000 for 10 second and flash-cooled in liquid nitrogen.

2.4.2.2 Diffraction, Data collection and processing

Diffraction data for Asp269Asn PCK complexed with ATP-Ca^{2+} -Mg^{2+} and pyruvate were collected from a single crystal at a wavelength of 0.98 Å, with a crystal-to-detector distance of 300 mm. Images were recorded on the MX300HE detector using the 08B1-1 beamline at the Canadian Macromolecular Crystallography Facility (CMCF) in Saskatoon. 360 diffraction images were collected with an oscillation range of 1° and with an exposure time of 3.5 second per image. The crystal was kept at 105°K under a cold stream of nitrogen gas during data

collection. Diffraction images were processed with HKL 2000 processing software (Otwinowski and Minor, 1997).

2.4.2.3 Phase Determination, Model Building, Refinement and Structure validation

One molecular replacement solution was found using the coordinates from *E.coli* PCK model PDB accession number 1AYL using Phaser-MR (Mccoy, 2007) in PHENIX (Adams *et al.,* 2010). ATP was added to the model, since the electron density for ATP was evident in the model. After refinement using Phenix.Refine (Afonine *et al.,* 2012), the electron densities of pyruvate, Ca^{2+}, and Mg^{2+} became evident, and these ligands were also included in the model. After several rounds of model building and structure refinement, no improvement in R-values was observed. As a result, water was added to the model, and the model was built using Coot (Emsley *et al.,* 2010) and refined until no improvement in R-values was observed. The model was validated using comprehensive validation (Chen *et al.,* 2010) in PHENIX.

2.4.3 *E.coli* PCK Lys254Ser-Ca^{2+}-Pyruvate Structure

2.4.3.1 Crystallization conditions

Lys255Ser PCK, previously purified by Novakovski, was successfully crystallized using microbatch under oil. A 2 µl drop containing 2 mg/ml K254S PCK, 5 mM $MnCl_2$, 5 mM $MgCl_2$, 2 mM ATP, 2 mM pyruvate, 1 mM EDTA, 200 mM ammonium acetate, 100 mM sodium acetate pH 4.8, 0.01 mM DTT, and 10% (w/v) PEG 4000, was added to a 2 µl drop containing 0.2 M calcium chloride ($CaCl_2$), and 20% (w/v) PEG 3350. Rod-like crystals formed after 7 days, were harvested, soaked in cryoprotectant solution containing 30% (v/v) glycerol, 1 mM EDTA, 100 mM sodium acetate, 200 mM ammonium acetate, and 12% PEG 4000 for 10 seconds, and flash-cooled in liquid nitrogen.

2.4.3.2 Diffraction, Data collection and processing

Diffraction data for Lys254Ser PCK complexed with Ca^{2+} and pyruvate were collected from a single crystal at a wavelength of 0.98 Å. Images were recorded on the Mar300CCD detector using the 081D-1 beamline at the Canadian Macromolecular Crystallography Facility (CMCF) in Saskatoon. 250 diffraction images were collected with an oscillation range of 1°, with an exposure time of 1 second per image, at a crystal to detector distance of 220 mm. The crystal was kept at 105°K under a cold stream of nitrogen gas during data collection. Diffraction images were processed with d*TREK (Pflugrath, 1999) processing software.

2.4.3.3 Phase Determination, Model Building, Refinement and Structure validation

One molecular replacement solution was found using the coordinates from *E. coli* PCK model PDB accession number 1OEN using Phaser-MR (Mccoy, 2007) in PHENIX (Adams *et al.*, 2010). After refinement using Phenix.Refine (Adams *et al.*, 2010), the electron densities for pyruvate and Ca^{2+} became evident, and these ligands were included in the model. After several rounds of model building and structure refinement, no improvement in R-values was observed. As a result, water was added to the model, and the model was built using Coot (Emsley *et al,* 2010) and refined until no improvement in R-values was observed. The model was validated using comprehensive validation (Chen *et al.*, 2010) in PHENIX.

2.4.4 *E.coli* PCK Arg65Gln ATP-Mg^{2+}-Mn^{2+} Structure

2.4.4.1 Crystallization conditions

Arg65Gln *E. coli* PCK, previously purified by Novakovski, was successfully crystallized using microbatch under oil. A 2 µl drop containing 8 mg/ml R65Q PCK, 5 mM $MnCl_2$, 5 mM $MgCl_2$, 2 mM ATP, 2 mM pyruvate, 1 mM EDTA, 200 mM ammonium acetate, 100 mM sodium acetate pH 4.4, and 12% (w/v) PEG 4000 was added to a 2 µl drop containing 0.2 M magnesium acetate and 20% (w/v) PEG 3350. Rod-like crystals formed after 7days, were

harvested, soaked in a cryoprotectant solution containing 30% (v/v) glycerol, 1 mM EDTA, 100 mM sodium acetate, 200 mM ammonium acetate, and 12% PEG 4000 for 10 seconds, and flash-cooled in liquid nitrogen.

2.4.4.2 Diffraction, Data collection and processing

Diffraction data for Arg65Gln PCK complexed with ATP-Mn^{2+} and pyruvate were collected from a single crystal at a wavelength of 0.98 Å. Images were recorded on the Mar300CCD detector using the 081D-1 beamline at the Canadian Macromolecular Crystallography Facility (CMCF) in Saskatoon. 200 diffraction images were collected with an oscillation range of 1° at a crystal-to-detector distance of 250 mm, with an exposure time of 1 second per image. The crystal was kept at 105°K under a cold stream of nitrogen gas during data collection. Diffraction images were processed with d*TREK (Pflugrath and JW, 1999) processing software.

2.4.4.3 Phase Determination, Model Building, Refinement and Structure validation

One molecular replacement solution was found using the coordinates from *E. coli* PCK model PDB accession number 1AYL using Phaser-MR (Mccoy, 2007) in PHENIX (Adams *et al.*, 2010). Since the electron density for ATP was very evident in the model, ATP was added to the model. After refinement using Phenix.Refine (Adams *et al.*, 2010), the electron densities for Mn^{2+} became evident and were also included in the model. After several rounds of model building and structure refinement, no improvement in R-values was observed. Consequently, water was added to the model, and the model was built using Coot (Emsley *et al.*, 2010) and refined until no improvement in R-values was observed. The model was validated using comprehensive validation (Chen *et al.*, 2010) in PHENIX.

3.0 Results

3.1 Site-directed mutagenesis

3.1.1 Restriction digest screens of mutants

Restriction digest screening was performed on mutant plasmids isolated using an alkaline lysis method. Migration of the fragment generated from mutant plasmids was compared to that of wild type pDBss, and molecular size standards were used to approximate the size of the fragments. As shown in Figure 3.1, digestion of pY207F (pDBss with Tyr207Phe mutation) with *KpnI* and *BssHII* produced fragments with the expected size of 1247 bp and 3503 bp. Digestion of pR333Q with *BsaI* did not produce fragments with the expected sizes of 450 bp, 1751 bp, and 2549 bp. Rather, two fragments of 2999 bp and 1751 bp similar to pDBss were produced (Fig 3.2).

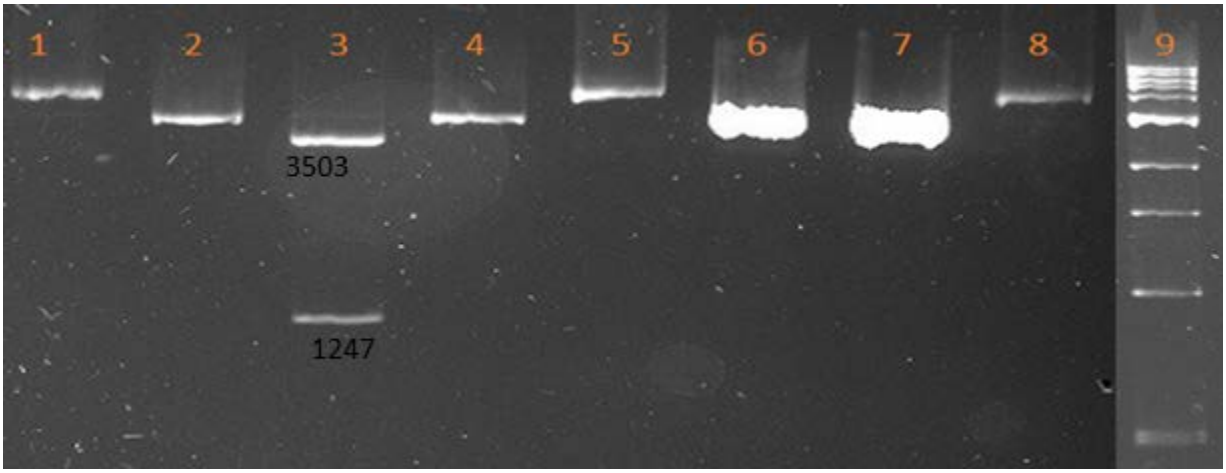

Figure 3.1: Restriction digest of pY207F and pDBss with *KpnI* and *BssHII*. Plasmid Y207F is present in lanes 1-4, while lanes 5-8 contain pDBss. No restriction enzyme is present in lanes 1 and 5, lanes 2 and 6 contain *BssHII* restriction enzyme, while lanes 4 and 8 contain *KpnI* restriction enzyme. *BssHII* and *KpnI* restriction enzymes are present in lanes 3 and 7. Lane 9 contains pDBss molecular weight standard, digest were several times and similar result was obtained.

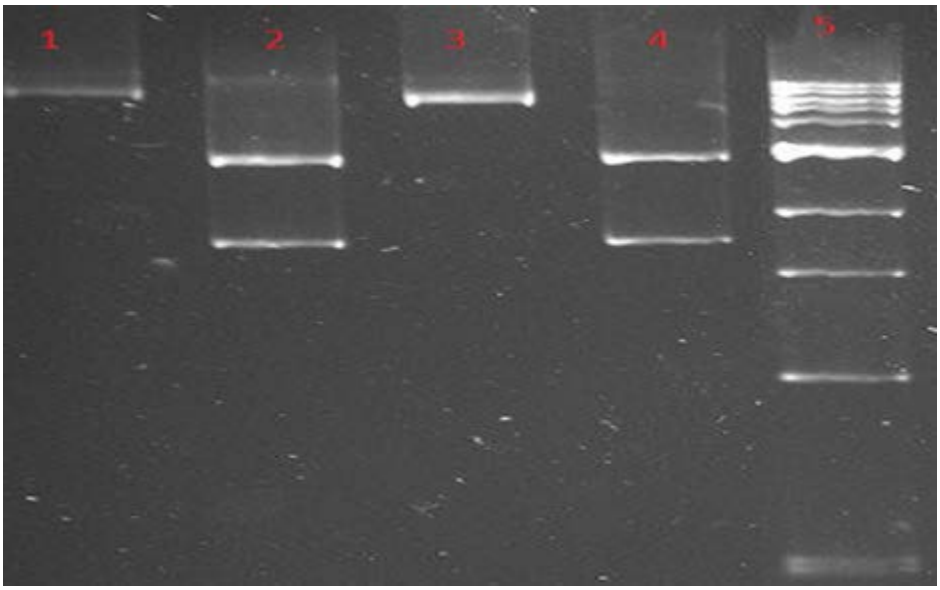

Figure 3.2: Restriction digest of pR333Q and pDBss with *BsaI* restriction enzyme: lanes 1 and 2 contain pR333Q, while lanes 3 and 4 contain pDBss. No restriction enzyme is present in lanes 1 and 3, while lanes 2 and 4 contain *BsaI* restriction enzyme. Lane 5 contains pDBss molecular weight standards. Digest were several times and similar result was obtained.

3.1.2 Sequencing results

The Sanger sequencing technique was used at the National Research Council Plant Biotechnology Institute to confirm the presence of the desired mutations (Fig. 3.3). All mutant plasmids contained the desired mutation, including pR333Q, which did not produce the correct-sized fragments during restriction digest screen.

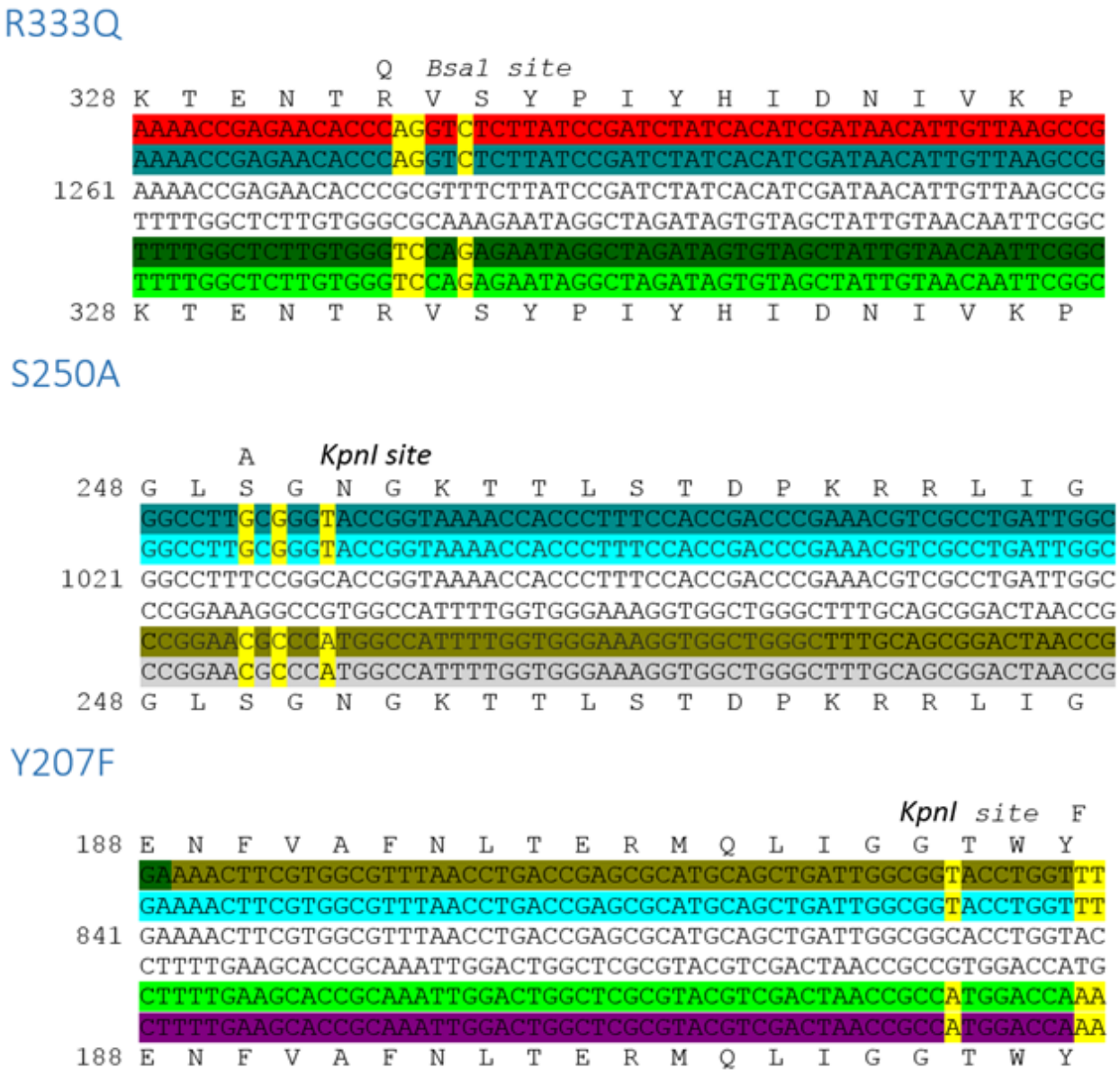

Figure 3.3: Sanger sequencing results obtained for each mutant. Each color represents a unique oligonucleotide used to sequence the *pckA* gene.

3.2 Protein purification

3.2.1 Culture growth on minimal medium plates

E. coli HG89 used in this study is *pckA*$^{-}$ and *pps*$^{-}$, as a result, it is unable to grow on pyruvate or succinate in the absence of plasmids containing *pckA* or *pps*. HG89 is also *recA1*$^{-}$, *his*$^{-}$, *tyr*$^{-}$, *pyrD*$^{-}$ and *argG*$^{-}$, hence it is sensitive to ultraviolet (UV) light damage, and requires histidine, tyrosine, uridine, and arginine for growth (Table 2.4). Transformation of *E.coli* HG89

with a pDBss or pDBss mutated plasmid restored its ability to grow on succinate, while slow or no growth on pyruvate was observed. Other phenotypes such as its sensitivity to UV damage and its requirement of histidine, tyrosine, uridine, and arginine for growth are still present in the transformed HG89 strain.

Table 3.1: Phenotype of *E. coli* K12 HG89 strain

Strain	Growth on carbon[A] source			Growth on medium lacking amino acid supplement[B]						Antibiotic[C]
	Glucose	Pyruvate	Succinate	Pro	His	Tyr	Ur	Arg	UV[c]	Ampicillin
HG89	+	-	-	+	-	-	-	-	S	-
HG89/pDBss	+	+/-	+	+	-	-	-	-	S	+

A. growth on plate with Medium A supplemented with 0.4% carbon source, 0.01% proline (pro), 0.01% histidine (His), 0.01% tyrosine (Tyr), 0.05% Uridine and 0.01% arginine (Arg)
B. growth on plate with Medium A lacking Pro or His or Tyr or Ur or Arg, supplemented with 0.4% glucose
C. growth on LB plate after exposure to u.v light for 20 secs.
+ Growth on plate, -No growth on plate, S- no growth after exposure to u.v, R- growth after exposure to u.v. (U.V sensitivity, cells were irradiated in the dark and plates were wrapped with aluminum foil to prevent photoreactivation)

3.2.2 Protein purification using DEAE cellulose and calcium phosphate column

SDS-Page gels of the fractions eluted from DEAE column showed that DEAE cellulose was effective at isolating but not purifying PCK from crude extract (Fig 3.3), hence ultra-gel filtration was used to further purify the fractions containing PCK (Fig 3.4). Pure PCK fractions were pooled together and dialyzed with 12 L of water, which was changed three times in 24 hours. Dialyzed PCK samples were lyophilized and stored at -20°C. For exchange assays, lyophilized PCK samples were dissolved in TE buffer and used at concentrations that produced below 40,000 counts per minute, since ^{14}C-bicarbonate was used at 400,000 counts per minute. 0.23 mg/ml, 0.24 mg/ml, 0.44 mg/ml, and 4.99 mg/ml of wild type Tyr207Phe, Ser250Ala, and Arg333Gln were used for exchange assays, respectively.

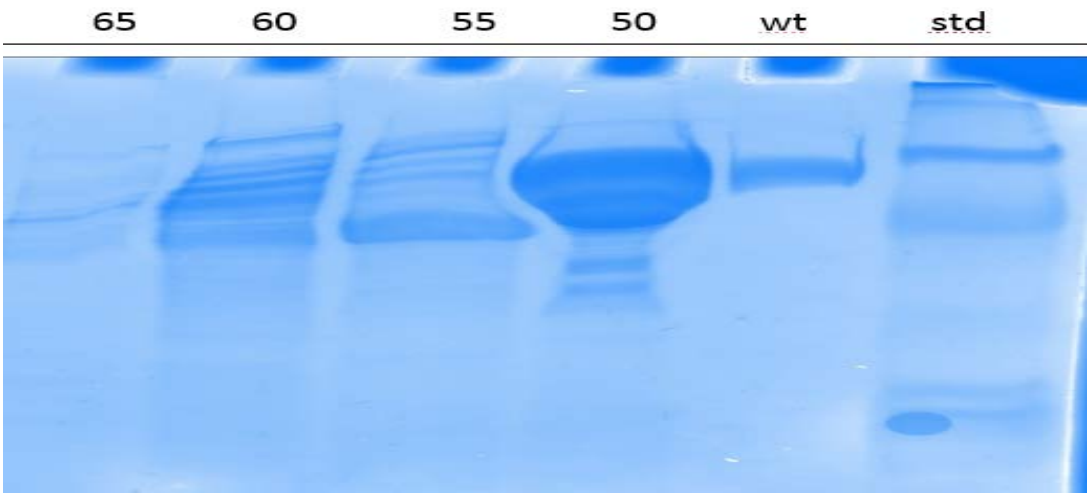

Figure 3.4: Early fractions collected from DEAE cellulose. R333Q PCK mutant is mainly present in fraction 50.

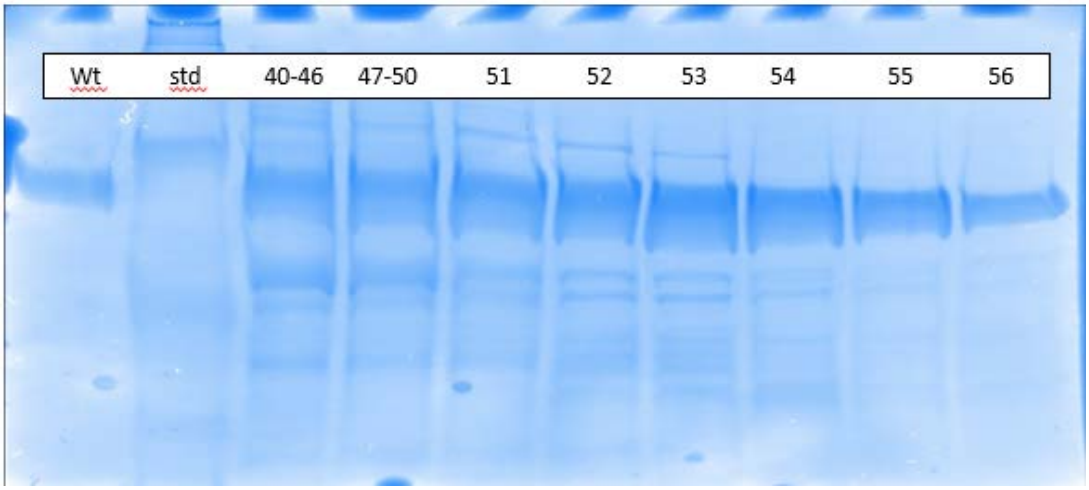

Figure 3.5: Fractions collected from ultra-gel filtration column

3.3 Enzyme assays and kinetics

3.3.1 Exchange assay results

Kinetic assays on the purified proteins using exchange assays were analyzed using the GraphPad Prism, which uses three methods of data analysis to evaluate data. The methods of analysis used are Non-linear (NL), Lineweaver-Burk (LB), and Eadie-Hofstee (EH) regression, which are used to generate Michaelis –Menten (M-M), Lineweaver-Burk, and Eadie-Hofstee plots, respectively. Michaelis –Menten plots give a rectangular hyperbola from which kinetic

parameters such as V_{max} and K_m can be obtained. However, the Michaelis –Menten (M-M) equation has been rearranged to produce other equations, such as the Lineweaver-Burk and Eadie-Hofstee equations, which give linear plots. The Lineweaver-Burk equation allows the generation of a plot of $1/v_0$ against $1/[S]$, which gives a straight line with a positive slope, where v_0 is the initial velocity and [S] the substrate concentrations. Eadie-Hofstee plots of v_0 vs $v_0/[S]$ give a straight line with a negative slope, however because v is on both axes, errors in measuring v are multiplied and result in low precision in the K_m and V_{max} values obtained with is plot. This also makes it difficult to include error bars in this plot when assay are replicated at a constant substrate concentration. While Lineweaver-Burk plot overemphasizes small errors in small values of initial velocity, Eadie-Hofstee plots overemphasizes errors in large v/[S] values, hence M-M plots are the best for the determination of kinetic parameters. Lineweaver-Burk and Eadie-Hofstee plots are mainly used for enzyme inhibition studies, for the determination of reaction types (Cornish-Bowden 1995, Nelson, 2008) and kinetic parameters obtained from them are used to compare those obtained from M-M plot in other to detect errors in experimental data. In this study, kinetic parameters obtained from Lineweaver-Burk and Eadie-Hofstee plots are compared to those obtained using M-M plots; however, final parameters for each mutate are obtained from M-M plots. Changes in values below 3-fold were generally not considered significant.

3.3.1.1 Kinetic parameters obtained for wild type

The K_m and V_{max} values obtained from all methods for Mg^{2+}ATP with and without Mn^{2+} or Ca^{2+} for wild type are less than 3-fold different from each other, while some of the values obtained for OAA are more than 3-fold different from each. No kinetic parameters for OAA in the presence of Mn^{2+} were obtained, because the data did not fit into a standard M-M curve, and increasing concentrations of OAA lead to precipitate formation, hence initial velocities obtained could not be regenerated. During exchange assays, counts per minute obtained for low

concentrations of OAA are very low, hence initial velocities calculated at these concentrations are less accurate and introduce errors in my data. The limited precision of the stability constants for OAA-metal complex (Gelles *et al.,* 1958) used for the determination of OAA concentrations required for assay in COMICS, may be responsible for the inaccurate initial velocities of the enzyme at low concentrations of OAA, hence the more than 3-fold difference in the values obtained for OAA. Using values obtained from M-M plots for data analysis, in the presence of Ca^{2+}, V_{max} increased by 4-fold under changing OAA concentrations, while V_{max} increased by 6-fold in the presence of Mn^{2+} and Ca^{2+} ion, when Mg^{2+}ATP concentrations were varied. In most cases K_m values changed by less than 3-fold in the presence of Mn^{2+} and Ca^{2+} ions. (Table 3.2).

Table 3.2: Kinetic parameters for wild type PCK enzyme obtained using GraphPad Prism

Varied substrate		OAA		Mg^{2+}ATP		
Constant substrate		[1]	[2]Ca^{2+}	[3]	[4]Mn^{2+}	[4]Ca^{2+}
Method	Parameters					
Nonlinear regression	K_m (mM)	1.84 ± 0.5	1.89 ± 0.2	0.49 ± 0.2	0.56 ± 0.07	0.13 ± 0.03
	V_{max} (µmol/min/mg)	4.75 ± 0.4	16.64 ± 0.6	2.94 ± 0.2	16.94 ± 0.7	16.9 ± 0.8
Linewaver-Burk regression	K_m (mM)	-0.012 ± 0.03	1.13 ± 0.3	-0.2 ± 0.03	-1.3 ± 0.03	-0.11 ± 0.003
	V_{max} (µmol/min/mg)	0.078 ± 0.2	-0.3 ± 0.7	1.01 ± 2.6	20.6 ± 6.6	12.37 ± 4.8
Eadie-Hoftsee regression	K_m (mM)	-0.097 ± 0.1	-0.64 ± 0.9	-0.63 ± 0.2	-0.72 ± 0.2	-0.15 ± 0.02
	V_{max} (µmol/min/mg)	1.76 ± 0.6	9.58 ± 3.6	2.83 ± 0.4	16.5 ± 3.2	17.02 ± 1.4

[1]Assays carried out under changing concentrations of OAA and constant Mg^{2+}-ATP concentrations. [2]Assays were performed under changing concentrations of OAA and constant Ca^{2+} and Mg^{2+}-ATP concentrations. [3]Assays were performed changing concentrations of Mg^{2+}-ATP and constant OAA concentration. [4]Assays were performed with changing Mg^{2+}-ATP concentrations, and constant OAA and Ca^{2+} or Mn^{2+} concentrations. Errors is standard error. Assays in the presence of Ca^{2+} were performed 12 times while other assays was performed 9 times.

3.3.1.2 Kinetic parameters obtained for the Tyr207Phe PCK mutant

K_m's and V_{max}'s for Mg^{2+}ATP displayed by Tyr207Phe PCK mutant obtained using all methods are less than 3-fold different from one another. The K_m and V_{max} values for OAA obtained using M-M and EH are less than 5-fold different from each other except in one case where 10 fold they are different, indicating errors in my data. As observed with wild type low count per minute were obtained for low OAA concentrations, and initial velocities calculated for

these OAA concentrations introduced error in my data. However, kinetic parameters obtained using M-M plot are discussed and used for k_{cat} calculation. In the presence of Mn^{2+} and Ca^{2+} change in the K_m for OAA was less than 3-fold; however, V_{max} increased by 1.7- and 4.4-fold, respectively. K_m for Mg^{2+}ATP decreased by 7-fold, while V_{max} increase by 2.9-fold in the presence of Ca^{2+} (Table 3.3).

Table 3.3: Kinetic parameters for Tyr207Phe PCK mutant obtained using GraphPad Prism

Varied substrate		OAA			Mg^{2+}ATP		
Constant substrate		[1]	[2]Mn^{2+}	[2]Ca^{2+}	[3]	[4]Mn^{2+}	[4]Ca^{2+}
Method	Parameters						
Nonlinear regression	K_m (mM)	0.98 ± 0.1	2.0 ± 0.4	0.57 ± 0.05	0.36 ± 0.09	0.39 ± 0.09	0.051 ± 0.02
	V_{max} (µmol/min/mg)	1.93 ± 0.06	3.32 ± 0.2	8.5 ± 0.2	2.55 ± 0.1	2.87 ± 0.2	7.56 ± 0.5
Linewaver -Burk regression	K_m (mM)	-0.33 ± 0.03	-0.69 ± 0.03	2.6 ± 0.1	-0.28 ± 0.03	-0.16 ± 0.003	-0.068 ± 2.6
	V_{max} (µmol/min/mg)	0.35 ± 0.2	0.33 ± 0.2	-11.7 ± 6.8	1.27 ± 3.4	1.3 ± 0.0003	7.16 ± 4.5
Eadie-Hoftsee regression	K_m (mM)	-0.88 ± 0.3	-0.51 ± 1.2	-0.75 ± 0.3	-0.56 ± 0.1	-0.34 ± 0.05	-0.066 ± 0.01
	V_{max} (µmol/min/mg)	1.55 ± 0.3	1.34 ± 0.8	8.2 ± 1.4	2.57 ± 0.4	2.66 ± 0.3	7.74 ± 0.7

[1]Assays carried out under changing concentrations of OAA and constant Mg^{2+}-ATP concentrations. [2]Assays were performed under changing concentrations of OAA and constant Mn^{2+} or Ca^{2+} and Mg^{2+}-ATP concentrations. [3]Assays were performed changing concentrations of Mg^{2+}-ATP and constant OAA concentration. [4]Assays were performed with changing Mg^{2+}-ATP concentrations, and constant OAA and Ca^{2+} or Mn^{2+} concentrations. Errors is standard error. Assays in the presence of Ca^{2+} were performed 12 times while other assays was performed 9 times.

3.3.1.3 Kinetic parameters obtained for the Ser250Ala PCK mutant

In most cases, K_m and V_{max} values for Ser250Ala mutant obtained using M-M and EH are less than 3-fold different from each other, while LB values are more than 3-fold different from M-M and EH values. Low initial velocities calculate for Ser250Ala PCK mutant at low concentrations of OAA, introduced errors in my data. Data obtained for OAA with Mn^{2+} did not follow standard M-M kinetics and were not reproducible, hence no kinetic data were obtained for OAA with Mn^{2+}. Using values obtained by M-M for analysis, the presence of Ca^{2+} did not change the K_m and V_{max} of OAA in the Ser250Ala PCK mutant, while K_m and V_{max} for Mg^{2+}ATP in the presence of Mn^{2+} increased 4- and 11-fold respectively (Table 3.4).

Table 3.4: Kinetic parameters for Ser250Ala PCK mutant obtained using GraphPad Prism

Varied substrate		OAA		Mg^{2+}ATP		
Constant substrate		[1]	[2]Ca^{2+}	[3]	[4]Mn^{2+}	[4]Ca^{2+}
Method	Parameters					
Nonlinear regression	K_m (mM)	2.4 ± 0.6	2.3 ± 0.3	0.69 ± 0.1	3.0 ± 0.6	0.22 ± 0.06
	V_{max} (µmol/min/mg)	0.67 ± 0.05	0.69 ± 0.024	0.68 ± 0.03	7.9 ± 0.9	0.74 ± 0.052
Linewaver-Burk regression	K_m (mM)	0.24 ± 0.03	-0.53 ± 0.1	-0.13 ± 0.03	-0.15 + 0.05	-0.055 ± 0.03
	V_{max} (µmol/min/mg)	-0.007 ± 0.004	0.15 ± 0.3	0.27 ± 0.6	0.52 ± 1.2	0.35 ± 1.05
Eadie-Hoftsee regression	K_m (mM)	-2.1 ± 0.8	-1.74 ± 0.6	-0.25 ± 0.07	1.3 ± 0.7	-0.092 ± 0.03
	V_{max} (µmol/min/mg)	0.51 ± 0.1	0.56 ± 0.1	0.5 ± 0.08	3.8 ± 1.5	0.59 ± 0.08

[1]Assays carried out under changing concentrations of OAA and constant Mg^{2+}-ATP concentrations. [2]Assays were performed under changing concentrations of OAA and constant Ca^{2+} and Mg^{2+}-ATP concentrations. [3]Assays were performed changing concentrations of Mg^{2+}-ATP and constant OAA concentration. [4]Assays were performed with changing Mg^{2+}-ATP concentrations, and constant OAA and Ca^{2+} or Mn^{2+} concentrations. Errors is standard error. Assays in the presence of Ca^{2+} were performed 12 times while other assays was performed 9 times.

3.3.1.4 Kinetic parameters obtained for the Arg333Gln PCK mutant

The K_m and V_{max} values obtained by all methods for the Arg333Gln mutant, are more than 3-fold different from each other, indicating error in my data. However, this is due to the very low counts per minute obtained with this mutant, even when high concentrations of Arg333Gln were used for assays. Less accurate initial velocities calculated at low OAA concentrations also introduced error in my data, hence the difference in the kinetic parameters obtained from all method. However, values obtained with M-M plots are discussed and used for k_{cat} determination. K_m for OAA in this mutant is high, especially in the presence with Mn^{2+}, where K_m increased 3-fold. K_m for Mg^{2+}ATP is also high in the presence of Mn^{2+}, but decreased by 7-fold in the presence of Ca^{2+}.

Table 3.5: Kinetic parameters obtained for Arg333Gln mutant using GraphPad Prism

Varied substrate		OAA			Mg^{2+}ATP		
Constant substrate		[1]	[2]Mn^{2+}	[2]Ca^{2+}	[3]	[4]Mn^{2+}	[4]Ca^{2+}
Method	Parameters						
Nonlinear regression	K_m (mM)	1.89 ± 0.4	5.96 ± 1.1	1.02 ± 0.15	0.29 ± 0.08	3.9 ± 1.6	0.04 ± 0.01
	V_{max} (µmol/min/mg)	0.02 ± 0.001	0.15 ± 0.01	0.03 ± 0.001	0.02 ± 0.001	0.1 ± 0.02	0.03 ± 0.002
Linewaver -Burk regression	K_m (mM)	-0.05 ± 0.03	-0.19 ± 0.03	-0.35 ± 0.1	-0.04 ± 0.03	-0.09 ± 0.03	-0.41 ± 0.03
	V_{max} (µmol/min/mg)	0.003 ± 0.01	0.013 ± 0.02	0.02 ± 0.2	0.01 ± 0.05	0.02 ± 0.06	0.09 ± 0.02
Eadie-Hoftsee regression	K_m (mM)	-0.26 ± 0.1	-0.4 ± 0.25	-0.5 ± 0.08	-0.02 ± 0.01	-0.26 ± 0.1	-0.04 ± 0.009
	V_{max} (µmol/min/mg)	0.01 ± 0.003	0.048 ± 0.02	0.03 ± 0.002	0.011 ± 0.002	0.04 ± 0.09	0.03 ± 0.002

[1]Assays carried out under changing concentrations of OAA and constant Mg^{2+}-ATP concentrations. [2]Assays were performed under changing concentrations of OAA and constant Mn^{2+} or Ca^{2+} and Mg^{2+}-ATP concentrations. [3]Assays were performed changing concentrations of Mg^{2+}-ATP and constant OAA concentration. [4]Assays were performed under changing Mg^{2+}-ATP concentrations, and constant OAA and Ca^{2+} or Mn^{2+} concentrations. Errors is standard error. Assays in the presence of Ca^{2+} were performed 12 times while other assays was performed 9 times.

3.4 X-ray Crystallography results

3.4.1 *E.coli*-Ser250Ala-PCK-ATP-Mn^{2+}-pyruvate Structure

The S250A-PCK crystal diffracted to a resolution of 1.8Å. After the last round of electron density fitting and model refinement, the final structure has a R_{work} of 0.16 and R_{free} of 0.21. Data collection and refinement statistics for the S250A-PCK mutant structure are shown in Table 3.6.

Table 3.6: Data collection and refinement statistics for Ser250Ala-PCK-ATP-Mn^{2+}-pyruvate structure. Values in parentheses are for the highest resolution shell.

Unit cell	
Space group	C 1 2 1
a (Å)	124.9
b (Å)	94.4
c (Å)	46.2
α (deg.)	90
β (deg.)	96.1
γ (deg.)	90
Data collection	
No. molecules in asymm. unit	1
Resolution range (Å)	38.97 – 1.80 (1.86 -1.80)
No. reflections measured	130208
No. unique reflections	48267
Completeness (%)	97.61 (98.32)
Redundancy	2.70 (2.63)
Mean I/σ(I)	13.5 (4.6)
R-merge	0.047 (0.195)

R-meas	0.058 (0.238)
Refinement statistics	
Resolution range (Å)	38.97 – 1.8 (18.64 – 1.8)
R_{free}	0.2109 (0.2834)
R_{work}	0.1615 (0.2213)
Total no of reflections	48192 (4866)
No. non-H protein atoms	4711
No. water molecules	536
Wilson B-factor	17.92
R.m.s. deviations from ideal geometry	
Bond distances (Å)	0.007
Bond angles (deg.)	1.11
Dihedral angles (deg.)	13.51
Ramachandran statistics	
Favored (%)	98
Allowed (%)	2.27
Outliers (%)	0.19
Clashscore	7.65
Average B-factor	21.50
macromolecules	20.60
Ligands	19.30
Solvent	28.50

Alignment of the atomic coordinates of Ser250Ala-PCK-ATP-Mn^{2+}-pyruvate structure, with wild type PCK-ATP-Mn^{2+}-Mg^{2+}-pyruvate structure, highlighted no noticeable difference in the position of the residues. However, Mn^{2+} instead of Mg^{2+} is complexed with ATP, hence Mn^{2+} is bound at two sites in the Ser250Ala mutant structure. The average distance between β- and γ-phosphate oxygen's of ATP and Mn^{2+} is 2.0Å compared to 2.1Å when Mg^{2+} is bound. The second Mn^{2+} is in a slightly distorted octahedral coordination with His232, Lys213, Asp269, two water molecules, and the γ-phosphate oxygen of ATP as observed in wild type PCK-ATP-Mn^{2+}-Mg^{2+}-pyruvate structure. However, the average coordination distance between Mn^{2+} and its coordinating ligands in this structure is 2.12 Å (Fig 3.6), instead of 2.68 Å (Fig 1.9) observed in the wild type structure. The ATP to pyruvate distance in the wild type structure is 4.3 Å (Fig 1.8), while the ATP to pyruvate distance in the Ser250Ala PCK mutant structure is 4.1 Å (Fig 3.6).

Ser250 is part of the kinase1a-loop essential for Mg^{2+}-ATP coordination, as shown in Figure 1.5. In the wild type PCK-ATP-Mn^{2+}-Mg^{2+}-pyruvate structure, Ser250 is hydrogen-bonded to one of the γ-phosphate oxygen's of ATP. Mutating Ser250 to Ala eliminates its ability to form an H-bond, and decrease the angle between residue 250 and one γ-phosphate oxygen of ATP from 137° observed in the wildtype to 130.8°. Therefore this mutation causing the γ-phosphate of ATP to be slightly extended toward pyruvate, hence the reduced ATP-to-pyruvate distance observed in the structure. In the wild type structure containing Mn^{2+}, the distance between the CH_2 group of pyruvate and the hydroxyl group of Tyr207 is 4.3. However, this distance is increased to 4.7 Å in the Ser250Ala PCK mutant structure, and also contributes to the reduced distance between the γ-phosphate of ATP and pyruvate measured in this structure.

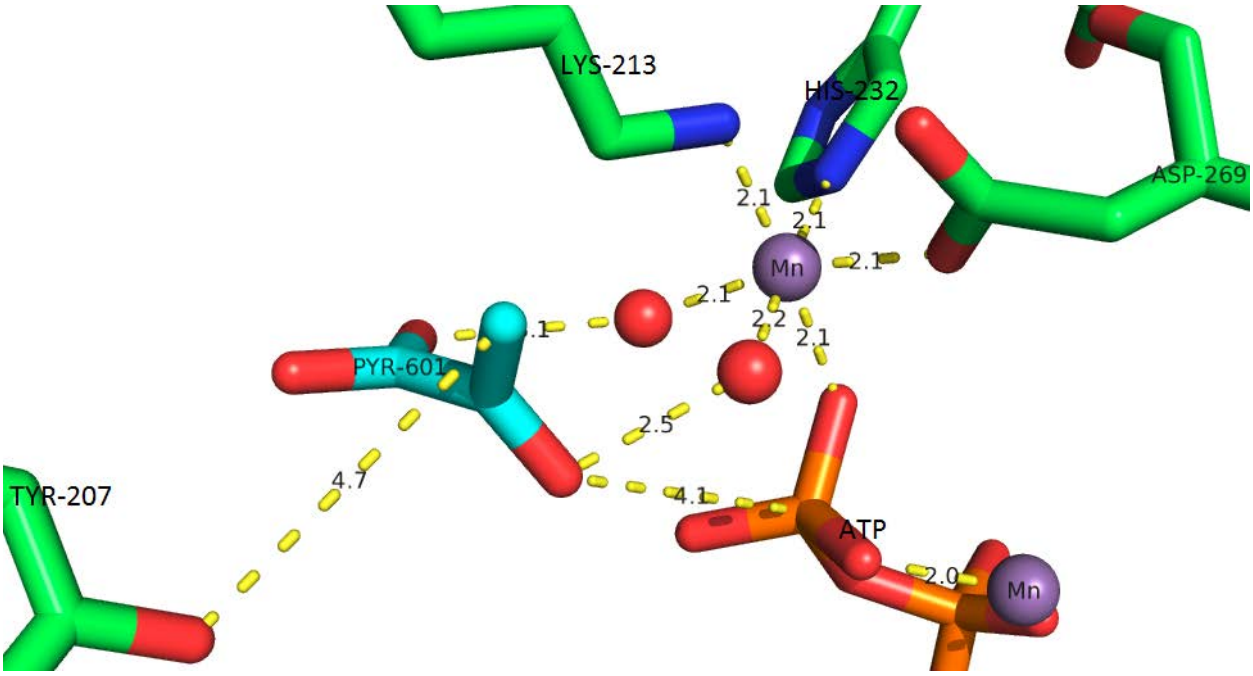

Figure 3.6: The octahedral coordination of Mn^{2+} in *E.coli* Ser250Ala-PCK-ATP-Mn^{2+}-pyruvate structure. Mn^{2+} is coordinated by Asp269, His232, Lys213 and two water molecules, which are interacting with pyruvate. Tyr207 is 4.7 Å away from the CH_2 group of pyruvate, while γ-phosphate of ATP is 4.1Å away from the carbonyl oxygen of pyruvate. A second Mn^{2+} ion forms a Mn^{2+}-ATP complex with ATP. Image was made with Pymol (DeLano, 2002).

3.4.2 *E.coli* PCK Asp269Asn-ATP-Mg^{2+}-Ca^{2+}-Pyruvate Structure

The D269N-ATP-Mg^{2+}-Ca^{2+}-pyruvate crystal diffracted to 2.3Å resolution. After the last round of electron density fitting and model refinement, the final structure has R_{work} and R_{free} of 0.16 and 0.22, respectively. Gly410 and Asp307 are in Ramachandran disallowed regions (Table 3.7); however, comparison of this structure with other PCK structures showed that Gly410 is always in a disallowed region, while Asp307 is usually in an allowed region. Compared to other PCK structures, D269N is one of the lowest-diffracting PCK crystals obtained so far; hence more constraints are applied to this structure during refinement. This is probably why Asp307 is in a disallowed region in this structure, because alignment of D269N Asp307 with other PCK structures shows that Asp307 in the D269N structure is in a similar position.

Table 3.7: Data collection and refinement statistics for Asp269Asn-PCK-ATP-Mg^{2+}-Mn^{2+}-pyruvate structure. Values in parentheses are for the highest resolution shell.

Unit cell	
Space group	C 1 2 1
a (Å)	124.6
b (Å)	94.18
c (Å)	46.46
α (deg.)	90
β (deg.)	94.77
γ (deg.)	90
Data collection	
No. molecules in asymm. unit	1
Resolution range (Å)	50 – 2.11 (2.15 – 2.11)
No. reflections measured	186602
No. unique reflections	
Completeness (%)	100 (100)
Redundancy	6.1 (5.4)
Mean I/σ(I)	39.175 (11.19)
R-symm	0.088 (0.25)
Refinement statistics	
Resolution range (Å)	47.09 – 2.3 (2.382 – 2.3)
R_{free}	0.22 (0.26)
Rwork	0.16 (0.16)
Total no of reflections	23811 (2360)
No. non-H protein atoms	4359
No. water molecules	4089
Wilson B-factor	22.99
R.m.s. deviations from ideal geometry	
Bond distances (Å)	0.008

Bond angles (deg.)	1.09
Dihedral angles (deg.)	
Ramachandran statistics	
Favored (%)	97
Allowed (%)	2.62
Outliers (%)	0.38
Clashscore	6.52
Average B-factor	24.20
macromolecules	24.10
Ligands	24.50
Solvent	26.40

Alignment of the Asp269Asn-ATP-Mg^{2+}-Ca^{2+}-pyruvate structure with the wild type *E. coli* PCK-ATP-Mg^{2+}-Ca^{2+}-pyruvate structure showed that Ca^{2+} is 2.2 Å away from its position in the wild type structure, and is coordinated by one γ-phosphate oxygen of ATP and two water molecules (Fig 3.7). One of the water molecules coordinating Ca^{2+} is interacting with His232, Asn269, and Lys213, which are directly coordinating Ca^{2+} in the wild type structure. Lys213 is interacting with the carbonyl oxygen of pyruvate, which is 6.1 Å away from the γ-phosphate of ATP. In the wildtype structure with Ca^{2+}, Tyr207 is interacting with the CH_2 group of pyruvate, however in D269N mutant structure with Ca^{2+}, Tyr207 is interacting with one of the carboxyl oxygen of pyruvate (Fig. 3.7).

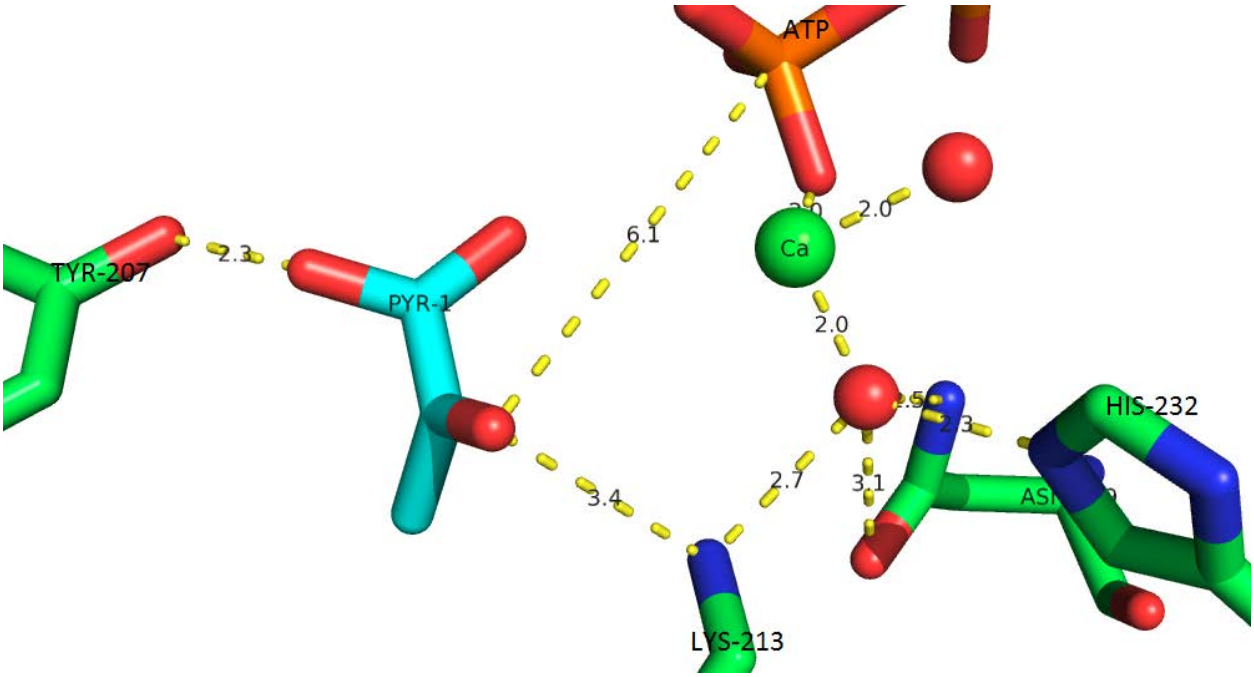

Figure 3.7: Ca^{2+} coordination in *E. coli* Asp269Asn-PCK-ATP-Mg^{2+}- Ca^{2+}-pyruvate structure. Ca^{2+} is coordinated by two molecules and one γ-phosphate oxygen of ATP. Asn269, His232 and Lys213 are interacting with one of the water molecules coordinating Ca^{2+}. Pyruvate is interacting with Lys213 and Tyr207. The γ-phosphate group of ATP is 6.1 Å away from the carbonyl group of pyruvate. Image was made with Pymol (DeLano, 2002).

Although adenine base, ribose sugar, the α- and β- phosphate group of ATP are still in similar positions found in the wild type structure, the γ-phosphate of ATP is 0.89 Å away from its position in the wild type structure. Mg^{2+} is 1.2 Å away from its position in the wild type structure and is coordinated by α, β and γ-phosphate oxygen of ATP, one water molecule, and Thr255. In the wild type structure, Mg^{2+} is coordinated by β-γ-phosphate oxygen's of ATP, three water molecules, and Thr255. Asp268 is indirectly coordinating Mg^{2+} through Thr255, instead of a water molecule. In the wild type structure, Lys254 is interacting with the β and γ-phosphate groups of ATP, however it is interacting with only the β-phosphate group of ATP in Asp269Asn mutant structure (Fig 3.8).

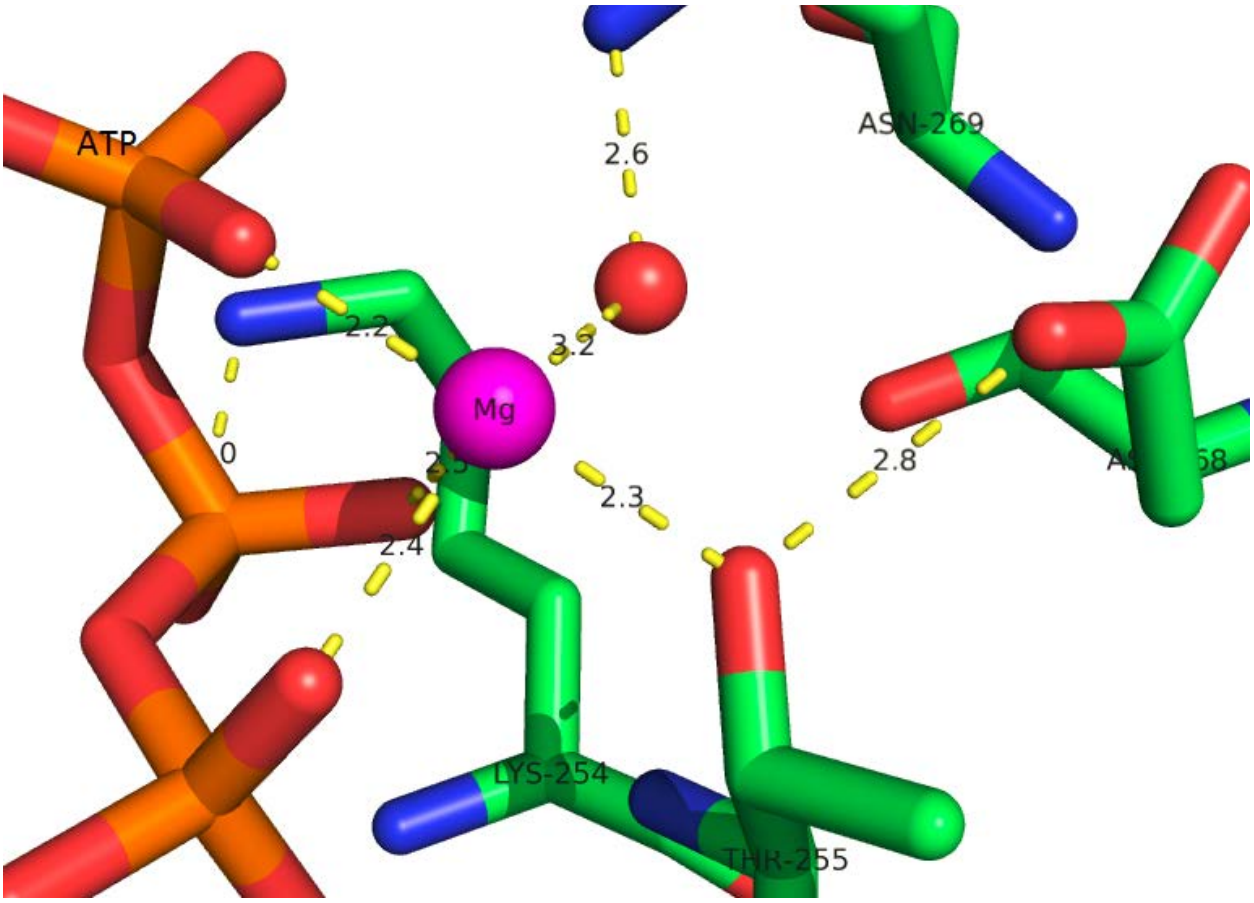

Figure 3.8: The coordination of Mg^{2+} in *E.coli* D269N-PCK-ATP-Mg^{2+}- Ca^{2+}-pyruvate structure. Mg^{2+} is coordinated by one α, β and γ-phosphate oxygen of ATP, one water molecule that is H-bonded to Asn269 and Thr255 which is interacting with Asn268. Lys542 is interacting with one β-phosphate oxygen of ATP. Image was made with Pymol (DeLano 2002).

Kinetic assays performed by Novakovski showed that the K_{cat} of D269N mutant is 15-fold less than the wild type, while K_m for OAA and Mn^{2+} are increased by about 240- and 1000-fold, respectively. Distorted coordination of Ca^{2+} observed in this structure supports the high K_m for Mn^{2+} observed by Novakovski, since Mn^{2+} and Ca^{2+} bind to similar sites in *E. coli* PCK. The Asp269Asn structure can be used to explain the high K_m for OAA displayed by this mutant. In the wild type structure, Lys213 coordinates Ca^{2+}; however, it interacts with the carbonyl group of pyruvate (3.4 Å away) in the D269N structure. Since Lys212 and Phe413 cause the pK_a of Lys213 to be reduced in *E.coli* PCK, electrostatic repulsion between Lys213 and OAA reduce the affinity of the enzyme for OAA, hence the high K_m for OAA observed by Novakovski, 2001.

3.4.3 *E. coli* PCK Lys254Ser-Ca^{2+}-Pyruvate Structure

The final model of the *E. coli* PCK Lys254Ser-Ca^{2+}-pyruvate structure has R_{work} and R_{free} of 0.18 and 0.22, respectively. It has a spacegroup of P2 instead of the C2 normally observed for most *E.coli* PCK structures (Table 3.8). No electron density was observed for residues, 1-5, 250-256, and 390 – 400 and ATP, hence these residues and ATP are missing in the final structure. Alignment of the Lys254Ser PCK mutant structure with the wild type *E. coli* PCK-ATP-Mg^{2+}-oxalate structure show that the residues in both structures are not in similar positions; they are slightly shifted away from one another. However, alignment of the Lys254Ser PCK mutant structure with the native wild type *E. coli* PCK structure (PDB 1OEN, this structure has no ATP bound to it), shows that residues in both structures are in similar positions. The active site of Lys254Ser and the native *E. coli* PCK structure is open, while that in *E. coli* PCK structures with ATP is closed, hence the difference in the position of residues in K254S and *E. coli* PCK-ATP-Mg^{2+}-oxalate structures.

The 69-fold higher K_m for Mg^{2+}ATP displayed by this mutant (Novakovski, 2001) provides kinetic evidence for this structure. The lack of electron density for residues 250 – 256 shows that this loop region is flexible and exposed to the surface in the absence of Mg^{2+}ATP. This region is also part of the kinase 1a region essential for Mg^{2+}ATP binding. Since pyruvate is bound to this structure, this structure supports a random ordered mechanism of PCK catalysis, where OAA binds before Mg^{2+}ATP binding occurs. Mg^{2+}ATP binding leads to active site closure which facilitates catalysis.

Table 3.8: Data collection and refinement statistics for Lys254Ser-PCK-Ca^{2+}-pyruvate structure. Values in parentheses are for the highest resolution shell.

Unit cell	
Space group	P 1 21 1
a (Å)	55.03
b (Å)	76.7
c (Å)	65.5
α (deg.)	90
β (deg.)	96.3
γ (deg.)	90
Data collection	
No. molecules in asymm. unit	1
Resolution range (Å)	39.79 -1.8 (1.86 – 1.8)
No. reflections measured	262297
No. unique reflections	50206
Completeness (%)	99.9 (100)
Redundancy	5.22 (5.24)
Mean I/σ(I)	6.9 (2.6)
R-merge	0.13 (0.47)
R-meas	0.14 (0.52)
Refinement statistics	
Resolution range (Å)	39.79 – 1.8 (1.864 -1.8)
R_{free}	0.22 (0.25)
Rwork	0.18 (0.23)
Total no of reflections	50185 (5005)
No. non-H protein atoms	4342
No. water molecules	297
Wilson B-factor	25.27
R.m.s. deviations from ideal geometry	
Bond distances (Å)	0.007
Bond angles (deg.)	1.07
Dihedral angles (deg.)	13.2
Ramachandran statistics	
Favored (%)	98
Allowed (%)	2.15
Outliers (%)	0.2
Clashscore	4.13
Average B-factor	28.60
macromolecules	28.30
Ligands	37.60
Solvent	33.50

3.4.4 *E.coli* PCK Arg65Gln ATP-Mg^{2+}-Mn^{2+} Structure

The *E.coli* PCK R65Q Mg^{2+}ATP-Mg^{2+}-Mn^{2+} crystal diffracted to a resolution of 2.0 Å, and the final structure has R_{work} and R_{free} of 0.21 and 0.27, respectively (Table 3.9). Alignment of

this structure with the wild type *E.coli* PCK-Mg^{2+}ATP-Mn^{2+}-pyruvate structure showed that all residues except mutated residue Arg65Gln are in similar positions. Gln65 in the mutant structure is pointing in the opposite direction away from the active site compared to Arg65 found in the wild type structure. In the R65Q PCK mutant structure, no electron density was observed for pyruvate, hence pyruvate is absent in this structure, and this supports the high K_m for OAA displayed by this mutant during kinetic analysis (Novakovski 2000). The closed confirmation of the active site of this mutant also supports a random ordered mechanism of catalysis, where OAA binding occurs before Mg^{2+}ATP binding which cause active site closure.

Table 3.9: Data collection and refinement statistics for Arg65Gln-PCK-Mg^{2+}ATP-Mn^{2+} structure. Values in parentheses are for the highest resolution shell.

Unit cell	
Space group	C 1 2 1
a (Å)	125.093
b (Å)	95.03
c (Å)	46.43
α (deg.)	90
β (deg.)	96.3
γ (deg.)	90
Data collection	
No. molecules in asymm. unit	1
Resolution range (Å)	38.26– 1.85 (1.92 -1.85)
No. reflections measured	191253
No. unique reflections	46034
Completeness (%)	100.0 (100.0)
Redundancy	4.15 (4.11)
Mean I/σ(I)	3.1 (1.7)
R-merge	0.35 (0.81)
R-meas	0.40 (0.94)
Refinement statistics	
Resolution range (Å)	46.05 – 1.995) (2.066 – 1.9995)
R_{free}	0.269 (0.364)
Rwork	0.214 (0.284)
Total no of reflections	30879 (2896)
No. non-H protein atoms	4597
No. water molecules	429
Wilson B-factor	21.03
R.m.s. deviations from ideal geometry	
Bond distances (Å)	0.007
Bond angles (deg.)	1.08
Dihedral angles (deg.)	14.31

Ramachandran statistics	
Favored (%)	96.98
Allowed (%)	2.84
Outliers (%)	0.19
Clashscore	5.47
Average B-factor	22.90
macromolecules	22.40
Ligands	20.10
Solvent	28.00

4.0 Discussion

4.1 Increased rate of catalysis by *E. coli* PCK in the presence of Ca^{2+} or Mn^{2+} ions

E. coli PCK has a strict Mg^{2+} requirement in the form of Mg^{2+}ATP to catalyze the conversion of OAA to PEP; however, for optimal catalysis the presence of Ca^{2+} or Mn^{2+} is also required. Catalysis in the presence of Ca^{2+} or Mn^{2+} increased by about 4-fold (Table 4.1) because they function to bring both substrates in close proximity to each other, increase the reactivity of the reaction intermediate and to further increase the susceptibility of the γ-phosphate of ATP for nucleophilic attack.

Comparison of the effect of Mn^{2+} and Ca^{2+} on the rate of catalysis displayed by each mutant shows that Mn^{2+} and Ca^{2+} increase the k_{cat} of Tyr207Phe mutant by 1.4 and 3.4-fold respectively. Ca^{2+} had no effect on the k_{cat} of Ser250Ala while Mn^{2+} increased k_{cat} of Ser250Ala mutant by 11.6-fold. Ca^{2+} increased k_{cat} of Arg333Gln by 1.7-fold, while Mn^{2+} increase k_{cat} by 6.9-fold (Table 4.1). The different k_{cat}'s displayed by these mutants in the presence of Ca^{2+} and Mn^{2+} ions, indicates that Tyr207, Ser250 and Arg333 play slightly different roles in catalysis when Ca^{2+} or Mn^{2+} is bound to the enzyme, thereby indicating that the mechanism of catalysis in the presence of either Ca^{2+} or Mn^{2+} may be different.

Table 4.1: Apparent k_{cat} values for wild type and *E. coli* mutant PCK'S with and without Ca^{2+} or Mn^{2+}

		Mn^{2+}	Ca^{2+}
	k_{cat} (s^{-1})	k_{cat} (s^{-1})	k_{cat} (s^{-1})
Enzyme			
Wild type	16.40 ± 1.34	72.00 ± 2.98	71.30 ± 1.33
Tyr207Phe	9.41 ± 0.43	12.99 ± 0.83	33.70 ± 1.50
Ser250Ala	1.52 ± 0.10	17.70 ± 2.00	1.62 ± 0.10
Arg333Gln	0.0036 ± 0.00020	0.025 ± 0.0003	0.0061 ± 0.00031

Errors are in standard error. Values for k_{cat} were calculated using the V_{max} values shown in the result section.

4.2 Mechanism of catalysis by *E. coli* PCK

4.2.1 Mechanism of catalysis by *E. coli* PCK in the presence of Mg^{2+}ATP and OAA

Analyses of Mg^{2+}ATP and oxalate bound *E. coli* PCK structures have shown that, Tyr207 is 3.2Å away from one of the carboxyl oxygen's of oxalate, Arg333 is interacting directly with oxalate and ATP, while Ser250 is hydrogen bonded to one γ-phosphate oxygen of ATP (Fig 4.1). The close proximity of Tyr207 to one of the carboxyl oxygen's of oxalate indicates that if OAA is bound in similar manner as oxalate, Tyr207 may be involved in OAA decarboxylation. However the mechanism proposed by Tari *et al.*, 1996, does not include Tyr207 and mutation of Tyr207 to Phe decrease k_{cat} by 1.7-fold compared to wildtype, therefore indicating that Tyr207 is probably not involved in OAA decarboxylation when only Mg^{2+}ATP and OAA are present for catalysis by *E. coli* PCK.

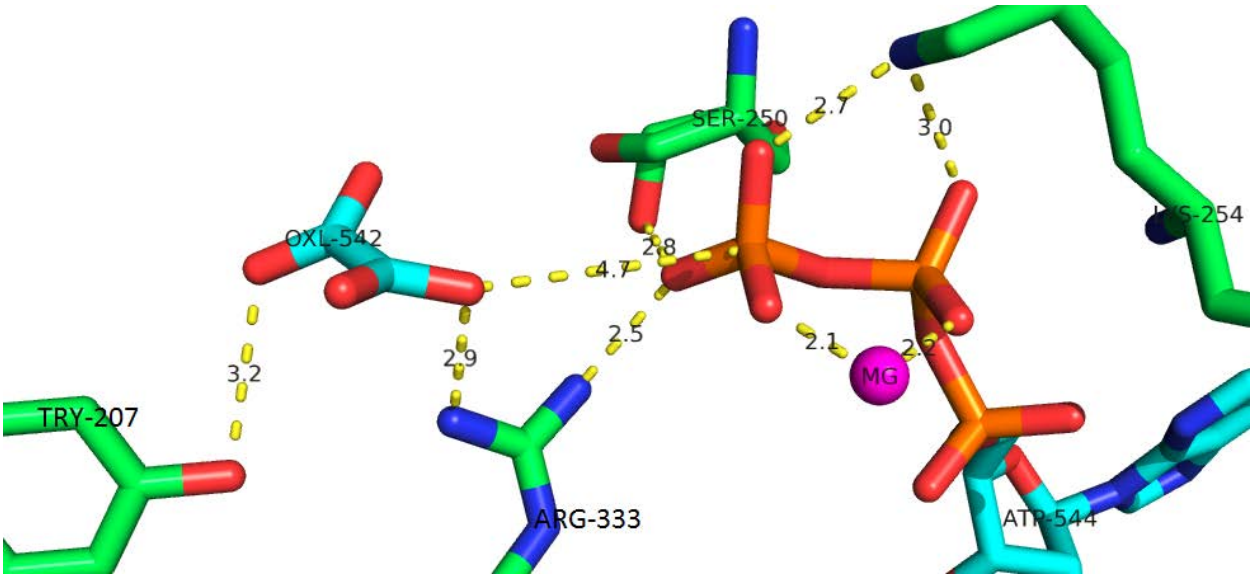

Figure 4.1: Coordination of Mg^{2+}ATP and oxalate by Tyr207, Ser250 and Arg333. Oxalate is interacting with Tyr207, Arg333 and one of its carboxyl oxygen is 4.7Å away from the γ-phosphate of ATP. The β and γ-phosphate oxygen's of ATP are interacting with Lys254, Ser250, Arg333 and Mg^{2+}. Image was made with pymol (DeLano, 2002) using 1AYL PDB.

Ser250Ala mutation reduced k_{cat} by about 10.8-fold and increase K_m for both substrates by about 1.4-fold compared to wildtype (Table 4.2). The 1.4-fold increase in K_m for Mg^{2+}-ATP displayed by this mutant is not surprising because other residues involved in Mg^{2+}-ATP binding are intact, hence the small change in K_m for Mg^{2+}ATP. Ser250 is hydrogen bonded to one γ-phosphate oxygen of ATP, this interaction is important to prevent steric hindrance of the γ-phosphate of ATP by that oxygen. As observed in Ser250Ala PCK mutant structure, Ser250Ala mutation decrease the angle between residue 250 and one γ-phosphate oxygen of ATP by 6.2°, hence the 10.8-fold decrease in k_{cat} may be due to the reduced accessibility of the nucleophilic carbonyl oxygen of *enol*-pyruvate to the electrophilic γ-phosphate of ATP. Phosphoryl transfer by *E. coli* PCK occur by an S_N2 mechanism where bond formation and breakage occur simultaneously, hence the nucleophile (carbonyl oxygen of pyruvate) has to attack the electrophile (γ-phosphate of ATP) at an angle 180° away from the leaving group (ADP) (Delbaere *et al.*, 2004). For this to occur the molecules (γ-phosphate oxygens of ATP) attached

to the electrophile has to be maintained in an eclipsed conformation, where they are less likely to prevent nucleophilic attack. Therefore hydrogen bond formation between Ser250 and one γ-phosphate oxygen of ATP, functions to keep the oxygen in an eclipse conformation important for phosphoryl transfer. Mg^{2+} and Lys254 function to maintain the other oxygens attached to the γ-phosphate of ATP in an eclipsed conformation.

Arg333 drives OAA decarboxylation and also functions to neutralize the charge between *enol*-pyruvate and ATP, thereby moving them in close proximity to each other. (Tari *et al.*, 1996). Arg333Gln mutation reduced k_{cat} by about 4555-fold (Table 4.2), hence our result supports the proposed mechanism of catalysis by *E. coli* PCK in the presence of Mg^{2+}-ATP and OAA as shown in Figure 1.12.

Table 4.2: Apparent kinetic parameters for wild type and *E.coli* mutant PCK

Enzyme	K_m (mM)		k_{cat} (s^{-1})
	OAA	Mg^{2+}ATP	
Wild type	1.84 ± 0.50	0.49 ± 0.17	16.4 ± 1.34
Tyr207Phe	0.98 ± 0.10	0.36 ± 0.10	9.41 ± 0.43
Ser250Ala	2.4 ± 0.60	0.69 ± 0.14	1.52 ± 0.10
Arg333Gln	1.89 ± 0.40	0.29 ± 0.10	0.0036 ± 0.00020

Errors are in standard error. Values for k_{cat} were calculated using the V_{max} values shown in the result section. K_m and k_{cat} values obtained in this project are less than 3-fold different from those obtained by Novakovski, 2000 (Table 1.1). However these are apparent values and vary with changing conditions. When OAA was the changing substrates Mg^{2+}ATP was used a constant concentration of 5.0 mM in this study and 2.0 mM by Novakovski, 2000. When Mg^{2+}ATP was the changing substrate OAA was used at a constant concentration of 10 mM in this project and 20 mM by Novakovski, 2000.

4.2.2 Mechanism of catalysis by *E. coli* PCK in the presence of Mg^{2+}ATP OAA and Mn^{2+}

In the *E. coli* PCK-Mg^{2+}ATP-Mn^{2+}-pyruvate structure, Arg333 is interacting with the carbonyl oxygen of pyruvate and one γ-phosphate oxygen of ATP. Tyr207 is 4.3 Å away from the CH_2 group of pyruvate, while Ser250 is 2.8 Å away from one γ-phosphate oxygen of ATP. Mn^{2+} is directly interacting with one γ-phosphate oxygen of ATP and indirectly interacting with pyruvate through two water molecules. Arg333Gln mutation caused a 2880-fold reduction in

k_{cat}, while Ser250Ala and Tyr207Phe mutations reduced k_{cat} by about 4 and 5.5-fold respectively compared to wild type (Table 4.3). This result indicates that Arg333 is important for catalysis, while Ser250 and Tyr207 may play marginal role in catalysis in the presence of Mg^{2+}-ATP, OAA and Mn^{2+}.

Table 4.3: Apparent kinetic parameters for wild type and *E. coli* mutant PCK with Mn^{2+}

Enzyme	K_m (mM)		k_{cat} (s^{-1})
	OAA	Mg^{2+}ATP	
Wild type		0.56 ± 0.070	72.0 ± 2.98
Tyr207 Phe	2.0 ± 0.40	0.39 ± 0.090	12.99 ± 0.83
Ser250 Ala		3.0 ± 0.65	17.7 ± 2.00
Arg333 Gln	5.96 ± 1.10	3.9 ± 1.60	0.025 ± 0.0030

Errors are in standard error. Values for k_{cat} were calculated using the V_{max} values shown in the result section.

Alignment of the wildtype *E. coli* PCK-ATP-Mg^{2+}-Mn^{2+}-pyruvate structure, with Ser250Ala *E. coli* PCK-ATP-Mn^{2+}-pyruvate structure, shows that ATP, pyruvate and Mn^{2+} are bound at similar position in both structures; however, the average distance between Mn^{2+} and its coordinating ligands in the S250A structure is 2.12 Å instead of 2.68 Å observed in wildtype structure. In the wild type structure with Mn^{2+} the angle between Ser250 and one γ-phosphate oxygen of ATP is 137°, however this angle is reduced to 130.8° when Ser250 is mutated to Ala. The carbonyl oxygen of pyruvate is 4.1 Å away from the γ-phosphate of ATP in S250A structure, however in the wildtype structure, the carbonyl oxygen of pyruvate is 4.3 Å away from the γ-phosphate of ATP. The distance between the CH_2 group of pyruvate and Tyr207 is 4.7 Å in S250A structure, instead of 4.3Å measured in the wildtype structure (Fig 4.3). This indicates that Ser250Ala mutation moved ATP and pyruvate closer to each other, but moved pyruvate further away from Tyr207. Therefore if OAA and pyruvate binding to the wildtype and S250A mutant structure are similar, the results indicate that Tyr207 is involved in the decarboxylation of OAA

in the presence of Mn^{2+}. Tyr207Phe and Ser250Ala mutations affect the decarboxylation step of *E. coli* PCK catalysis, because Ser250Ala mutation moves one of the carboxyl group of OAA further away from Tyr207, while Tyr207Phe mutation eliminates the hydroxyl group that can interact with that carboxyl group of OAA. The interaction between the hydroxyl group of Tyr207 and the carboxyl group of OAA is important for OAA decarboxylation, hence the 4 and 5.5-fold reduction in k_{cat} displayed by Ser250Ala and Tyr207Phe *E.coli* PCK mutants respectively.

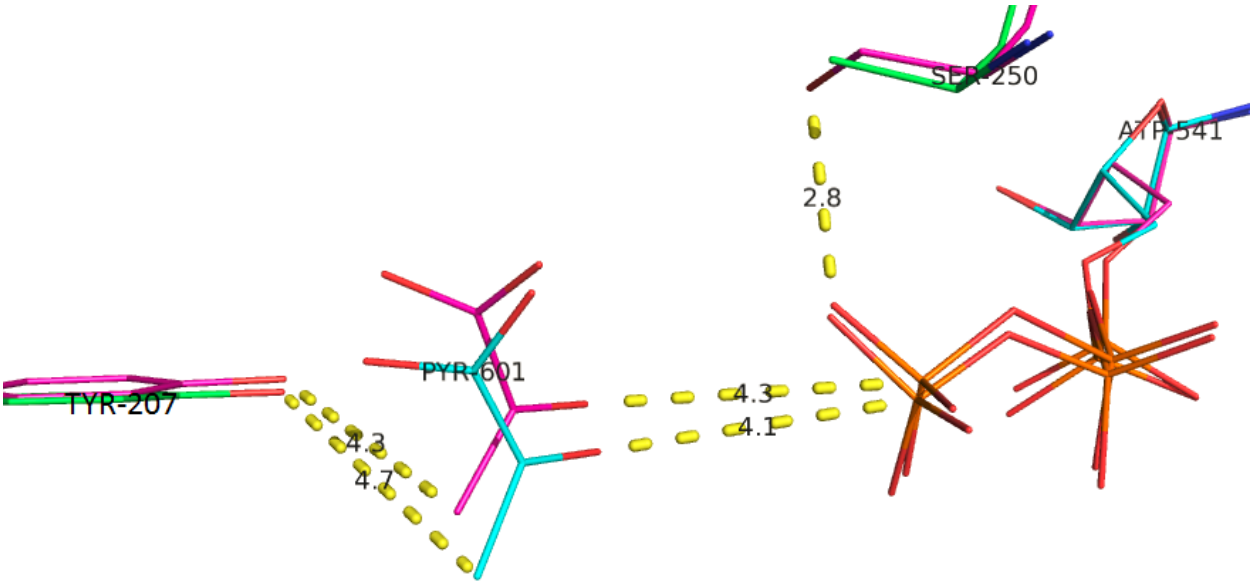

Figure 4.2: Alignment of wild type *E. coli* PCK-ATP-Mg^{2+}-Mn^{2+}- pyruvate with the Ser250Ala *E. coli* PCK-ATP-Mn^{2+}-pyruvate structure. In wildtype structure, Tyr207 is 4.3 Å away from the CH_2 group of pyruvate, the carbonyl oxygen of pyruvate is 4.3 Å away from the γ-phosphate of ATP, while Ser250 is 2.8 Å away from one γ-phosphate oxygen of ATP. Ser250Ala mutant structure, Tyr207 is 4.7 Å away from the CH_2 group of pyruvate, the carbonyl oxygen of pyruvate is 4.1 Å away from the γ-phosphate of ATP, while Ala250 is not interacting with ATP. Image was made with Pymol (DeLano, 2002) using coordinates from wildtype structure with Mn^{2+} (1AQ2) and Ser250Ala mutant structure with Mn^{2+}.

The Tyr207Phe mutation decrease k_{cat} by 5.5-fold, while Arg333 decreased k_{cat} by 2880-fold, indicating that Arg333 is important for catalysis, while Tyr207 enhances OAA decarboxylation in the presence of Mn^{2+}. k_{cat} of Tyr207Phe and Ser250Ala in the presence of Mn^{2+} is 12.99 s^{-1} and 17.7s^{-1} compared to 16.40 s^{-1} displayed by wildtype *E. coli* PCK in the presence of Mg^{2+}-ATP and OAA. This indicates that enhanced decarboxylation in the presence

of Mn^{2+} by Tyr207, contributes to the increased rate of catalysis by *E. coli* PCK observed in the presence of OAA, Mg^{2+}-ATP and Mn^{2+}.

Based on our results, the new mechanism of catalysis proposed for *E. coli* PCK in the presence of Mg^{2+}-ATP, OAA and Mn^{2+} ion is as follows (Fig 4.3). Interaction of OAA with Tyr207 and Arg333 drives OAA decarboxylation and formation of *enol*-pyruvate which displaces water from the coordination sphere of Mn^{2+}. Arg333 and Mn^{2+} now function to neutralize the electrostatic repulsion between *enol*-pyruvate and ATP, bringing the nucleophilic carbonyl oxygen of *enol*-pyruvate in close proximity to the electrophilic γ-phosphate of ATP. PEP and ADP formation occurs when the carbonyl oxygen of pyruvate attacks and displaces the γ-phosphate of ATP.

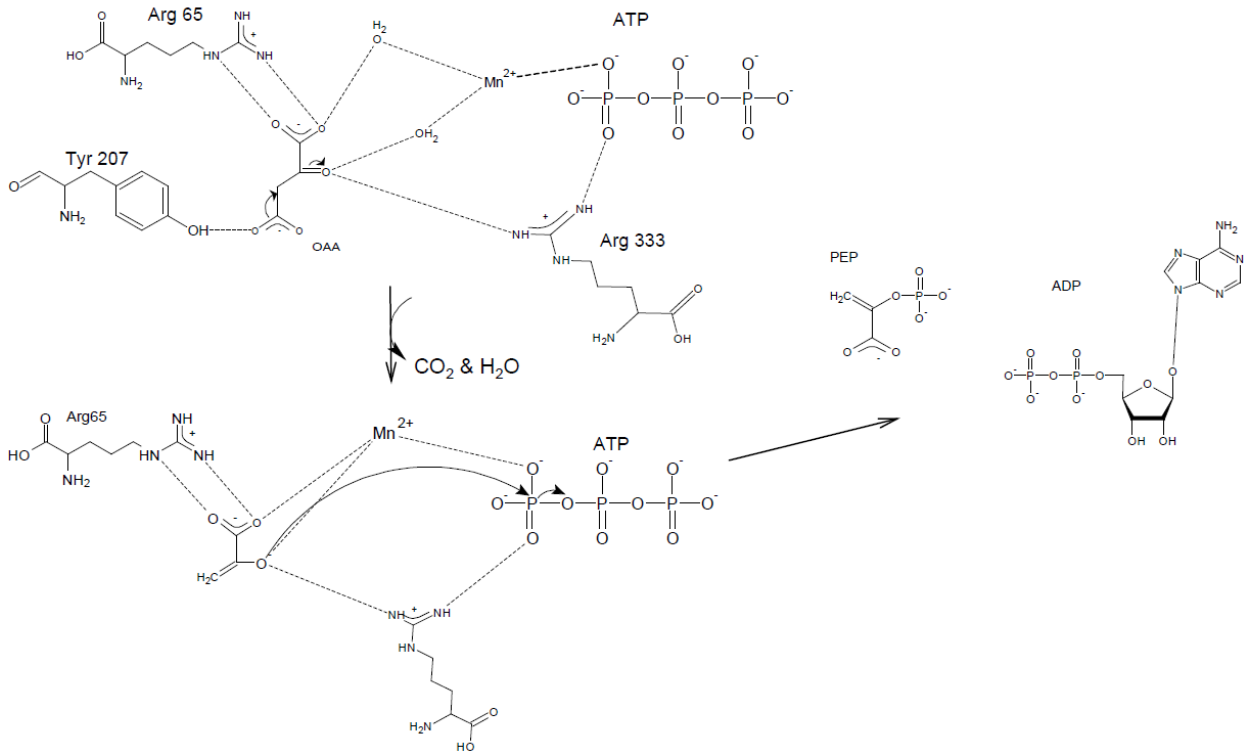

Figure 4.3: Mechanism of PCK catalysis in the presence of Mn^{2+}. Hydrogen bond formation between the hydroxyl group of Tyr207 and one of the carboxyl oxygen's of OAA leads to OAA decarboxylation and formation of pyruvate enolate, which attacks and displaces the γ-phosphate of ATP.

4.2.3 Mechanism of catalysis by *E. coli* PCK in the presence of Mg^{2+}ATP OAA and Ca^{2+}

Analysis of the *E. coli* PCK-Mg^{2+}ATP-Ca^{2+}-pyruvate structure shows that, Ca^{2+} is 2.6 Å and 3.1 Å away from one γ-phosphate oxygen of ATP and one carboxyl oxygen of pyruvate, while Tyr207 is 2.8 Å away from the CH_2 group of pyruvate. Arg333 is 3.0 Å and 3.2 Å away from ATP and Ser250, while Ser250 is interacting with Arg333, pyruvate and ATP. According to Sudom *et al.*, 2003, superposition of OAA over the pyruvate binding site in the Ca^{2+} structure, indicates that Arg333 also interacts with OAA. The carbonyl oxygen of pyruvate is 6.0 Å away from the γ-phosphate of ATP, however it is 3.3 Å away from a water molecule which is directly interacting with Ca^{2+} and the γ-phosphate of ATP. Hence water has to be displaced from the coordination sphere of Ca^{2+}, in order for Ca^{2+} to directly interact with the carbonyl oxygen of pyruvate and bring it in close proximity to the γ-phosphate of ATP.

Tyr207Phe mutation reduced k_{cat} by 2-fold, Ser250Ala mutation reduced k_{cat} by 44-fold, while Arg333Gln mutation decreased k_{cat} by 11,688 fold (Table 4.4). This result indicates that Arg333 is important for catalysis, Ser250 plays a marginal role in catalysis, while Tyr207 is probably not involved in catalysis when Mg^{2+}-ATP, OAA and Ca^{2+} are used for catalysis by *E. coli* PCK.

Table 4.4: Apparent Kinetic parameters for wild type and *E. coli* mutant PCK with Ca^{2+}

Enzyme	K_m (mM)		k_{cat} (s^{-1})
	OAA	Mg^{2+}ATP	
Wild type	1.89 ± 0.20	0.13 ± 0.030	71.3 ± 1.33
Tyr207 Phe	0.57 ± 0.050	0.051 ± 0.020	33.7 ± 1.50
Ser250 Ala	2.3 ± 0.25	0.22 ± 0.060	1.62 ± 0.10
Arg333 Gln	1.02 ± 0.15	0.042 ± 0.013	0.0061 ± 0.00031

Errors are in standard error. Values for k_{cat} were calculated using the V_{max} values shown in the result section.

Based on our results the proposed mechanism of *E. coli* PCK catalysis in the presence of Ca^{2+} is as follows. Binding of OAA to Arg333 and Ca^{2+}, drives OAA decarboxylation and the formation of *enol*-pyruvate. The carbonyl oxygen of *enol*-pyruvate forms an inner coordination

sphere with Ca^{2+}, while water is displaced from the coordination sphere of Ca^{2+}, and this brings the carbonyl oxygen of *enol*-pyruvate closer to the γ-phosphate of ATP. Interaction between Ca^{2+}, *enol*-pyruvate and ATP, neutralizes the electrostatic repulsion between *enol*-pyruvate and ATP, moves them in closer proximity to each other and orient the carbonyl oxygen of *enol*-pyruvate to attack and displace the γ-phosphate of ATP (Fig 4.4). Compared to wild type Ser250Ala mutation reduced k_{cat} by 44 fold, however, k_{cat} of S250A PCK mutant in the presence of Ca^{2+} is $1.62s^{-1}$ compare to $1.52s^{-1}$ in the absence of Ca^{2+} or Mn^{2+}, this result indicates that in the presence of Ca^{2+} Ser250 is important to maintain one γ-phosphate oxygen of ATP in an eclipse conformation which facilities catalysis, as previously discussed.

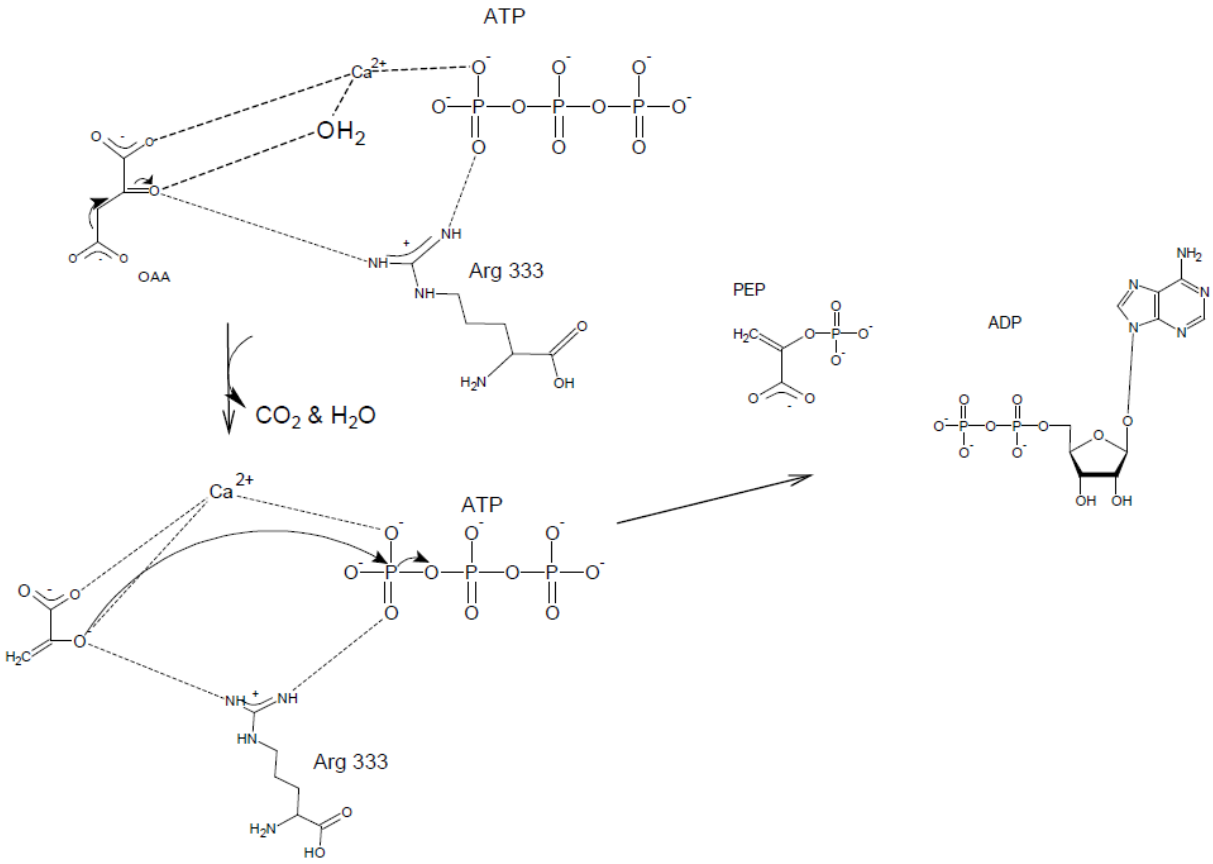

Figure 4.4: Mechanism of PCK catalysis in the presence of Ca^{2+}. Arg333 and Ca^{2+} function to bring both substrates in close proximity to each other, and this drives the decarboxylation of OAA and the formation of *enol*-pyruvate, which attack and display the γ-phosphate of ATP. Made with ACD/ChemSketch software.

4.2.4 Function of Arg333, Ser250 and Tyr207 during catalysis by *E. coli* PCK

Arg333 is important for the decarboxylation of OAA and phosphorylation of *enol*-pyruvate during catalysis by *E. coli* PCK. It plays a role in *enol*-pyruvate phosphorylation because it brings *enol*-pyruvate and ATP in close proximity to each other, it puts the carbonyl oxygen of *enol*-pyruvate in the right position that facilitate catalysis and increases the electrophilicity of the γ-phosphate of ATP. Arg333 also functions to keep one γ-phosphate oxygen of ATP in an eclipse conformation. Since Gln333 is able to form hydrogen bond with *enol*-pyruvate and ATP, the reduced k_{cat} displayed by the *E. coli* PCK Arg333Gln mutate with and without Mn^{2+} or Ca^{2+}, shows that the positive charge on Arg333 is important for catalysis. The positive charge on Arg333 has also be shown to be important for catalysis using *S. cereviase* Arg336Lys PCK mutant (Llanos *et al.*, 2001).

In the presence of Mn^{2+}, Tyr207 plays a role in the decarboxylation of OAA, since Tyr207Phe mutation eliminate the hydroxyl group involved in hydrogen bond formation with one of the carboxyl group of OAA. In the Ca^{2+} containing *E. coli* PCK structure, Ca^{2+} is directly interacting with Mg^{2+}-ATP and pyruvate, while Tyr207 is 2.8 Å away from the CH_2 group of pyruvate. In Mn^{2+} containing *E. coli* PCK structure, Mn^{2+} is directly interacting with Mg^{2+}-ATP, but indirectly interacting with pyruvate through two water molecules, while Tyr207 is 4.3 Å away from the CH_2 group of pyruvate (Fig. 4.5). Although the distance between Tyr207 and the CH_2 group of pyruvate is less in the presence of Ca^{2+}, decarboxylation of OAA driven by Tyr207 in the presence of Mn^{2+} is required to remove water from the coordination sphere of Mn^{2+}, to enable Mn^{2+} directly interact with *enol*-pyruvate. Hence the k_{cat} of Tyr207Phe *E. coli* PCK mutant is reduced by 2-fold in the presence of Ca^{2+}, and 5.5-fold in the presence of Mn^{2+}, even though Ca^{2+} and Mn^{2+} increase k_{cat} by 4-fold. Since OAA is larger than pyruvate, we suspect that

the distance between Tyr207 and one of the carboxyl groups of OAA in the Mn^{2+} structure will be less than 4.3 Å, when OAA is bound to the enzyme. Interaction between the hydroxyl group of Tyr207 and CO_2 has been suggested to be important for the reverse reaction catalyzed by *E. coli* PCK in the presence of Mn^{2+} (Cotelesage, 2007). Polarization of CO_2 and OAA by the hydroxyl group of Tyr207 has been suggested to facilitate carboxylation and decarboxylation in *S. cerevisiae*, because Tyr207Leu mutation increased K_m for CO_2 by 15-fold (Castillo *et al.*, 2009). Mutation of the equivalent Tyr235 in human cytosolic-PCK to Ala and Ser reduced PEP production and OAA decarboxylation by human PCK-C (Dharmarajan *et al.*, 2008). Structural studies has also shown that Tyr235 plays a role in catalysis by chicken liver PCK-M in the presence of Mn^{2+} (Holyoak *et al.*, 2006).

Ser250 is part of the kinase 1a loop important for ATP binding in *E. coli* PCK, it is hydrogen bonded to one γ-phosphate oxygen of ATP, where it functions to keep one γ-phosphate oxygen of ATP in an eclipsed conformation which facilities S_N2 mechanism of phosphoryl transfer. Analysis of S250A mutant structure with Mn^{2+} has shown that Ser250Ala mutation reduced the distance between pyruvate and ATP, by 0.2Å and increased the angle between them from 134° to 137°. This reduced distance and increases angle bring both substrate closer to each other, hence the 4-fold reduction in k_{cat} displayed by S250A PCK mutant in the presence of Mn^{2+}. Therefore the 10 and 44-fold reduction in k_{cat} displayed by this mutant in the absence and presence of Ca^{2+} respectively, maybe due to lack of change in the distance and angle between pyruvate and ATP that moved them closer to each other, as a result of Ser250Ala mutation in the absence and presence of Ca^{2+}. Ca^{2+} and Mn^{2+} are 2.6 Å and 2.1 Å away from the γ-phosphate oxygen of ATP (Fig 4.5) and the carbonyl oxygen of pyruvate is 6.0 Å and 4.3 Å away from the γ-phosphate of ATP in Ca^{2+} and Mn^{2+} structure respectively. In the wildtype structure without

Mn^{2+} or Ca^{2+}, the distance between the carbonyl oxygen of pyruvate and γ-phosphate of ATP is 4.7 Å. Hence little changes in the position and angle between pyruvate and the γ-phosphate of ATP as a result of Ser250Ala mutation that bring them closer to each other in the presence of Mn^{2+}, will have no effect in the presence and absence of Ca^{2+}, because the distance between ATP and pyruvate might still be considerably large. Analysis of the crystal structure of chicken liver PCK-M have shown that the equivalent residue S305 may be involved in phosphoryl transfer during catalysis (Holyoak *et al.,* 2006). Mutation of Ser252 to Ala caused a 50-fold increase in the K_m for OAA, hence Ser252 was suggested to be important for OAA binding in *S. cerevisiae* (Andrade *et al.,* 2010).

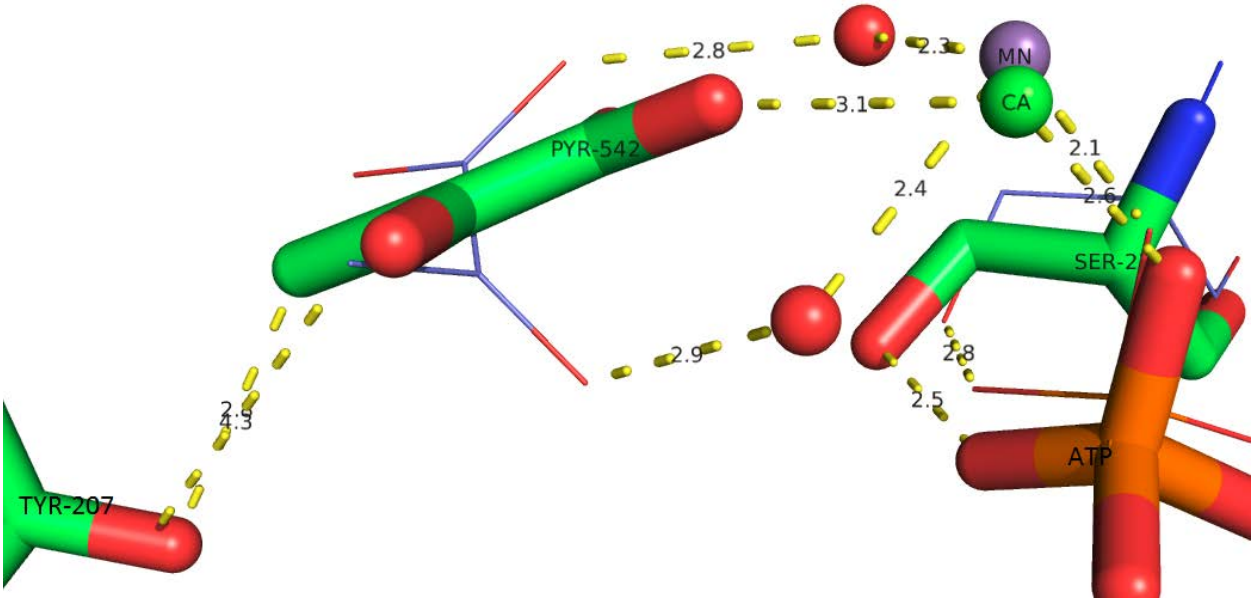

Figure 4.5*:* Alignment of wild type *E. coli* PCK Mg^{2+}ATP-pyruvate Mn^{2+} structure to *E. coli* PCK Mg^{2+}ATP-pyruvate-Ca^{2+}. In the Ca^{2+} structure Ca^{2+} is 3.1 Å and 2.6 Å away from one carboxyl oxygen of pyruvate and the γ-phosphate of ATP, Ser250 is 2.5 Å away from one γ-phosphate oxygen, while Tyr207 is 2.8Å away the CH_2 group of pyruvate. In the Mn^{2+} structure, Mn^{2+} is 2.1 Å away from one γ-phosphate oxygen, 2.3 Å and 2.4 Å away from two water molecules which are 2.8 Å and 2.9 Å away from carboxyl and carbonyl oxygen's of pyruvate. Tyr207 is 4.3 Å away from the CH_2 group of pyruvate, while Ser250 is 2.8 Å away from one γ-phosphate oxygen. (PCK Mg^{2+}ATP-pyruvate Mn^{2+} structure is represented with lines, while *E. coli* PCK Mg^{2+}ATP-pyruvate-Ca^{2+} is represented with sticks). Image was made with Pymol (DeLano, 2002).

4.2.5 Comparison of the different mechanisms of catalysis by *E. coli* PCK

Analysis of *E. coli* PCK structures with Ca^{2+} or Mn^{2+}, show that Ca^{2+} directly interacts with Mg^{2+}-ATP and pyruvate, while Mn^{2+} interacts indirectly with pyruvate; hence, it was expected that catalysis in the presence of Ca^{2+} will be greater than catalysis with Mn^{2+}. However, Ca^{2+} and Mn^{2+} increased k_{cat} by about 4-fold. In the wild type *E. coli* PCK-Mg^{2+}-ATP-pyruvate-Ca^{2+} structure, the carbonyl oxygen of pyruvate is 6.0 Å (4.3 Å in the Mn^{2+} structure) away from the γ-phosphate of ATP, hence for the carbonyl oxygen of enol pyruvate to move closer to the γ-phosphate of ATP, and water has to be displaced from the coordination sphere of Ca^{2+}. Mn^{2+} is indirectly coordinating pyruvate through two water molecules, which have to be displaced during catalysis. Although Ca^{2+} is more efficient in terms of water exchange compared to Mn^{2+} (Sudom *et al.*, 2003), Ca^{2+} and Mn^{2+} change k_{cat} at a similar rate because, in addition to excluding water from the active site, the carbonyl oxygen of *enol*-pyruvate and γ-phosphate of ATP have to brought in close proximity to each other during catalysis in the presence of Ca^{2+}.

4.2.6 Physiological relevance and role of calcium, manganese and magnesium in *E. coli* cells

Divalent metal cations are essential for most cellular functions in eukaryotic and prokaryotic cells. They have been implicated in physiological processes such as spore formation, cell cycles, bacteria pathogenesis, competence, and chemotaxis. Absence of divalent metal cations in growth medium have been associated with changes in the ultrastructure of *E. coli* and slow metabolism (Arancia *et al.*, 1980). Mg^{2+} is an essential cofactor for many enzymatic reactions and is tightly regulated in bacteria cells. The total cellular concentration of Mg^{2+} is approximately 100 mM (Downing *et al.*, 2009), and this indicates that the Mg^{2+} requirement for catalysis by *E. coli* PCK is physiologically plausible *in vivo*.

Although the role of calcium is poorly defined in bacteria, the presence of Ca^{2+} transporters, Ca^{2+} binding proteins, and tight regulation of Ca^{2+} levels in response to environmental stimuli indicate that Ca^{2+} is essential for bacteria growth. During stationary growth phase, the intracellular Ca^{2+} levels in *E. coli* have been shown to be tightly regulated in the micromolar range (Naseem *et al.,* 2008); however, changes in the cytosolic Ca^{2+} levels of *E. coli* cells in response to repellents and attractants has been described by Tisa and Adler, who reported that, repellents such as acetate, L-leucine, and indole, which cause *E. coli* to tumble, cause an increase in free cytosolic Ca^{2+} levels, while attractants such as L-serine and L-aspartate, which cause *E. coli* to run, caused transient decreases in free cytosolic Ca^{2+} levels. How changes in cytosolic Ca^{2+} levels cause tumbling and running still needs to elucidated (Tisa and Adler, 1995), but the increase in cytosolic Ca^{2+} levels under certain conditions shows that it is plausible for *E. coli* PCK to use Mg^{2+} and Ca^{2+} for catalysis during stationary growth phase when expression from *pckA* gene is increased and during other conditions that lead to increased levels of cytosolic free Ca^{2+}.

Manganese is an essential cofactor for many bacteria enzymes. It has an ionic radius of 0.8 Å, which lies between the ionic radii of Mg^{2+} (0.65 Å) and Ca^{2+} (0.99 Å), and replace them in the metal binding site of some proteins (Jakubovics and Jenkinson, 2001); hence, the presence of Mn^{2+}-ATP instead of Mg^{2+}-ATP complex in Ser250Ala *E. coli* PCK mutant structure is not unusual. The total Mn^{2+} concentration in *E. coli* cell is 10-fold lower than that of Zn^{2+}, which has an apparent concentration of 10^{-4} M in *E. coli* (Ma *et al.,* 2009). The low Mn^{2+} concentration in *E. coli* cells suggests that catalysis by *E. coli* PCK in the presence of Mn^{2+} is likely an *in vitro* artifact and not plausible in *vivo*; hence, the different mechanism of OAA decarboxylation observed in the presence of Mn^{2+}.

4.3 Arg65Gln mutation

Arg65 is important for OAA binding, hence the high K_m for OAA displayed by the Arg65Gln *E. coli* PCK mutant (Novakovski, 2000). The crystal structure of Arg65Gln solved in this study has no pyruvate bound to the active site. Alignment of the R65Q mutant structure with the wild type structure containing Mn^{2+} showed that most residues interacting with Mg^{2+}ATP, and Mn^{2+} are in similar positions, except for Gln65 in the mutant structure, whose side chain is pointing away from the active site (Fig 4.6). In the wild type *E. coli* PCK structure, Arg65 is interacting with the carboxyl group of pyruvate; however, the CH_2 group of pyruvate will interact with Gln65 if pyruvate is bound to the Arg65Gln *E. coli* PCK structure. If OAA and pyruvate binding to PCK are similar, this indicates that the interaction between the carboxyl group of OAA and Arg65 is important for OAA binding to *E. coli* PCK.

The Arg65Gln mutant has a k_{cat} similar to wild type, therefore indicating that Arg65 is not essential for catalysis (Novakovski, 2000). If pyruvate is bound to the Arg65Gln mutant structure with Mn^{2+}, as shown in Fig 4.6, Tyr207 will be 4.4 Å away from the CH_2 of pyruvate, while Mn^{2+} will still indirectly interact with pyruvate through two water molecules. Hence, at very high concentrations of OAA, Arg65Gln can catalyze the reaction at a rate similar to wild type PCK.

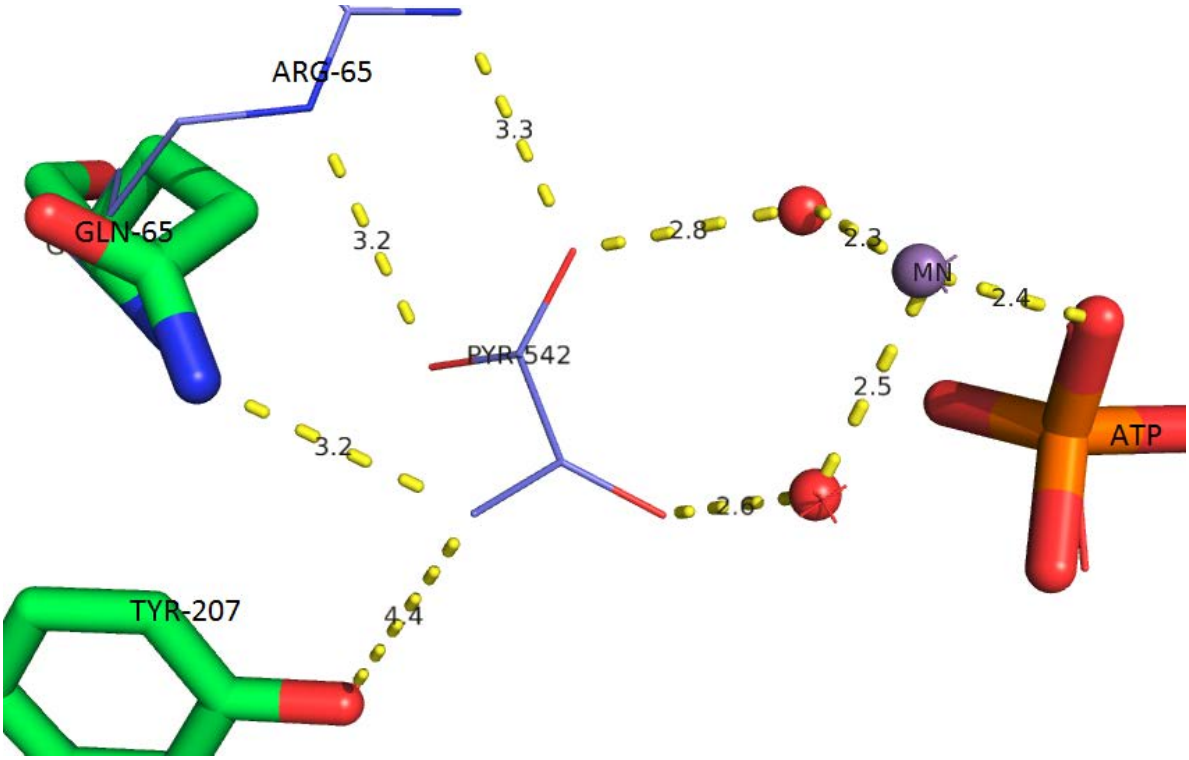

Figure 4.6: Alignment of Arg65Gln *E. coli* PCK-Mn^{2+}-Mg^{2+}-ATP structure with the wild type *E. coli* PCK-Mg^{2+}ATP-Mn^{2+}-pyruvate structure. Arg65 in the wild type structure is 3.3 Å and 3.2 Å away from the carboxyl group of pyruvate, while Gln65 and Tyr207 in the mutant structure are 3.2 Å and 4.4 Å away from the CH_2 group of pyruvate present in the wild type structure. If pyruvate in Arg65Gln mutant and wild type structure are bound in similar position and manner, Mn^{2+} will indirectly interact with pyruvate through two water molecules in the Arg65Gln *E. coli* PCK-Mn^{2+}-ATP structure. Residues and ligands from the Arg65Gln *E. coli* PCK-Mn^{2+}-Mg^{2+}-ATP structure *are* represented with thick sticks, while those from wild type *E. coli* PCK-Mg^{2+}ATP-Mn^{2+}-pyruvate structure are represent with lines. Image was made with Pymol (DeLano, 2002).

4.4 Asp269Asn mutation

Asp269 is part of the kinase la loop involved in ATP binding to *E. coli* PCK. It also functions with ATP to connect Mg^{2+} to Mn^{2+} or Ca^{2+} bound to the bridging site. In the 2.3Å resolution structure of the Asp269Asn *E. coli* PCK mutant with Ca^{2+} presented in this study, Ca^{2+} is coordinated by one carboxyl oxygen of pyruvate and one γ-phosphate oxygen of ATP. The distance between Ca^{2+} and ATP is reduced by 0.6 Å and Ca^{2+} is 2.2 Å away from its position in the wild type structure (Fig. 4.7). Asp269Asn mutation increased K_m for Mn^{2+} 1000-fold. Since Mn^{2+} and Ca^{2+} bind to similar sites in *E. coli* PCK, the distorted coordination of Ca^{2+} observed in Asp269Asn structure provide structural evidence to support the high K_m for Mn^{2+} observed by

Novakovski, 2000. Therefore, Asp269 is important for coordination of metal ions that bind to the bridging site of *E. coli* PCK.

In the Asp269Asn mutant structure, Mg^{2+} interacts with all the triphosphate groups of ATP, while the average distance between Lys254 and β- & γ-phosphate of ATP is 3.34 Å, instead of the 2.8 Å distance observed in the wild type structure (Fig 4.7). It has previously been said that the interaction between the β and γ-phosphates of ATP with Mg^{2+} and Lys254 allows ATP to adopt a sterically strained conformation that promotes catalysis by reducing the activation energy. Therefore, the reduced k_{cat} (15-fold reduction) displayed by this mutant is due to the distorted interaction between Lys254, Mg^{2+} and ATP as a result of the Asp269Asn mutation.

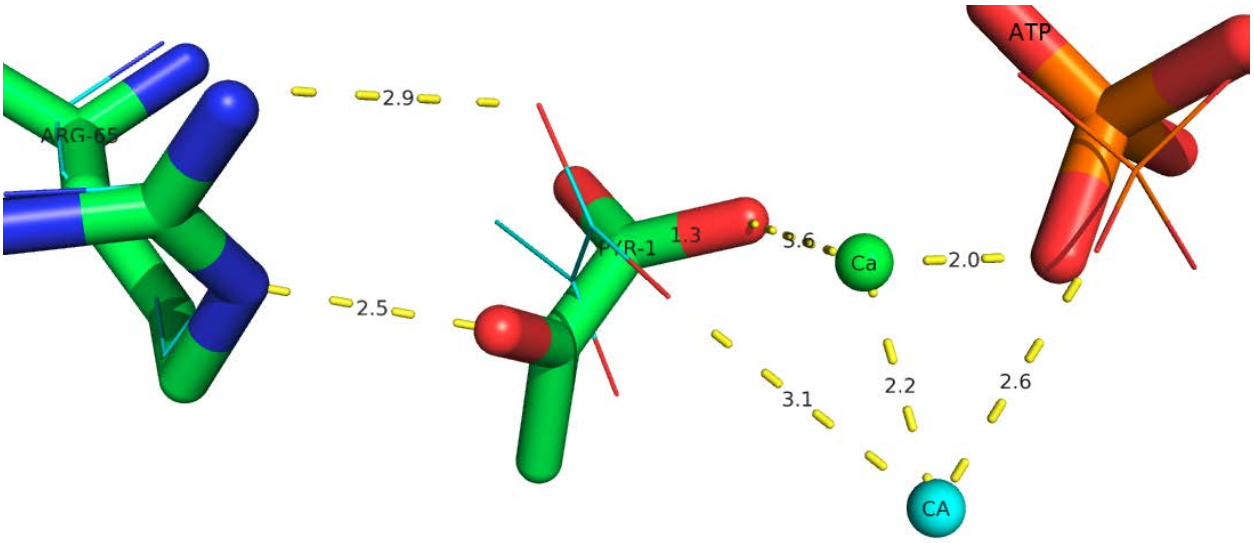

Figure 4.7: Alignment of *E. coli* PCK Asp269Asn-Mg^{2+}ATP-Ca^{2+}-pyruvate structure with wild type *E. coli* PCK Mg^{2+}ATP-Ca^{2+}-pyruvate structure. In D269N structure, Ca^{2+} is 2.2 Å away from its position while its coordinating ligands are in similar position compared to the wild type structure. Pyruvate in D269N mutate structure is 3.6 Å and 2.5 Å away from Ca^{2+} and Arg65, while pyruvate in the wild type structure is 2.9 Å and 3.1 Å away from Arg65 and Ca^{2+}repectively. *E. coli* PCK D269N-Mg^{2+}ATP-Ca^{2+}-pyruvate structure is represented with thick sticks, while wild type *E. coli* PCK Mg^{2+}ATP-Ca^{2+}-pyruvate structure is represented with lines. Image was made with Pymol (DeLano, 2002)

In the wild type *E. coli* PCK structure, Arg65 interacts with the carboxyl group of pyruvate; however, in the Asp269Asn mutant structure, Arg65 interacts with the carbonyl oxygen of pyruvate (Fig. 4.7). Since the Asp269Asn mutation increased the K_m for OAA by about 240-fold, this structure provides further evidence that the interaction between Arg65 and the carboxyl group of OAA is important for OAA binding.

The Asp268Asn *E. coli* PCK mutant has a high OAA decarboxylase activity, while the Asp269Asn mutant has low OAA decarboxylase activity (Novakovski, 2000). Analyses of wild type *E. coli* PCK structures have shown that Asp268 and Asp269 interact with Mg^{2+} indirectly by interacting with two water molecules that directly coordinate Mg^{2+}. In the Asp269Asn PCK mutant structure, Asn269 is still interacting with Mg^{2+} indirectly through a water molecule; however, Asp268 is interacting indirectly with Mg^{2+} by interacting with Thr255 (Fig. 3.7). This shows that the Asp268Asn mutation probably has a similar effect on the conformation of ATP as observed in the Asp269Asn mutant structure; hence, in the D268N PCK mutation, ATP probably adopts a conformation that does not facilitate catalysis. The high decarboxylase activity observed in the Asp268Asn mutant shows that decarboxylation of OAA in PCK occurs independently of phosphoryl transfer. Since Asp268Asn is not involved in the coordination of Mn^{2+} or Ca^{2+}, it is expected that OAA will still interact with Arg65 and Ca^{2+} or Tyr207, which drive decarboxylation, in the D268N mutant. However, the low decarboxylase activity displayed by the Asp269Asn *E. coli* PCK mutant is probably related to its high K_m for OAA; hence, the lack of OAA binding in Asp269Asn results in low decarboxylase activity displayed by this mutant. Asp268Asn *E. coli* PCK mutant has high decarboxylase activity because D268N mutant does not affect OAA binding to the enzyme, while D269N mutation affect OAA binding to the enzyme, hence the low decarboxylase activity displayed by Asp269Asn *E. coli* PCK mutant.

4.5 Lys254Ser mutation

Lys254 is a key conserved residue in the kinase la-loop involved in ATP binding and directly interacts with ATP. Lys254 to Ser mutation reduced k_{cat} by 17 fold and increased K_m for Mg^{2+}ATP 69 fold (Novakovski, 2000). Lys254 interacts with the β and γ-phosphate of ATP and works with Mg^{2+} to maintain the sterically strained conformation of ATP essential for catalysis and to increase the electrophilicity of the γ-phosphate of ATP (Tari *et al.*, 1997). The structure of Lys254Ser presented in this study has no Mg^{2+}ATP present and is missing residues 250 – 256. This supports the high K_m for Mg^{2+}ATP observed in this mutant, and shows that Lys254 plays a role in the flexibility of the kinase1a-loop, since this region is not missing in the wild type native structure which is also missing Mg^{2+}ATP.

Although pyruvate and Ca^{2+} are bound to the active site of the Lys254Ser mutant PCK, the active site is still exposed to the surface (Fig. 4.8). This structure therefore provides evidence that catalysis by *E. coli* PCK occurs by a random ordered mechanism where OAA and Ca^{2+} or Mn^{2+} binds to the enzyme before Mg^{2+}-ATP, which induces active site closure.

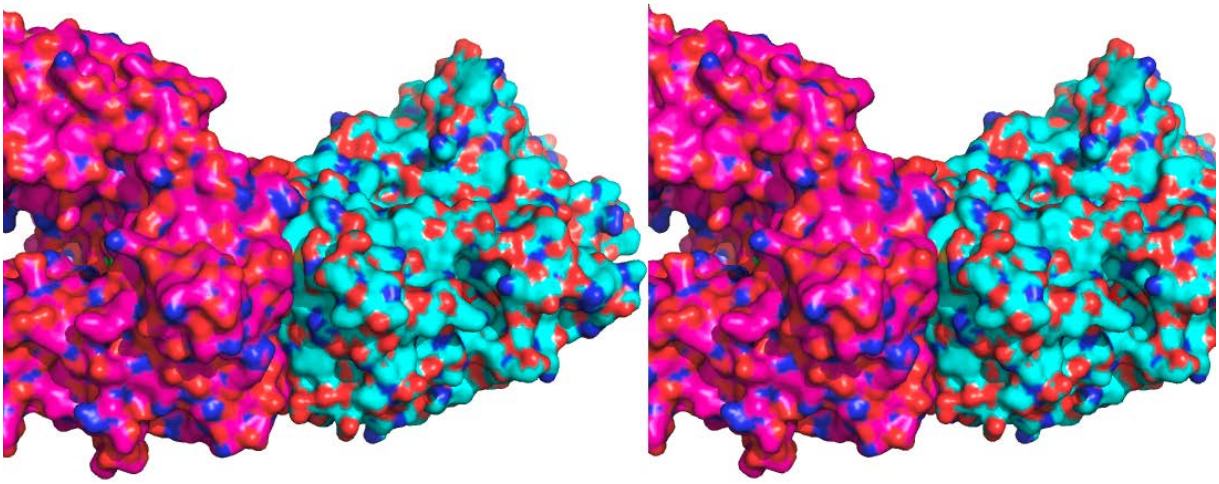

Figure 4.8: Stereo view of *E. coli* Lys254Ser PCK-Ca^{2+}-pyruvate structure and wild type *E. coil* PCK –Mg^{2+}ATP-Ca^{2+}-pyruvate structure. The ATP bound structure has a closed conformation compared to K254S which has only pyruvate. Stereo image was made with Pymol (DeLano, 20012).

5.0 Summary

Transgenic mice overexpressing PCK have high amount of insulin in their serum and are hyperglycemic (Valera *et al.*, 1994), hence PCK inhibitors can be used to treat NIDDM patients with increased PCK levels. Active site residues involved in metal and substrate binding are conserved in ATP and GTP dependent PCKs, therefore inhibitors that interact with these residues may be effective against both forms of PCK. Information obtained from the mechanism of catalysis by PCK can be used to design these inhibitors. The mechanism of catalysis by ATP dependent *E. coli* PCK in the presence of divalent metal ions was analyzed in this study.

In the presence of Ca^{2+} or Mn^{2+} k_{cat} increased, however a larger increase in k_{cat} was not observed in the presence of Ca^{2+} as expected. The result obtained in this study supports the hypothesis that Arg333Gln *E. coli* PCK mutant will display a reduced k_{cat} in the presence of Mg^{2+}-ATP and OAA with or without Ca^{2+} or Mn^{2+}. Tyr207Phe mutation cause a 5.5 and 2-fold reduction in k_{cat} in the presence of Mn^{2+} and Ca^{2+}, this did not support the hypothesis that Tyr207Phe mutation will cause a larger decrease in k_{cat} in the presence of Ca^{2+}. Ser250Ala mutation caused a bigger reduction in k_{cat} in the presence of Ca^{2+} as hypothesized.

Decarboxylation of OAA driven by Tyr207 in the presence of Mn^{2+} but not in the presence of Ca^{2+} supports our hypothesis that the function of Ty207 depends on the presence or absence of Mn^{2+} or Ca^{2+} during catalysis by *E.coli* PCK. The function of Arg333 and Ser250 during catalysis by *E. coli* PCK does not depend on the presence or absence of Mn^{2+} or Ca^{2+}.

Crystal structures obtained for Asp269Asn, Lys254Ser and Arg65Gln provided structural evidence that Asp269, Lys254 and Arg65 are important for Ca^{2+} or Mn^{2+}, Mg^{2+}-ATP and OAA binding respectively.

6.0 Future investigation

This study has contributed to the understanding of catalysis by *E. coli* PCK and the role of key residues in the active site of the enzyme. How the rate of catalysis by *E. coli* PCK varies with changing Ca^{2+} concentration needs to be investigated in the future. $^{14}CO_2$ exchange assay can be used to determine the maximum velocity of *E. coli* PCK under varying concentrations of Ca^{2+}. *E. coli* HG89 is unable to use succinate as a carbon and energy source, unless it is transformed with plasmid carrying PCK gene. How the growth rate of *E. coli* HG89 transformed with pDBss plasmid changes with changing concentrations of Ca^{2+} in succinate medium can be used to determine if varying Ca^{2+} concentrations increases PCK activity *in vivo*.

7.0 Appendices

7.1 Wild type

Plots were made using GraphPad Prism, with kinetic values obtained using $^{14}CO_2$ exchange assays, which was performed in triplicates or duplicates and repeated three to four times.

7.1.1 Michaelis-Menten plots

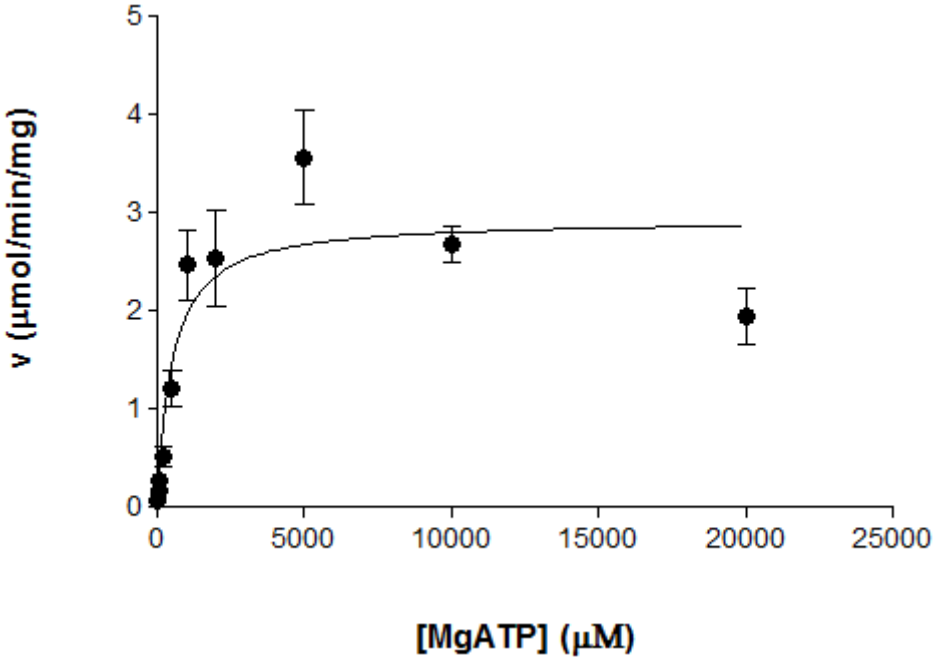

Figure 7.1: Michaelis-Menten plot of v as a function of [MgATP] for wild type PCK. K_m obtained from this plot is shown in table 3.2 and 4.2. V_{max} value obtained from this plot is shown in table 3.2 and used to calculate the k_{cat} value for wild type PCK shown in table 4.1 and 4.2

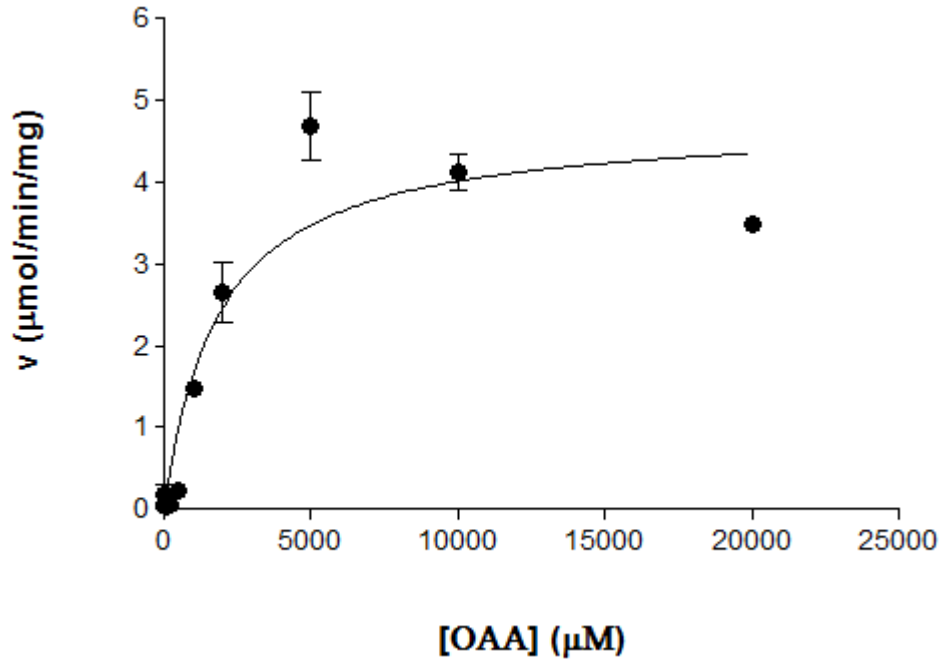

Figure 7.2: Michaelis-Menten plot of v as a function of [OAA] for wild type PCK. K_m obtained from this plot is shown in table 3.2 and 4.2. V_{max} value obtained from this plot is shown in table 3.2 and used to calculate the k_{cat} value for wild type PCK shown in table 4.1 and 4.2

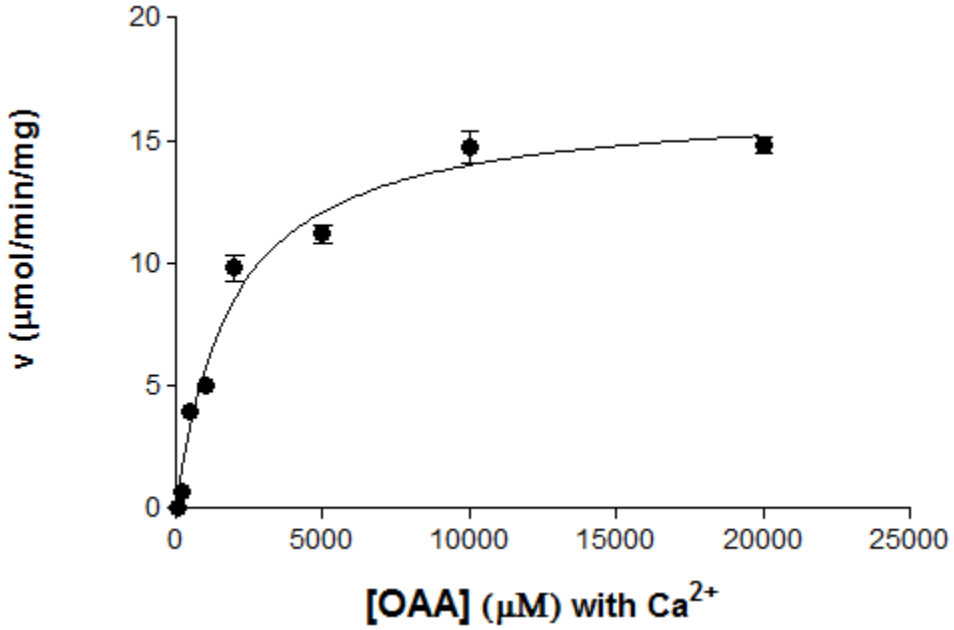

Figure 7.3: Michaelis-Menten plot of v as a function of [OAA] in the presence of calcium for wild type PCK. K_m obtained from this plot is shown in table 3.2 and 4.2. V_{max} value obtained from this plot is shown in table 3.2 and used to calculate the k_{cat} value for wild type PCK shown in table 4.1 and 4.2

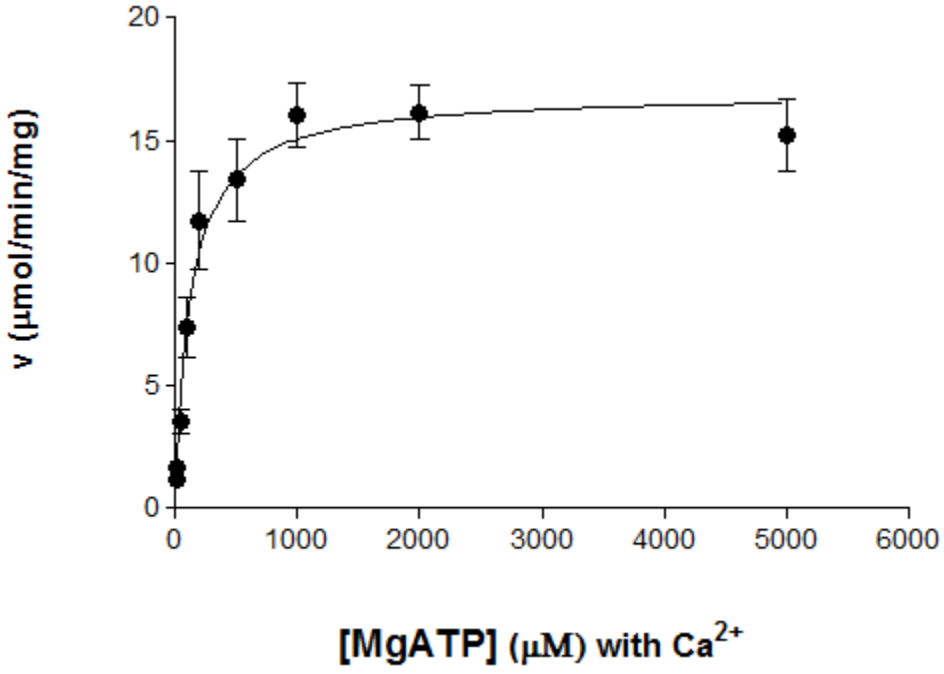

Figure 7.4: Michaelis-Menten plot of v as a function of [MgATP] in the presence of calcium for wild type PCK. K_m obtained from this plot is shown in table 3.2 and 4.2. V_{max} value obtained from this plot is shown in table 3.2 and used to calculate the k_{cat} value for wildtype PCK shown in table 4.1 and 4.2

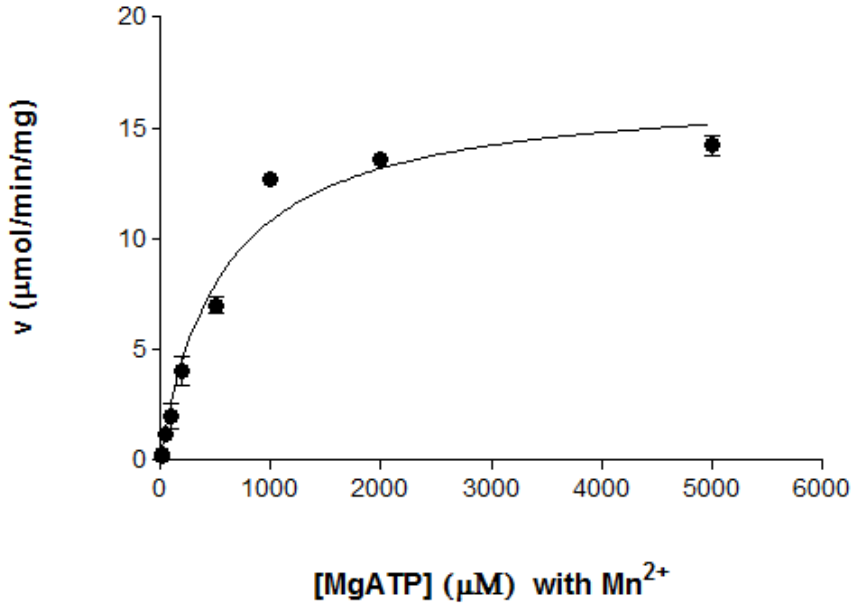

Figure 7.5: Michaelis-Menten plot of v as a function of [MgATP] in the presence of manganese for wild type PCK. K_m obtained from this plot is shown in table 3.2 and 4.2. V_{max} value obtained from this plot is shown in table 3.2 and used to calculate the k_{cat} value for wild type PCK shown in table 4.1 and 4.2

7.1.2 Lineweaver-Burk plots

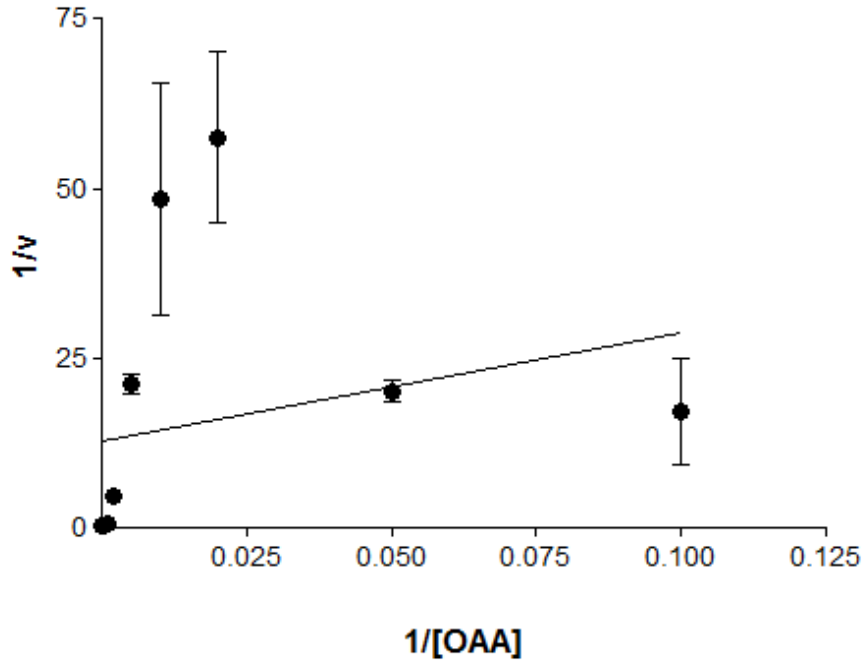

Figure 7.6: Lineweaver-Burk plot of 1/v as a function of 1/[OAA] for wildtype PCK. K_m and V_{max} obtained from this plot is shown in table 3.2

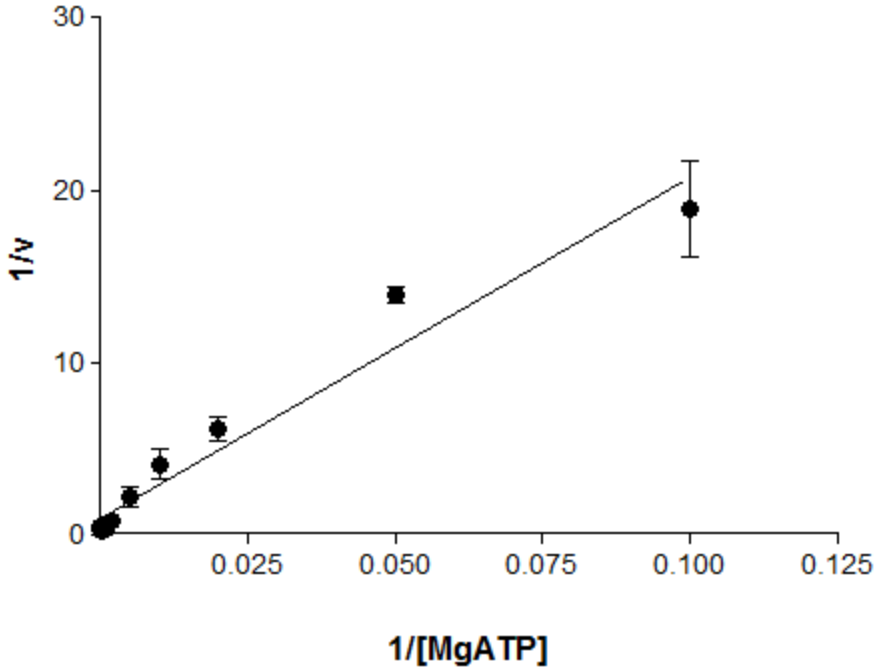

Figure 7.7: Lineweaver-Burk plot of 1/v as a function of 1/[MgATP], for wild type PCK. K_m and V_{max} obtained from this plot is shown in table 3.2

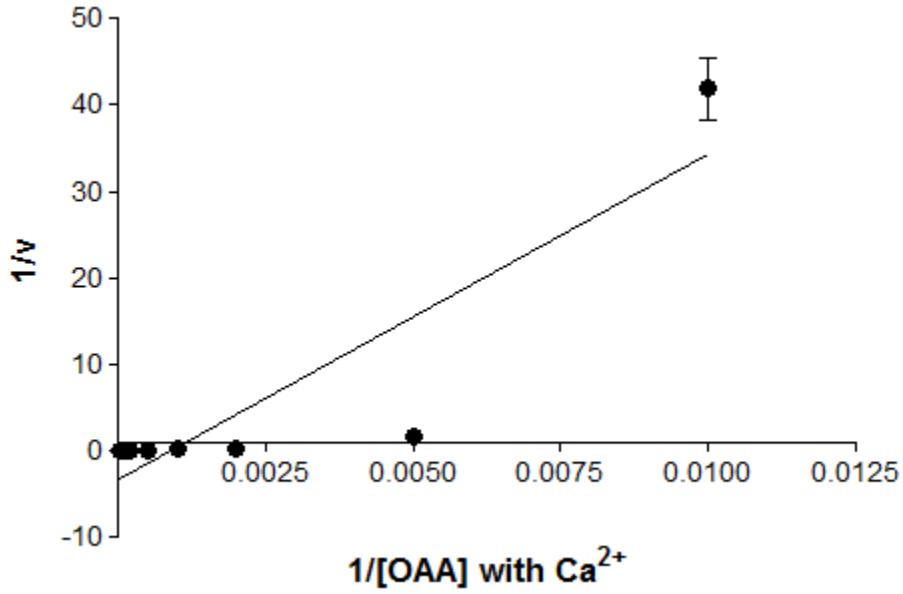

Figure 7.8: Lineweaver-Burk plot of 1/v as a function of 1/[OAA] in the presence of calcium for wild type PCK. K_m and V_{max} obtained from this plot is shown in table 3.2

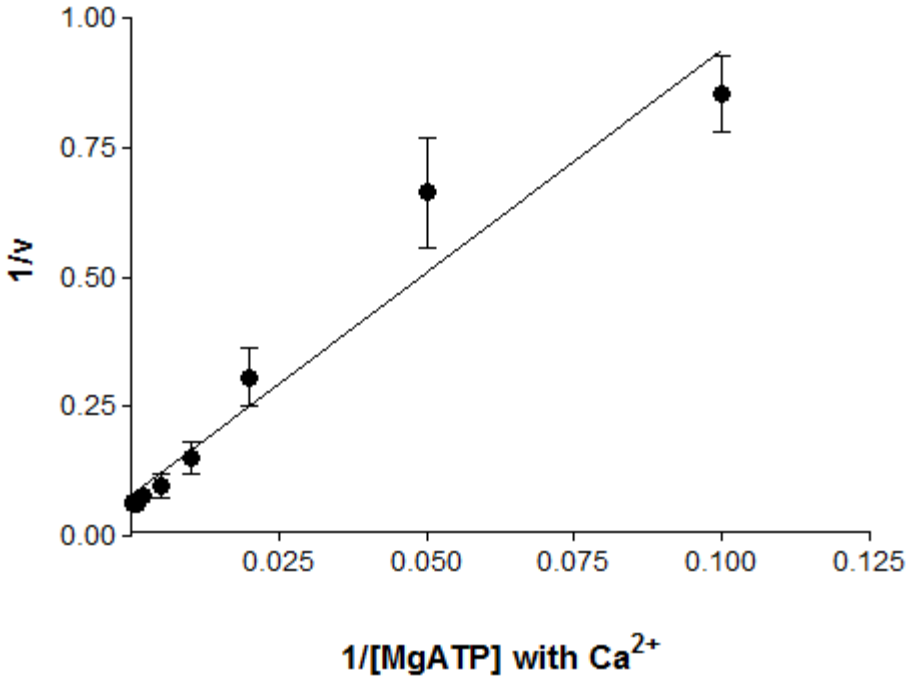

Figure 7.9: Lineweaver-Burk plot of 1/v as a function of 1/[MgATP] in the presence of calcium for wild type PCK. K_m and V_{max} obtained from this plot is shown in table 3.2

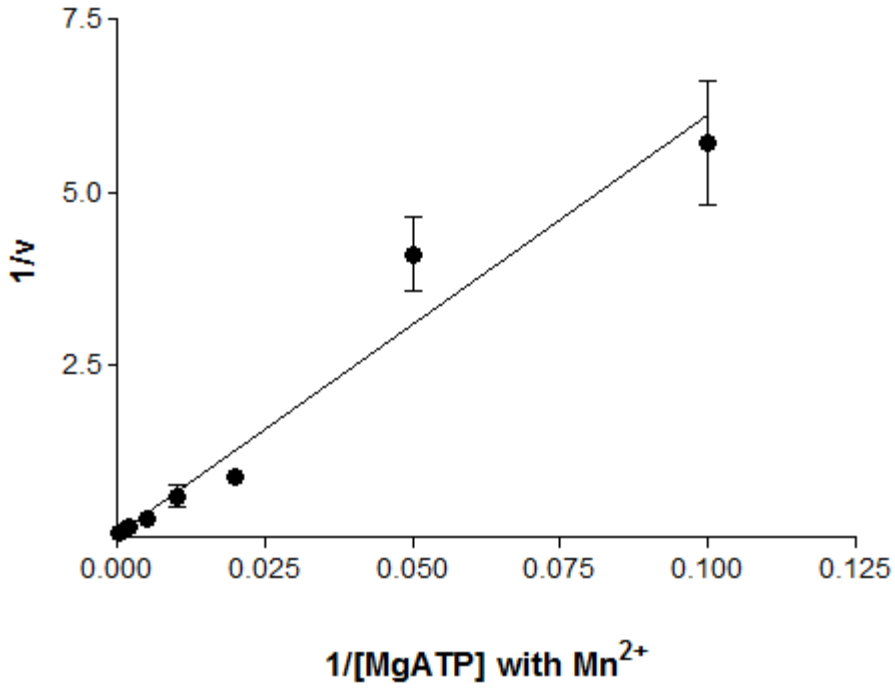

Figure 7.10*:* Lineweaver-Burk plot of 1/v as a function of 1/[MgATP] in the presence of manganese for wild type PCK. K_m and V_{max} obtained from this plot is shown in table 3.2

7.1.3 Eadie-Hofstee plot

Average velocities was used to calculate the velocities used for Eadie-Hofstee plots because v is present on both axes, hence error bars are not shown for these plots

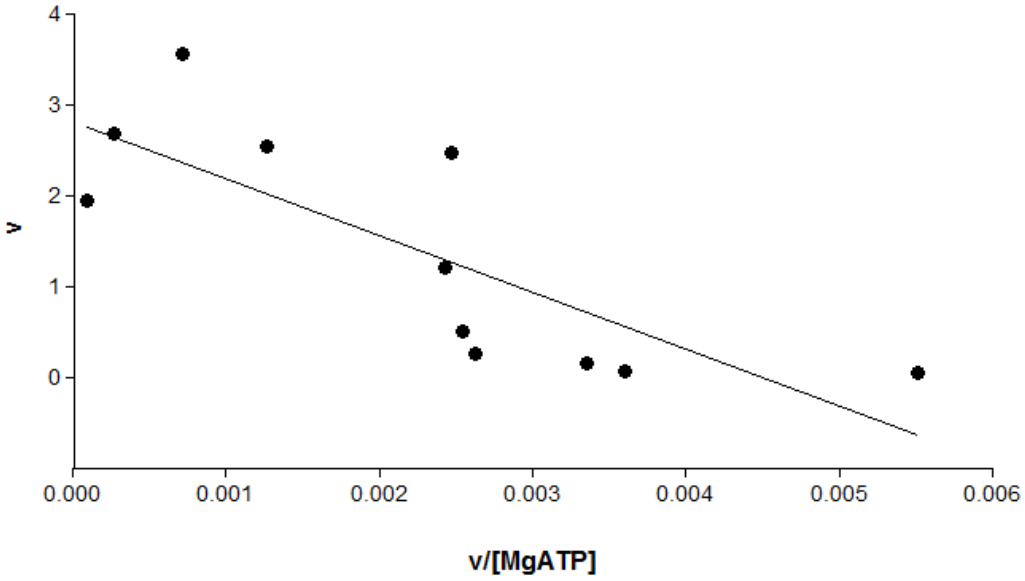

Figure 7.11: Eadie-Hofstee plot of v as a function of v/[MgATP] for wildtype PCK. K_m and V_{max} obtained from this plot are shown in table 3.2

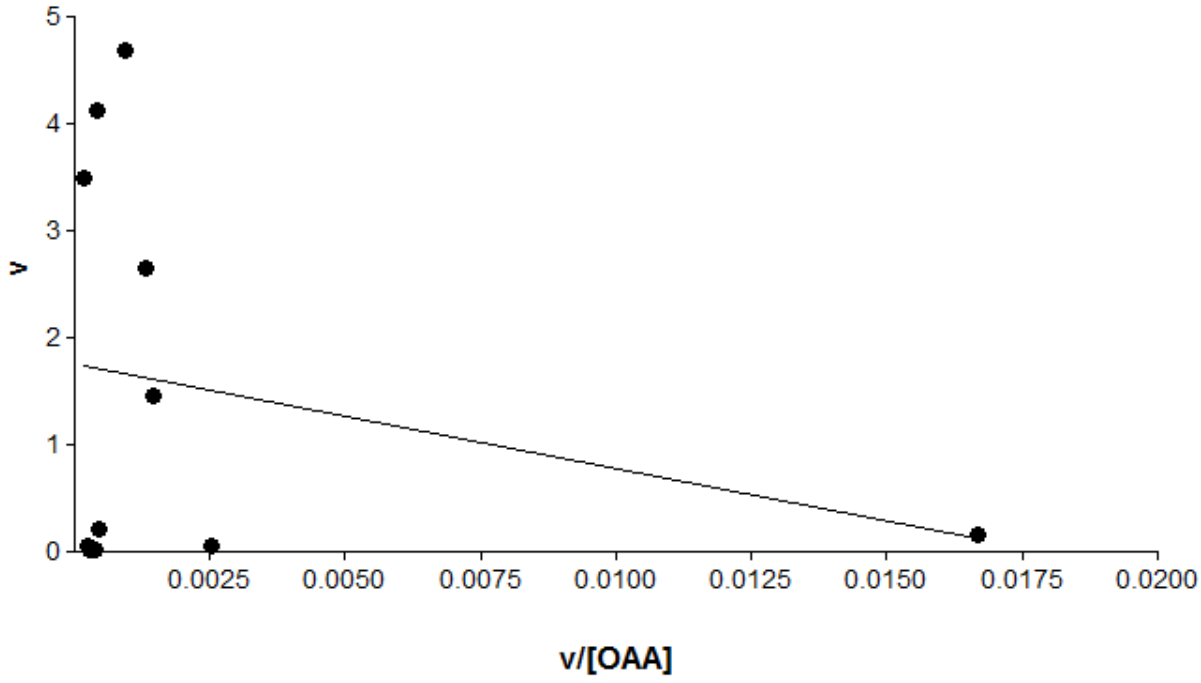

Figure 7.12: Eadie-Hofstee plot of v as a function of v/[OAA] for wildtype PCK. K_m and V_{max} obtained from this plot are shown in table 3.2

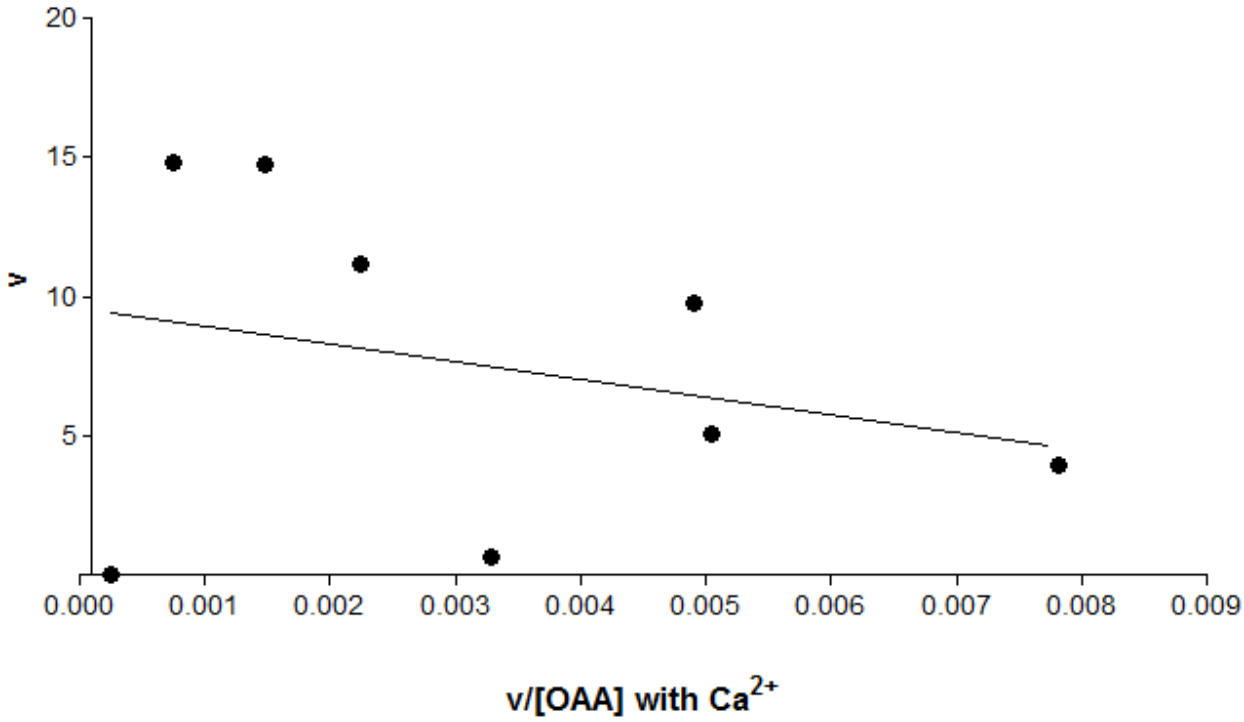

Figure 7.13: Eadie-Hofstee plot of v as a function of v/[OAA] in the presence of calcium for wildtype PCK. K_m and V_{max} obtained from this plot are shown in table 3.2

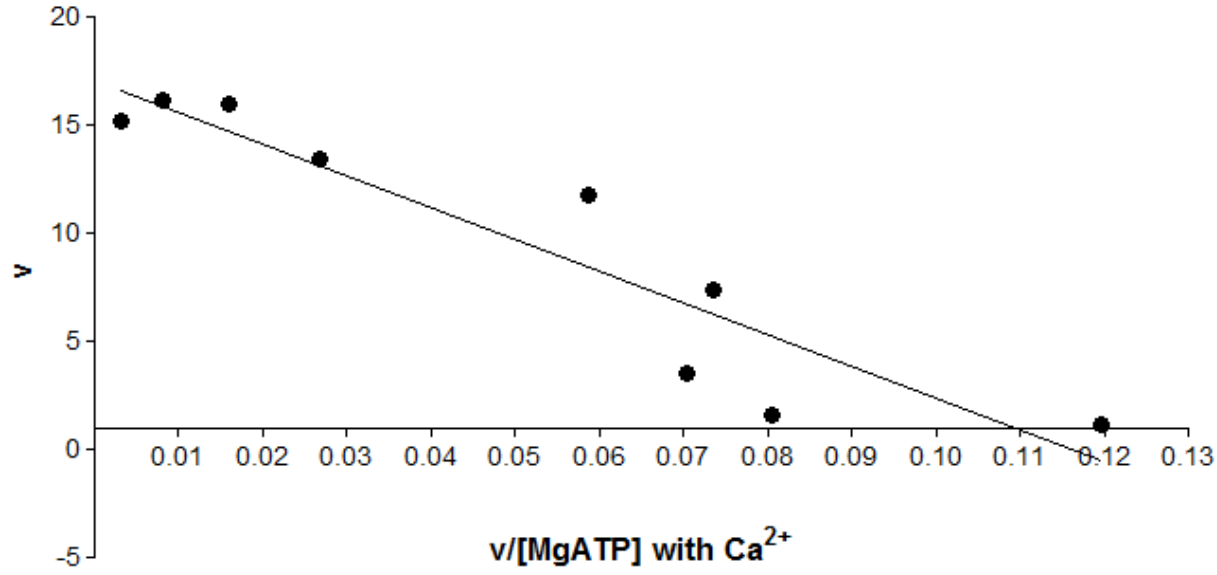

Figure 7.14: Eadie-Hofstee plot of v as a function of v/[MgATP] in the presence of calcium for wildtype PCK. K_m and V_{max} obtained from this plot are shown in table 3.2

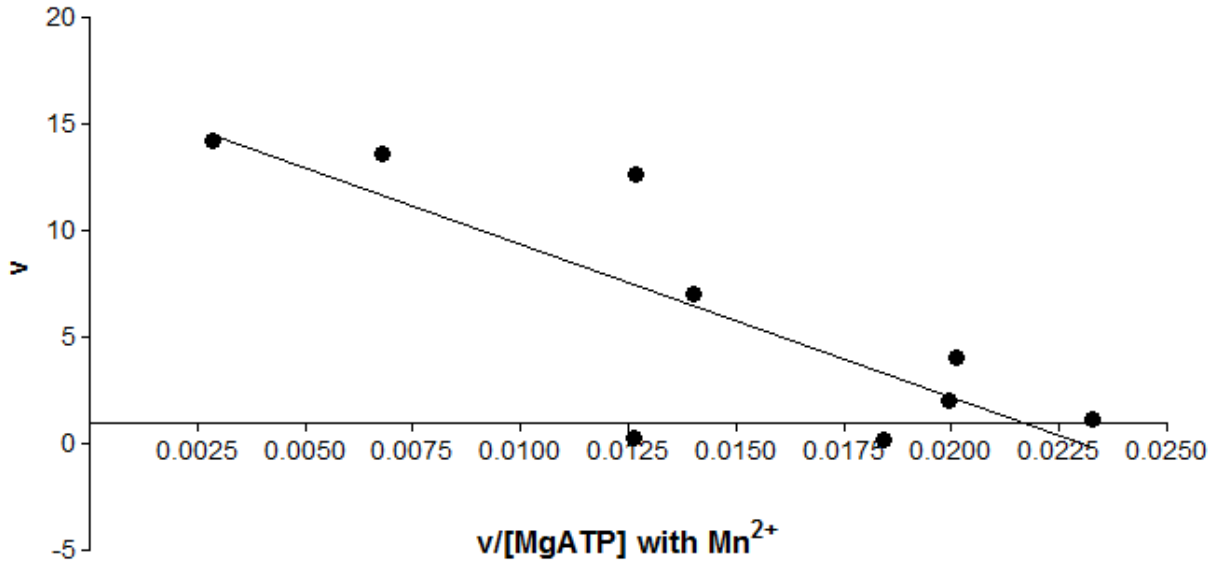

Figure 7.15: Eadie-Hofstee plot of v as a function of v/[MgATP] in the presence of manganese for wildtype PCK. K_m and V_{max} obtained from this plot are shown in table 3.2

7.2 Tyr207Phe

7.2.1 Michaelis-Menten Plot

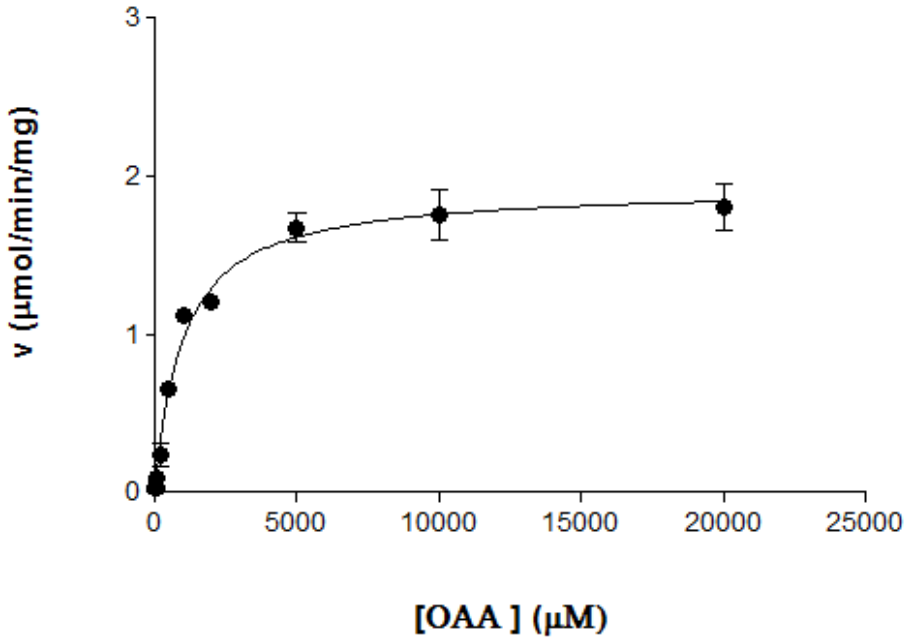

Figure 7.16: Michaelis-Menten plot of v as a function of [OAA] for Tyr207Phe mutant PCK. K_m obtained from this plot is shown in table 3.3 and 4.2. V_{max} value obtained from this plot is shown in table 3.3 and used to calculate the k_{cat} value for Tyr207Phe mutant PCK shown in table 4.1 and 4.2

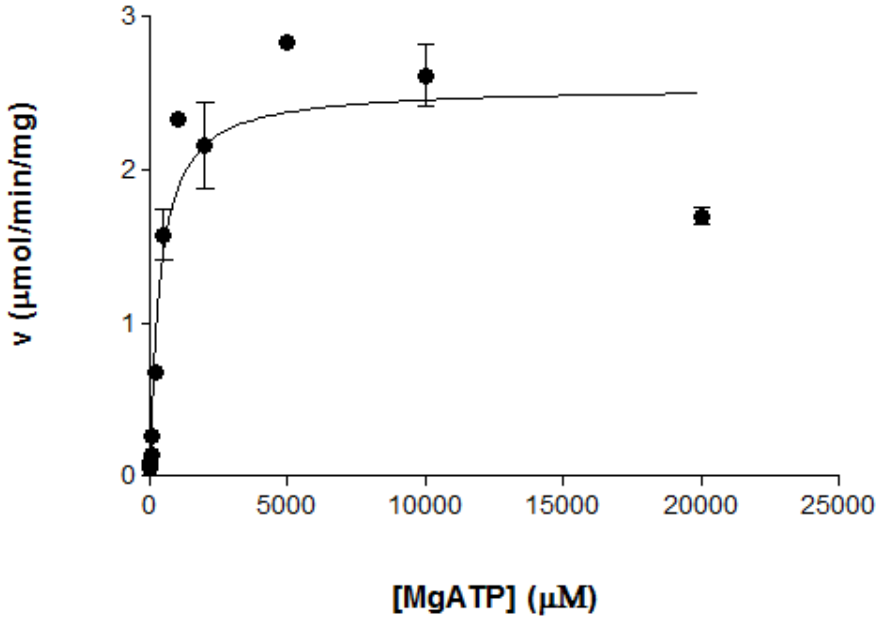

Figure 7.17: Michaelis-Menten plot of v as a function of [MgATP] for Tyr207Phe mutant PCK. K_m obtained from this plot is shown in table 3.3 and 4.2. V_{max} value obtained from this plot is shown in table 3.3 and used to calculate the k_{cat} value for Tyr207Phe mutant PCK shown in table 4.1 and 4.2

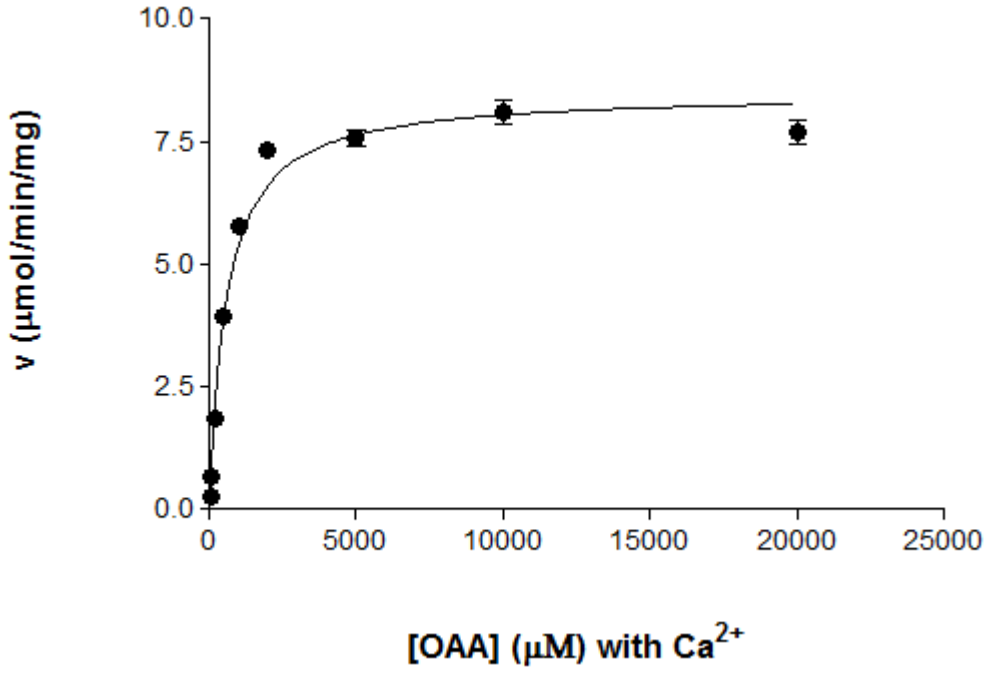

Figure 7.18: Michaelis-Menten plot of v as a function of [OAA] in the presence of calcium for Tyr207Phe mutant PCK. K_m obtained from this plot is shown in table 3.3 and 4.4. V_{max} value obtained from this plot is shown in table 3.3 and used to calculate the k_{cat} value for Tyr207Phe mutant PCK shown in table 4.1 and 4.4

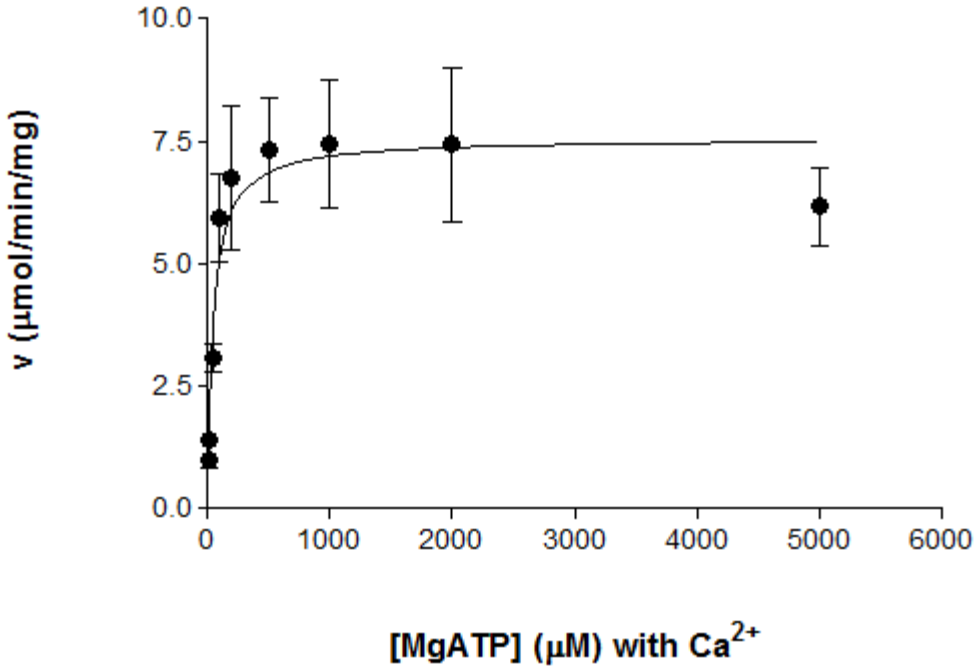

Figure 7.19: Michaelis-Menten plot of v as a function of [MgATP] in the presence of calcium for Tyr207Phe mutant PCK. K_m obtained from this plot is shown in table 3.3 and 4.4. V_{max} value obtained from this plot is shown in table 3.3 and used to calculate the k_{cat} value for Tyr207Phe mutant PCK shown in table 4.1 and 4.4

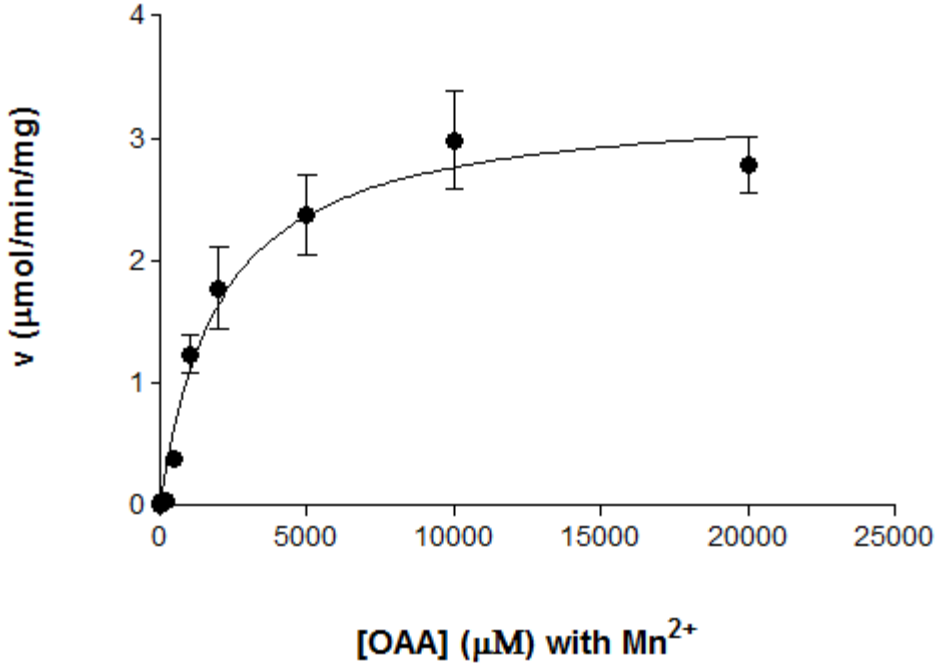

Figure 7.20: Michaelis-Menten plot of v as a function of [OAA] in the presence of manganese for Tyr207Phe mutant PCK. K_m obtained from this plot is shown in table 3.3 and 4.3. V_{max} value obtained from this plot is shown in table 3.3 and used to calculate the k_{cat} value for Tyr207Phe mutant PCK shown in table 4.1 and 4.3

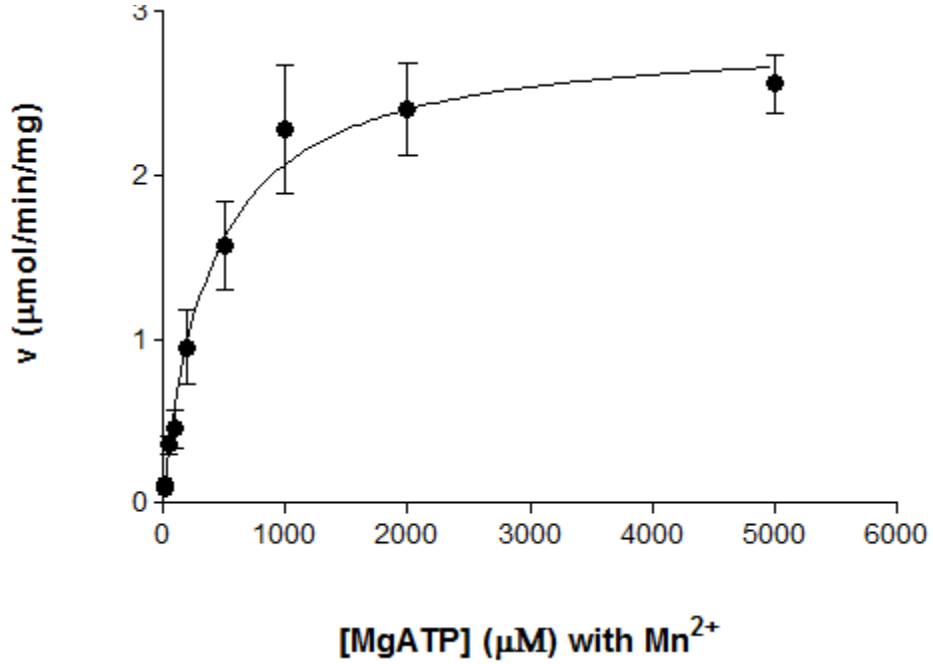

Figure 7.21: Michaelis-Menten plot of v as a function of [MgATP] in the presence of manganese for Tyr207Phe mutant PCK. K_m obtained from this plot is shown in table 3.3 and 4.3. V_{max} value obtained from this plot is shown in table 3.3 and used to calculate the k_{cat} value for Tyr207Phe mutant PCK shown in table 4.1 and 4.3

7.2.2 Lineweaver-Burk plots

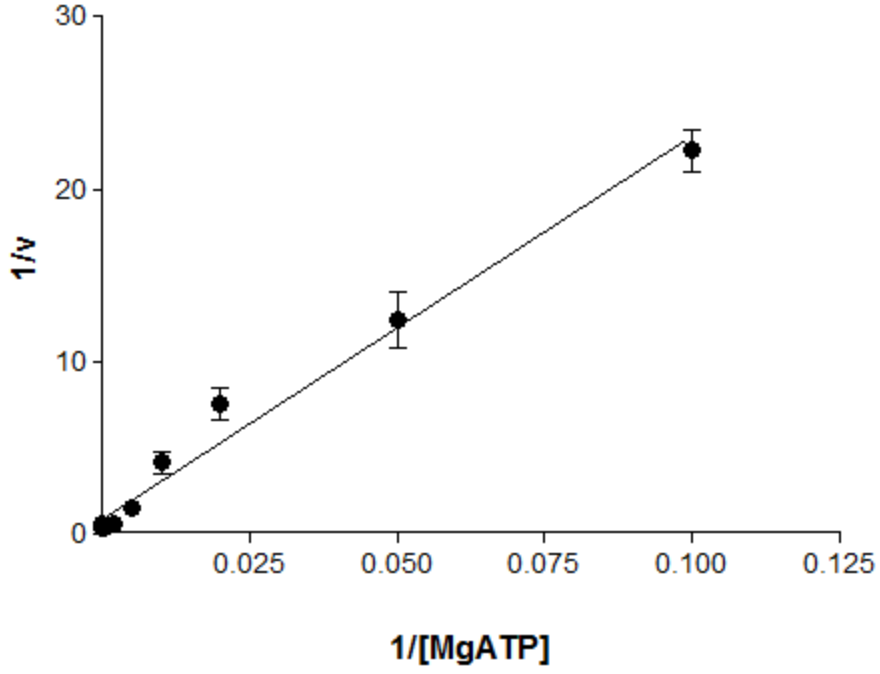

Figure 7.22: Lineweaver-Burk plot of 1/v as a function of 1/[MgATP] for Tyr207Phe mutant PCK. K_m and V_{max} values obtained from this plot are shown in table 3.3

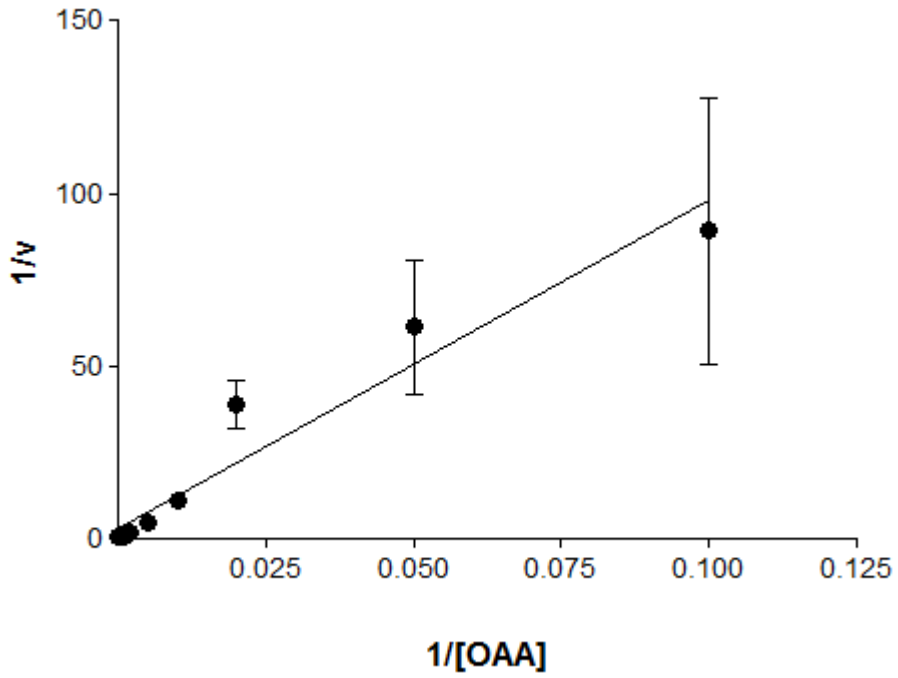

Figure 7.23: Lineweaver-Burk plot of 1/v as a function of 1/[OAA] for Tyr207Phe mutant PCK. K_m and V_{max} values obtained from this plot are shown in table 3.3

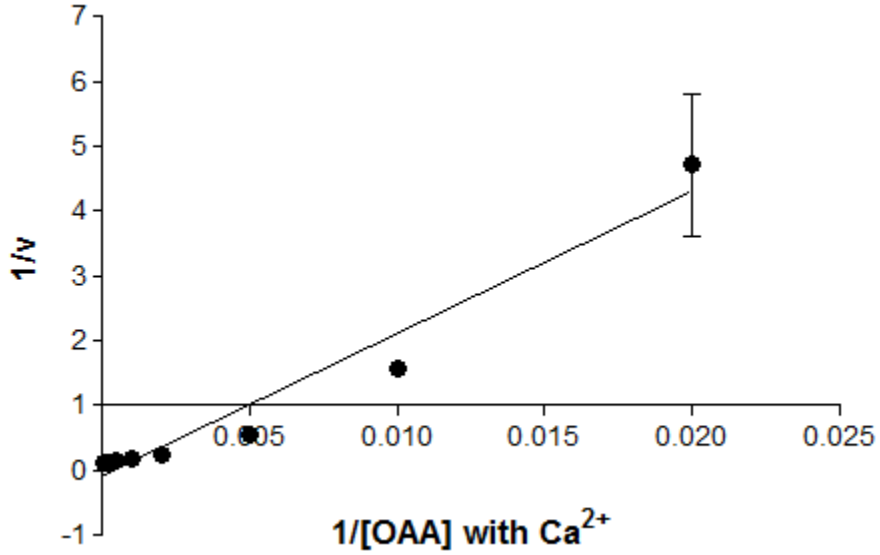

Figure 7.24: Lineweaver-Burk plot of 1/v as a function of 1/[OAA] in the presence of calcium for Tyr207Phe mutant PCK. K_m and V_{max} values obtained from this plot are shown in table 3.3

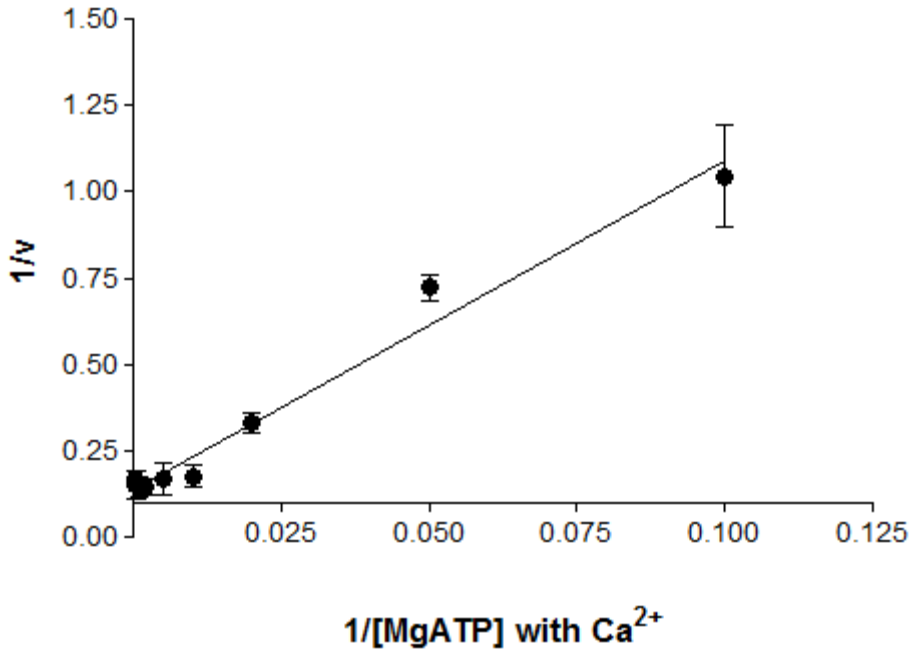

Figure 7.25: Lineweaver-Burk plot of 1/v as a function of 1/[MgATP] in the presence of calcium for Tyr207Phe mutant PCK. K_m and V_{max} values obtained from this plot are shown in table 3.3

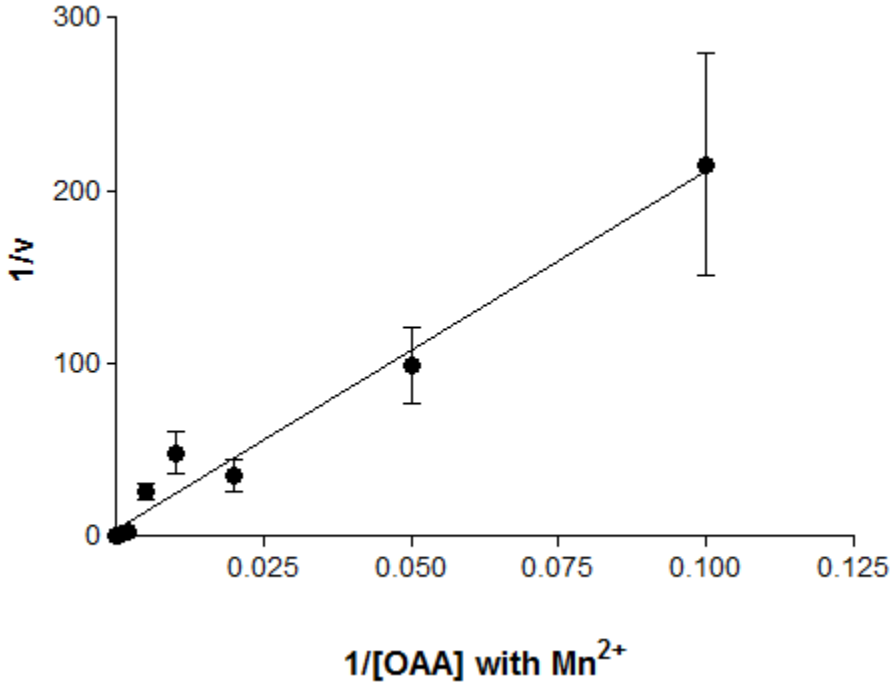

Figure 7.26: Lineweaver-Burk plot of 1/v as a function of 1/[OAA] in the presence of manganese for Tyr207Phe mutant PCK. K_m and V_{max} values obtained from this plot are shown in table 3.3

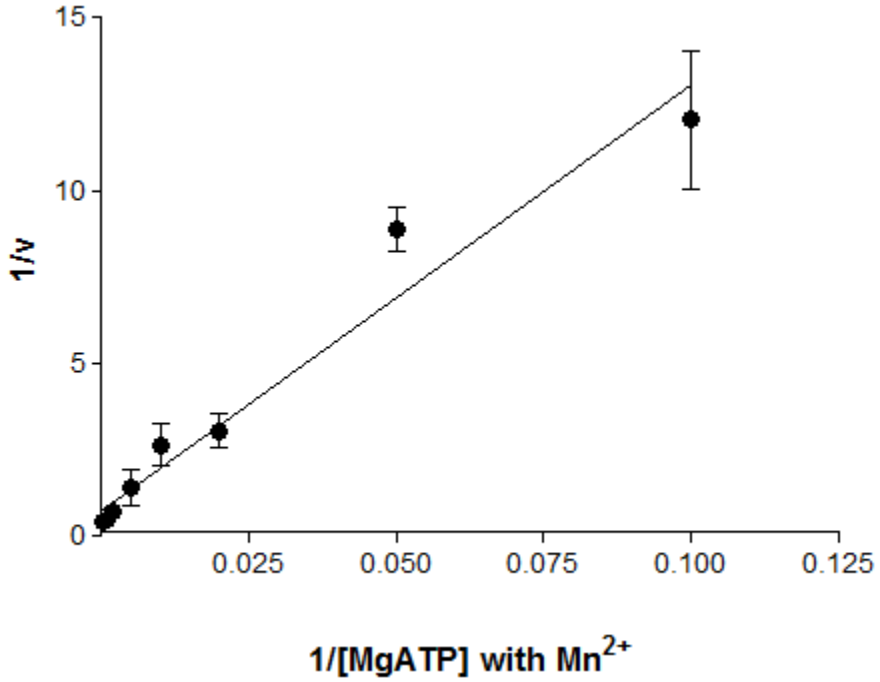

Figure 7.27: Lineweaver-Burk plot of 1/v as a function of 1/[MgATP] in the presence of manganese for Tyr207Phe mutant PCK. K_m and V_{max} values obtained from this plot are shown in table 3.3

7.2.3 Eadie-Hofstee plots

Average velocities was used to calculate the velocities used for Eadie-Hofstee plots because v is present on both axes, hence error bars are not shown for these plots.

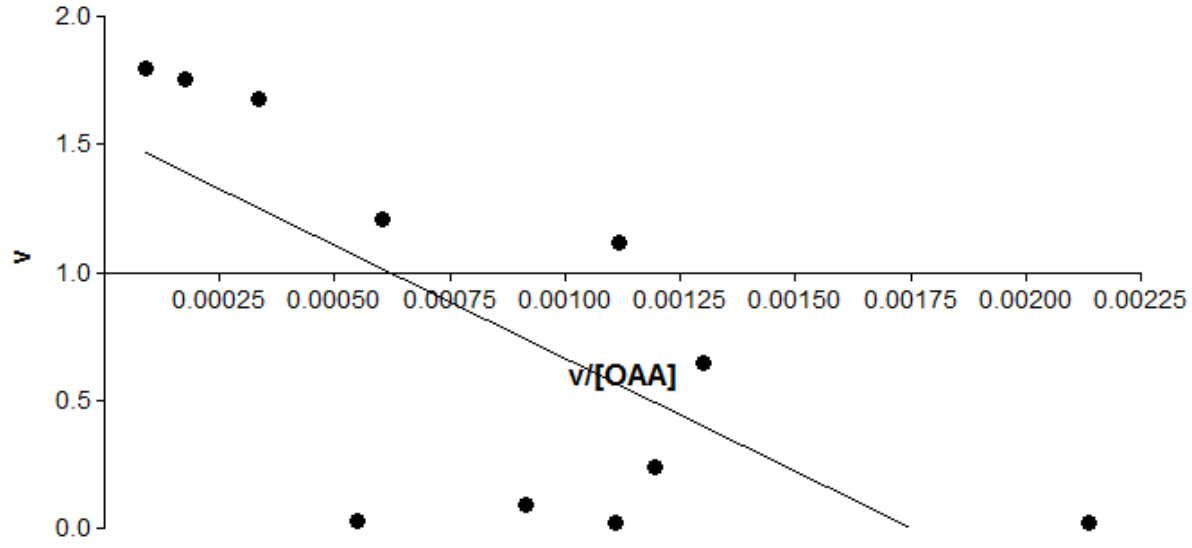

Figure 7.28: Eadie-Hofstee plot of v as a function of v/[OAA] for Tyr207Phe mutant PCK. K_m and V_{max} values obtained from this plot are shown in table 3.3

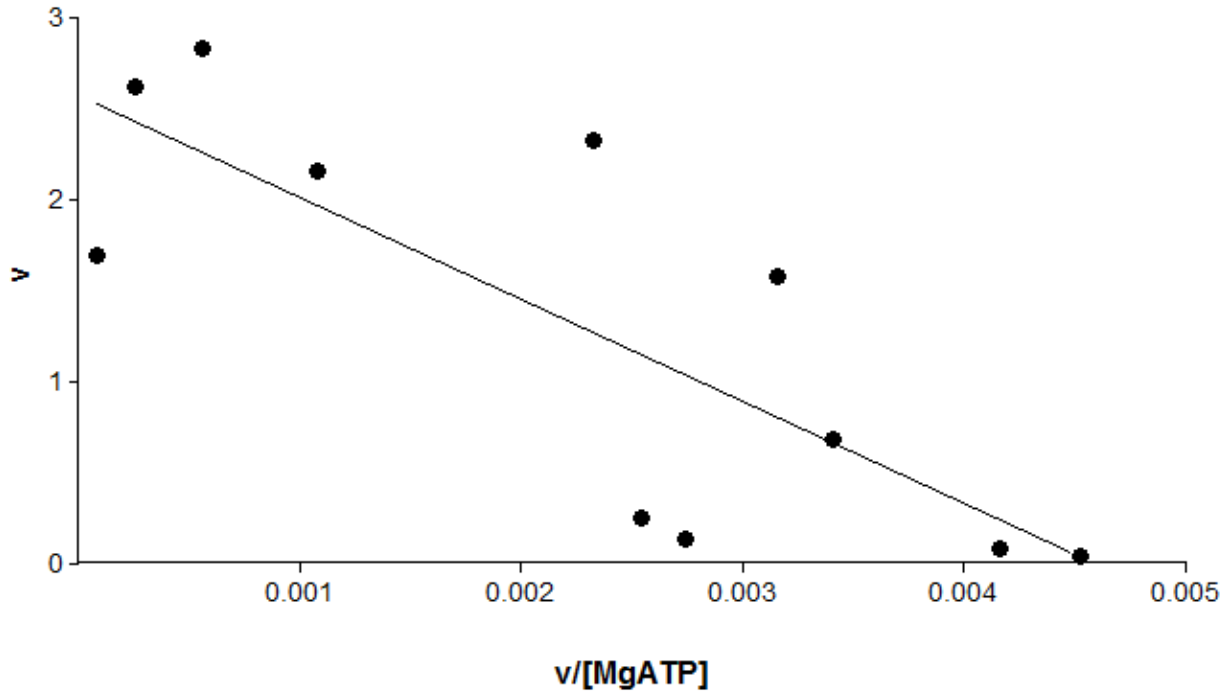

Figure 7.29: Eadie-Hofstee plot of v as a function of v/[MgATP] for Tyr207Phe mutant PCK. K_m and V_{max} values obtained from this plot are shown in table 3.3

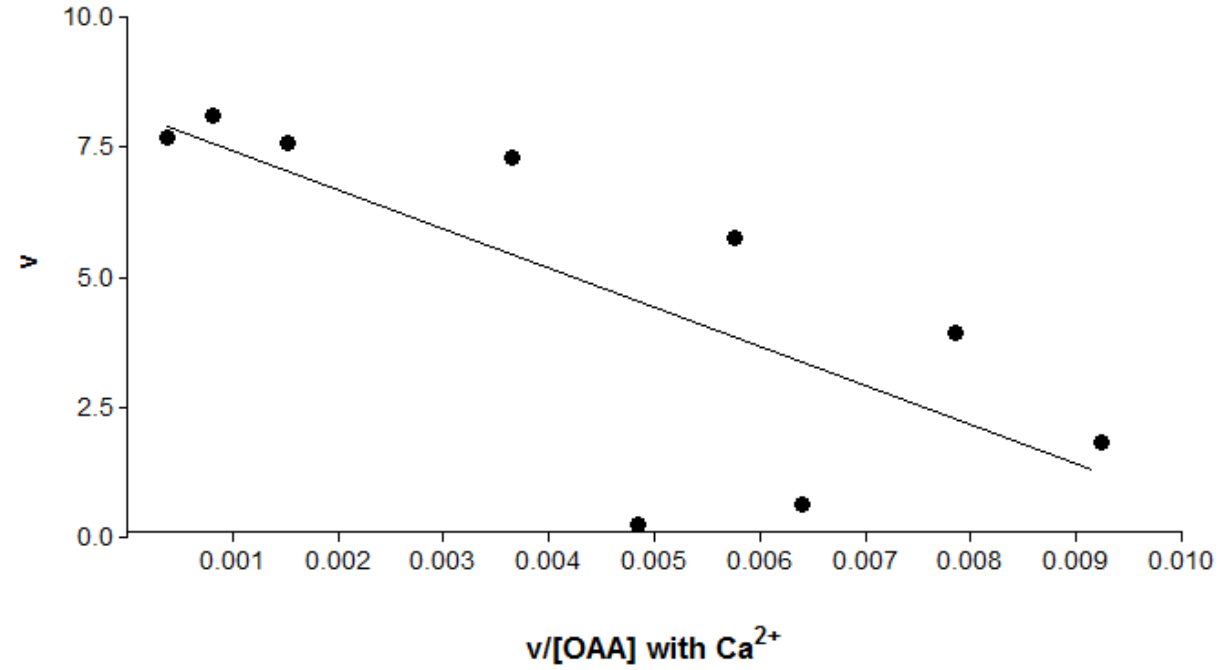

Figure 7.30: Eadie-Hofstee plot of v as a function of v/[OAA] in the presence of calcium for Tyr207Phe mutant PCK. K_m and V_{max} values obtained from this plot are shown in table 3.3

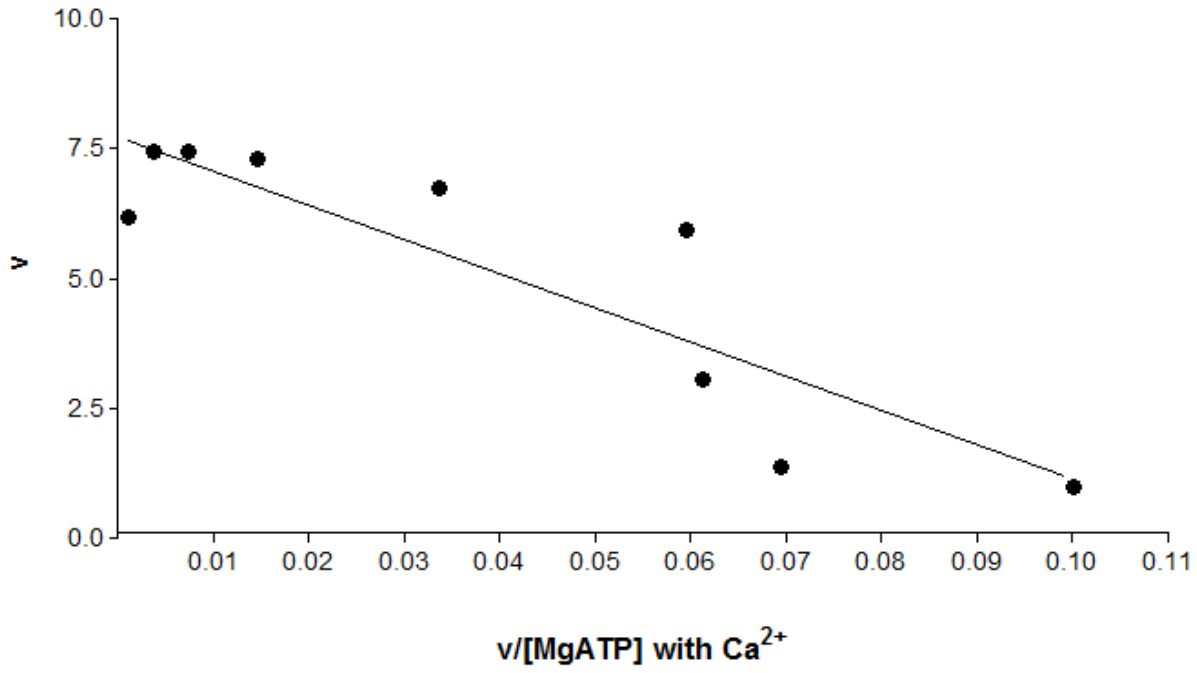

Figure 7.31: Eadie-Hofstee plot of v as a function of v/[MgATP] in the presence of calcium for Tyr207Phe mutant PCK. K_m and V_{max} values obtained from this plot are shown in table 3.3

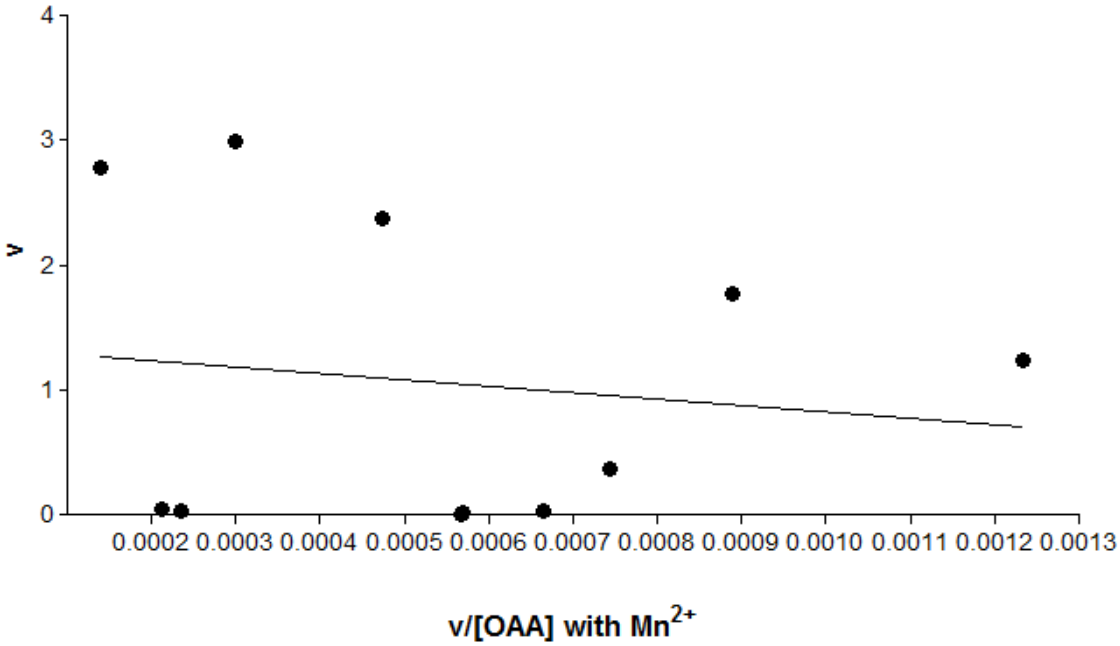

Figure 7.32: Eadie-Hofstee plot of v as a function of v/[OAA] in the presence of manganese for Tyr207Phe mutant PCK. K_m and V_{max} values obtained from this plot are shown in table 3.3

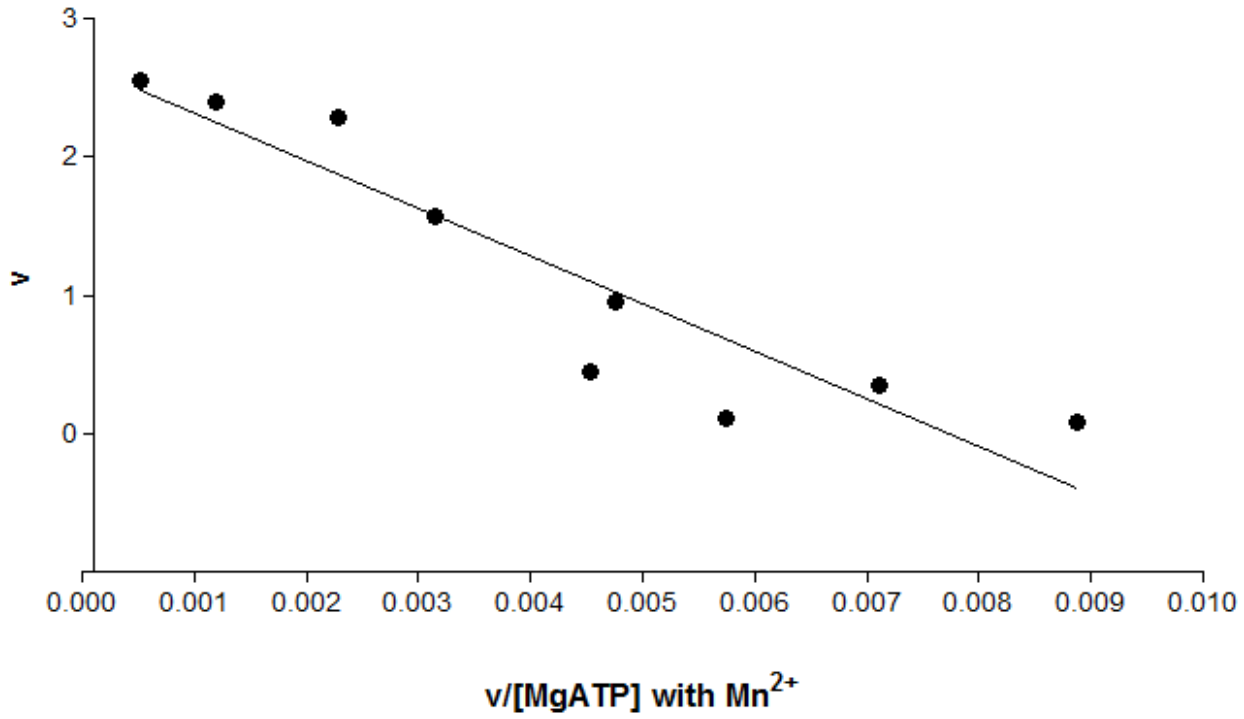

Figure 7.33: Eadie-Hofstee plot of v as a function of v/[MgATP] in the presence of manganese for Tyr207Phe mutant PCK. K_m and V_{max} values obtained from this plot are shown in table 3.3.

7.3 Ser250Ala

7.3.1 Michaelis-Menten plots

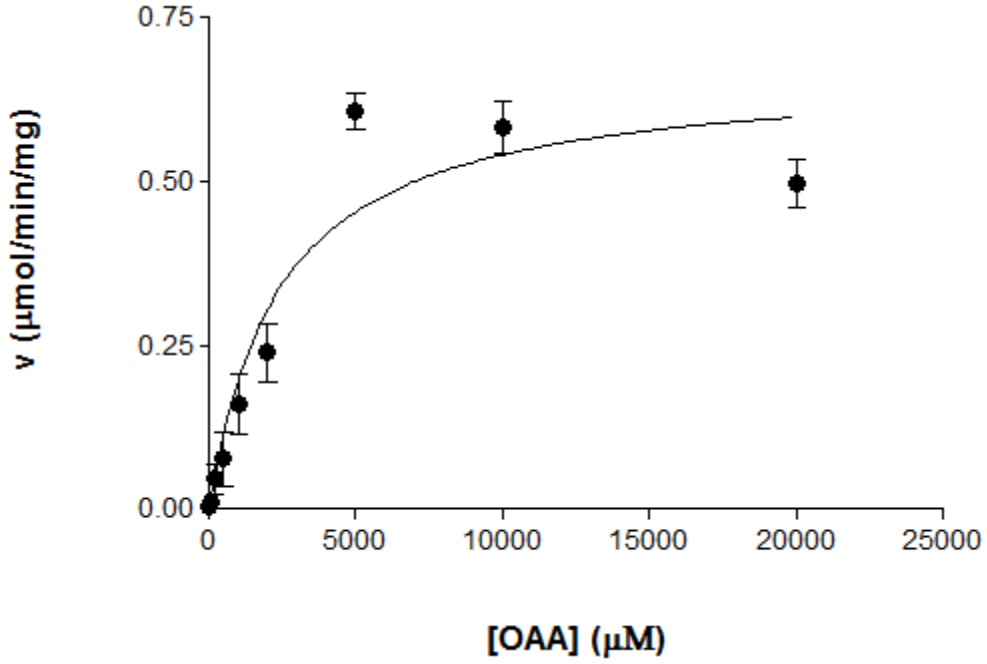

Figure 7.34: Michaelis-Menten plot of v as a function of [OAA] for Ser250Ala mutant PCK. K_m obtained from this plot is shown in table 3.4 and 4.2. V_{max} value obtained from this plot is shown in table 3.4 and used to calculate the k_{cat} value for Ser250Ala mutant PCK shown in table 4.1 and 4.2

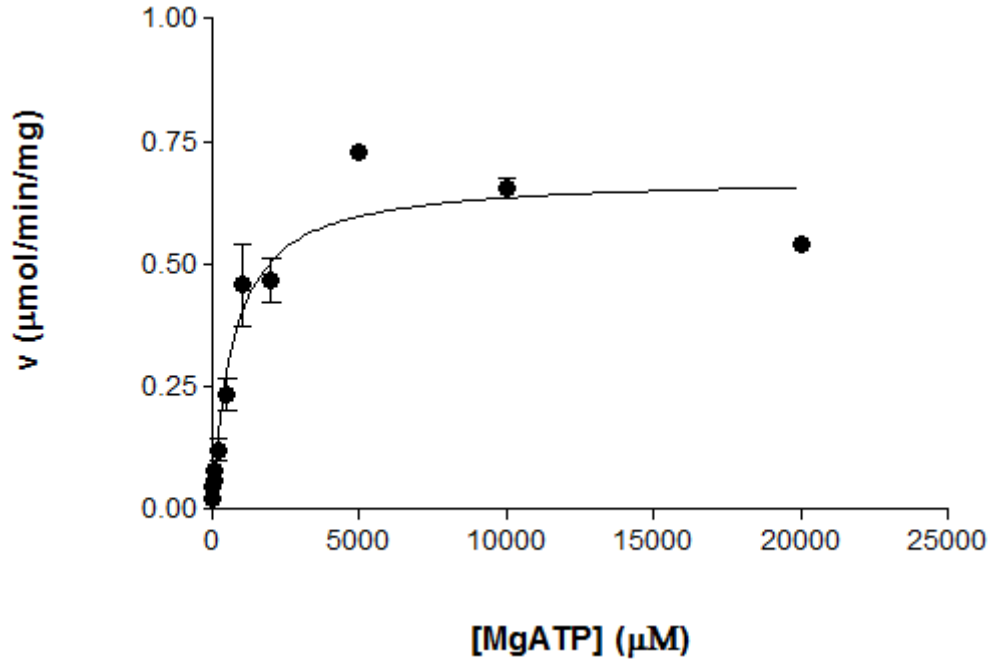

Figure 7.35: Michaelis-Menten plot of v as a function of [MgATP] for Ser250Ala mutant PCK. K_m obtained from this plot is shown in table 3.4 and 4.2. V_{max} value obtained from this plot is shown in table 3.4 and used to calculate the k_{cat} value for Ser250Ala mutant PCK shown in table 4.1 and 4.2

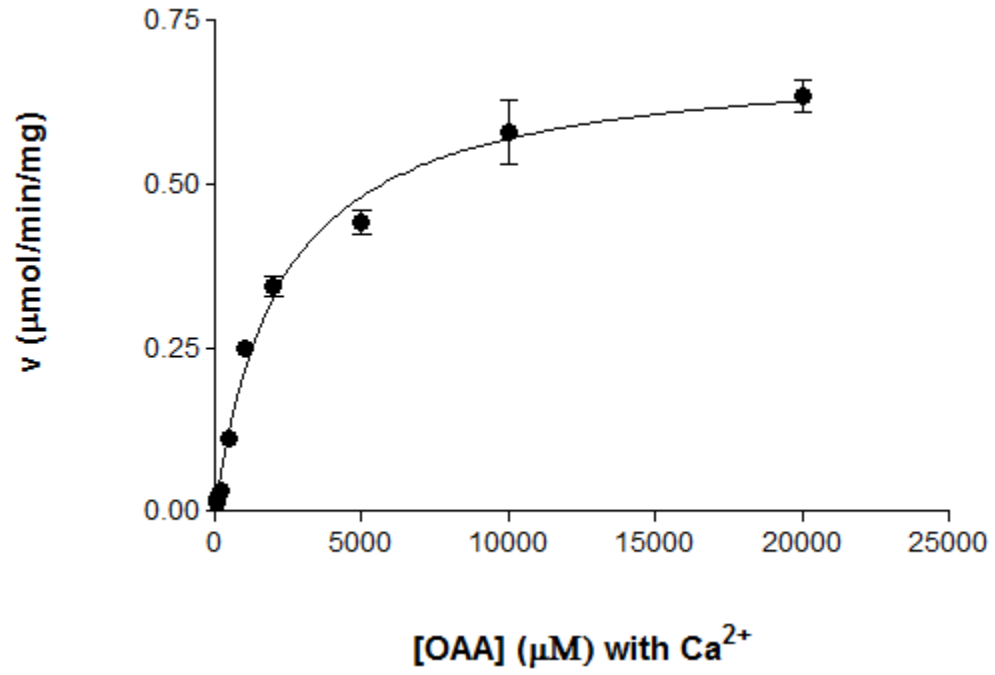

Figure 7.36: Michaelis-Menten plot of v as a function of [OAA] in the presence of calcium for Ser250Ala mutant PCK. K_m obtained from this plot is shown in table 3.4 and 4.4. V_{max} value obtained from this plot is shown in table 3.4 and used to calculate the k_{cat} value for Ser250Ala mutant PCK shown in table 4.1 and 4.4

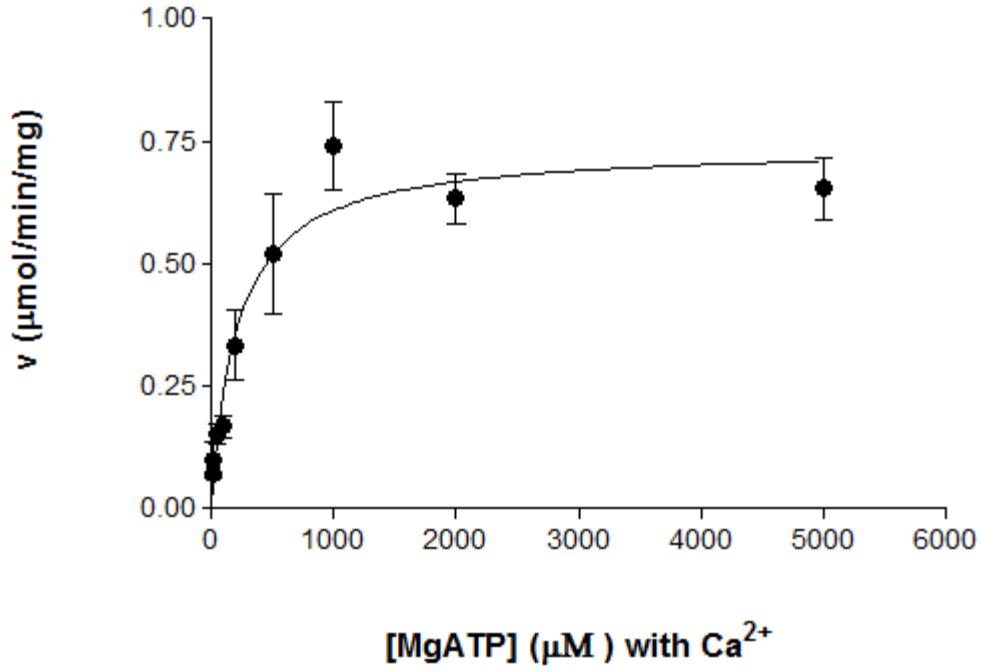

Figure 7.37: Michaelis-Menten plot of v as a function of [MgATP] in the presence of calcium for Ser250Ala mutant PCK. K_m obtained from this plot is shown in table 3.4 and 4.4. V_{max} value obtained from this plot is shown in table 3.4 and used to calculate the k_{cat} value for Ser250Ala mutant PCK shown in table 4.1 and 4.4

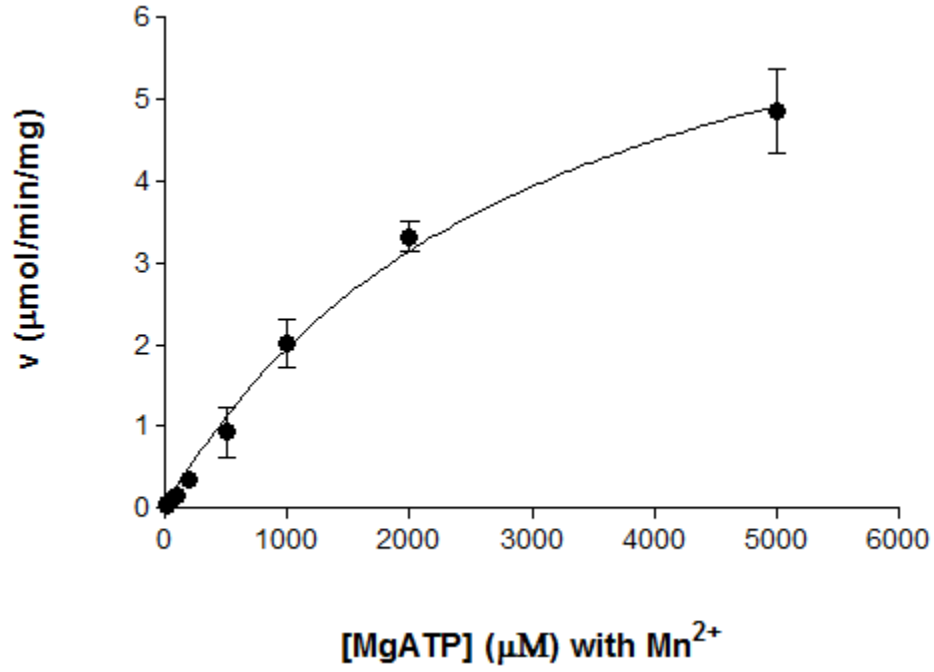

Figure 7.38: Michaelis-Menten plot of v as a function of [MgATP] in the presence of manganese for Ser250Ala mutant PCK. K_m obtained from this plot is shown in table 3.4 and 4.3. V_{max} value obtained from this plot is shown in table 3.4 and used to calculate the k_{cat} value for Ser250Ala mutant PCK shown in table 4.1 and 4.3

7.3.2 Lineweaver-Burk plot

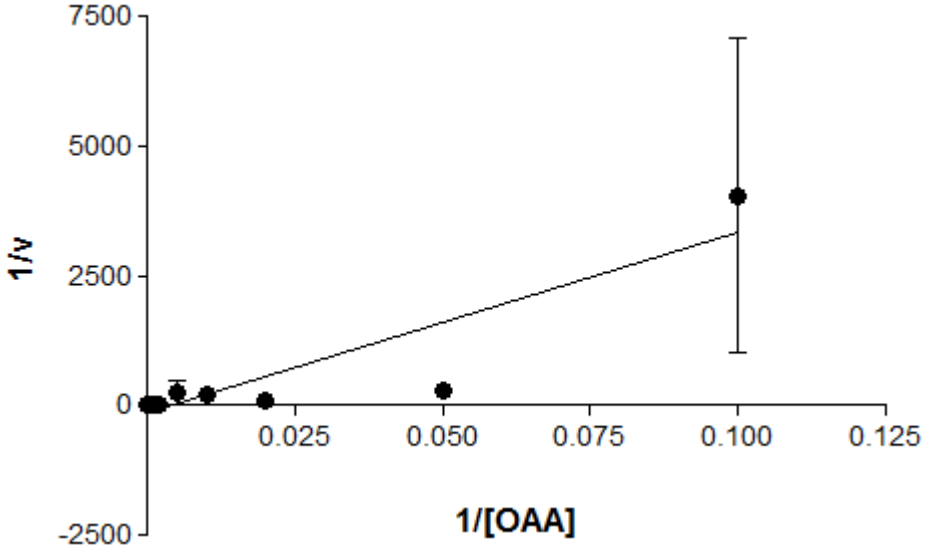

Figure 7.39: Lineweaver-Burk plot of 1/v as a function of 1/[OAA] for Ser250Ala mutant PCK. K_m and V_{max} values obtained from this plot are shown in table 3.4

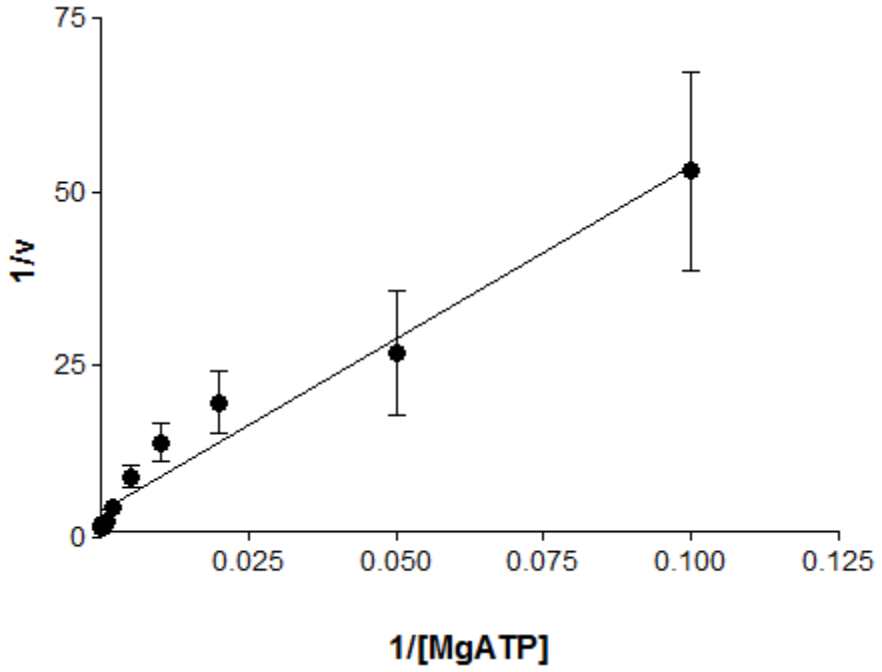

Figure 7.40: Lineweaver-Burk plot of 1/v as a function of 1/[MgATP] for Ser250Ala mutant PCK. K_m and V_{max} values obtained from this plot are shown in table 3.4

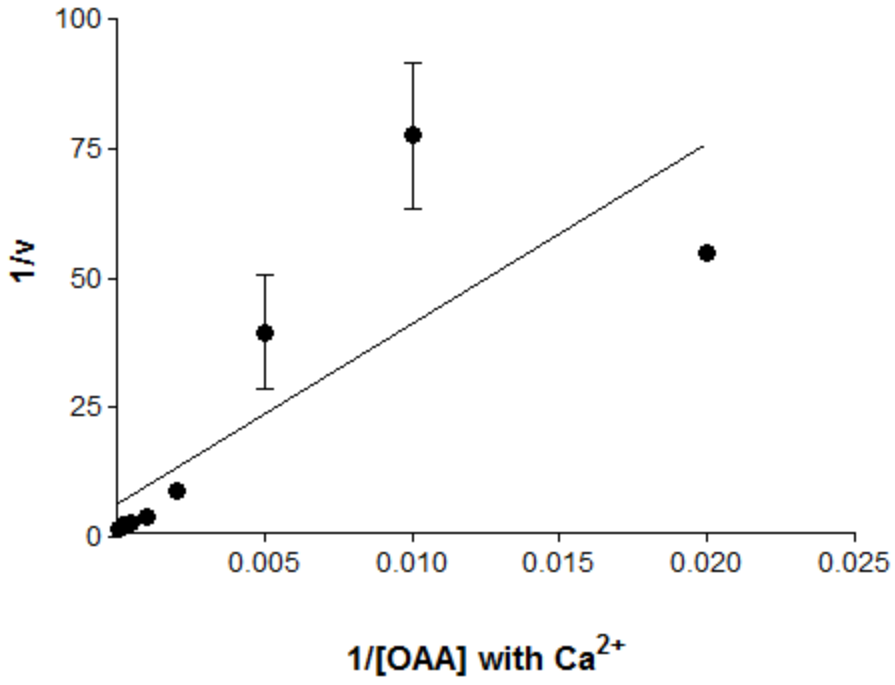

Figure 7.41: Lineweaver-Burk plot of 1/v as a function of 1/[OAA] in the presence of calcium for Ser250Ala mutant PCK. K_m and V_{max} values obtained from this plot are shown in table 3.4

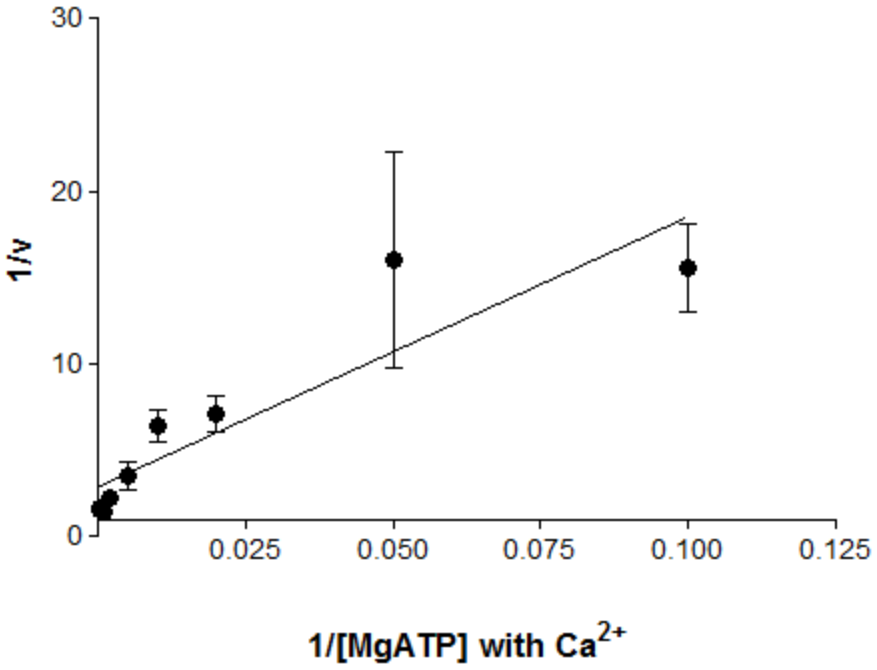

Figure 7.42: Lineweaver-Burk plot of 1/v as a function of 1/[MgATP] in the presence of calcium for Ser250Ala mutant PCK. K_m and V_{max} values obtained from this plot are shown in table 3.4

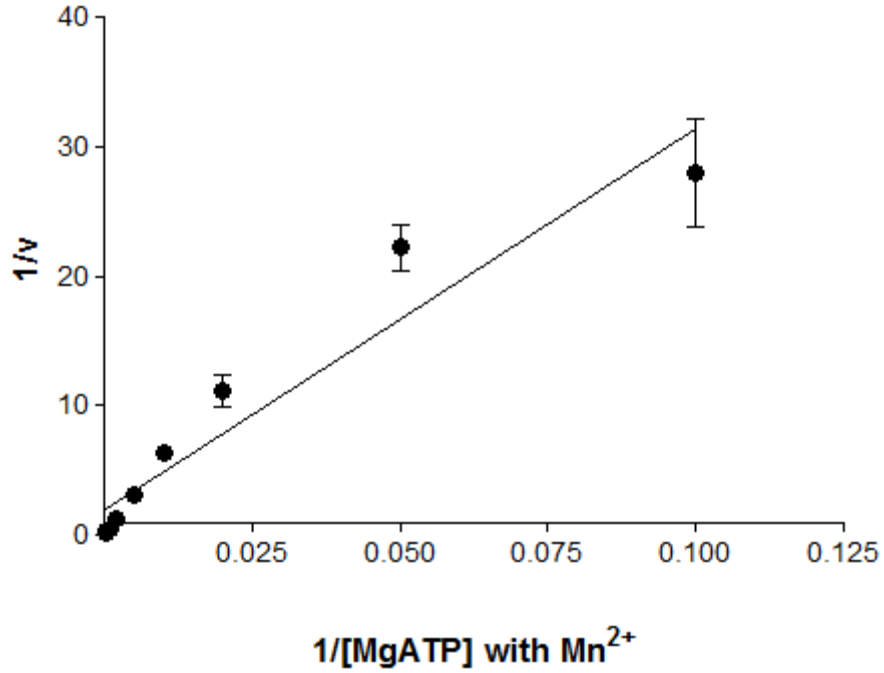

Figure 7.43: Lineweaver-Burk plot of 1/v as a function of 1/[MgATP] in the presence of manganese for Ser250Ala mutant PCK. K_m and V_{max} values obtained from this plot are shown in table 3.4

7.3.3 Eadie-Hofstee plot

Average velocities was used to calculate the velocities used for Eadie-Hofstee plots because v is present on both axes, hence error bars are not shown for these plots

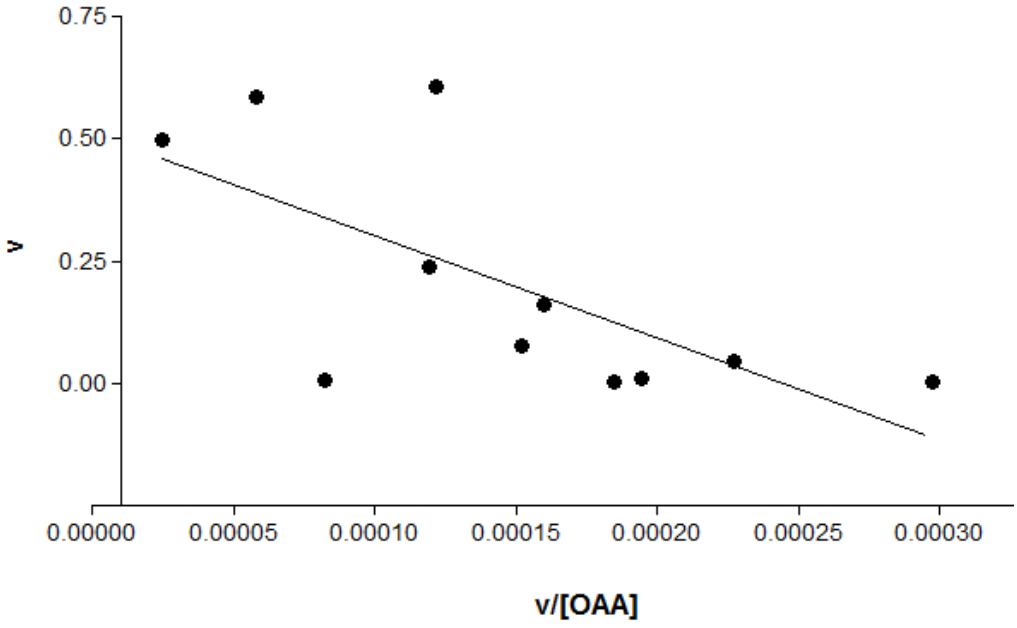

Figure 7.44: Eadie-Hofstee plot of v as a function of v/[OAA] for Ser250Ala mutant PCK. K_m and V_{max} values obtained from this plot are shown in table 3.4

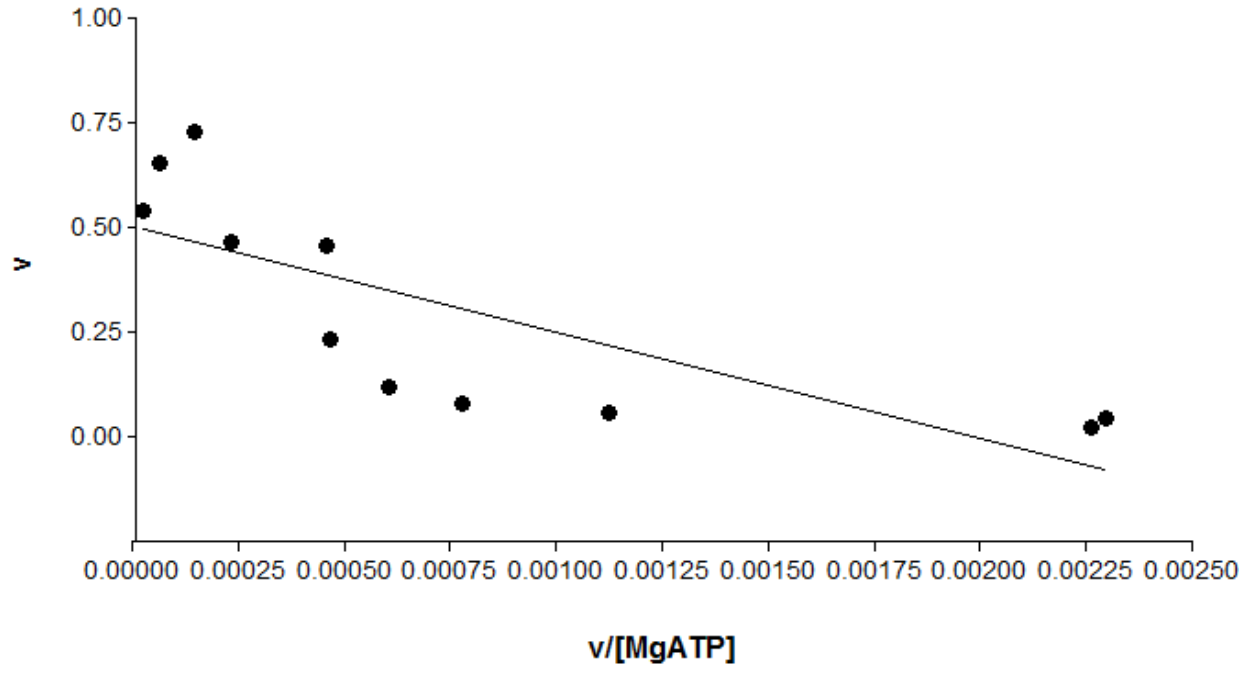

Figure 7.45: Eadie-Hofstee plot of v as a function of v/[MgATP] for Ser250Ala mutant PCK. K_m and V_{max} values obtained from this plot are shown in table 3.4

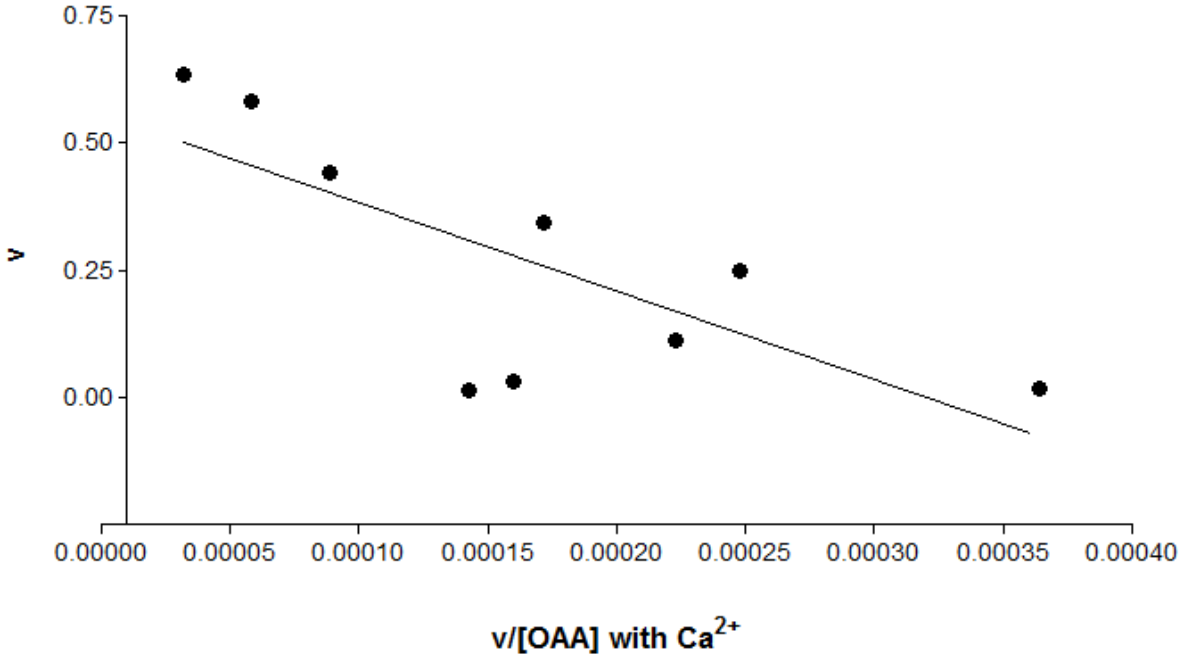

Figure 7.46: Eadie-Hofstee plot of v as a function of v/[OAA] in the presence of calcium for Ser250Ala mutant PCK. K_m and V_{max} values obtained from this plot are shown in table 3.4

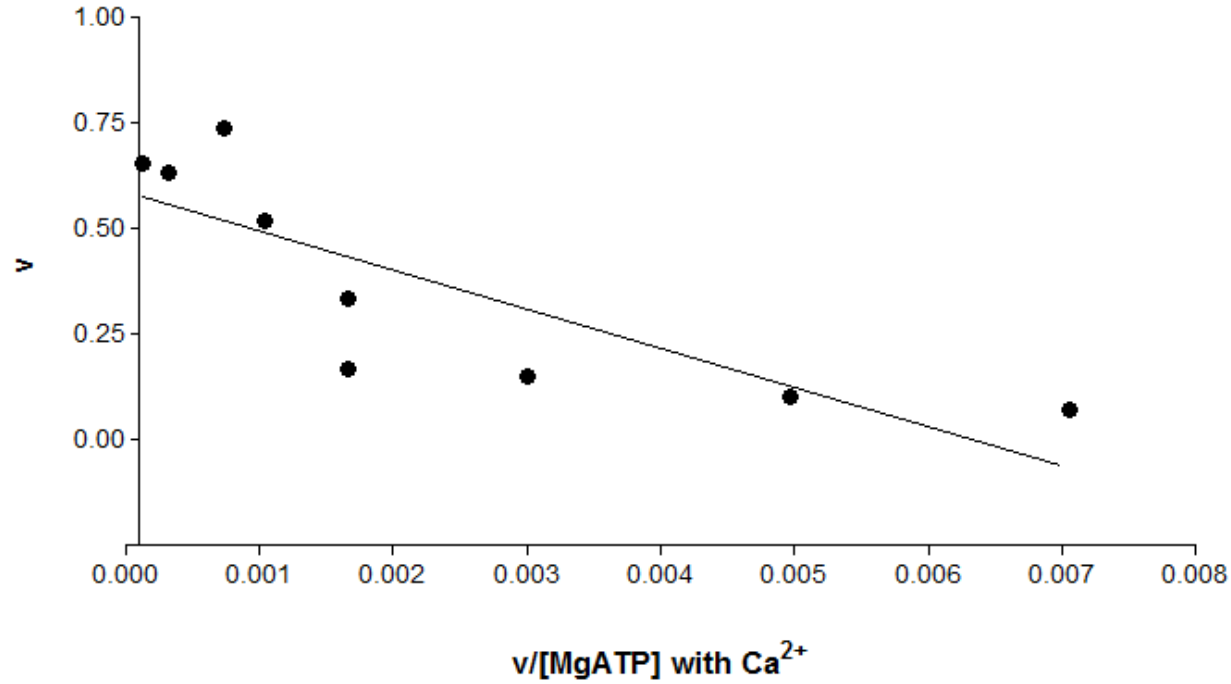

Figure 7.47: Eadie-Hofstee plot of v as a function of v/[MgATP] in the presence of calcium for Ser250Ala mutant PCK. K_m and V_{max} values obtained from this plot are shown in table 3.4

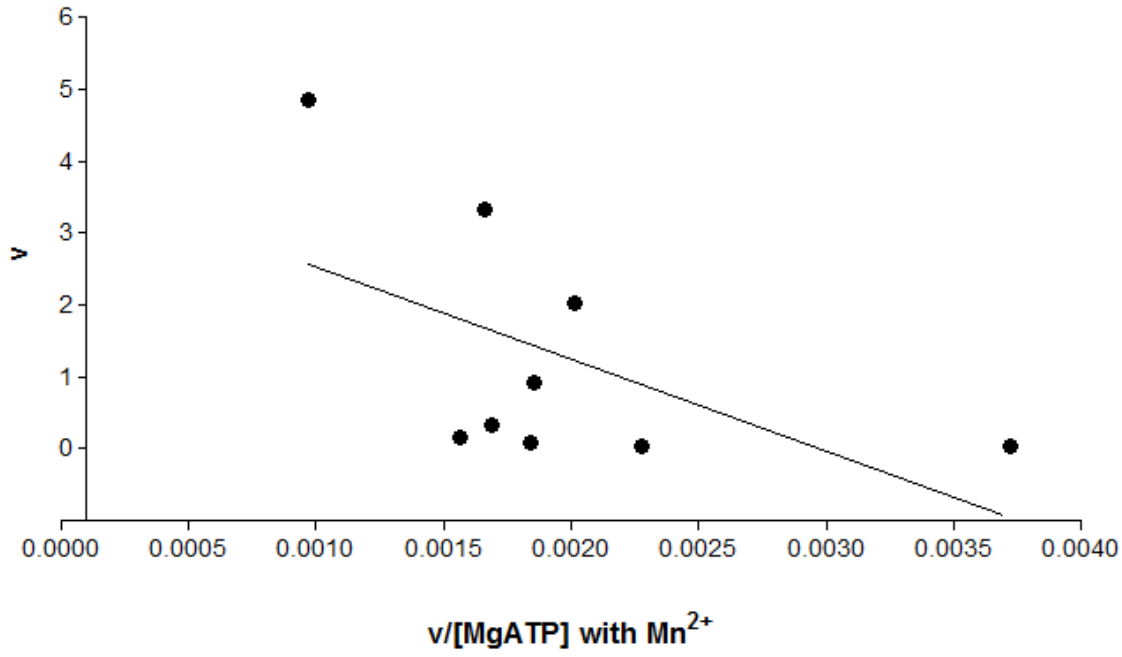

Figure 7.48: Eadie-Hofstee plot of v as a function of v/[MgATP] in the presence of manganese for Ser250Ala mutant PCK. K_m and V_{max} values obtained from this plot are shown in table 3.4

7.4 Arg333Gln

7.4.1 Michaelis-Menten plot

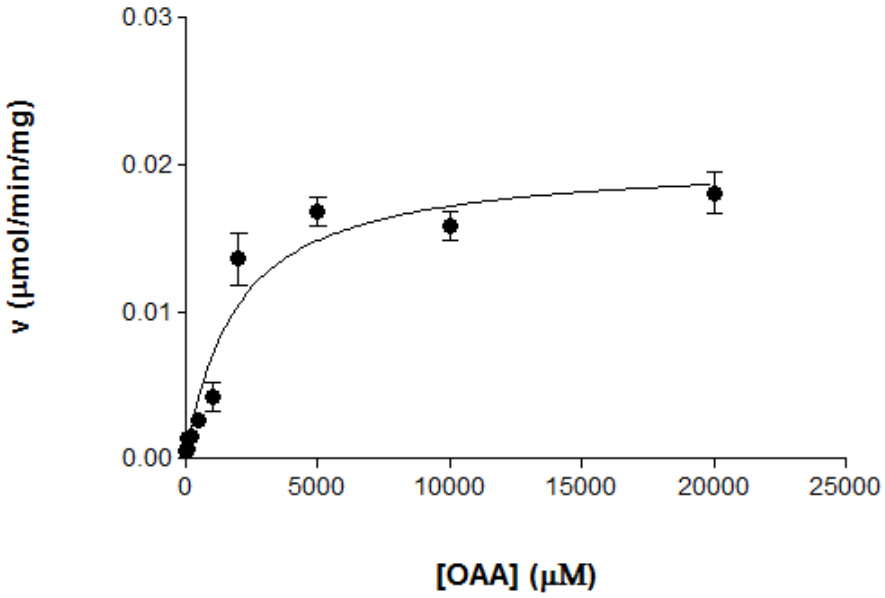

Figure 7.49: Michaelis-Menten plot of v as a function of [OAA] for Arg333Gln mutant PCK. K_m obtained from this plot is shown in table 3.5 and 4.2. V_{max} value obtained from this plot is shown in table 3.5 and used to calculate the k_{cat} value for Arg333Gln mutant PCK shown in table 4.1 and 4.2

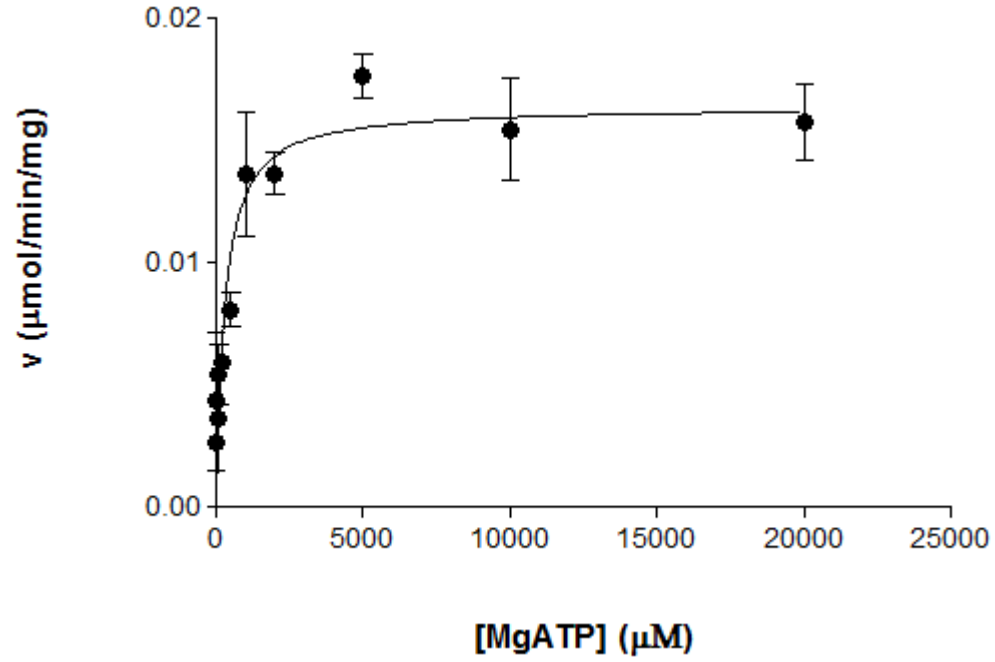

Figure 7.50: Michaelis-Menten plot of v as a function of [MgATP] for Arg333Gln mutant PCK. K_m obtained from this plot is shown in table 3.5 and 4.2. V_{max} value obtained from this plot is shown in table 3.5 and used to calculate the k_{cat} value for Arg333Gln mutant PCK shown in table 4.1 and 4.2

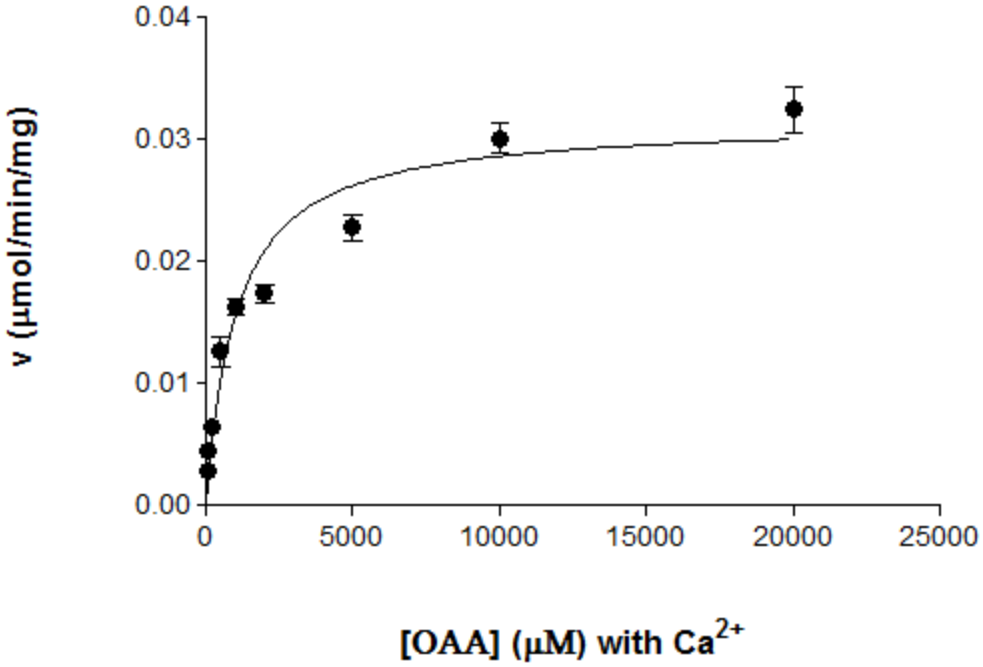

Figure 7.51: Michaelis-Menten plot of v as a function of [OAA] in the presence of calcium for Arg333Gln mutant PCK. K_m obtained from this plot is shown in table 3.5 and 4.4. V_{max} value obtained from this plot is shown in table 3.5 and used to calculate the k_{cat} value for Arg333Gln mutant PCK shown in table 4.1 and 4.4

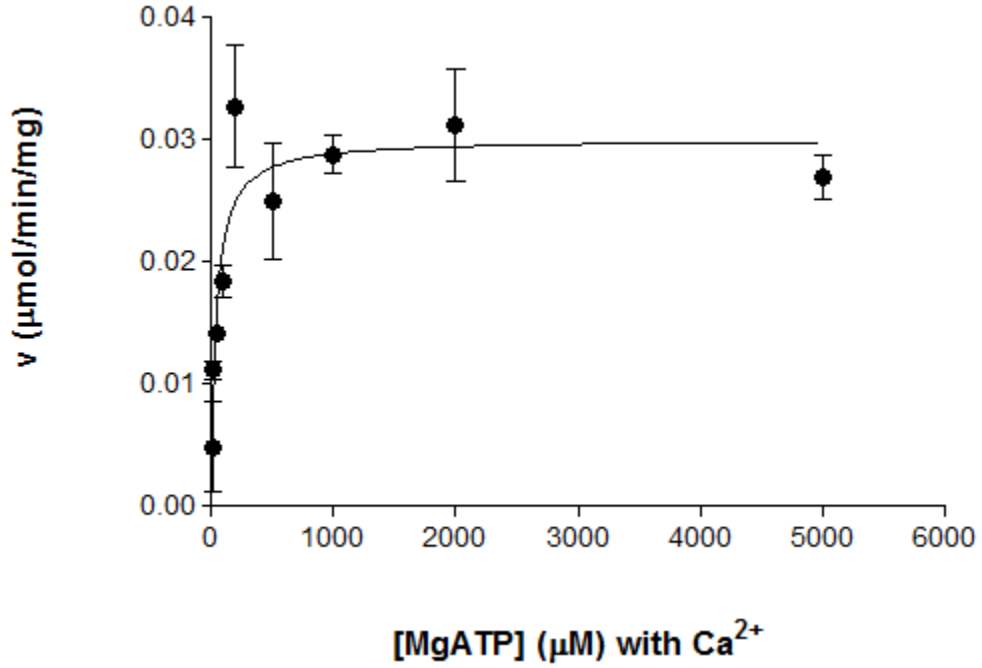

Figure 7.52: Michaelis-Menten plot of v as a function of [MgATP] in the presence of calcium for Arg333Gln mutant PCK. K_m obtained from this plot is shown in table 3.5 and 4.4. V_{max} value obtained from this plot is shown in table 3.5 and used to calculate the k_{cat} value for Arg333Gln mutant PCK shown in table 4.1 and 4.4

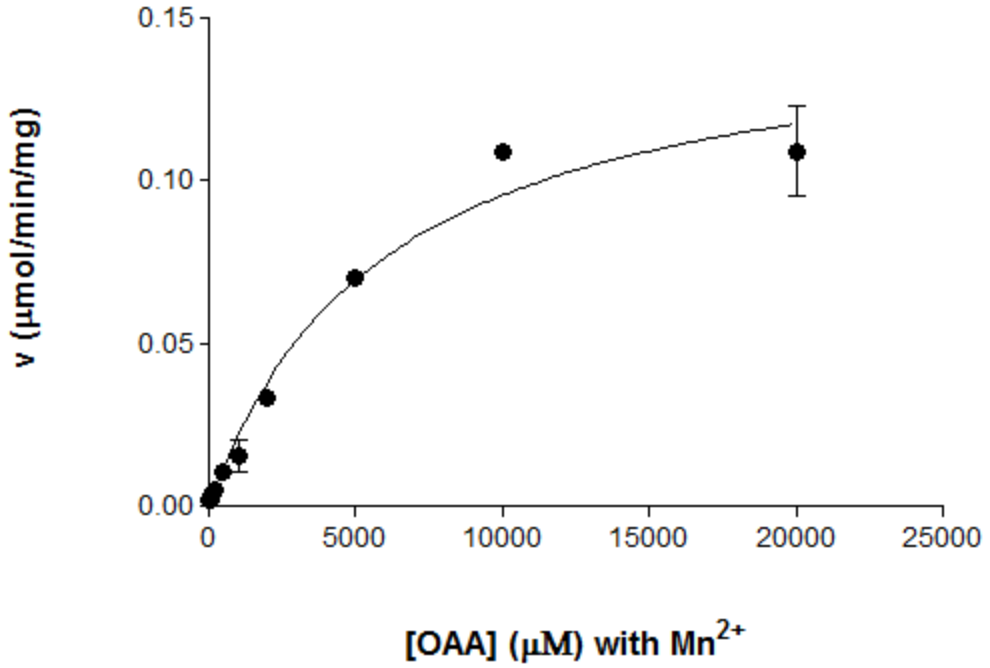

Figure 7.53: Michaelis-Menten plot of v as a function of [OAA] in the presence of manganese for Arg333Gln mutant PCK. K_m obtained from this plot is shown in table 3.5 and 4.3. V_{max} value obtained from this plot is shown in table 3.5 and used to calculate the k_{cat} value for Arg333Gln mutant PCK shown in table 4.1 and 4.3

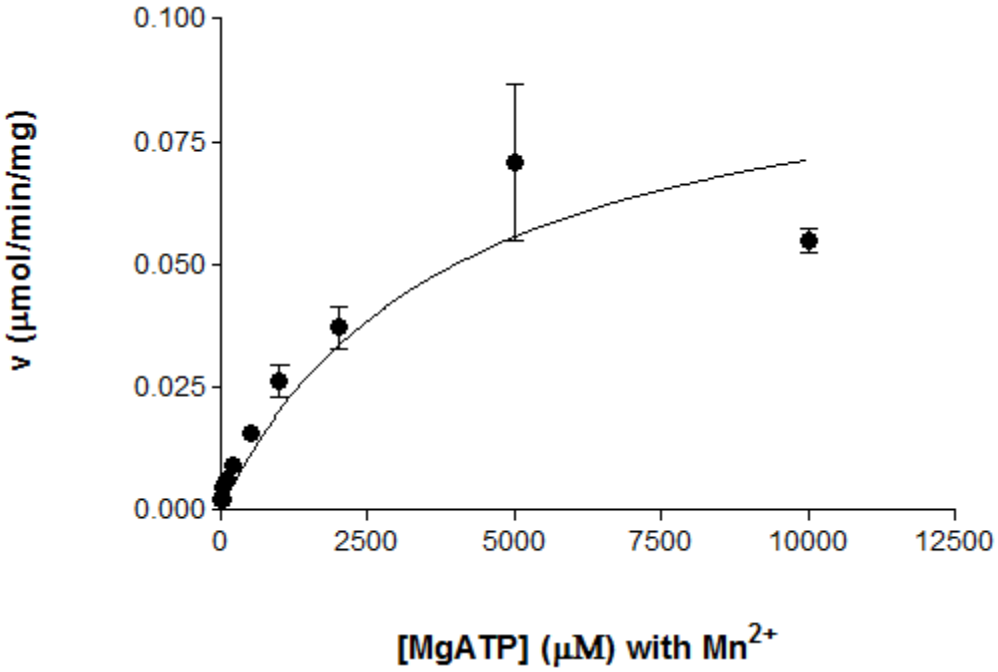

Figure 7.54: Michaelis-Menten plot of v as a function of [MgATP] in the presence of manganese for Arg333Gln mutant PCK. K_m obtained from this plot is shown in table 3.5 and 4.3. V_{max} value obtained from this plot is shown in table 3.5 and used to calculate the k_{cat} value for Arg333Gln mutant PCK shown in table 4.1 and 4.3

7.4.2 Lineweaver-Burk plot

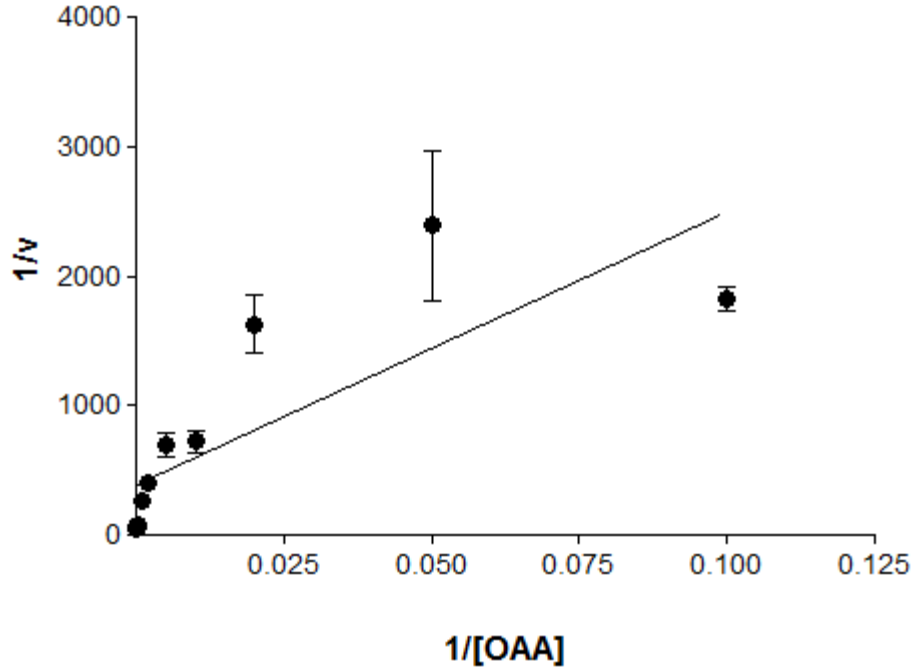

Figure 7.55: Lineweaver-Burk plot of 1/v as a function of 1/[OAA] for Arg333Gln mutant PCK. K_m and V_{max} values obtained from this plot are shown in table 3.5

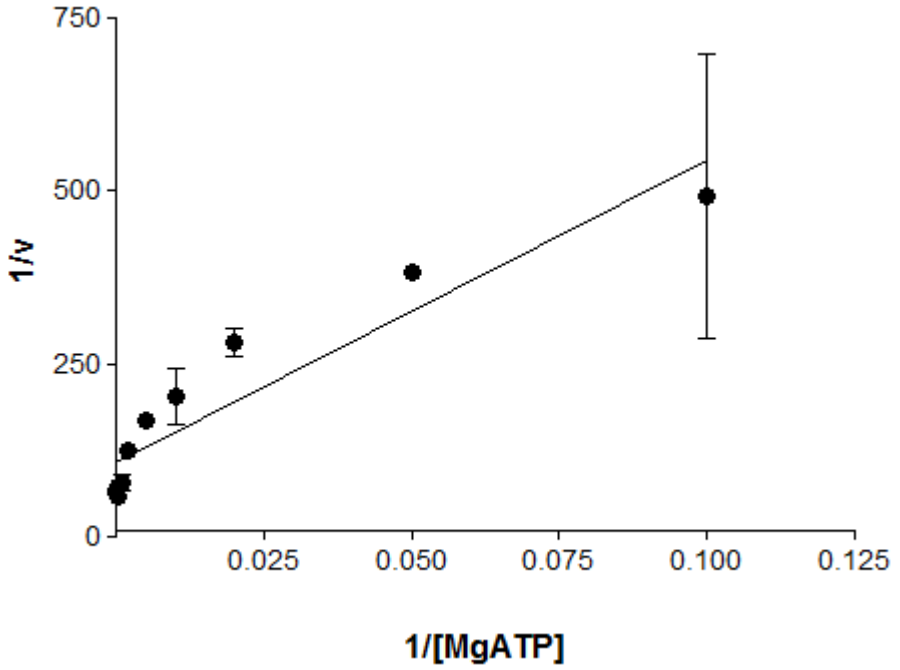

Figure 7.56: Lineweaver-Burk plot of 1/v as a function of 1/[MgATP] for Arg333Gln mutant PCK. K_m and V_{max} values obtained from this plot are shown in table 3.5

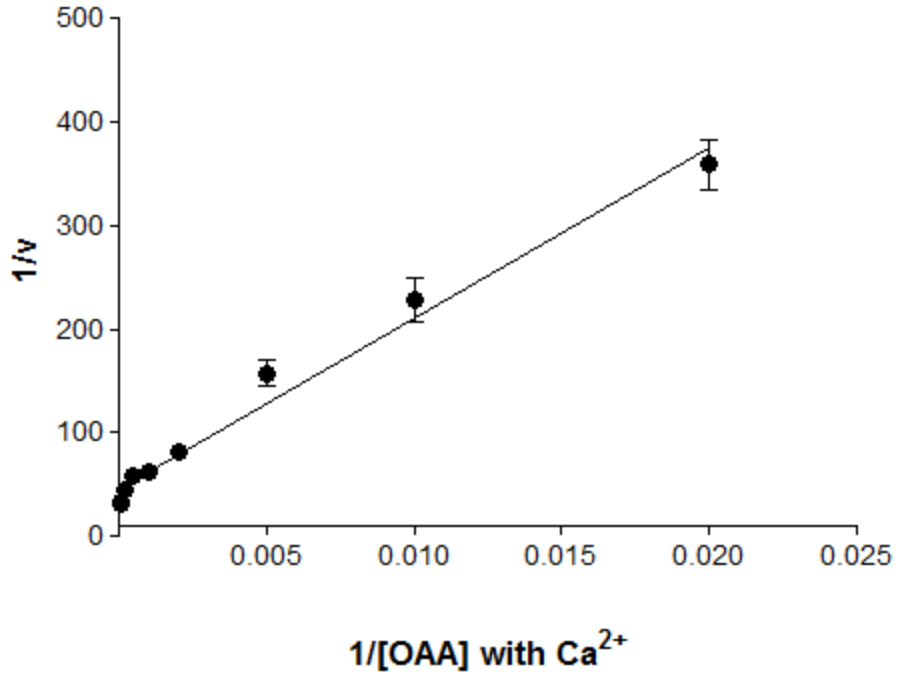

Figure 7.57: Lineweaver-Burk plot of 1/v as a function of 1/[OAA] in the presence of calcium for Arg333Gln mutant PCK. K_m and V_{max} values obtained from this plot are shown in table 3.5

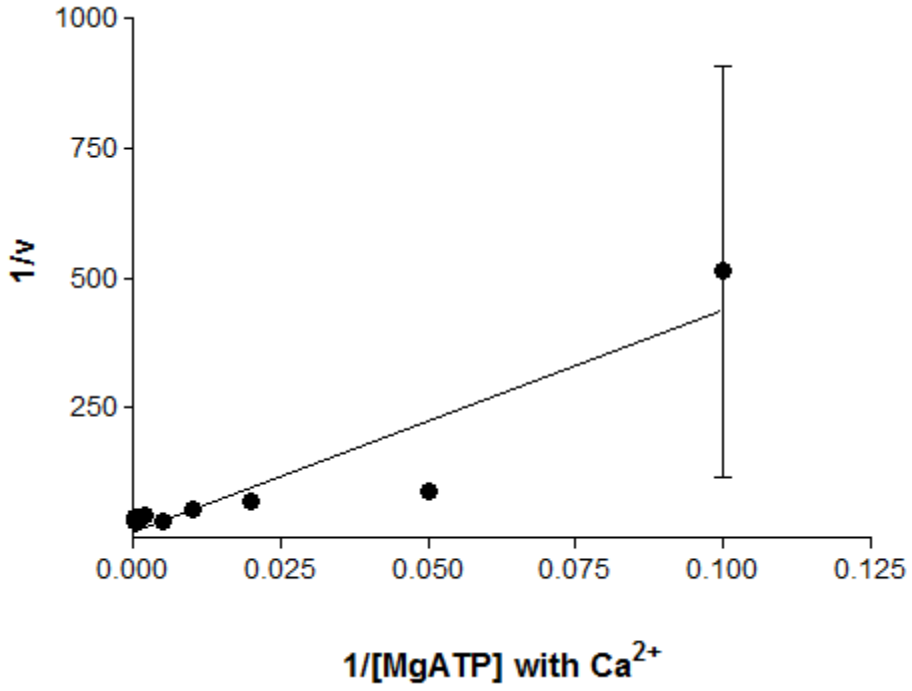

Figure 7.58: Lineweaver-Burk plot of 1/v as a function of 1/[MgATP] in the presence of calcium for Arg333Gln mutant PCK. K_m and V_{max} values obtained from this plot are shown in table 3.5

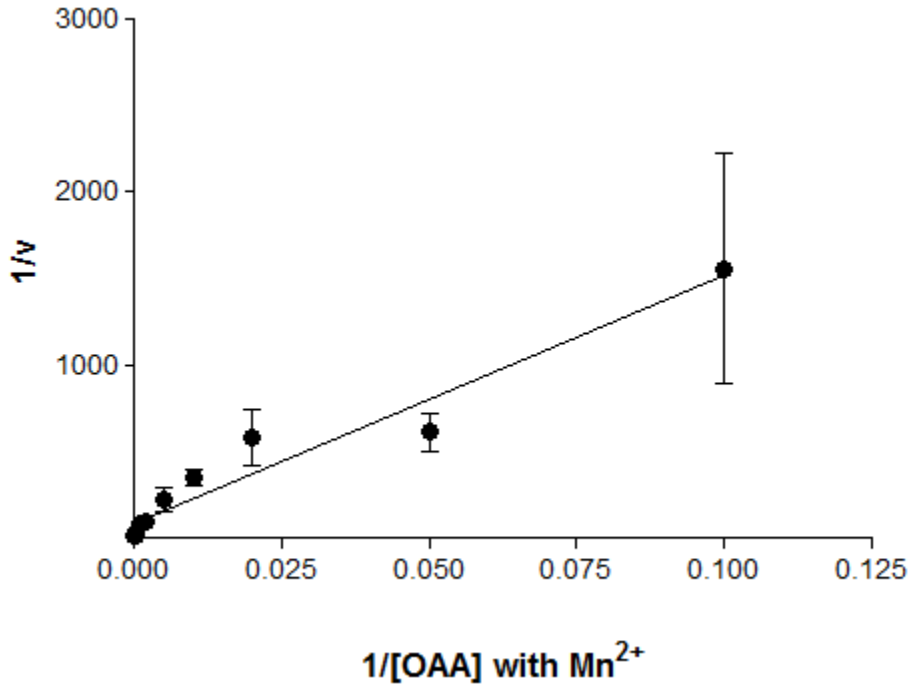

Figure 7.59: Lineweaver-Burk plot of 1/v as a function of 1/[OAA] in the presence of manganese for Arg333Gln mutant PCK. K_m and V_{max} values obtained from this plot are shown in table 3.5

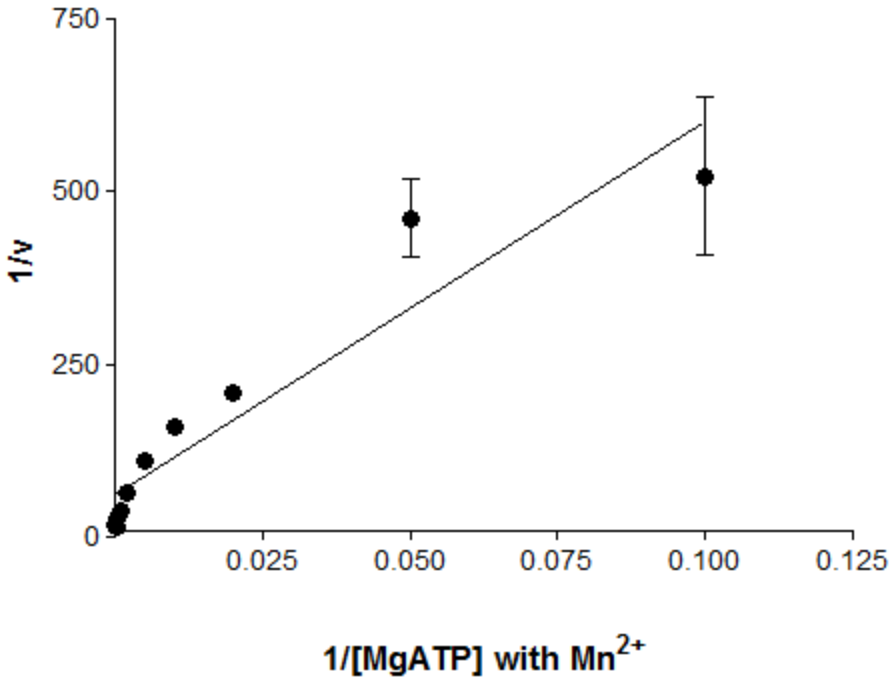

Figure 7.60: Lineweaver-Burk plot of 1/v as a function of 1/[MgATP] in the presence of manganese for Arg333Gln mutant PCK. K_m and V_{max} values obtained from this plot are shown in table 3.5

7.4.3 Eadie-Hofstee plot

Average velocities was used to calculate the velocities used for Eadie-Hofstee plots because v is present on both axes, hence error bars are not shown for these plots

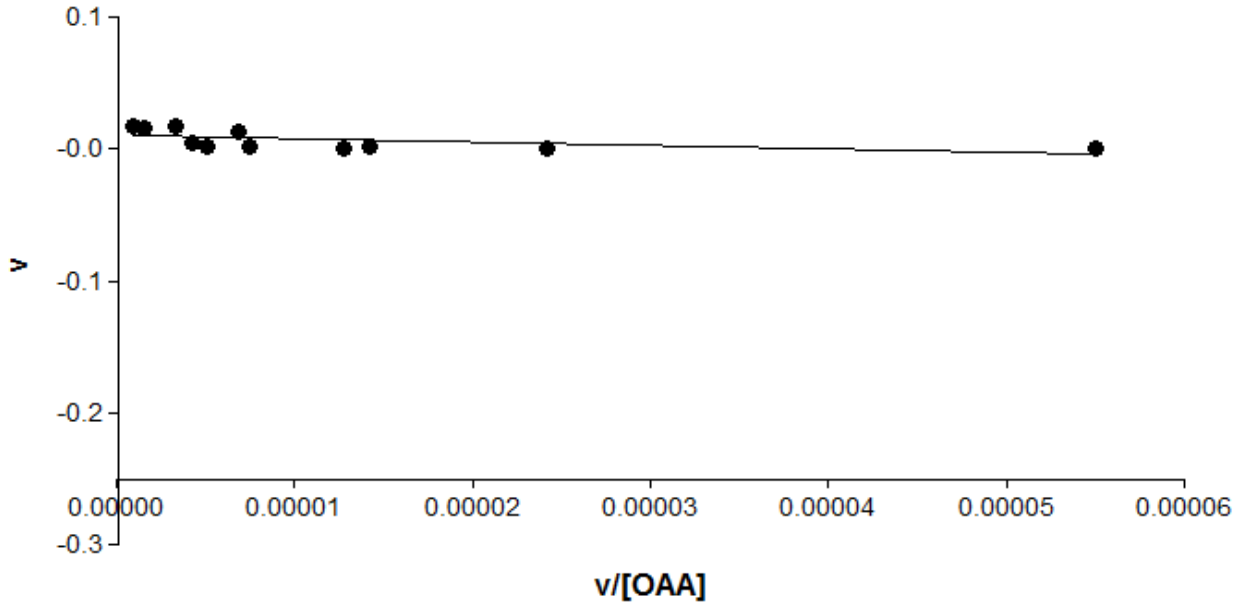

Figure 7.61: Eadie-Hofstee plot of v as a function of v/[OAA] for Arg333Gln mutant PCK. K_m and V_{max} values obtained from this plot are shown in table 3.5

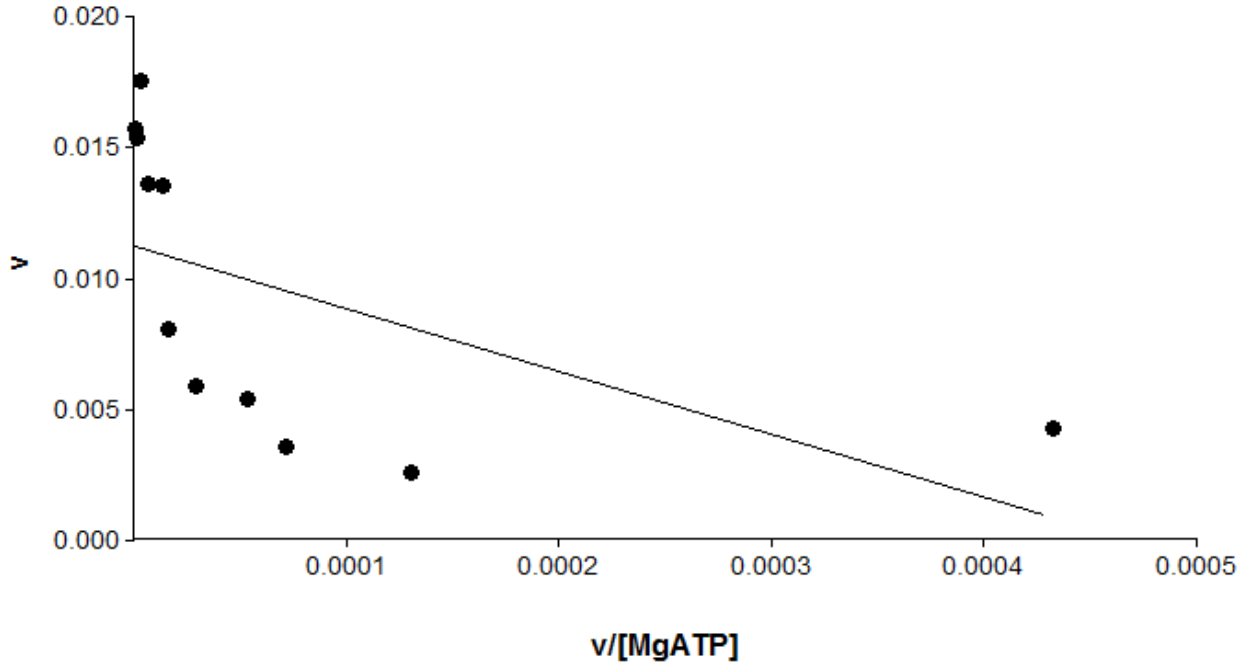

Figure 7.62: Eadie-Hofstee plot of v as a function of v/[MgATP] for Arg333Gln mutant PCK. K_m and V_{max} values obtained from this plot are shown in table 3.5

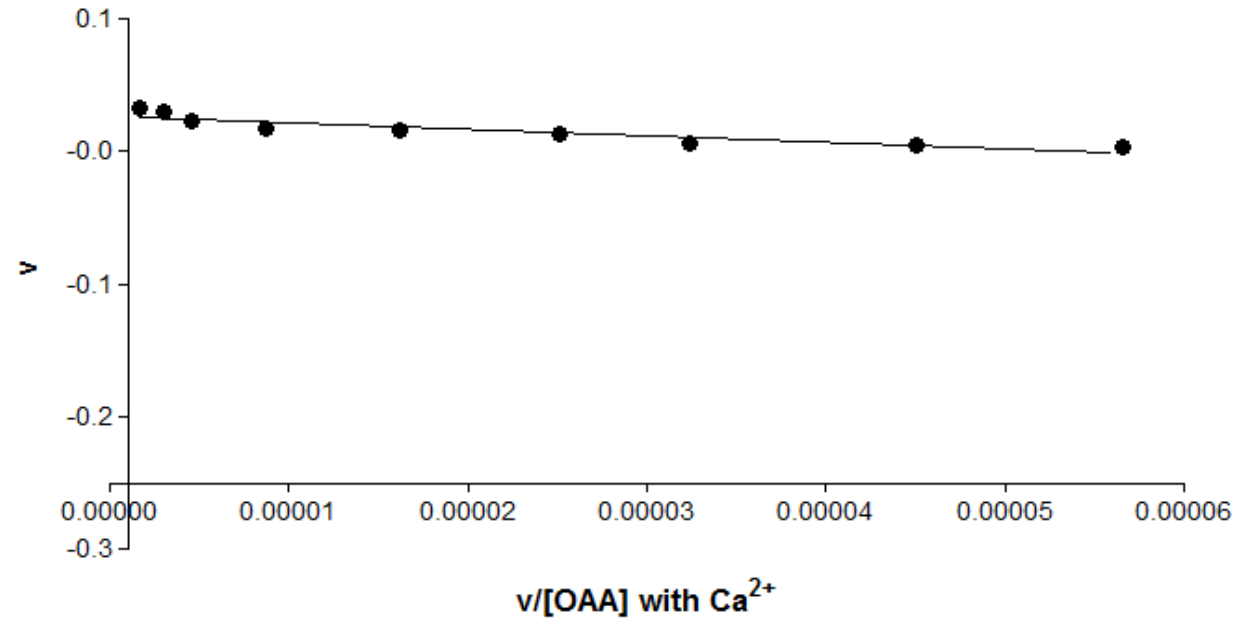

Figure 7.63: Eadie-Hofstee plot of v as a function of v/[OAA] in the presence of calcium for Arg333Gln mutant PCK. K_m and V_{max} values obtained from this plot are shown in table 3.5

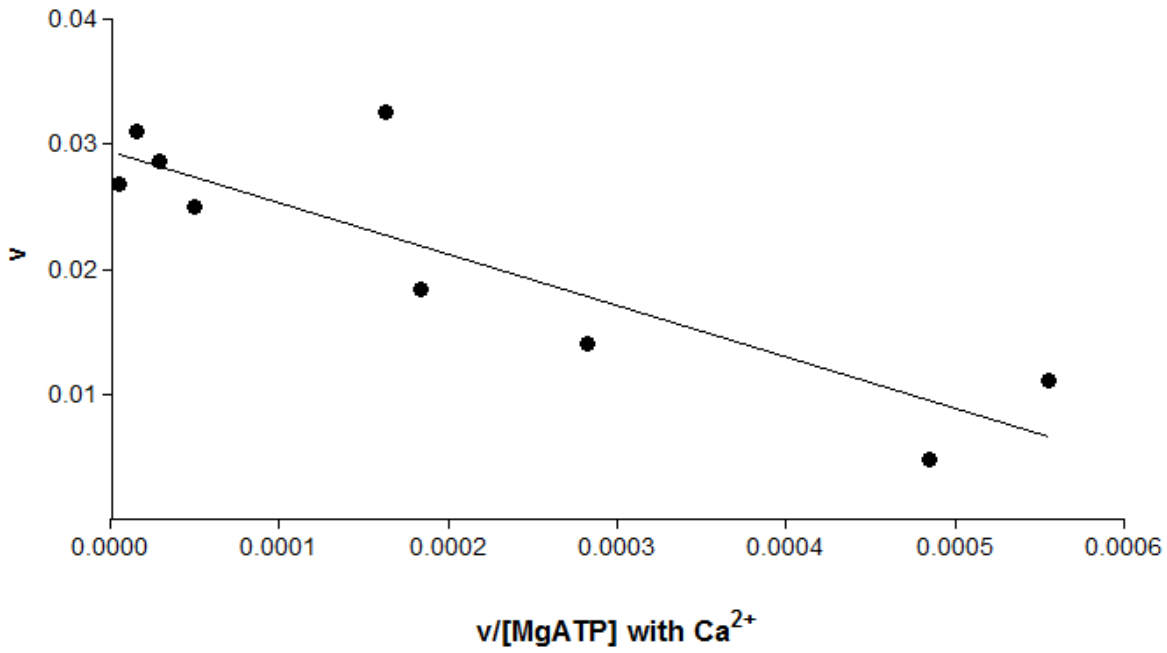

Figure 7.64: Eadie-Hofstee plot of v as a function of v/[MgATP] in the presence of calcium for Arg333Gln mutant PCK. K_m and V_{max} values obtained from this plot are shown in table 3.5

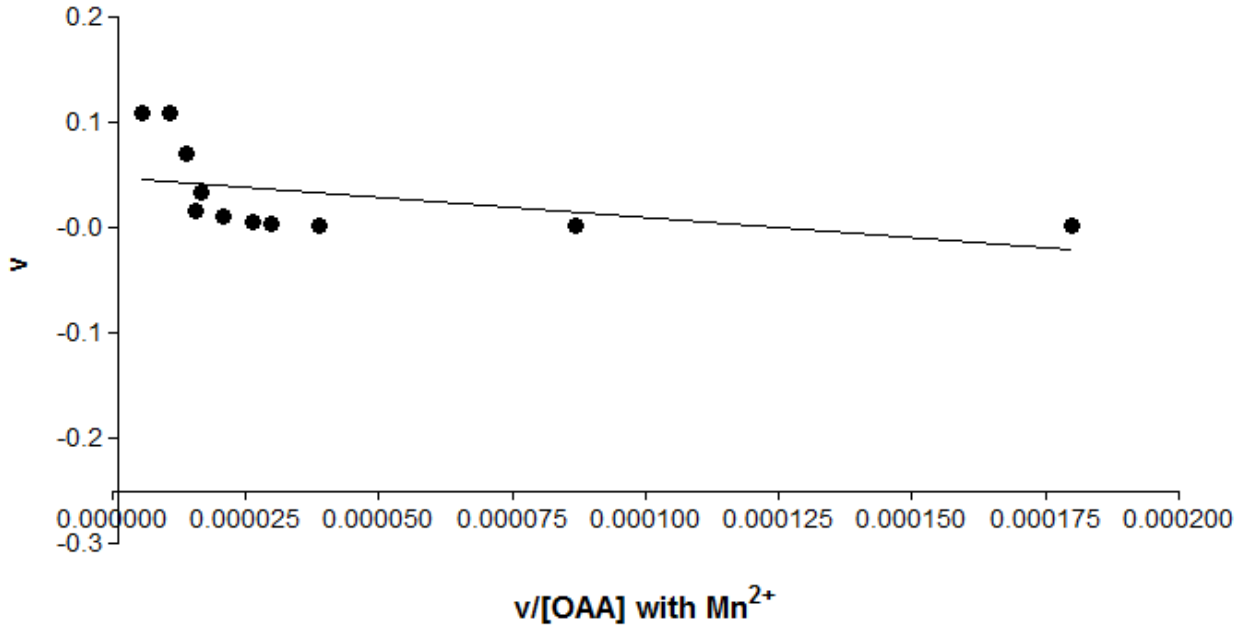

Figure 7.65: Eadie-Hofstee plot of v as a function of v/[OAA] in the presence of manganese for Arg333Gln mutant PCK. K_m and V_{max} values obtained from this plot are shown in table 3.5

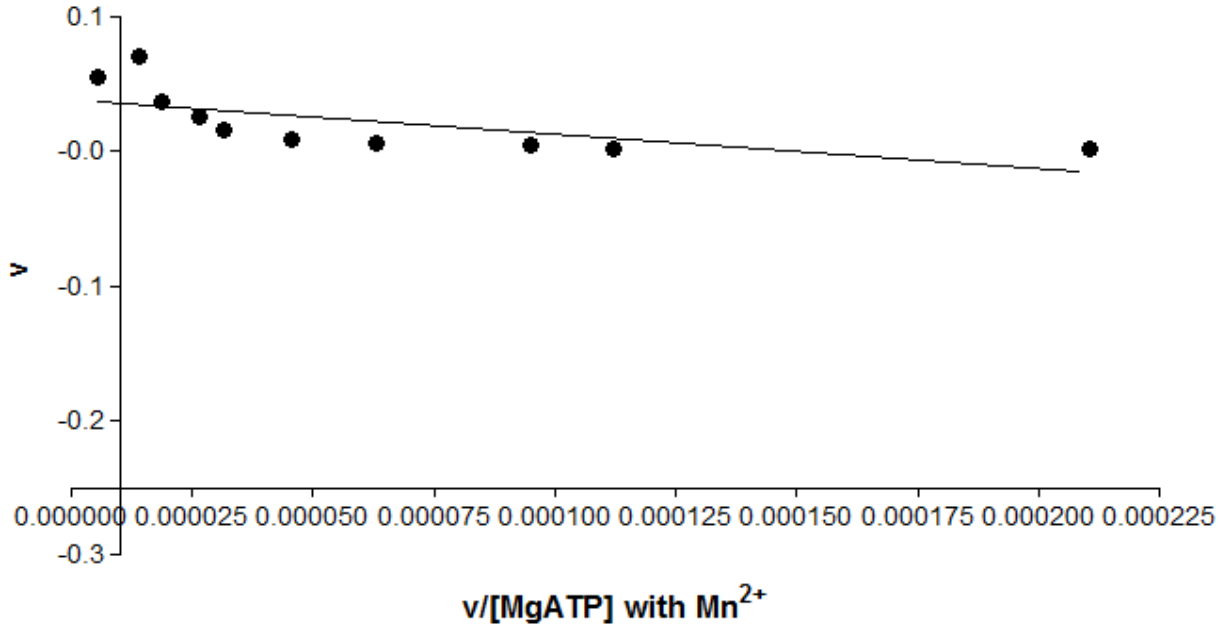

Figure 7.66: Eadie-Hofstee plot of v as a function of v/[MgATP] in the presence of manganese for Arg333Gln mutant PCK. K_m and V_{max} values obtained from this plot are shown in table 3.5

8.0 References

ACD/ChemSketch, freewre version. Advanced chemistry Development, Inc, Toronto, ON, Canada. www.acdlabs.com 2015. (n.d.).

Adams, P.D., Afonine, P.V., Bunkoczi, G., Chen, V.B., Davis, I.W., Echols, N., Headd, J.J., Hung, L.W., Kapral G.J., Grosse-Kunstleve R.W., McCoy, A.J., Moriarty, N.W., Oeffner, R., Read, R.J., Richardson, D.C., Richardson, J.S., Terwilliger, T.C., and Zwart, P.H. (2010). Phenix: a comprehensive python-based system for macromoleculear structure solution. *Acta Crysta*, 213-221.

Afonine, P.V., Grosse-Kunstleve, R.W., Echols, N., Headd, J.J., Moriarty, N.W., Mustyakimov, M., Terwilliger, T.C., Urzhumtsev, A., Zwart, P.H., & Adams P.D. (2012). Towards Automated crystallographic structure refinement with phenix.refine. *Acta Crystallogr D Biol Crystallogr* 68, 352-67.

Aich, S., & Delbaere, L. T. (2007). Phylogenetic study of the evolution of PEP-carboxykinase. *Evolutionary Bioinformatics Online, 3*, 333-340.

Andrade, C., Sepulveda, C., Cardemil, E., & Jabalquinto, A. M. (2010). The role of tyrosine 207 in the reaction catalyzed by *Saccharomyces cerevisiae* phosphoenolpyruvate carboxykinase. *Biological Research, 43*(2), 191-195.

Arancia, G., Belli, S., Donelli, G., & Trovalusci, P. (1980). Ultrastructural changes in *Escherichia coli* grown in divalent cation-deficient medium. *Journal of General Microbiology, 119*(1), 155-164.

Ash, D. E., Emig, F. A., Chowdhury, S. A., Satoh, Y., & Schramm, V. L. (1990). Mammalian and avian liver phosphoenolpyruvate carboxykinase. Alternate substrates and inhibition by analogues of oxaloacetate. *The Journal of Biological Chemistry, 265*(13), 7377-7384.

Short protocols in molecular biology: (3rd edition). A compendium of methods from “current protocols in molecular biology”. Edited by F. ausubel, R. brent, R. E. kingston, D. D. moore, J. G. seidman, J. A. smith and K. struhl. Published 1995 by john wiley & sons, inc., New York. ISBN: 0-471-13781-2(1996).

Barnett, B. L., & Uchtman, V. A. (1979). Structural investigations of calcium- binding molecules. 4. Calcium binding to aminocarboxylates. Crystal structures of ca(CaEDTA)·7H 2 O and na(CaNTA). *Inorganic Chemistry, 18*(10), 2674-2678.

Baudry, A., Leroux, L., Jackerott, M., & Joshi, R. L. (2002). Genetic manipulation of insulin signaling, action and secretion in mice. Insights into glucose homeostasis and pathogenesis of type 2 diabetes. *EMBO Reports, 3*(4), 323-328.

Bazaes, S., Silva, R., Goldie, H., Cardemil, E., & Jabalquinto, A. M. (1993). Reactivity of cysteinyl, arginyl, and lysyl residues of *Escherichia coli* phosphoenolpyruvate carboxykinase against group-specific chemical reagents. *Journal of Protein Chemistry, 12*(5), 571-577.

Bolshakova, T. N., Gabrielyan, T. R., Bourd, G. I., & Gershanovitch, V. N. (1978). Involvement of the *Escherichia coli* phosphoenolpyruvate-dependent phosphotransferase system in regulation of transcription of catabolic genes. *European Journal of Biochemistry / FEBS, 89*(2), 483-490.

Castillo, D., Sepulveda, C., Cardemil, E., & Jabalquinto, A. M. (2009). Functional evaluation of serine 252 of *Saccharomyces cerevisiae* phosphoenolpyruvate carboxykinase. *Biochimie, 91*(2), 295-299.

Chakravarty, K., Cassuto, H., Reshef, L., & Hanson, R. W. (2005). Factors that control the tissue-specific transcription of the gene for phosphoenolpyruvate carboxykinase-C. *Critical Reviews in Biochemistry and Molecular Biology, 40*(3), 129-154.

Chakravarty, K., & Hanson, R. W. (2007). Insulin regulation of phosphoenolpyruvate carboxykinase-c gene transcription: The role of sterol regulatory element-binding protein 1c. *Nutrition Reviews, 65*(6 Pt 2), S47-56.

Chao, Y. P., Patnaik, R., Roof, W. D., Young, R. F., & Liao, J. C. (1993). Control of gluconeogenic growth by *pps* and *pck* in *Escherichia coli*. *Journal of Bacteriology, 175*(21), 6939-6944.

Chen, V.B., Arendall, W.B., Headd, J.J., Keedy, D.A., Immormino, R.M., Kapral, G.J., Murray, L.W., Richardson, J.S., & Richardson D.C. (2010). MolProbity all atom struture validation for macromolecular crystallograpphy. Acta Cryst. D66, 16-21.

Cheek, S., Zhang, H., & Grishin, N. V. (2002). Sequence and structure classification of kinases. *Journal of Molecular Biology, 320*(4), 855-881.

Christ, B., & Nath, A. (1996). Impairment by interleukin 1 beta and tumor necrosis factor alpha of the glucagon-induced increase in phosphoenolpyruvate carboxykinase gene expression

and gluconeogenesis in cultured rat hepatocytes. *The Biochemical Journal, 320 (Pt 1)*, 161-166.

Cornish-Bowden, A. (1995). *Fundamentals of enzyme kinetics* (Rev. Ed.). London: Brookfield, Vt., USA: London: Portland; Brookfield, Vt., USA: Ashgate Pub. Co. distributor.

Cotelesage, J. (2007). Structural and functional studies of phosphoenolpyruvate carboxykinase ProQuest Dissertations Publishing.

Cotelesage, J. J., Prasad, L., Zeikus, J. G., Laivenieks, M., & Delbaere, L. T. (2005). Crystal structure of *Anaerobiospirillum succiniciproducens* PEP carboxykinase reveals an important active site loop. *The International Journal of Biochemistry & Cell Biology, 37*(9), 1829-1837.

Cotelesage, J. J., Puttick, J., Goldie, H., Rajabi, B., Novakovski, B., & Delbaere, L. T. (2007). How does an enzyme recognize CO_2? *The International Journal of Biochemistry & Cell Biology, 39*(6), 1204-1210.

Delbaere, L. T., Sudom, A. M., Prasad, L., Leduc, Y., & Goldie, H. (2004). Structure/function studies of phosphoryl transfer by phosphoenolpyruvate carboxykinase. *Biochimica Et Biophysica Acta, 1697*(1-2), 271-278.

DeLano, W. (2002). The PyMOL Molecular Graphics System. *DeLano Scientific*, www.delanoscientific.com.

Dharmarajan, L., Case, C. L., Dunten, P., & Mukhopadhyay, B. (2008). Tyr235 of human cytosolic phosphoenolpyruvate carboxykinase influences catalysis through an anion-quadrupole interaction with phosphoenolpyruvate carboxylate. *The FEBS Journal*, *275*(23), 5810-5819.

Dittrich, P., Campbell, W. H., & Black, C. C. (1973). Phosphoenolpyruvate carboxykinase in plants exhibiting crassulacean acid metabolism. *Plant Physiology*, *52*(4), 357-361.

Downing, B. P., Rutenberg, A. D., Touhami, A., & Jericho, M. (2009). Subcellular min oscillations as a single-cell reporter of the action of polycations, protamine, and gentamicin on *Escherichia coli*. *PloS One, 4*(9), e7285.

Ehleringer, J. R., Cerling, T. E., & Helliker, B. R. (1997). C_4 photosynthesis, atmospheric CO_2, and climate. *Oecologia, 112*(3), 285-299.

Emsley, P., Lohkamp, B., Scott, W.G., & Cowtan, K. (2010). Features and development of Coot. Acta Cryst. D66, 486-501.

Fersht, A., 1943-. (1999). Structure and mechanism in protein science: A guide to enzyme catalysis and protein folding. New York: New York: W.H. Freeman.

Finan, T. M., Oresnik, I., & Bottacin, A. (1988). Mutants of *Rhizobium meliloti* defective in succinate metabolism. *Journal of Bacteriology*, *170*(8), 3396-3403.

Finnegan, P. M., Suzuki, S., Ludwig, M., & Burnell, J. N. (1999). Phospho*enol*pyruvate Carboxykinase in the C_4 Monocot *Urochloa panicoides* is encoded by Four Differentially Expressed Genes. *Plant Physiology*, *120*(4), 1033–1042.

Fukuda, W., Fukui, T., Atomi, H., & Imanaka, T. (2004). First characterization of an archaeal GTP-dependent phosphoenolpyruvate carboxykinase from the hyperthermophilic archaeon *Thermococcus kodakaraensis* KOD1. *Journal of Bacteriology, 186*(14), 4620-4627.

Gelles, E., & Salama, A. (1958). 737. The interaction of transition- metal ions with oxaloacetic acid. Part II. Thermodynamics of chelation. *Journal of the Chemical Society (Resumed),* 3683-3688.

Goldie, A. (1979). The regulation of phosphoenolpyruvate carboxykinase and other gluconeogenic enzymes in Escherichia coli *K12* ProQuest Dissertations Publishing.

Goldie, A. H., & Sanwal, B. D. (1980). Allosteric control by calcium and mechanism of desensitization of phosphoenolpyruvate carboxykinase of *Escherichia coli*. *The Journal of Biological Chemistry, 255*(4), 1399-1405.

Goldie, H. (1984). Regulation of transcription of the *Escherichia coli* phosphoenolpyruvate carboxykinase locus: Studies with *pck-lacZ* operon fusions. *Journal of Bacteriology, 159*(3), 832-836.

Goldstein, B. J. (2002). Insulin resistance as the core defect in type 2 diabetes mellitus. *The American Journal of Cardiology, 90*(5A), 3G-10G.

Gomez-Valades, A. G., Vidal-Alabro, A., Molas, M., Boada, J., Bermudez, J., Bartrons, R., et al. (2006). Overcoming diabetes-induced hyperglycemia through inhibition of hepatic phosphoenolpyruvate carboxykinase (GTP) with RNAi. *Molecular Therapy: The Journal of the American Society of Gene Therapy, 13*(2), 401-410.

Guss, J. M. (2011). Biomolecular crystallography: Principles, practice, and application to structural biology, by Bernard Rupp. *Crystallography Reviews, 17*(1), 65-67.

Hanson, R. W., & Patel, Y. M. (1994). Phosphoenolpyruvate carboxykinase (GTP): The gene and the enzyme. *Advances in Enzymology and Related Areas of Molecular Biology, 69*, 203.

Hanson, R., & Reshef, L. (1997). Regulation of phosphoenolpyruvate carboxykinase (GTP) gene expression. *Annual Review of Biochemistry, 66*(1 1), 581-611.

Holyoak, T., Sullivan, S. M., & Nowak, T. (2006). Structural insights into the mechanism of PEPCK catalysis. *Biochemistry, 45*(27), 8254-8263.

Hou, S. Y., Chao, Y. P., & Liao, J. C. (1995). A mutant phosphoenolpyruvate carboxykinase in *Escherichia coli* conferring oxaloacetate decarboxylase activity. *Journal of Bacteriology, 177*(6), 1620-1623.

Jabalquinto, A. M., & Cardemil, E. (1993). The kinetic mechanism of yeast phosphoenolpyruvate carboxykinase. *Biochimica Et Biophysica Acta, 1161*(1), 85-90.

Jakubovics, N. S., & Jenkinson, H. F. (2001). Out of the Iron Age: New insights into the critical role of manganese homeostasis in bacteria. *Microbiology (Reading, England), 147*(Pt 7), 1709-1718.

Jo, J., Ishihara, N., & Kikuchi, G. (1974). Occurrence and properties of four forms of phosphoenolpyruvate carboxykinase in the chicken liver. *Archives of Biochemistry and Biophysics, 160*(1), 246-254.

Jomain-Baum, M., & Schramm, V. L. (1978). Kinetic mechanism of phosphoenolpyruvate carboxykinase (GTP) from rat liver cytosol. Product inhibition, isotope exchange at equilibrium, and partial reactions. *The Journal of Biological Chemistry, 253*(10), 3648-3659.

Klaffl, S., Brocker, M., Kalinowski, J., Eikmanns, B. J., & Bott, M. (2013). Complex regulation of the phosphoenolpyruvate carboxykinase gene *pck* and characterization of its GntR-type regulator IolR as a repressor of myo-inositol utilization genes in *Corynebacterium glutamicum*. *Journal of Bacteriology, 195*(18), 4283-4296.

Karczmarewicz, E., Matyaszczyk, M., Vorbrodt, Z., & Lorenc, R. (1985). Activation of liver cytosol phosphoenolpyruvate carboxykinase by Ca^{2+} through intracellular redistribution of Mn2+. *European Journal of Biochemistry / FEBS, 151*(3), 561-565.

Krautwurst, H., Bazaes, S., Gonzalez, F. D., Jabalquinto, A. M., Frey, P. A., & Cardemil, E. (1998). The strongly conserved lysine 256 of saccharomyces cerevisiae phosphoenolpyruvate carboxykinase is essential for phosphoryl transfer. *Biochemistry, 37*(18), 6295-6302.

Krebs, A., & Bridger, W. A. (1980). The kinetic properties of phosphoenolpyruvate carboxykinase of *Escherichia coli*. *Canadian Journal of Biochemistry, 58*(4), 309-318.

Kung, F. C., Raymond, J., & Glaser, D. A. (1976). Metal ion content of *Escherichia coli* versus cell age. *Journal of Bacteriology, 126*(3), 1089-1095.

Kwon, Y., Yup Lee, S., & Kim, P. (2008). A physiology study of *Escherichia coli* overexpressing phosphoenolpyruvate carboxykinase. *Bioscience, Biotechnology, and Biochemistry, 72*(4), 1138.

Lea, P. J., Chen, Z. -., Leegood, R. C., & Walker, R. P. (2001). Does phosphoenolpyruvate carboxykinase have a role in both amino acid and carbohydrate metabolism? *Amino Acids, 20*(3), 225-241.

Lee, S. J., Song, H., & Lee, S. Y. (2006). Genome-based metabolic engineering of *Mannheimia succiniciproducens* for succinic acid production. *Applied and Environmental Microbiology, 72*(3), 1939-1948.

Leegood, R. C., & Walker, R. P. (2003). Regulation and roles of phosphoenolpyruvate carboxykinase in plants. *Archives of Biochemistry and Biophysics, 414*(2), 204-210.

Leduc, Y. A., Prasad, L., Laivenieks, M., Zeikus, J. G., & Delbaere, L. T. (2005). Structure of PEP carboxykinase from the succinate-producing *Actinobacillus succinogenes*: A new conserved active-site motif. *Acta Crystallographica.Section D, Biological Crystallography, 61*(Pt 7), 903-912.

Liao, J. C., Chao, Y. P., & Patnaik, R. (1994). Alteration of the biochemical valves in the central metabolism of *Escherichia coli*. *Annals of the New York Academy of Sciences, 745*, 21-34.

Llanos, L., Briones, R., Yevenes, A., Gonzalez-Nilo, F. D., Frey, P. A., & Cardemil, E. (2001). Mutation Arg336 to lys in *Saccharomyces cerevisiae* phosphoenolpyruvate carboxykinase

originates an enzyme with increased oxaloacetate decarboxylase activity. *FEBS Letters, 493*(1), 1-5.

Ma, Z., Jacobsen, F. E., & Giedroc, D. P. (2009). Coordination chemistry of bacterial metal transport and sensing. *Chemical Reviews, 109*(10), 4644-4681.

Magnusson, I., Rothman, D. L., Katz, L. D., Shulman, R. G., & Shulman, G. I. (1992). Increased rate of gluconeogenesis in type II diabetes mellitus. A 13C nuclear magnetic resonance study. *Journal of Clinical Investigation*, *90*(4), 1323–1327.

Matte, A. (1996). In Delbaere L. (Ed.), Crystallographic studies of *Escherichia coli* phosphoenolpyruvate carboxykinase ProQuest Dissertations Publishing.

Matte, A., Goldie, H., Sweet, R. M., & Delbaere, L. T. (1996). Crystal structure of *Escherichia col*i phosphoenolpyruvate carboxykinase: A new structural family with the P-loop nucleoside triphosphate hydrolase fold. *Journal of Molecular Biology, 256*(1), 126-143.

Matte, A., Tari, L. W., Goldie, H., & Delbaere, L. T. J. (1997). Structure and mechanism of phosphoenolpyruvate carboxykinase. *Journal of Biological Chemistry, 272*(13), 8105-8108.

McCoy, A.J., Grosse-Kunstleve, R.W., Adams, P.D., Winn, M.D., Storoni, L.C., & Read, R.J. (2007). Phaser crystallographic software. *J Appl Crystallogr* 40, 658-674.

Medina, V., Pontarollo, R., Glaeske, D., Tabel, H., & Goldie, H. (1990). Sequence of the *pckA* gene of *Escherichia coli* K-12: Relevance to genetic and allosteric regulation and homology of *E. coli* phosphoenolpyruvate carboxykinase with the enzymes from *Trypanosoma brucei* and *Saccharomyces cerevisiae*. *Journal of Bacteriology, 172*(12), 7151-7156.

Nakano, M., Ogasawara, H., Shimada, T., Yamamoto, K., & Ishihama, A. (2014). Involvement of cAMP-CRP in transcription activation and repression of the *pck* gene encoding PEP carboxykinase, the key enzyme of gluconeogenesis. *FEMS Microbiology Letters, 355*(2), 93-99.

Naseem, R., Holland, I. B., Jacq, A., Wann, K. T., & Campbell, A. K. (2008). pH and monovalent cations regulate cytosolic free Ca2+ in E. coli. *Biochimica Et Biophysica Acta (BBA) - Biomembranes, 1778*(6), 1415-1422.

Naseem, R., Wann, K. T., Holland, I. B., & Campbell, A. K. (2009). ATP regulates calcium efflux and growth in *E. coli*. *Journal of Molecular Biology, 391*(1), 42-56.

National institute of standards and technology. Ciritical selected stability constants of metals complexes .Database version two. (1995). U.S. Commerce department 100 Bureau Drive Gathersburg M.D., U.S.A 20899-23460.

Nelson, D. L. (. L., 1942-. (2008). In Lehninger A. L., Cox M. M. (Eds.), *Lehninger principles of biochemistry* (5th ed.). New York: New York: W.H. Freeman.

Novakovski, B. A. A. (2000). Mutations which alter substrate and metal ion kinetics of *Escherichia coli* phosphoenolpyruvate carboxykinase: A thesis.. Thesis (M.Sc.)--University of Saskatchewan, 2001).

Osteras, M., Finan, T. M., & Stanley, J. (1991). Site-directed mutagenesis and DNA sequence of *pckA* of rhizobium NGR234, encoding phosphoenolpyruvate carboxykinase: Gluconeogenesis and host-dependent symbiotic phenotype. *Molecular & General Genetics: MGG, 230*(1-2), 257-269.

Perrin, D. D., & Sayce, I. G. (1967). Computer calculation of equilibrium concentrations in mixtures of metal ions and complexing species. *Talanta, 14*(7), 833-842.

Pflugrath, J. W. (1999). d*trek. *Acta cryst*, 1718-1725.

Podkovyrov, S. M., & Zeikus, J. G. (1993). Purification and characterization of phosphoenolpyruvate carboxykinase, a catabolic CO2-fixing enzyme, from *Anaerobiospirillum succiniciproducens*. *Journal of General Microbiology, 139*(2), 223-228.

Saier, M.,H. (1996). Cyclic AMP- independent catabolite repression in bacteria. *FEMS Microbiology Letters, 138*(2), 97-103.

Simoni, R. D., Roseman, S., & Saier, M. H.,Jr. (1976). Sugar transport. Properties of mutant bacteria defective in proteins of the phosphoenolpyruvate: Sugar phosphotransferase system. *The Journal of Biological Chemistry, 251*(21), 6584-6597.

Sudom, A., Walters, R., Pastushok, L., Goldie, D., Prasad, L., Delbaere, L. T., et al. (2003). Mechanisms of activation of phosphoenolpyruvate carboxykinase from *Escherichia coli* by Ca^{2+} and of desensitization by trypsin. *Journal of Bacteriology, 185*(14), 4233-4242.

Sugahara, M., Ohshima, N., Ukita, Y., Sugahara, M., & Kunishima, N. (2005). Structure of ATP-dependent phosphoenolpyruvate carboxykinase from *Thermus thermophilus* HB8 showing the structural basis of induced fit and thermostability. *Acta Crystallographica. Section D, Biological Crystallography, 61*(Pt 11), 1500-1507.

Tari, L. W., Matte, A., Goldie, H., & Delbaere, L. T. (1997). Mg^{2+}-Mn^{2+} clusters in enzyme-catalyzed phosphoryl-transfer reactions. *Nature Structural Biology, 4*(12), 990-994

Tari, L. W., Matte, A., Pugazhenthi, U., Goldie, H., & Delbaere, L. T. (1996). Snapshot of an enzyme reaction intermediate in the structure of the ATP-Mg2+-oxalate ternary complex of *Escherichia coli* PEP carboxykinase. *Nature Structural Biology, 3*(4), 355-363.

Tisa, L. S., & Adler, J. (1995). Cytoplasmic free-Ca2+ level rises with repellents and falls with attractants in *Escherichia coli* chemotaxis. *Proceedings of the National Academy of Sciences of the United States of America, 92*(23), 10777-10781.

Valera, A., Pujol, A., Pelegrin, M., & Bosch, F. (1994). Transgenic mice overexpressing phosphoenolpyruvate carboxykinase develop non-insulin-dependent diabetes mellitus. *Proceedings of the National Academy of Sciences of the United States of America, 91*(19), 9151-9154.

Walker, R. P., Acheson, R. M., Técsi, L. I., & Leegood, R. C. (1997). Phosphoenolpyruvate carboxykinase in C4 plants: Its role and regulation. *Functional Plant Biology, 24*(4), 459-468.

Wiese, T. J., Lambeth, D. O., & Ray, P. D. (1991). The intracellular distribution and activities of phosphoenolpyruvate carboxykinase isozymes in various tissues of several mammals and birds. *Comparative Biochemistry and Physiology.B, Comparative Biochemistry, 100*(2), 297-302.

Yang, J., Kalhan, S. C., & Hanson, R. W. (2009). What is the metabolic role of phosphoenolpyruvate carboxykinase? *The Journal of Biological Chemistry, 284*(40), 27025.

Yevenes, A., Gonzalez-Nilo, F. D., & Cardemil, E. (2007). Relevance of phenylalanine 216 in the affinity of saccharomyces cerevisiae phosphoenolpyruvate carboxykinase for Mn (II). *The Protein Journal, 26*(2), 135-141.

Zhang, X., Jantama, K., Moore, J. C., Jarboe, L. R., Shanmugam, K. T., & Ingram, L. O. (2009). Metabolic evolution of energy-conserving pathways for succinate production in *Escherichia coli*. *Proceedings of the National Academy of Sciences of the United States of America, 106*(48), 20180-20185.

Zimmer, D. B., & Magnuson, M. A. (1990). Immunohistochemical localization of phosphoenolpyruvate carboxykinase in adult and developing mouse tissues. *The Journal of Histochemistry and Cytochemistry: Official Journal of the Histochemistry Society*, *38*(2), 171-178.